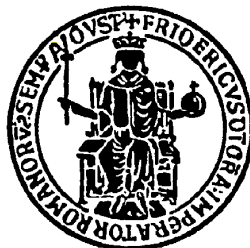


UNIVERSITA' DEGLI STUDI DI NAPOLI FEDERICO II



*Dottorato di Ricerca in Ingegneria Chimica
(XXIII Ciclo)*

HIGH PRESSURE CATALYTIC COMBUSTION

scientific committee :

Prof. Gennaro Russo

Prof. Piero Salatino

Ing. Raffaele Pirone

Candidate:

Paola Sabrina Barbato

ABSTRACT

The study of catalyst behavior at pressure up to 12 bar during CH₄, H₂, CO and their mixtures combustion is the main purpose of this PhD thesis. Actually the interest towards catalytic combustion as an alternative route to produce electric power is renewed due to the use of Low-Btu fuels. Therefore the research activity was focused notably on CH₄ but also on H₂ and CO combustions and on the effect of their addition on methane combustion at variable pressure.

At this purpose it was necessary to design and realize an innovative lab scale plant which operates at temperatures up to 1000°C and pressure up to 12 bar and, with the proper reactor configuration and operative conditions, in two different operating modes: isothermal and auto-thermal.

The active phases considered in this experimental activity are a conventional Pt catalyst (1%wt), and a more thermally stable catalyst, a supported perovskite (20%wt LaMnO₃), and a bi-functional Pt-perovskite catalyst. Perovskites are cheap and show an activity only slightly lower compared to noble metals at condition relevant for GT engines. Moreover their behavior under pressure is quite unknown. The need for low combustor pressure drops makes necessary the use of an appropriate substrate. For this reason particular attention was devoted to deposit efficaciously the catalysts powders over appropriate planar (α -Al₂O₃) and honeycomb monolithic (cordierite) substrates.

The materials used in this thesis were completely characterized by means of temperature programmed reductions of the different catalysts under H₂ or CO flows. Results revealed that the reducibility of the catalysts, characteristic temperatures and reduction degrees strongly depends on the reducing agent. In particular, H₂ is the most reducing agent for Pt, while perovskite preferentially interacts with CO. The bi-functional Pt-perovskite catalyst show intermediate properties with respect to the single phases.

Since the availability of reliable heterogeneous kinetic data is necessary for the correct description of the catalytic processes, CH₄, CO and H₂ combustions under isothermal conditions have been separately studied on the perovskite and the noble metal catalyst. Particular attention was devoted to study the fluid dynamics of the reactor and to characterize the mass transfer properties of the systems in order to find the conditions free from diffusion limitations. Moreover a proper reactor model was developed in order to find the best kinetic models.

Concerning the Pt catalyst, H₂ combustion apart, in all cases it was possible to derive a simple reaction rate well fitting all experimental data; fractional rate expressions, derived from models including both fuel and oxygen adsorption, provided the best description of the experimental results. With regard to the Perovskite catalyst, in the investigated temperature range methane combustion rate can be expressed with a single fractional equation taking into account only methane adsorption. An apparent linear reaction rate could be used to fit the data only at atmospheric pressure. As a consequence, the extension of such kinetics at higher pressures leads to an overestimation of the reaction rate. The evidence that oxygen dependence is negligible is in agreement with literature data and is due to the occurrence of the reaction with lattice oxygen. On the contrary, both CO and H₂ combustions on perovskite are influenced by changes of oxygen partial pressure. In both cases, the best models suggest the reaction of at least a fraction of the fuel with α -oxygen, generally weakly bonded to the catalyst surface. Moreover, according to the strong CO affinity with perovskite the CO combustion rate must take into account the negative effect of CO accumulation on the surface, leading to a less than linear reaction order with respect to the fuel.

As a general conclusion, excluding some conditions of H₂ combustion on Pt, the effect of pressure on the combustion kinetics is positive even if less than linear.

Concerning the effect of the pressure under autothermal conditions, it was found that methane can be ignited simply by increasing the pressure, due to two concomitant effects: higher reaction rates, according to the conclusions of the kinetic study, and longer contact times, due to the reduction of the flow velocity. Moreover, once ignited, the pressure can be lowered without the occurrence of quenching phenomena, i.e. keeping stable operation.

A positive effect of Low BTU fuels co-feeding on methane light off has been detected on perovskite-based catalysts, eventually doped with Pt. As a matter of fact, lower pre-heating temperatures are needed in order to ignite methane. Ignition occurrence could be obtained by changing the operating pressure too. The main reason of such effect is due to thermal causes. As a matter of fact, depending on the catalyst formulation, low BTU fuels can be easily converted in the first part of the reactor and the produced heat increases the temperature (and consequently the kinetics) downstream up to the imbalance between generated and exchanged heat is reached.

GENERAL INDEX

Abstract	ii
I INTRODUCTION	1
I.1 Energetic-Environmental Issues	1
I.2 Conventional and Alternatives Fuels	3
I.3 Gas Turbine System	7
<i>I.3.1. Application Contexts</i>	7
<i>I.3.2. Primary Measure To Reduce NO_x Emissions</i>	11
I.4 Catalytic Combustion	15
<i>I.4.1 Total Oxidation Catalysts</i>	17
<i>I.4.2. Catalytic Combustors</i>	21
<i>I.4.3 High Pressure Catalytic Combustion Literature</i>	27
I.5 Aim of the thesis	33
II MATERIALS AND METHODS	36
II.1 Structured Catalyst Preparation	36
<i>II.1.1 Planar Substrates Catalytic Systems</i>	36
<i>II.1.2 Monolith Catalysts</i>	40
II.2 Catalyst Characterization	42
II.3 Activity Test at Atmospheric Pressure: Study of H₂-CCM under autothermal condition	44
<i>II.3.1. Atmospheric Rig Description</i>	44
<i>II.3.2 Reactor Configuration</i>	46

II.3.3 Operative Conditions	47
II.4 Activity Test under Pressure	48
II.4.1 Design and Description of High-Pressure Test Rig	48
II.4.2. Kinetic Studies Under Pressure	54
II.4.3 Autothermal Test	59
III CATALYSTS CHARACTERIZATION.....	62
III.1 BET Analysis on Powders Catalysts.....	62
III.2 H₂-CO Temperature Programmed Reduction	63
III.2.1 H ₂ -TPR	63
III.2.2 CO-TPR.....	67
III.3 Pt volatilization study for the bi-functional 1Pt-LM20.....	75
IV-ATMOSPHERIC AUTOTHERMAL RESULTS.....	77
IV.1 Methane Ignition And Quenching.....	77
IV.2 H₂ assisted ignition and quenching of methane	86
V KINETIC STUDY UNDER PRESSURE.....	91
V.1CH₄ Combustion	91
V.1.1 CH ₄ combustion on supported LaMnO ₃	91
V.1.2 CH ₄ combustion on supported Pt.....	105
V.2 H₂ combustion	116
V.2.1 H ₂ combustion on supported LaMnO ₃	116
V.2.2 H ₂ combustion on supported Pt.....	124
V.3 CO combustion	133

<i>V.3.1 CO combustion on supported LaMnO₃</i>	133
<i>V.3.2 CO combustion on supported Pt</i>	144
VI AUTHO-THERMAL TEST UNDER PRESSURE	151
VI.1 Effect of pressure on CH₄ ignition	151
VI.2 Pressure ignition: total flow rate effect	157
VI.3 Pressure effect on steady state operation	161
VI.4 Pressure effect on ignition of a CH₄/CO/H₂ mixture	163
VII Conclusions and future work	165
VII.1 Conclusions	165
VII.2 Future work	168
Appendix	169
1.1 Fluid Dynamic Regime Individuation	170
1.2 Plug flow approximation	174
1.3 Heat And Mass Transfer	176
1.4 Interphase limitation to mass transfer	178
1.4 Intraphase limitation to mass transfer	182
Notation	185
References	189

I INTRODUCTION

I.1 Energetic-Environmental Issues

The environmental issues associated with the energy production are more and more of concern for the scientific community and for the civil society too. In particular the attention is addressed to the energy production from fossil fuel for essentially two reasons: (i) it is the major source of pollutants (soot and NO_x) and green-house gasses, mainly CO₂ and (ii) also in the next future it remains the most important method to cover the world energetic requirements. Actually, it is expected that fossil fuels (coal, oil and natural gas), will remain the most used primary source for energy production for several decades, as reported in Fig. I.1.1(International Energy Outlook 2008).

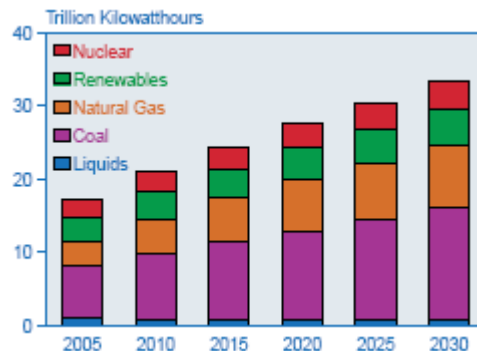


Fig.I.1.1 World electricity generation by fuel 2005-2030 (Trillion kWh)-Energy information Administration/International Energy Outlook 2008

As shown in figure I.1.2, the world consumptions of primary energy are constantly growing, especially those of China and India, where about 40% of worldwide people are living.

In the World Energy Outlook of the 2008, the International Energy Agency (IEA) estimates that, in the reference scenario (“business as usual”), the increase of oil demand and of CO₂ emission in 2050 will be respectively 70% and 130%. Therefore, the Europe Council, in the meeting of March 8-9th 2007, has signed up an international agreement on emission reduction in the post-Kyoto period

(2020) of 30% respect to 1990. In general the EU objective is a pollutants emission reduction by 20% until 2020. The aim of this policy is to reach a reduction of 60-80% till 2050.

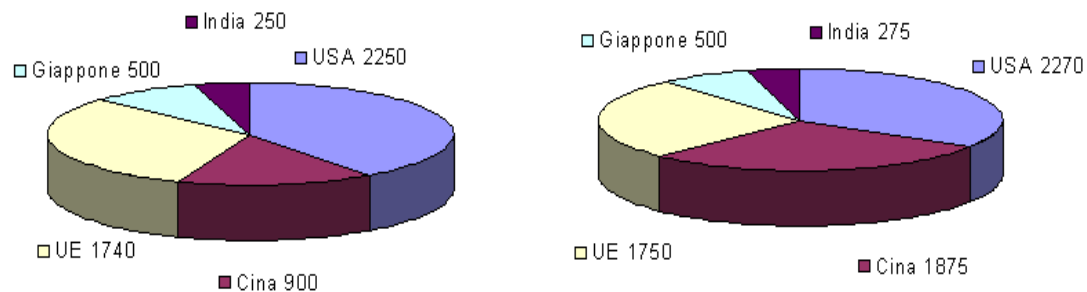


Fig.I.1.2 The world consumptions of primary energy 2000-2007 (Mtoe)-Source ENEA Report 2008

The rigorousness of these objectives leads to severe regulations. Moreover, starting from these consideration, in the IEA opinion, derives the necessity of a new world way of energy production and consumption that implies

- the use of different existing technologies with a significant improvement of their efficiencies
- the development of new technologies based on the exploitation of renewable sources
- the CO₂ capture and storage (fuel decarbonisation)

Among these different strategies, the improvement of efficiencies of existing technologies turn out to be the most effective approach in term of emission reduction (43%), followed by renewable (21%), power generation with CO₂ capture (19%), fuel substitution in end-use sector (i.e. use of energy vectors) (11%) and nuclear (6%). It is note worthy that new concepts of power generation proposed generally are based on more than one strategies listed above.

Besides, among the existing technologies, Gas Turbines (GT) are very promising since they not only show high efficiencies, but also the possibility (i) to increase global efficiencies when combined with steam turbine in Combined Cycle Plant (CC), (ii) to co-generate heat and power (Combined Heat and Power generation (CHP)) and (iii) to be used in Integrated Gasification Combined Cycle (IGCC) with

several advantages as will be presented in section I.3. Nevertheless, still some improvements are required as will be highlighted in paragraph I.3.2.

Likewise, in the last decades it is accrued the awareness that the use of catalysis could be very important for the aim of a sustainable future (Catalysis for Sustainable Energy Production 2009). Actually, in the case of power generation application, Catalytic Combustion has received increasing attention due to: (i) the safety of the operation, extending stable combustion with very lean mixtures too, and (ii) the possibility to achieve ultra-low NO_x emission without compromising combustion efficiency.

Firstly in the section I.2 fuels other than Natural Gas, will be introduced. Then some features of Gas Turbine and Catalytic Combustion will be deepened respectively in section I.3 and I.4.

I.2 Conventional and Alternatives Fuels

Historically Gas Turbine (GT) have been primary developed for Natural Gas (NG) utilisation and currently are the best available technologies to convert the chemical potential of this fuel to power. This “symbiosis” implies that not only GT benefits by the great availability of NG but also that the use of GT has increased the widespread use of NG. In addition, the latter is the most clean among fossil fuels (Coal, oil and NG) with the higher H/C ratio allowing a lower CO₂/kWh ratio (Pilavachi et al 2009; see Fig.I.2.1). As a consequence, as highlighted in the International Energy Outlook 2008, it is expected that NG will replace oil whenever it is possible and that worldwide natural gas consumption, in the reference case, increases from 104 trillion cubic feet in 2005 to 158 trillion cubic feet in 2030.

Nevertheless, the actual situation pushes towards the use of an energy vector that has: (i) virtual no environmental impact, (ii) the possibility to be produced by different interchangeable and widespread available primary sources and (iii) the possibility to be easily distributed by means of a net.

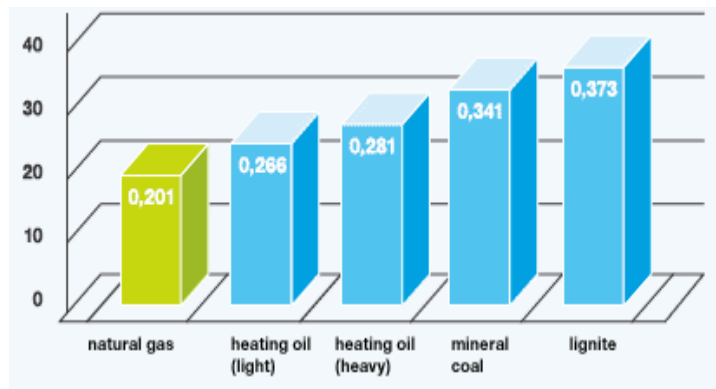


Fig. I.2.1. Kg CO₂ produced for KWh for several fossil fuels

Therefore in the meanwhile the interest towards hydrogen is grown since it partially comes up to the above mentioned expectations. As a matter of fact, H₂ could be produced by several sources either fossil or renewable (Fig. I.2.2). thus allowing to valorise the local renewables and, as a consequence, to reduce the dependence on imported source of energy leading to a more free and stable energy market (European school on Hydrogen Safety 2006).

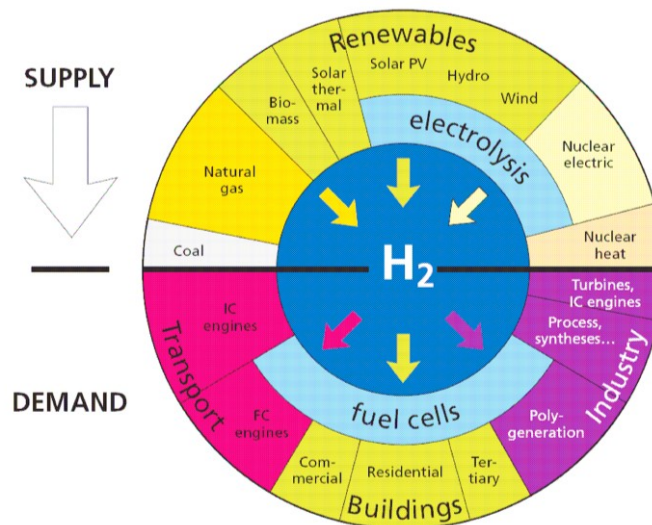


Fig. I.2.2 Sources and uses of hydrogen (European school on Hydrogen Safety 2006)

The use of this energy vector is considered a key aspect for a sustainable future but also at the same time it boosts the diffuse use of renewables and makes compatible the use of fossil fuels with environmental demands.

Actually, concerning the H₂ production from fossil fuels (that currently represents the only method of H₂ production on a large scale; see table I.2.1) its economic–environmental justification is the easy CO₂ removal at the point of production instead of the more expensive CO₂ capture at the end of combustion processes due to the large N₂ dilution (Towns et al 2007).

Tab I.2.1– Annual global hydrogen production share by source

Source	Billion cubic meters/yr	Share, %
NG	240	48
Oil	150	30
Coal	90	18
Electrolysis	20	4
<u>Total</u>	500	100

(Balat, 2008)

The use of hydrogen as energy vector requires several integrated infrastructures making its use cheap and reliable. Among these infrastructures, the use of a distribution net is very important. In this direction, the use of NG distribution net is an attractive option to allow the H₂ penetration in the energy market.

Thus, in the last years the combustion processes of CH₄-H₂ mixtures have received huge interest, since the higher H/C ratio i.e. lower CO₂/kWh ratio of this new fuel. This interest is witnessed by a considerable number of works concerning the homogeneous combustion of this mixtures. For example Yilmaz et Ilbas (2008) pointed out that hydrogen addition makes the fuel more reactive resulting in performance improvement. Nevertheless, the same authors state that increasing the H₂ amount higher flame temperature are achieved. Park et al (2006), in a numerical work concerning the effect of H₂ adding to methane (up to 30%) on flame structure and NO_x emission, affirmed that the structure is deeply modified and NO_x emission are higher.

Moreover, they stated that the CH₄ consumption rate increases substituting CH₄ with H₂ due to the preferential attack of H radicals to CH₄ even though methane molar fraction diminishes. As far as

NO_x emissions thermal NO_x increase as H₂ substitution increases due to higher flame temperature. Moreover, Prompt NO_x, which are associated with CH radicals, firstly increases with H₂ content and then decrease at higher H₂ due to the decrease of methane molar fraction.

On the contrary Degaut et Nicolle (2005) focused their attention on the stabilizing effect of H₂ adding on flame. As a matter of fact, they report that the lean blowout limit decreases as H₂ increases and they proposed the use of very lean methane-hydrogen mixtures for gas turbine application in order to limit the temperature and, as a consequence, the extent of NO_x emissions.

The interest towards alternative fuels is not limited to H₂ pure feed, but it is extended also to hydrogen-rich mixtures. Respect to NG, these mixtures show lower heat of combustion (see Table I.2.2), for this reason they are also called *Low-Btu fuels*.

Tab I.2.2- Heat of combustion for CH₄, H₂ and CO

fuel	ΔH_{com}, kJ/mol
CH ₄	802.6
H ₂	241.8
CO	283.0

As a matter of fact, except for electrolysis processes and thermo-chemical cycles, hydrogen is not produced pure. Actually, a mixtures mostly constituted by H₂ and CO, the so called syngas, is produced mainly by steam reforming processes of NG and partial oxidation of light hydrocarbons or by gasification processes as will be highlighted in paragraph I.3.1. Lastly, other hydrogen-rich mixtures are produced as by-products in industrial processes like those of carbon and steel. In these cases the interest towards these Low Btu fuels is driven by the possibility of their valorisation and overall efficiency improvement.

The use of syngas appears very interesting because it could be produced by solid or liquid fuels gasification with a reduction of pollutants emission like soot or sulphur oxides. As a matter of fact the use of syngas allows an easier and cheaper cleaning process as will be focused in paragraph I.3.1.

Moreover, the syngas production from biomass gasification is very attractive since biomass are carbon neutral. But, during biomass gasification products there are also N-containing compounds, mainly NH_3 , that in flame are easily oxidized to NO_x (Johansson et al, 2002).

In addition, associated with the use of Low-Btu fuels there is generally an increase in flame temperature with respect to a NG/air mixtures developing the same power. This is due to the lower N_2 dilution and as a consequence higher adiabatic temperature.

The behaviour of these Low-Btu fuels was studied at condition relevant for GT application in several numeric and experimental studies (Natarajan et al 2009, Davis et al, 2004; Li et al, 2007). These studies mostly concern the laminar flame speed measurements in order to gain fundamental information regarding reactivity, diffusivity and exothermicity and to validate several detailed kinetics mechanisms (Natarajan et al 2009).

I.3 Gas Turbine System

I.3.1. Application Contexts

Gas Turbine burning natural gas (NG) represent a reliable and efficient power generation technology that is widely used (Wright and Gibbons, 2007). Actually, the number of gas turbines used worldwide has grown significantly during the last decade, and nowadays gas turbines are increasingly used for electricity production in base and intermediate loads not only for peaking duty. This increase may be explained by the abundant supply of natural gas at a favourable price (Pilavachi, 2009) and by the development of a new generation of gas turbines with higher output, efficiency, and reliability.

In order to improve GT efficiencies, new materials for blade covering have been tested in order to increase inlet turbine temperature up to 1400-1600°C (Wright and Gibbons, 2007)

Gas turbines are used within a wide range of output power, from small gas turbines at about 100 kWe up to large gas turbines of 310 MWe. Aero-derivative gas turbines are available up to 50 MWe with efficiencies up to 42 %. Heavy duty gas turbines with power outputs from 200 – 300 MWe can reach efficiencies up to 39 %.

GT are installed in different types of combustion plants such as (i) combined cycle units in order to achieve efficiency up to 55-59% (Ol'khovskii, 2005), (ii) co-generation of heat and power plants (CHP) (Fig. I.3.1), (iii) Integrated Gasification Combined Cycle plants (IGCC) of different solid fuels like coal or biomass (Fig. I.3.2 a) and liquid fuels like residual oil (Fig. I.3.2 b).

In particular, as visible in Fig. I.3.2 a, the syngas can be eventually added with NG in order to increase the heat of combustion and then delivered to the turbine.

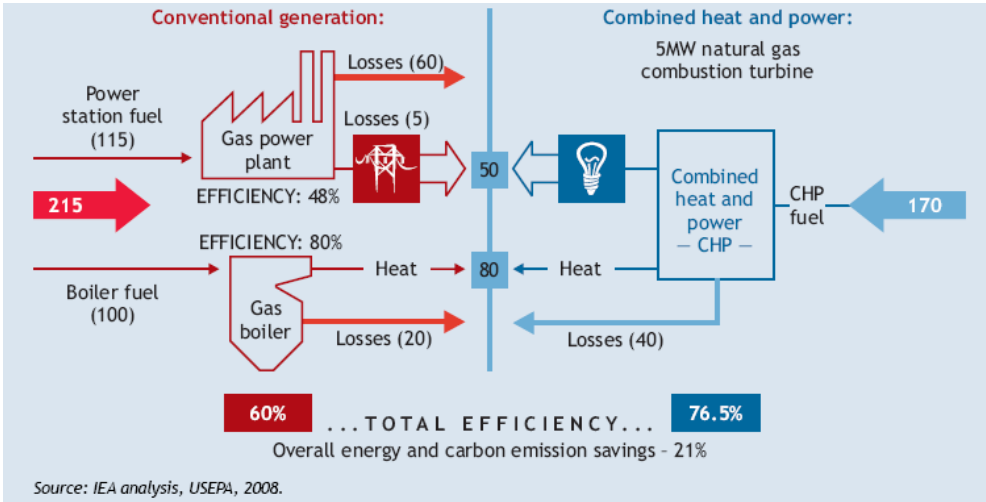


Fig. I.3.1 General example of efficiency gain of heat and power co-generation.

As reported in fig. I.3.1, according to IEA in the World Outlook of 2006, CHP system are able to convert 75-80% of the fuel in a useful form of energy. Instead, as stated by Pilavachi (2000), the utilisation factor of CHP could be as high as 85-90% providing 40% of electrical energy and 50% of thermal energy for large systems. Usually CHP systems with an output of 50 MW are more and more used for municipal power supply while only 15kWe are required for the individual house consumptions (Pilavachi, 2000; Ol'khovskii, 2005).

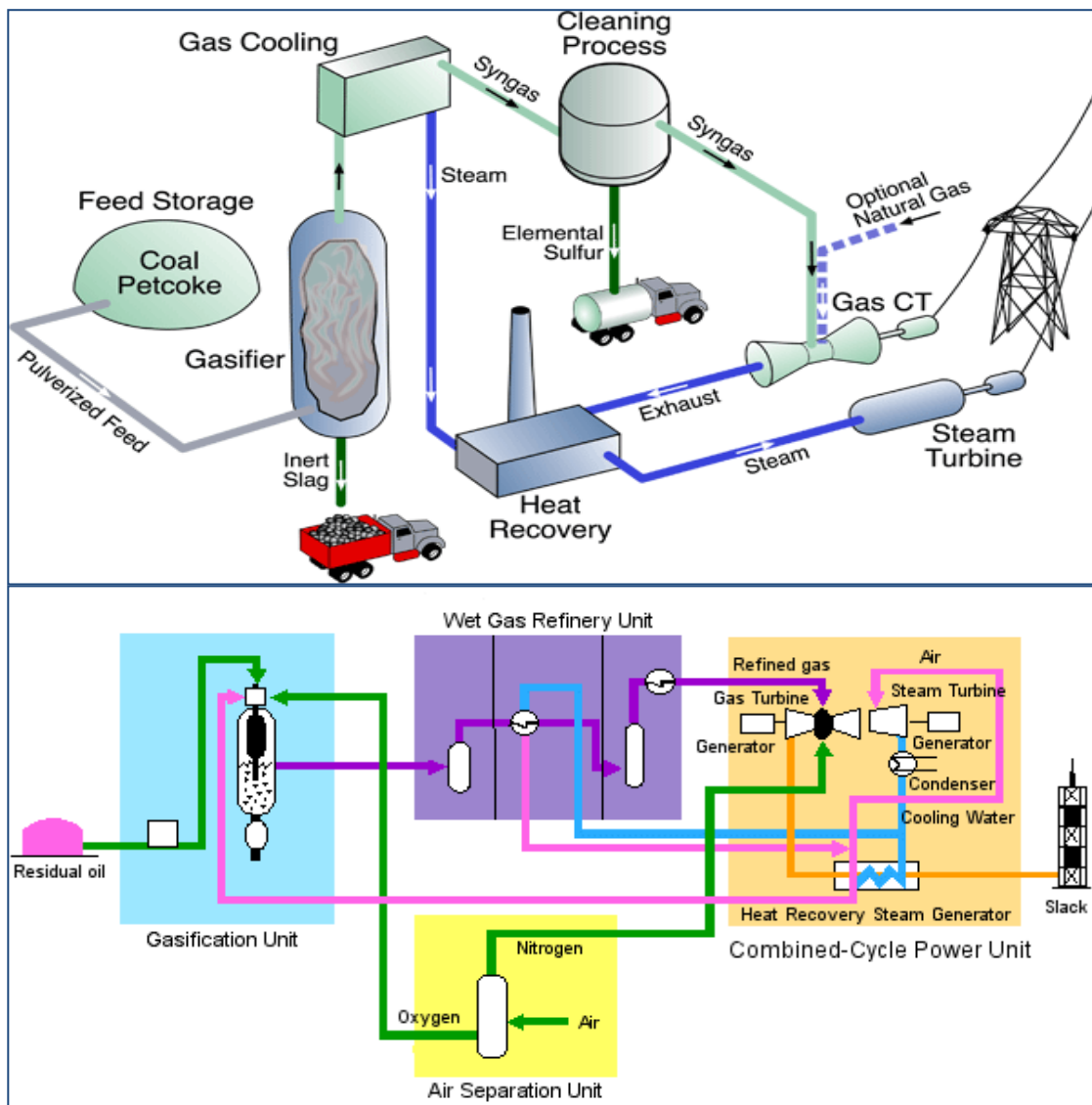


Fig. I.3.2 Conceptual diagram of IGCC: (a) general scheme of a IGCC based on Coal Gasification; (b) Diagram of the API plant in Falconara (Italy).

As reported by Neathery et al. (1999), a new type of plant concept based on IGCC principle has attracted huge interest. The principle at the base is the simultaneous co-production of electricity and added value products from coal, but also other fuels, gasification. In particular, only a part of coal-derived synthesis gas is fed to a unit producing fuels/chemicals. The unreacted mixtures is combined with the remainder of syngas and then burnt, eventually with added NG, in the combined cycle power generation unit (Fig. I.3.4) .

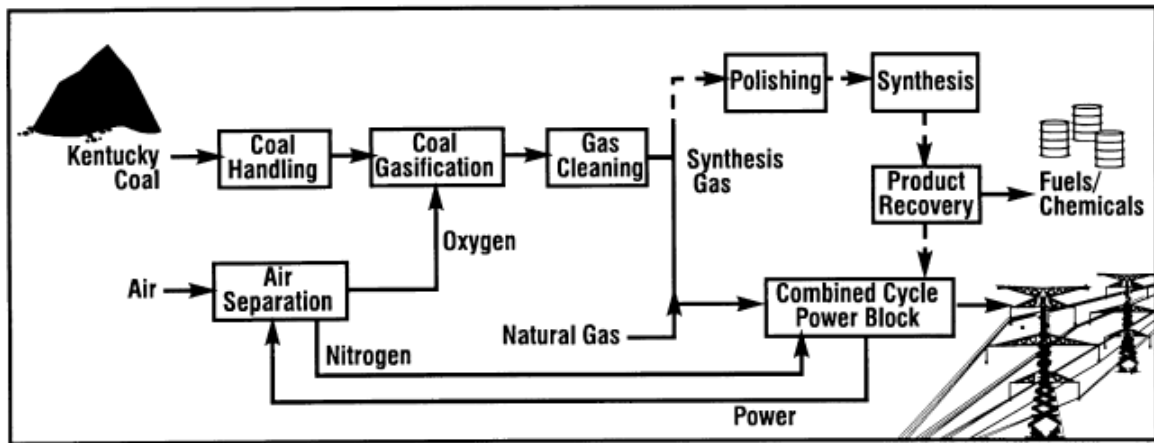


Fig. I.3.4 Schematic of the pioneer plant concept - Neathery et al. (1999).

In conclusion the success of IGCC is essentially based over the following advantages: (i) the ability of the gasifier to accept a range of feeds of varying quality (solid/liquid) (ii) the production of a gaseous fuel that could be simply and cheaply cleaned and (iii) the use of a combined cycle with high efficiency.

Finally, in principle the off-gas of High-Temperature fuel cell operating at 850 °C (Solide Oxide Fuel Cell SOFC) could be used as power source for a gas turbine or a combined cycle. Some installations in USA show the possibility to reach 70% overall efficiency using natural gas with internal reforming. SOFC could be either fed with synthesis gas or pure hydrogen obtained also from coal gasification. Of course the high cost of fuel cell units currently make this choice unfavorable (Ol'khovoskii, 2005).

It is note worthy that for GT emission of soot and SO₂ are insignificant, the latter justified by the easy desulfurization in the case of a gaseous fuel (i.e. NG or Syngas). On the other hand, more significant are the NO_x emissions caused by high temperature in the combustion chamber (1800-2000 K). As stated by Andreini and Facchini (2002), in the last 20 years many efforts were made to modify the combustion chamber in order to face with the most stricter NO_x emission regulations in most of the countries. As a matter of fact, in the last 30 years generally the maximum emission levels allowable were reduce by one order of magnitude from 100 ppm to 10 ppm (corrected by 15% of O₂). In areas like California, which has the stricter normative, the NO_x emissions are required to be less than 2.5 ppm (Smith et al, 2005) while in the most stringently regulated areas in Japan and Europe the limit is 5 ppm (Appel et al, 2002). So primary measures to reduce NO_x formation are becoming more and

more relevant especially when secondary measures turn out to be very expensive (see paragraph I.3.2.1). In the following paragraph some primary measure for NO_x reduction are deepened.

I.3.2. Primary Measure To Reduce NO_x Emissions

It is known that, in order to achieve stable combustion i.e. high combustion efficiency in an conventional -diffusion flame combustor, very high flame temperature are required (1600°C-1800°C) thus exalting thermal NO_x formation mechanism (Lefebvre, 1999). Thereof it clearly appears that every primary criteria for NO_x reduction is based on lowering flame temperature. As a consequence it is necessary to burn lean mixtures and also it is crucial to avoid local stoichiometric zone. The latter goal could be achieved improving the degree of mixing.

Generally lowering flame temperature causes the combustion efficiency decrease, thus resulting in higher CO and UHC emissions.

The most common strategies widely used in the case of conventional combustors retrofit, i.e. without a substantial modification of the combustor geometry, are water/steam injection and exhaust gas recirculation. These measure, as it could be seen in table I.1 and figure I.3.5, are unable to reach single digit level emissions.

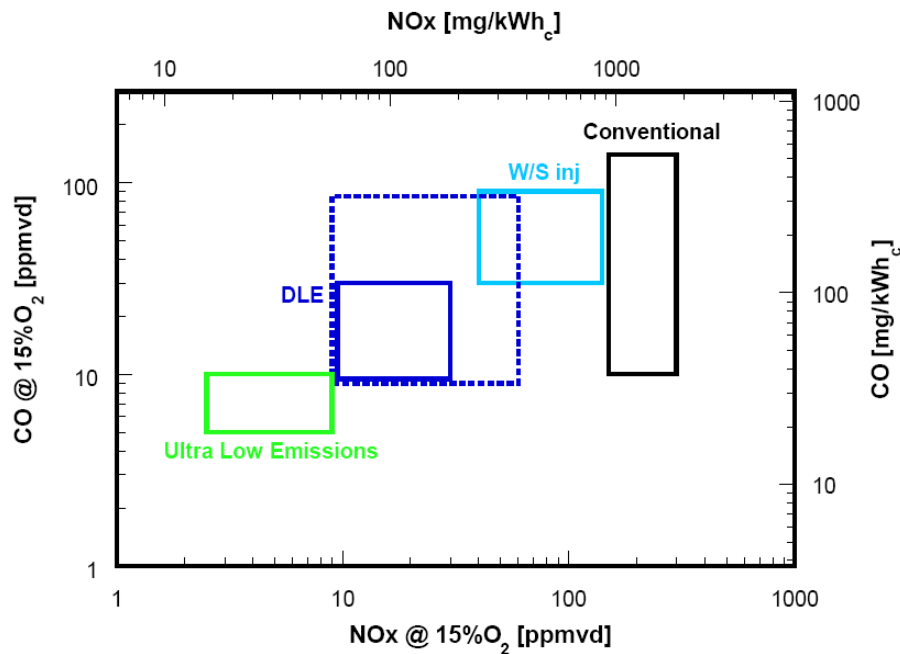


Fig. I.3.5- NO_x and CO emissions in combustors fuelled with NG.

Tab. I.3.1 Some primary measures to control NO_x emissions

	Exhaust Gas recirculation	Steam/ water Injection	Lean Premixed Combustion	Catalytic Combustion
Emission reduction, %	20-50	40-60	76-90	>97
Emissions, ppm	84-52	>42	25-9	<3
Limitation	Very clean fuels are needed	<ul style="list-style-type: none"> ✓ Flame instabilities ✓ Reduction of combustion efficiency 	Especially at low load: <ul style="list-style-type: none"> ✓ Flame instabilities ✓ Acoustic oscillations ✓ Reduction of combustion efficiency 	Durability and cost of catalytic materials

(Integrated Pollution Prevention and Control, 2006)

Therefore, quite complex combustors were designed and realized in order to work in the optimal temperature range (Fig I.3.6) for simultaneous reduction of NO_x and CO. The basic idea is to control the flame temperature acting on the appropriate mixing of fuel and oxidizer. Essentially there are two principle: (i) variable geometry and staged combustion.

The variable geometry consists in varying the share of air destined to the primary and the secondary zone varying the power load in such a way that the temperature is always optimal (Micklow et al., 1993).Of course the complexity of the control constitute the major drawback.

More diffused respect to variable geometry is the staged combustion or fuel staging. This technique allow to operate in a stable manner also at low load since extended to a limited zone the equivalence ratio are high enough to move the lean blowout to lower global equivalence ratio. Another possibility is the so called Rich Burn Quick Quench Combustion (RQL) that is based on the creation of two different reactive zones: the first that operate in air defect and a secondary combustion zone in which there is an oxygen excess to ensure complete burn-out. Each of this zone works at temperature lower than expected from the global equivalence ratio. Some drawbacks are the complication of the mixing of products obtained in the first zone with air and the complexity of the

first zone geometry in order to avoid gas recirculation and consequently NO_x formation (Micklow et al.,1993).

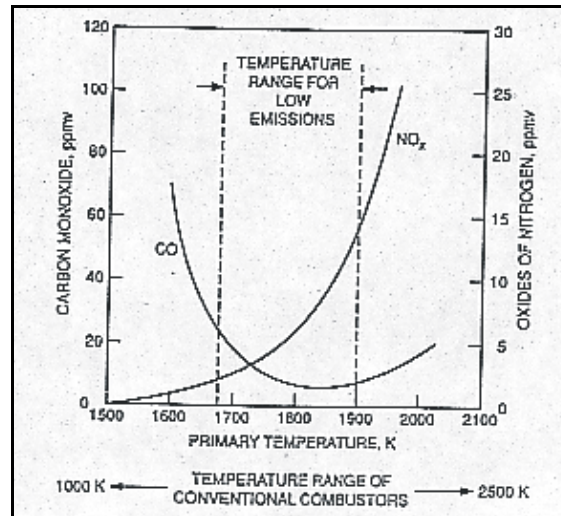


Fig. I.3.6- NO_x and CO emissions varying the temperature of conventional combustors fuelled with NG. (Lefebvre, 1999)

To date, according to IEA, the best available techniques to reduce NO_x formation at single digit level are Lean Premixed Combustion (LPM)- the principle at the base of Dry Low NO_x (DLN) combustors- and Catalytic Combustion (Integrated Pollution Prevent and Control for Large Combustion Plant, 2006).

The basic characteristic of DLN combustors is that air and fuel are firstly mixed upstream the combustion chamber, thus creating a premixed flame with an homogeneous temperature distribution and a lower flame temperature is achieved, but it necessary that the that equivalence ratio chosen is close to lean blowout limit. Even though LPM is an effective technique and allows high combustion efficiencies, the major disadvantage is the difficulty to guarantee stable combustion at low load i.e. to even lower equivalence ratio. As a matter of fact, lean conditions, especially at low load, leads to flame instabilities, more CO and UHC emissions other than acoustic oscillations responsible of the turbine deterioration and breaking. In order to overcome these problems, a “pilot” flame that burn, in a diffusion mode or partially premix mode, only a fraction of the fuel (2-10%) is used imparting stability to the main flame (Karim et al, 2003). Lower is the load

higher is the fraction of fuel burnt in the pilot. Moreover, the pilot flame is able to guarantee stability during start up, transient and load ramping. Due to higher temperatures associated with the pilot flame NO_x emission level cannot be lower than 9 ppm at baseload (Karim et al.2003). For these reasons, DLN combustors show good performance in terms of CO and NO_x reduction only at high loads (85-100%). A further problem related to the operation at high load is due to the high pressure and temperature reached at the compression exit, that can cause mixture auto ignition in the mixing zone.

Despite of these inconveniences, currently DLN combustors are widely used since they are a reliable and mature technology at cost comparable to those of conventional combustors. But catalytic combustion appears to be the most preferred solution for gas turbine application where ultra-low NO_x emissions are required. As a matter of fact, the use of a catalyst allows operation with very diluted-mixtures without compromising combustion efficiencies also at temperatures below 1000 °C thus virtually avoid the NO_x formation (Forzatti, 2003). In the last 4 decades different catalytic strategies were proposed and will be introduced in section I.4.2.

I.3.2.1 Economics Considerations

The cost analysis presented in this paragraph is drawn from a study that was committed by the US Department of Energy (DOE) in the 1999. This study remains the most complete and up to date document concerning the costs of technologies of NO_x emissions reduction that were available or being commercialized at that time about NG fired turbines. The economic impact of the different technologies, including the secondary measures (i.e. *conventional, high and low temperature Selective Catalytic Reduction* and *SCONO_xTM*), is evaluated depending on the turbine's class of power (5 MW, 25 MW e 150 MW).

The results are summarized in table I.3.2 in terms of cost per ton of NO_x removed (\$/Ton di NO_x) and of cost per kWh produced (€/kWh). The latter represent the cost of the technologies that must be added to the others capital costs associated with the GT design, which is independent from the amount of NO_x removed.

The data reported in table I.3.2 refer to the annual cost of operation and take in account the amortization cost of capital investment (15 year lifetime, annual interest rate 10%), operation and maintenance costs, as declared by the different technologies' manufacturers. Moreover, it is assumed that the GT work 8,000 hr per year at full load. Since the different technologies has

different initial and final NO_x emissions, a direct comparison, in terms of \$/Ton of NO_x, could not be strictly done. Similarly, also the comparison among costs per kWh is correct only at equal final concentration. Therefore, the comparison in terms of cost among different control measures could be done with caution and only general consideration could be drawn.

One of this is the trend of costs that generally are higher decreasing the turbine size. This trend is more pronounced for the secondary measures. So for this class of turbines the most preferred solution where ultra-low NO_x emissions are required is catalytic combustion.

Tab.I.3.2 Costs of several technologies of NO_x emission control for GT (Major B., B. Powers (1999), cost analysis of NO_x control alternatives for stationary gas turbine, Contract DE-FC02-97CH10877)

Power Class		5MW		25MW		150MW	
Control Technology		\$/ton	€/kWh	\$/ton	€/kWh	\$/ton	€/kWh
DLN (25ppm)		260	0.075	210	0.124	122	0.054
Steam/water Injection (42 ppm)		1652	0.410	984	0.240	476	0.152
Catalytic Combustion (3 ppm)		957	0.317	692	0.215	371	0.146
SCR	Conventional	6274	0.469	3541	0.204	1938	0.117
	High T	7148	0.530	3841	0.221	2.359	0.134
	Low T	5894	1.060	2202	0.429	Nd	Nd
SCONOX		16327	0.847	11554	0.462	6.938	0.289

I.4 Catalytic Combustion

With reference to the issues presented above, it appears that Catalytic Combustion is a safety and clean technology and, potentially, the preferred one to produce energy with high efficiency. As a matter of fact it has the potential to extend flammability limits of fuel/air mixtures and achieve stable combustion at lower temperature compared to flame temperature. In this way, instabilities and pollutants formation (CO, NO_x, soot), that are typical of conventional combustion processes, are avoided.

With respect to other primary measures of NO_x control, Catalytic combustion is the only one that have demonstrate to achieve single digit NO_x emission lower than 3ppm and lower than 1ppm in the 90-100% load range (Cocchi et al, 2006) not affecting the combustion efficiency: low CO and UHC emission too (< 10 ppm) without requiring expensive clean-up systems. Actually as reported in paragraph 1.3.2.1, catalytic combustion is very attractive for small size gas turbine, for which secondary measures turn out to be very expensive.

The reduction of nitric oxides formation, similarly to other techniques above mentioned, is due principally to the lower temperature. It was found that the NO_x reduction was even higher than that could be ascribed only to the lowering in temperature. This effect was explained taking into account the effect of catalytic surface that acts as a sink for CH radicals thus reducing the Prompt NO_x mechanism and on the other hand, that release H₂O which represses NO_x formation (Barbaro and Bianchini, 2009).

Last but not least consideration concern the application of Catalytic Combustion when Low-Btu fuels that, as reported in paragraph I.2, could partially replace the use of NG, are used. In this case Catalytic Combustion appears advantageous compared to flame combustion because it limits not only Thermal NO_x formation, but also the conversion of fuel-N to fuel-NO_x (Johnsson, 2002). Besides, the choice of the right catalytic system could allows the H₂ and CO combustion at very low temperature, close to those of compressor exit (290-450°C depending on load), providing the necessary heat to increase combustor temperature enough to cause methane ignition. This is essentially the concept of the H₂-assisted catalytic combustion of methane that was successfully studied by several authors (Deutschmann et al 2000, Cimino et al, 2003, Demoulin et 2006, Barbato et al, 2009).

On the other hand, catalytic combustion suffers from materials limitation associated with their durability since the severe conditions (temperature pressure, environment) of Gas Turbine power generators.

As a matter of fact, even though the conditions are variable depending the turbine product line and load, the most common are:

- Compressor discharge temperature: 290-450°C
- Velocity as high as 20-30 m/s
- Pressure < 10 bar (small size turbine 1-10 MW) and as high as 30 bar (> 50 MW).
- Turbine inlet temperature as high as 1500°C

Moreover, as pointed out by Kolaczkowski (1995), one of the major challenge is the design of a catalytic system that is able to face with load variations involving variation of pressure, equivalence ratio and total gas flow in wide ranges. This heavily affects the catalyst durability which minimum target is set to 8800 hr, that correspond to one operation year. In order to better understand the rest of this section the properties of catalytic materials for total oxidation are firstly introduced in paragraph 1.4.1, while paragraph 1.4.2 reports the different applied solutions of catalytic combustion to GT systems. Finally, the paragraph 1.4.3 deals with the state of art of high pressure catalytic combustion.

1.4.1 Total Oxidation Catalysts

From the study of the abundant literature concerning the catalytic combustion it appears that essentially the classes of catalysts could be identified:

- Noble metals
- Metal oxides
- Hexaaluminates

(Zwinkels et al. 1993; Choudhary, 2002).

As concerning noble metals, it could be stated that all the platinum group metals show high activity for the combustion of hydrocarbons as well as H₂ and CO at low temperature too. For these reasons they are widely used as active phases for the VOC oxidation at low and medium temperature in the three way catalysts, and are the best candidates to be used in the first stages of catalytic combustors as “igniters”. The major drawback is related to their rarity, and as a consequence cost, and tendency to volatilize and/or sinter at high temperature, which limit their use to Pd and Pt only. The reactivity scale towards total oxidation reactions is Ru<Rh<Pd<Os<Ir<Pt (Parsad et al. 1984) but however the choice of the better active phase depends on the fuel. As a matter of fact, the platinum is the most active for H₂, CO and alkanes except the methane, that is oxidized more rapidly on Pd; the latter is the best choice in the case of olefins too. As a consequence the Pd is the most employed catalyst for NG-fuelled GT. It is widely recognized that, at low temperature the catalyst is in an oxidized form PdO_x that is the most active, but increasing the temperature, about 800°C, the reduction to metallic form occurs with a consequent loss of activity. Groppi et al (2001), has shown the possible occurrence of two different types of palladium oxide with different activity for methane oxidation. The first PdO species is supposed to be transformed into the second one increasing the

temperature; however the change occurs at lower temperatures than for the PdO/Pd transformation. These processes are reversible, re-oxidation from metallic form occurring at about 600 °C in air (Quick and Kamitomi 1995, McCarty 1995; Specchia et al. 2009). Since the re-oxidation reaction is very slow, and reformation of the oxide occurs at different temperature, hysteresis phenomena happens leading to instabilities in performance of catalytic combustion (Ersson et al, 2003). It is known that the decomposition of PdO takes place at different temperature varying the pressure (Carroni et al, 2003).

Several authors proposed to exploit the self-regulating capacity of the catalyst to preserve itself from sintering due to high temperature (Dalla Betta, 1997; McCarty (1999) and Farrauto (1990). As stated noble metals undergo to sintering and volatility phenomena above 800°C. For example, it was estimated that an exposure of 15 h at 1000°C is enough to causes the loss of 70% of the original Pt loading (Dalla Betta, 1997).

The supports over which noble metals are dispersed can play a relevant role, not only improving sintering resistance but also improving the catalytic performance (Choudhary, 2002). This is the case of CeO₂ which, thanks to its oxygen fast release from its lattice was proven to assist Pd in surface O₂ bonding, thus slowing the transition to Pd metallic and to minimize the its reduction in activity (Specchia et al., 2009). Therefore Pd/CeO₂-ZrO₂ systems have been extensively studied (Specchia et al. 2010).

Another class of catalysts is constituted by metal oxides, which are relatively inexpensive and have the potential to reduce fuel NO_x (Choudhary et al 2002). However they show lower activity and higher temperature light-off with respect to noble metals. As concerning single metal-oxide, many studies were devoted to identification of a scale of reactivity but the results were often discordant (Zwinkels et al. 1993). Generally Co₃O₄ is the most active metal oxide but also CuO, NiO, Mn₂O₃, Fe₂O₃ and Cr₂O₃ show an activity a little be lower compared to Co₃O₄, while Ti and Zn oxide are not active. Also these single metal oxides, that generally are dispersed onto a high surface area support, suffer of thermal deactivation due to interaction of active phase with the support. This is the case of alumina, a typical support, that interacts with many transition metals to form spinels of general formula MAl₂O₄ (Zwinkels et al. 1993).

Amongst different types of metal oxides (single, doped metal oxides, perovskites, spinels and other mixed metals) perovskites have been extensively considered as total oxidation catalysts (Choudhary 2002, Tejuca et al. 1989 Seyama 1992). As a matter of fact, some of these oxides show a significant activity, similar to that of platinum under specific condition, already at relatively low temperature

(Seiyama et al., 1992, Alifanti et al., 2005, Arai et al., 1986). They are a group of mixed oxides represented by the general formula ABO_3 with a cubic structure that is similar to $CaTiO_3$, in which the larger cation A has a dodecahedral co-ordination and the smaller B cation has a six-fold co-ordination. The number of perovskites with potential interest in total oxidation is elevated since that a large number of the metallic elements can be employed in different combinations to give robust perovskite-oxide structure: about the 90 % of periodic table elements could be arranged in a perovskite structure on condition that the cationic radius in the A site is $>0.90 \text{ \AA}$ and $r_B > 0.51 \text{ \AA}$ (Choudhary 2002). Moreover the robustness of the structure permits the partial substitution of A and B cations with metals with a different oxidation state ($A_xA'_{1-x}B_yB'_{1-y}O_{3-\delta}$). The partial substitution results in the profound modification of the activity since it leads to the formation of structural defects which influences catalytic activity of the material (Seiyama, 1992).

Also for unsubstituted perovskite, the activity in oxidation reactions is ascribed to structural defects involving cation vacancies in their lattice, in A sites and to a lesser extent in B side. As a result, an extra lattice oxygen may be accommodated in these systems thus causing their typical nonstoichiometry. This nonstoichiometry can be controlled by partial substitution of the A and B cations (Tejuca et al., 1989).

From temperature programmed desorption and thermogravimetric studies it was found that this mixed oxides are characterized by two type of oxygen called α and β oxygen. The type of oxygen (β oxygen), that is more bounded to the perovskite structure, plays a determinant role in high temperature Mars-Van-Krevelen oxidation mechanism being much more reactive than that transferred to the surface from the gas phase (Forni and Rossetti, 2002). The β oxygen, that is observed both for substituted and unsubstituted samples, is more specific to the B cation. Accordingly, for the unsubstituted perovskite oxides, the catalytic activity is mainly dependent on B cation. On the other hand the β oxygen is affected also by A cation substitution. (Seiyama 1992).

While as concern the low temperature activity it was demonstrated that an important role was determined by oxygen weakly adsorbed species (α oxygen) which amounts is greatly increased by partial substitution especially of A cation but also depend on the nature of B cations (Forni and Rossetti, 2002; Russo et al. 2008).

To date, the better active phase formulation for methane combustion are those in which A site are occupied by La or La-Sr and B site are occupied by Co, Fe, or Mn (Arai et al. 1986, McCarty and Wise 1990). For instance, $LaMnO_3$ is considered the most active formulation (Saracco et al., 1999, Marchetti and Forni, 1998).

Nevertheless, the application of perovskites is limited by their low surface area (De Collongue et al., 1991). Moreover, operation at temperatures above 800°C leads to sintering of perovskite-oxides caused by the 3D growth of crystals. After exposure to temperature above 900°C, the surface area diminishes and consequently catalytic activity decreases (Arai e Machida 1996). In order to overcome these problems, different research group have dispersed active phases on high surface area supports like La-stabilized alumina or La-stabilized MgO or spinels with an increase in activity and thermal stability (Cimino et al, 2000; Marti et al, 1994). One of the most employed support is γ -Al₂O₃, characterized by a specific area of about 200 m²/g. Nevertheless, close to 1000°C, γ -alumina undergoes a phase transition to α -alumina, which exhibits a lower specific area. In order to overcome such an inconvenient, it has been proposed to kinetically inhibit γ to α phase transition, by adding small quantities (typically 5wt % as regards the total amount of support is considered enough) of lanthanum oxide to the γ -alumina lattice (Arai e Machida., 1996).

In order to increase perovskites activity towards combustion reactions, the use of bi-functional catalysts has been proposed, in which perovskite phase is promoted by small amounts of noble metal (Cifà et al., 2003, Kucharczyk and Tylus, 2004, Cimino et al., 2004, Civera et al., 2005, Uenishi et al., 2005, Petrovic et al., 2005, Cimino et al., 2007, Giebeler et al., 2007). Perovskite, besides exhibiting its own catalytic activity, may be an ideal environment to host noble metals causing an high dispersion of the active phase and avoiding noble metal volatilization and sintering. Moreover, particular synergies may occur especially due to eventual interactions of the noble metal with the extra lattice oxygen of perovskites. On the other hand, the noble metal, even if in small quantities but well-dispersed, may increase catalyst activity at low temperature. Despite numerous studies concerning catalytic combustion on Pd-perovskite catalysts (Cimino et al., 2004, Cimino et al., 2007, Uenishi et al., 2005, Petrovic et al., 2005, Cifà et al., 2003, Kucharczyk e Tylus, 2004, Civera et al., 2005), Pt-perovskites are less studied. Recent works of Giebeler and co-workers (2007) and Scarpa et al (2009) demonstrated that platinum promoting is not effective in enhancing perovskites activity towards methane combustion at least on oxidized samples. Also respect to H₂ combustion, the Pt-perovskite samples showed a catalytic reactivity slightly lower than a catalyst with the same amount of platinum (Scarpa et al, 2009).

The highest thermal stability is showed by the last class of catalysts, the hexaaluminates, thus resulting very suitable for very high temperature applications. So they have been extensively studied since the pioneering work by Arai and co-workers (Machida et al. 1987 e 1989). The general formula of these materials is AAl₁₂O₁₉ where A is an alkaline or alkaline-earth element (La or Ba). The high thermal stability is derived by its lamellar structure, which consists of stacked spinel

blocks separated by a monolayer of oxides. The presence of the Ba or La cation blocks the crystal growth thus conferring superior stability properties (surface area $>20 \text{ m}^2/\text{g}$ at $T >1200^\circ\text{C}$ and stable operation till 1600°C).

Nevertheless they exhibit very low activity. In order to improve the activity, large efforts have been made to dope these materials. It should be however noted that, differently to perovskites, the crystal structure is less available for partial substitution of La or Ba cation with Sr or Ca. Also transition metals like Fe, Co and especially Mn could be introduced in the lattice structure thus improving activity towards methane combustion but only slightly. As a matter of fact, the activity of these materials towards methane combustion remains very low compared to Pd. It is worth noting that, with respect to other groups of catalyst, the difference among the activities towards the total oxidation of alternative fuels (carbon monoxide, hydrogen, syngas and diesel) is less significant [Groppi et al. 1996]. Extruded monolith of substituted hexaaluminates were employed as high temperature catalytic stages in GT application (Sadamori et al. 1995).

1.4.2. Catalytic Combustors

It appears that, despite the great number of materials and formulations proven as total oxidation catalyst, it was not found an active phase that is able to conjugate high activity with high thermal stability and durability at condition relevant for GT applications. As a matter of fact, some of the major difficulties are the elevated mass flows, and as a consequence linear velocity (15-30 m/s) and the wide temperature range (virtually from 260 to 1400°C) that makes impossible the use of an unique catalytic system¹ that operates in a so wide temperature range. Actually, catalytic combustors that were firstly proposed (Dalla Betta and Rostrup-Nielsen(1999), Sadamori (1995), McCarty (1999)) involved the use of several catalytic stages with different formulation, that were more and more stable (i.e. less and less active) increasing the temperature along the streamwise direction. The first catalytic stages with more active formulations, prevalently Pd-based catalysts, were called “igniters”. Their function was to increase the temperature to achieve the light-off one of the next catalytic stages. The last catalytic stages usually were hexaalluminates stable till 1200°C (Sadamori 1995).

¹ Generally, for GT application, a catalytic system is constituted by a catalyst powder supported on a honeycomb monolithic substrate which permits high catalyst load minimizing the impact of pressure drops.

As highlighted by Sadamori (1999) this solution is disadvantageous due to the limited power throughputs, i.e. mass flows limited by the necessary contact times to ensure complete catalytic conversion, that makes these combustors less competitive.

More recently, catalytic combustors based on the concept of partial use of catalytic combustion followed by homogeneous combustion were developed. Different solutions were proposed:

- Fuel Staging hybrid combustion
- Partial Catalytic Hybrid Combustion
- Rich Catalytic –Lean burn systems
- Pilot catalytic flame

The common aim of these solution is to limit the temperature of the catalytic zone well below 1000°C in order to use active catalyst formulations without damaging the active phase and/or support. In the fuel staging hybrid concept, the catalyst converts all the fed fuel and adiabatic temperature of the mixtures is achieved. Therefore the temperature tuning is obtained by modifying the mixture composition in order to limit the adiabatic temperature below 900°C. In the post catalytic zone, the remainder of the fuel is added to the hot gasses, and burnt with the large amount of oxygen still present together with total oxidation products. Under these conditions homogeneous combustion is highly sustained by the heat released by the catalytic section.

An example of this approach is the combustor equivalent to a 20 MW class gas turbine that was designed and tested by the Central Research Institute of Electrical Power Industry of Japan (Ozawa et al, 1999). In this combustor the six catalytic segments were arranged alternately with six premixing nozzles and about the 50% of the fuel was fed to the catalyst (Pd/Pt/Rh supported on ZrO₂ stabilized alumina) while the remainder was burnt in a premixed flame stabilized not only by the catalytic section but also by recirculating the flow. In this way the lean premixed combustion occurred at 1300°C while the catalytic combustion occurs at temperatures less than 1000°C. Moreover the combustor was provided with a premixed preburner whose function was to increase the temperature up to the light-off of the catalytic segments.

The NO_x emissions turned out to be less than 4 ppm. This value was reached for the combustor outlet gas temperature of 1350°C (Ozawa et al, 2003).

The principal drawback of this systems, adopted by Toshiba Corp. (Furuya et al., 1995) and Kansai Electric Power (Ozawa et al, 1999 and 2003), is the greater combustor complexity, and, as a

consequence, difficulty of control, due to the presence of a further feed of fuel. Besides, the advantages in terms of NO_x reduction, catalyst preservation and combustion efficiency are attained providing that the mixture added to the catalyst section is well mixed and no local richer zones are present, leading to dishomogeneities and hot spots.

Another concept of hybrid combustion is Partial Catalytic Hybrid Combustors that was proposed by Catalytica, Engelhard e Johnson & Matthey (Dalla Betta et al., 1995). In this case all the fuel is fed to the catalyst zone but only a fraction of the fuel, typically 40-60%, is catalytically oxidized while the remainder is burned downstream the catalyst in homogeneous combustion mode (Kajita and Dalla Betta, 2003). This zone, that is often called burn-out zone, is designed in order to minimize unburnt emissions (Dalla Betta et al, 1995, Dalla Betta and Rostrup Nielsen ,1999; Cutrone et al1999).

In this case the thermal management is achieved limiting the conversion in the catalytic zone thanks to two concomitant modes: first, the aforementioned auto regulation mechanism of PdO; and second the one-side coating strategy. The latter consists in alternatively coating of channels of the monoliths so that an half of them is active and the remainder is inert (Dalla Betta et al, 1993). Combustion goes to completion in the active channels while in the adjacent uncoated channels no combustion occurs. The net effect is that an half of the fuel is catalytically converted, assuming that all the channels have equals dimension. Moreover, the flow through the inert channels provides cooling for the active channels thus keeping the catalyst surface at acceptable temperatures (Carroni et al, 2003). Last but not least this bypassing flows is pre-heated up to 800-900°C . A sketch of this configuration is reported in Fig I.4.1.

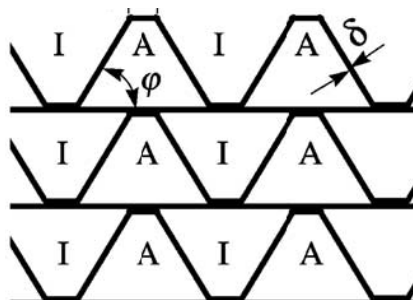


Fig. I.4.1- Schematic of one-side coating. A-active channels-I Inert channels (Carroni et al, 2003)

In order to improve the radial heat exchange between channels, an high conductivity of the substrates is required. Consequently, metallic substrates, especially FeCrAlloy, are employed.

On the base of these concept Catalytica has developed and commercialized the XONON technology in collaboration with many gas turbine supplier like General Electrics (Cocchi et al, 2006), Pratt&Whitney, Allison Engine, Kawasaki (Kajita and Dalla Betta,2003) and Solar Turbines (Fant et al,2000; Dutta et al 1997).

In particular, the XONON module consists in two metallic monoliths alternatively coated with Pd-based catalysts. The first stage is designed to be very active at about 400°C and to increase the temperature to the light-off one of the second catalytic stage which formulation has a slightly higher thermal resistance (Dalla Betta et al 1995; Cocchi et al. 2006). Usually, since the compressor exit temperatures are low, especially at low load operation, the combustor is also equipped with a preburner (see Fig. I.4.1) generally working with a diffusion flame that is responsible of NO_x emission at low load. Even with a premixed preburner, the NO_x emission are higher than 2.5 ppm for loads lower than 70%(Cocchi et al. 2006).

Nevertheless, in 1999, a 1.5 MWe gas turbine engine, supplied by Kawasaki, equipped with a XONON module, was firstly tested for the silicon valley power generation. The system has demonstrated to operate for more than 4000 hr guaranteeing the following emission levels at 70-100% load: NO_x<2ppm (corrected to @15% O₂), CO<2ppm,UHC<1 ppm. More recently, in 2003, this system has demonstrated a reliability of 99%, working for 14000 hr as reported in table I.4.1.

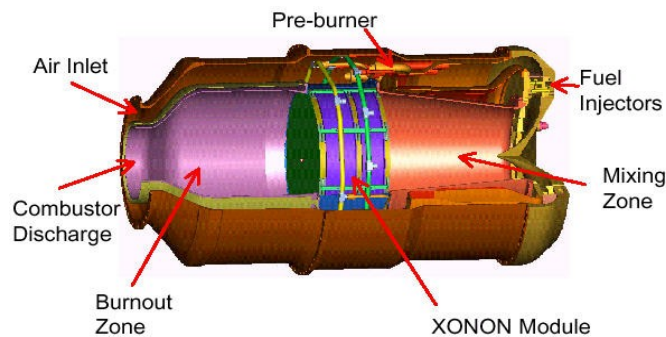


Fig. I.4.1-Combustor equipped with XONON module

Tab.I.4.1 Fields results of Silicon Valley Power-Kawasaki-XONON

Performance Criteria	Results
Operating Hours	> 14000
NOx emissions	< 2.5 ppm (corrected to 15% O ₂)
CO emissions	< 6 ppm (corrected to 15% O ₂)
VOC emissions	< 2 ppm
Reliability ¹	> 98%
Reliability ²	> 99%

¹ Total turbine engine and catalytic combustor system reliability

² Catalytic combustion system reliability

In the 2000, also General Electrics launched a program to develop a catalytic combustion systems for the GE-10-1 engine. This gas turbine, rated at 11 MW, was equipped with a XONON module (Cocchi et al, 2006). In 2006 the test campaign demonstrated satisfactory performance concerning CO and UHC but the NOx emission at low load operation (< 70%) were less satisfactory as reported in figure I.4.2. The authors suggested a new preburner desig in order to limit the NOx emissions at low load in order to commercialize their system.

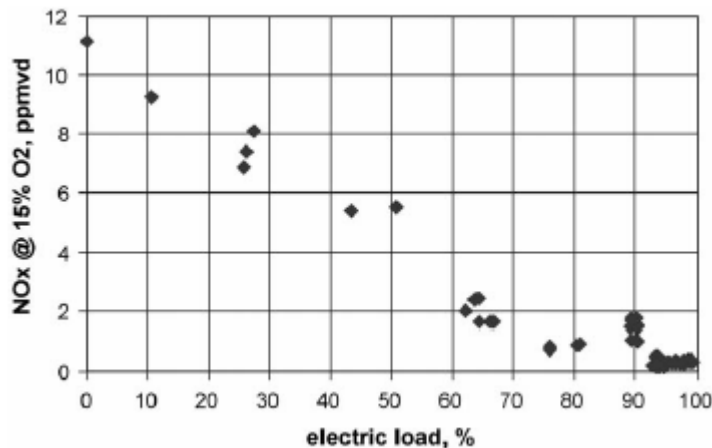


Fig. I.4.2 . NOx emission varying the electric load for GE10-1 gas turbine equippe with a XONON module.(Cocchi et al, 2006)

Actually, as already reported, the NOx emissions at low loads depend on the need to preheat the reacting mixture to light-off temperature of the first catalytic stage. Moreover, as reported by Cocchi et al(2006), the catalyst aging leads to an increase in light-off temperature and implies a more fraction dedicated to preburning and consequently higher NOx emissions.

On the other hand, Solar Turbines was devoted to the development of catalytic combustors for small engines (<20 MW). In Particular a 5 MW gas turbine (Mercury 50) equipped with a recuperated cycle was successful developed reaching emissions at full load as low as 1.5 ppm NO_x 8 ppm CO and 4 ppm UHC (Kajita and Dalla Betta,2003). The ultra low NO_x emissions were obtained thanks to the recuperated cycle that, preheating the air flow at temperature sufficiently high for catalyst operation, avoid the use of the preburner (Dutta et al, 1997; Kajita and Dalla Betta,2003; Fant et al, 2000).

From this overview it is evident that one of the outstanding issues in catalytic combustion is the use of the preburner in order to gap the temperature difference between compressor exit and light-off temperature of the catalyst.

An alternative means to limit the extent of the reaction is to operate the catalyst under fuel rich conditions.

The fuel and a fraction of the air, less than the stoichiometric amount, are fed to the catalyst module, while the air remainder is added downstream the catalyst in order to complete the fuel combustion. This is the principle at the base of the Rich-Catalytic Lean burn system concept that was proposed by PCI and trademark as *RCL* (Smith et al., 2005) (Fig I.4.3). The homogeneous reaction is carried out in the presence of total and partial oxidation products, the latter having a great stabilizing effect on the homogeneous combustion.

Moreover fuel-rich operation of the catalyst provides many advantages such as the use of catalyst with lower light-off temperature and improved catalyst durability, due to low temperatures and non oxidizing environment (Cocchi et al. 2006). As a matter of fact, the catalyst became active at temperature as low as 320°C (Smith et al., 2005) and the experimental campaign on a modified Solar Turbine (Saturn T1200 rated at 750 kW) demonstrated the feasibility of such technology with emission levels below 3 ppm in the load range 30-60%. A further advantage is the minor sensitivity of catalyst temperature to fuel/air ratio, allowing safe operation also with up to ±10% uniformity (Karim et al, 2003).

Moreover, recently it was proposed to install RCL system as pilot stabilizers in lean premixed burner instead of the aforementioned diffusion pilot flame (Karim et al. , 2003) (Fig. I.4.4). The catalytic pilot concept focus on replacing the highest temperature zone with the catalytic burner which provides stability to the main flame thank to enhanced reactivity of partial oxidation

products. The catalytic pilot is a good candidate for retrofit application without major modification and cost.

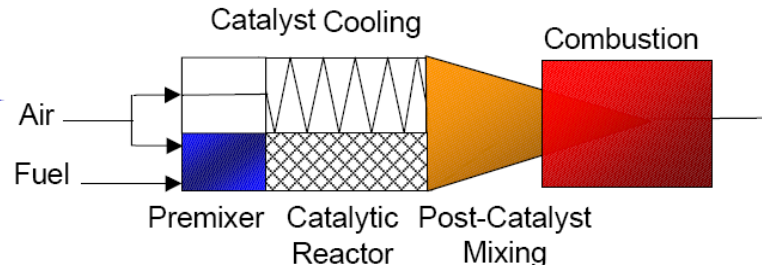


Fig. I.4.3 RCL system

In particular, as depicted in Fig. I.4.4, fuel and a fraction of the air are mixed before entering the catalyst under fuel rich conditions. The remainder fraction of the air acts as cooler for the catalyst. The cooling air and the gas exiting the catalyst are subsequently rapidly mixed giving rise to a fuel lean reactive mixture without the risk of autoignition.

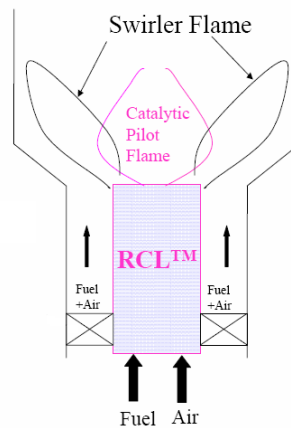


Fig. I.4.4 Catalytic pilot flame

1.4.3 High Pressure Catalytic Combustion Literature

The great interest towards catalytic combustion is witnessed by the large number of publications devoted to the experimental, prevalently conducted in lab-scale atmospheric pressure rigs and numerical/theoretical studies. The emphasis on atmospheric pressure is mainly due to a matter of

simplicity and ease of control of the test facility. In some cases a considerable effort is done to extrapolate the behavior of the catalyst at atmospheric condition to higher pressure by means of numerical models/schemes and predictions. Nevertheless in the case of GT application, it is evident the need to compare, not only with models but especially experimentally, the behaviour of the catalyst at condition relevant to GT, including pressure above the atmospheric. This is because catalytic combustion is a complex process, in which several transport and reaction mechanisms are involved and the high pressure behaviour and interplay of the different concurrent phenomena are not always predictable from atmospheric studies (reaction kinetics, mechanical and thermal resistance of catalyst, the adhesion of washcoat to substrate, hot spot formation and hetero/homogeneous reaction coupling). As a matter of fact, concerning reaction kinetics, it is noteworthy that the emphasis of schemes is on low-pressure and often also on low temperature and extrapolation and extension to higher pressure leads to erroneous evaluations. This is what for example happens in the case of Pd, as reported by Carroni et al (2003); As a matter of fact at atmospheric pressure the process can be well simulated by assuming mass-transfer controlled surface reaction while, this assumption leads to conversion that are larger than the measured ones at high pressure implying that at gas turbine condition, heterogeneous process is kinetically controlled.

On the contrary, from the study of the literature concerning high pressure catalytic combustion, it clearly appears a lack of fundamental studies of catalyst behaviour under pressure. In addition several studies have been performed by industrial research groups or in a joint venture with an industrial partner. In this cases the articles are more focused on the emission performances of the combustor equipped with catalytic modules, whose complete formulation and operative condition remain usually unknown (Ozawa, 1999; Dalla Betta et al, 1995; Dalla Betta and Rostrup Nielsen 1999; Cutrone et al 1999; Beebe, 2000; Smith et al, 2005; Cocchi, 2006). Another great part of literature is dedicated to the study of the different catalytic combustion concepts as already reported in the paragraph I.4.2 (Sadamori, 1999; Dalla Betta, 1997; Fant 2000).

Among the research groups, the most active were that of the KTH (Royal Institute of Technology) and of the Paul Scherrer institute both with some collaborations with Alstom Power (Ersson et al 2003, Carroni et al 2003).

The KTH works are based either on a bench-scale laboratory testing or on some results on a pilot-scale facility. The first attempt concerned the development of Mn-substituted lanthanum hexaaluminates for the combustion of Gasified Biomass (Johansson et al, 2002). These catalysts

were well studied in a lab-scale rig at atmospheric pressure with focus on temperature ignition of a synthetic gas constituted by CO, H₂ and CH₄, in composition that are typical of the gasification of wood. The following scale of activity was found: CO>H₂> CH₄. Another aspect addressed by these authors is the reduction of the 60% of NH₃ to N₂ thanks to the proposed catalyst. The results of the testing of these promising catalyst in an high pressure pilot-scale units are still not reported. In 2003, the activity of different bimetallic (Pd/Pt or Pd/Rh) catalysts was investigated by means of transient activity and steady-state tests in a lab scale annular reactor and at 5 bar in a high pressure test rig supplied by Alstom Power. This work compared the catalytic performance of the bimetallic formulation with respect to that of the 5%Pd/Al₂O₃. The addition of a second metal was proposed in order to improve the stability of Pd based catalysts: These catalysts showed, in pilot-scale rig, the decrease of their initial activity at temperature below the PdO/Pd transition, thus suggesting the presence of two different types of palladium oxides (Ersson et al, 2003, Groppi et al 2001).

It was found that the Pt addition increased the stability of the catalyst in the low temperature region. It was supposed that the improved stability was the result of increased resistance towards sintering of the Pd/Pt particles with respect to the Pd ones. Nevertheless, no attempt to extrapolate the influence of pressure on the catalyst behaviour was made by these authors.

On the contrary, Kuper et al (1999), testing different Pd based catalyst in a pressurized test rig simulating a partial catalytic combustor, focused their attention on the influence of various parameters pressure included. They, assuming a first reaction order with respect to methane, found that the apparent reaction order with respect to the pressure was 0.4±0.1. Moreover they stated that bimetallic Pd-Pt catalyst are not useful for partial catalytic concept due to their low transition temperature. As a matter of fact they proposed to use high temperature active phases in order to increase the temperature of the gas leaving the catalyst and allow the initiate and completion of homogeneous reactions at short residence times.

The effect of the pressure was also studied for methane combustion over supported palladium-platinum catalysts by Jaräs and co-workers (Persson et al, 2005). The authors showed that methane conversion decreases increasing pressure at constant velocity (i.e. increasing the mass flow and Re number). This effect is more pronounced at low pressure. They suggested that, even though the surface reaction is promoted by pressure, the maximum achievable conversion is limited by the growing mass transport limitation due to higher mass flows. Andrae et al (2005) numerically studied the effect of pressure at constant mass flow in the catalytic combustion of syngas over 1%Pt/Al₂O₃. The authors showed that, at constant mass flow, the conversion (i.e. combustion

efficiency) increases with pressure. This increase is more pronounced for relatively low pressures (<6 bar). Moreover they stated that the higher residence times at higher pressure compensate for the decreasing diffusion velocity.

Another approach is to numerically simulate the combustion and to validate the well-known schemes obtained at atmospheric pressure with the aid of some experimental results (Carroni et al, 2003; Andrae et al, 2005) The most preferred catalyst for these schemes was platinum since the well stated reaction mechanism including all the phenomena occurring on its surface (adsorption/desorption of species, co-adsorption effect and surface reaction).

For instance, the high pressure (5-16 bar) catalytic combustion of gasified biomass on 1%Pt/Al₂O₃ was studied by means of a parabolic two dimensional steady state model that was used to simulate the flow onto a single channel (Andrae et al, 2005). A detailed multi-step mechanism of Vlachos and co-worker (2003), developed for a polycrystalline surface, was used to describe the heterogeneous process. The model validation consisted in the comparison of predicted combustion efficiencies with only 5 experimental test.

This approach was extensively used by Mantzaras and co-worker (Reinke et al, 2002, 2004, 2005; Mantzaras et al 2007; 2009) who performed experiment up to 16 bar in an optically accessible catalytic channel reactor constituted by two Pt-coated ceramic plate. The rig is provided with two optical measuring techniques: OH-LIF (OH Laser Induced Fluorescence) used to monitor the OH radical along the streamwise plane of symmetry and the onset of homogeneous (gas-phase) ignition, and one dimensional Raman to measure major species concentration across the reactor boundary layer in order to assess the heterogeneous process. The most important aim of these articles is the discrimination among different homogeneous heterogeneous schemes and validation of an hetero/homogeneous scheme from the measurements of gas phase ignition distances for both hydrogen (Appel et al; 2002; Mantzaras et al, 2009) and methane (Reinke et al, 2002; 2004). Usually these heterogeneous schemes (Deutschmann or Vlachos) involves many elementary steps (> 30) including adsorption and desorption of the major species and radicals (see table I.4.3). Similarly also the homogeneous scheme, like those of Warnatz or Gri 3.0, involves many reaction.

The agreement of model prediction with experimental data was often poor with errors also higher than 10%. For example, in the case of methane, the scheme of Deutschmann/Warnatz, the best among the schemes tested, was able to predict the homogeneous ignition distance within 10% only in a limited range of pressure (up to 6 bar) while above 8 bar the over prediction of homogeneous ignition distances was about 25% (Reinke et al, 2002).

However, some fundamental aspects were addressed by the authors. For example they stated that catalytic reactivity increases less than linearly by increasing pressure because the platinum surface is more and more covered by O adsorbed atoms (Reinke et al 2004).

Nevertheless, often the attention is devoted to the homogeneous phase. For example, the work of Reinke et al (2005), focused on the role of H₂O and CO₂ on the gas phase ignition of methane in air. The authors found that the addition of H₂O promoted chemically homogeneous ignition whereas the addition of CO₂ had a minor chemical impact.

Another investigating point is the effect of H₂O and CO₂ on homogeneous (Reinke et al. 2005) and heterogeneous (Reinke et al. 2006) reactions. In particular, they found that the addition of H₂O chemically promoted homogeneous methane ignition whereas the addition of CO₂ had a less relevant impact. At the same time, they showed that the addition of water inhibits the catalytic methane conversion because of the reduction of the available free Pt sites due to higher OH(s) surface coverage. The H₂O-induced heterogeneous inhibition is more pronounced at higher pressures and lower catalyst temperatures. On the contrary the addition of CO₂ has no direct chemical impact on the catalytic pathway.

Methane apart, also H₂, propane and simulated syngas were studied, even though the latter only numerically. The hetero-/homogeneous combustion of fuel-lean hydrogen/air mixtures over platinum was experimentally and numerically investigated in the pressure range up to 10 bar. It was found that the homogeneous ignition was suppressed at pressure above 4 bar even at wall temperatures as high as 723 and 1250 K. This was attributed to the combined effects of the intrinsic homogeneous hydrogen kinetics and of the hetero/homogeneous chemistry coupling via the catalytically produced water over the gaseous induction zone (Mantzaras et al, 2009).

The catalytic combustion of syngas/air mixtures over Pt has been investigated numerically at pressure up to 15 bar (Mantzaras, 2008). The author highlighted that, due to the diffusional imbalance of hydrogen, superadiabatic surface temperatures could be achieved causing catalyst deactivation (sintering and volatilisation). Moreover he stated that the gas-phase H₂ combustion moderates the superadiabatic wall temperatures by shielding the catalyst from the hydrogen-rich channel core.

As concern the coupling of H₂ and CO chemistry, at temperature below 700 K, the carbon monoxide predominantly covers the catalytic surface inhibiting the catalytic conversion of both fuel components.

Table I.4.3-Heterogeneous Chemical reaction mechanisms for methane-(Reinke et al, 2004)

	Deutschmann ^b		Vlachos ^c			
	A (γ)	E	A_f (γ)	E_f	A_b	E_b
Adsorption reactions						
1. $\text{CH}_4 + 2\text{Pt}(s) \rightarrow \text{CH}_3(s) + \text{H}(s)$	0.01	0.0	1.0	50.2	-	-
2. $\text{O}_2 + 2\text{Pt}(s) \rightarrow 2\text{O}(s)$	0.023	0.0	0.03	0.0	-	-
3. $\text{O}_2 + 2\text{Pt}(s) \rightarrow 2\text{O}(s)$	4.9×10^{12}	0.0	-	-	-	-
4. $\text{CH}_3 + \text{Pt}(s) \rightarrow \text{CH}_3(s)$	-	-	1.0	0.0	-	-
5. $\text{CH}_2 + \text{Pt}(s) \rightarrow \text{CH}_2(s)$	-	-	1.0	0.0	-	-
6. $\text{CH} + \text{Pt}(s) \rightarrow \text{CH}(s)$	-	-	1.0	0.0	-	-
7. $\text{C} + \text{Pt}(s) \rightarrow \text{C}(s)$	-	-	1.0	0.0	-	-
8. $\text{H}_2 + 2\text{Pt}(s) \rightarrow 2\text{H}(s)$	0.046	0.0	0.25	0.0	-	-
9. $\text{H} + \text{Pt}(s) \rightarrow \text{H}(s)$	1.0	0.0	1.0	0.0	-	-
10. $\text{O} + \text{Pt}(s) \rightarrow \text{O}(s)$	1.0	0.0	1.0	0.0	-	-
11. $\text{H}_2\text{O} + \text{Pt}(s) \rightarrow \text{H}_2\text{O}(s)$	0.75	0.0	0.7	0.0	-	-
12. $\text{OH} + \text{Pt}(s) \rightarrow \text{OH}(s)$	1.0	0.0	1.0	0.0	-	-
13. $\text{CO}_2 + \text{Pt}(s) \rightarrow \text{CO}_2(s)$	-	-	1.0	0.0	-	-
14. $\text{CO} + \text{Pt}(s) \rightarrow \text{CO}(s)$	0.84	0.0	1.0	0.0	-	-
Pure surface reactions						
15. $\text{H}(s) + \text{O}(s) = \text{OH}(s) + \text{Pt}(s)$	1.0×10^{13}	11.5	1.7×10^{10}	50.6	5.6×10^{11}	102.1
16. $\text{H}(s) + \text{OH}(s) = \text{H}_2\text{O}(s) + \text{Pt}(s)$	1.0×10^{13}	17.4	3.5×10^{11}	51.9	1.2×10^{10}	77.0
17. $\text{OH}(s) + \text{OH}(s) = \text{H}_2\text{O}(s) + \text{O}(s)$	1.0×10^{13}	48.2	1.0×10^{11}	79.1	1.0×10^{11}	52.7
18. $\text{C}(s) + \text{OH}(s) \rightarrow \text{CO}(s) + \text{H}(s)$	-	-	1.0×10^{11}	16.7	1.0×10^{11}	168.6
19. $\text{C}(s) + \text{O}(s) \rightarrow \text{CO}(s) + \text{Pt}(s)$	1.0×10^{13}	62.8	1.0×10^{11}	18.0	-	-
20. $\text{CO}(s) + \text{Pt}(s) \rightarrow \text{C}(s) + \text{O}(s)$	2.7×10^9	184.0	1.0×10^{11}	221.8	-	-
21. $\text{CO}(s) + \text{O}(s) \rightarrow \text{CO}_2(s) + \text{Pt}(s)$	1.0×10^{13}	105.0	1.0×10^{11}	15.1	1.0×10^{11}	88.7
22. $\text{CO}(s) + \text{OH}(s) \rightarrow \text{CO}_2(s) + \text{H}(s)$	-	-	1.0×10^{11}	35.1	1.0×10^{11}	56.9
23. $2\text{CO}(s) \rightarrow \text{C}(s) + \text{CO}_2(s)$	-	-	1.0×10^{11}	0.0	1.0×10^{11}	129.7
24. $\text{CH}(s) + \text{O}(s) \rightarrow \text{CO}(s) + \text{H}(s)$	-	-	1.0×10^{11}	0.0	1.0×10^{11}	336.8
25. $\text{CH}_3(s) + \text{Pt}(s) \rightarrow \text{CH}_2(s) + \text{H}(s)$	1.0×10^{13}	20.0	5.0×10^{12}	107.9	1.0×10^{11}	25.5
26. $\text{CH}_3(s) + \text{O}(s) \rightarrow \text{CH}_2(s) + \text{OH}(s)$	-	-	1.0×10^{11}	84.5	1.0×10^{11}	52.3
27. $\text{CH}_3(s) + \text{OH}(s) \rightarrow \text{CH}_2(s) + \text{H}_2\text{O}(s)$	-	-	1.0×10^{11}	77.8	1.0×10^{11}	21.3
28. $\text{CH}_2(s) + \text{Pt}(s) \rightarrow \text{CH}(s) + \text{H}(s)$	1.0×10^{13}	20.0	1.0×10^{11}	104.6	1.0×10^{11}	51.0
29. $\text{CH}_2(s) + \text{OH}(s) \rightarrow \text{CH}(s) + \text{H}_2\text{O}(s)$	-	-	1.0×10^{11}	81.6	1.0×10^{11}	55.2
30. $\text{CH}_2(s) + \text{O}(s) \rightarrow \text{CH}(s) + \text{OH}(s)$	-	-	1.0×10^{11}	83.3	1.0×10^{11}	80.8
31. $\text{CH}(s) + \text{Pt}(s) \rightarrow \text{C}(s) + \text{H}(s)$	1.0×10^{13}	20.0	1.0×10^{11}	22.6	1.0×10^{11}	157.3
32. $\text{CH}(s) + \text{OH}(s) \rightarrow \text{C}(s) + \text{H}_2\text{O}(s)$	-	-	1.0×10^{11}	0.4	1.0×10^{11}	159.4
33. $\text{C}(s) + \text{O}(s) \rightarrow \text{CO}(s) + \text{Pt}(s)$	-	-	1.0×10^{11}	6.3	1.0×10^{11}	192.0
Desorption reactions						
34. $\text{CH}_3(s) + \text{H}(s) \rightarrow \text{CH}_4 + 2\text{Pt}(s)$	-	-	1.0×10^{11}	23.0	-	-
35. $2\text{O}(s) \rightarrow \text{O}_2 + 2\text{Pt}(s)$	1.0×10^{13}	213.2-600 _O	1.0×10^{13}	213-133.9 _O	-	-
36. $\text{CH}_3(s) \rightarrow \text{CH}_3 + \text{Pt}(s)$	-	-	1.0×10^{13}	159.0	-	-
37. $\text{CH}_2(s) \rightarrow \text{CH}_2 + \text{Pt}(s)$	-	-	1.0×10^{13}	284.5	-	-
38. $\text{CH}(s) \rightarrow \text{CH} + \text{Pt}(s)$	-	-	1.0×10^{13}	405.8	-	-
39. $\text{C}(s) \rightarrow \text{C} + \text{Pt}(s)$	-	-	1.0×10^{13}	627.6	-	-
40. $2\text{H}(s) \rightarrow \text{H}_2 + 2\text{Pt}(s)$	1.0×10^{13}	67.4-6 _H	1.0×10^{13}	83.7-25.1 _H	-	-
41. $\text{H}(s) \rightarrow \text{H} + \text{Pt}(s)$	-	-	1.0×10^{13}	251.9-20.1 _H	-	-
42. $\text{O}(s) \rightarrow \text{O} + \text{Pt}(s)$	-	-	1.0×10^{13}	387.4-107.1 _O	-	-
43. $\text{H}_2\text{O}(s) \rightarrow \text{H}_2\text{O} + \text{Pt}(s)$	1.0×10^{13}	40.3	1.0×10^{13}	41.8	-	-
44. $\text{OH}(s) \rightarrow \text{OH} + \text{Pt}(s)$	1.0×10^{13}	192.8	1.0×10^{13}	263.6-138.1 _O	-	-
45. $\text{CO}_2(s) \rightarrow \text{CO}_2 + \text{Pt}(s)$	1.0×10^{13}	20.5	1.0×10^{13}	71.1	-	-
46. $\text{CO}(s) \rightarrow \text{CO} + \text{Pt}(s)$	1.0×10^{13}	125.5	1.0×10^{13}	142.3-62.8 _{CO}	-	-

^a In all pure surface and desorption reactions, the reaction rate coefficient is $k = AT^b \exp(-E/RT)$ with $b = 0$. The units are A (s^{-1}) and E (kJ/mol) yielding reaction rates in (s^{-1}); to convert to standard surface reaction rate units ($\text{mol}/\text{cm}^2 \text{ s}$), A must be multiplied by Γ^{1-m} where m is the reaction order. In all adsorption reactions A denotes a sticking coefficient (γ), except in Deutschmann's reaction S3, where $k = AT^b \exp(-E/RT)$ with $b = -0.5$ and A in ($\text{mol}^{-1} \text{cm}^3 \text{K}^{0.5} \text{s}^{-1}$); A in S3 must be multiplied by $1/\Gamma$ to convert to standard surface rate units.

^b Reactions S2 and S3 are duplicate. Reactions S1, S8, and S14 have a Pt order of 2.3, 1, and 2, respectively.

^c Parameters are given for the forward (f) and, when appropriate, for the reverse (b) reactions. The activation energies of the adsorption and pure surface reactions are valid for an uncovered surface ($\theta_{\text{Pt}} = 1$); at other surface coverage, they were calculated using BOC (bond order conservation) formulae considering interactions of heats of chemisorption, according to Ref. [7].

Even though in the work of Mantzaras many important features of catalytic combustion, such as hetero-homogeneous coupling, presence of a second fuel or of inert gasses (CO_2 , H_2O), are treated, the major drawback is the interest limited only to Pt catalyst. But as stated above, the interest in Pt catalyst is limited only to fuel containing H_2 and CO and on low temperature operation since the volatility showed by this noble metal.

Therefore, the durability target of 8800 hr of operation makes necessary to propose and study different catalysts under conditions relevant to gas turbine application. To date the most preferred catalyst for methane combustion are Pd-based eventually with the addition of a second noble metal, as Pt, or Mn. The bimetallic palladium-manganese systems were successful studied by Requies et al (2008) showing high stability . As a matter of fact the $5\text{Mn}0.25\text{Pd}$ was able to maintain stable operation along a 100 hr activity test.

I.5 Aim of the thesis

The study of catalyst behavior at pressure above 1 bar during methane, H_2 , CO and their mixtures combustion is the main purpose of this PhD thesis. As a matter of fact, as stated above, the concurrent phenomena occurring in a catalytic reactor could deeply affect the catalyst performances. As a matter of fact, as reported by Kolaczkowski (1996), many catalysts that appear to have worked well in a laboratory environment but do not so when installed in a High Pressure pilot-scale rig. Kolaczkowski, attributed this evidence only to interphase and intraphase mass transfer limitation that arise in condition relevant to GT application. But, as already mentioned, heterogeneous processes at gas turbine conditions could be largely influenced by kinetics (Carroni et al, 2003). Thus implying that the discordance between catalyst behavior at different pressure is not only ascribed to the mass transfer limitations but also to the inability of proposed kinetic schemes to predict the effective behavior of the catalyst under pressure. As a matter of fact, the availability of reliable, heterogeneous, kinetic data, is necessary for the correct description of the catalytic processes.

As highlighted in paragraph I.4.3 the fundamental studies on high pressure catalytic processes are relatively few. Besides they are almost focalized on noble metals Pd for methane combustion and Pt. The latter was extensively studied in numerical works because, even though is less active than Pd, it allows to validate kinetic schemes known at low pressure under pressure and to derive simplified hetero/homogeneous scheme (Reinke et al, 2004).

Nevertheless, as reported in paragraph I.4.1, the Pd-based catalysts show instabilities also at temperature below that of the transition of PdO_x/Pd, requiring the addition of a second noble metal, Pt, in order to improve their low temperature stability. Moreover, noble metals are very expensive and their use is not suitable in high temperature applications due to the occurrence of sintering, highly accelerated with excursion over 1000°C, and volatilization phenomena resulting in loss of durability (Fant et al, 2000).

As a consequence the research has been focused on catalysts with higher thermal resistance. These catalysts can be used in fully catalytic combustor for GT application with turbine inlet temperatures lower than 1100°C (see Fig. I.5.1). Moreover, in the catalytically stabilized concept, the temperature of the gasses leaving the catalytic stage markedly affects the following homogeneous reaction (Kuper et al, 1999). As a matter of fact, higher temperature results in higher stability of homogeneous combustion and reduction of Burn-Out Zone volume due to the increase of reaction rates.

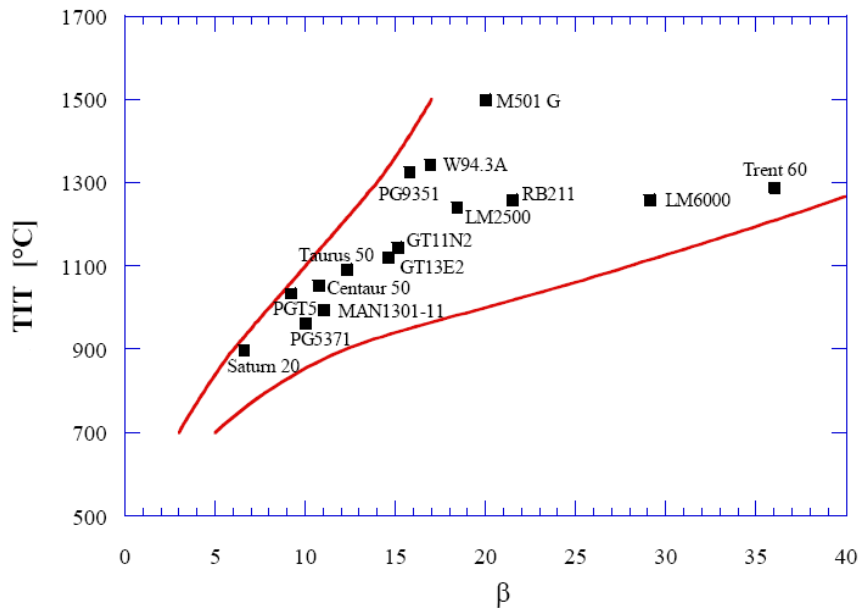


Fig.I.5.1-Compression ratio (β) and turbine inlet temperatures (TIT) for some GT.

Hence, the active phases considered in this experimental activity are supported perovskites that, as previously stated, are very cheap and thermally stable with an activity only slightly lower compared to noble metals at condition relevant for GT engines. Moreover their behavior under pressure is very less known. However, the effect of promoting perovskite with a little amount of platinum was studied with particular focus on the Pt volatilization at high temperature. The desire for low

combustor pressure drop makes necessary the use of an appropriate substrates. For this reason catalysts powders were deposited on appropriate planar ($\alpha\text{-Al}_2\text{O}_3$) and honeycomb monolithic (cordierite) substrates.

Since catalytic combustion is very attractive for the use of Low-Btu fuels, the research activity will be focused notably on CH_4 but also on focused on H_2 and CO combustions and on the effect of their addition on methane combustion at variable pressure. At atmospheric pressure, supported perovskites showed the reactivity scale $\text{CO} > \text{H}_2 > \text{CH}_4$ and, as a consequence, the partial substitution of methane with hydrogen and CO results in lower ignition temperature over these materials (Cimino et al, 2003); thus suggesting a positive effect at higher pressure too.

The first part of the thesis will be devoted to the study of physical-chemical properties of different materials ($\text{LaMnO}_3/\text{La}_2\text{O}_3\text{-}\gamma\text{-Al}_2\text{O}_3$; bi-functional $\text{Pt-La MnO}_3/\text{La}_2\text{O}_3\text{-}\gamma\text{-Al}_2\text{O}_3$ and $\text{Pt}/\text{La}_2\text{O}_3\text{-}\gamma\text{-Al}_2\text{O}_3$). At the same time the experimental high pressure test rig will be designed and realized. Moreover, an atmospheric experimental campaign was carried out to study methane combustion and the effect of H_2 addition under autothermal condition with respect to the behaviour of the bi-functional catalyst at ignition and extinction. This campaign will help to outline many important effects at atmospheric pressure and the similarities and differences of the catalyst behavior at pressure above the atmospheric one under autothermal conditions

Due to the lack of kinetic data at pressure higher than the atmospheric one, especially for perovskite based catalyst, it seems necessary to study H_2 , CO and CH_4 oxidation kinetics. They will be studied under isothermal condition on both perovskite and Pt catalyst at temperature of interest for ignition and for pressure up to 12 bar that are relevant notably in the case of small size turbine but also in order to gain information on the pressure influence on the heterogeneous reactions.

A second part of the high pressure study will be dedicated to pseudo-autothermal operation. In particular, the effect of pressure, H_2 and or CO addition on methane ignition over perovskite catalyst will be investigated. moreover in order to enhance low-Btu co-feeding effect another catalyst configuration will be studied. A Pt based catalyst, active at low temperature towards H_2 and CO combustion, will be placed upstream the perovskite catalyst in order to burn hydrogen and carbon monoxide and to increase the temperature up to the methane light off one over perovskite. Moreover, this configuration could preserve Pt catalysts from the highest temperature reached inside the perovskite, thus avoiding sintering and volatilization of the noble metal.

II MATERIALS AND METHODS

In this PhD activity the LaMnO₃-based catalysts were studied in comparison with Pt ones both supported on La₂O₃-stabilized γ -Al₂O₃. The active phase loadings are respectively of 20 wt% and 1 wt% as regards the total weight of the supported catalysts.

The research activity involved the preparation of structured (planar and monolithic) catalytic systems and the use of several characterization techniques as well as different activity tests (i.e. at atmospheric/under pressure test, high diluted/Autothermal condition) conducted in their own appropriate experimental rigs.

The applied methods and experimental apparatus description are reported in this chapter. First, the catalyst preparation was described.

II.1 Structured Catalyst Preparation

II.1.1 Planar Substrates Catalytic Systems

The preparation of planar substrates catalysts is divided in three fundamental steps:

- α -Al₂O₃ Platelet preparation
- Catalyst powder preparation
- Coating of the substrates with the active phase

Detailed description of the above mentioned steps is presented below

II.1.1.1 Preparation of The Platelet Substrates

Alumina platelets, characterized by an elevated thermal (maximum working temperature as high as 2000°C), mechanical and chemical resistance, have been prepared starting from products supplied by Cotronics Corp.. Preparation technique includes the preparation of a slurry constituted by a liquid activator used as binder and by α -Al₂O₃ pure powder. The slurry is dried overnight at room temperature and it is further fired at 950°C in air. The platelets are prepared in the required shape and dimensions through the use of specific home-made flexible and impermeable moulds; in particular they are made in the shape of a parallelepiped, 0.5 cm thick, 1.5 cm wide and 3.0 cm long. The manufacturing tolerance on the finished product is 0.1 mm. A detailed description of the preparation technique is reported below.

In order to prepare the mould, a plate in the required shape and dimensions is realized in a piece of brass by means of a milling machine. A silicone-like slurry is poured inside the block and it is dried overnight at room temperature. The silicone part, removed from the block, is the mould employed for preparing the platelets (Figure II.1.1c).

According to the recipe supplied by Cotronics, a specific amount of alumina powder (Rescor 780) and liquid activator are poured in a beaker and properly mixed until obtaining a slurry provided with a certain consistency. The slurry is then poured in the formerly prepared mould. The mould is successively stirred for about 15 min in order to take out from the slurry the remaining air bubbles, thus avoiding the occurrence of cracks in the further thermal treatments. After about 20 min the slurry in excess is removed by the mould using a shovel. The slurry inside the mould is dried at room temperature for about 20h. After such operation the mechanical resistance is high enough to allow the removal of the platelet from the mould and the sample is further fired at 950°C for 5 hours. Such thermal treatment determines a further increase in the substrate mechanical resistance besides allowing the removal of the organic part present in the liquid activator. However, thermal treatment may causes over pressure because of the air still present in the platelet and the thermal decomposition of the organic part. So, in order to avoid cracks in the finished product, a very low heating rate (1°C/min) has been used. In Figure II.1.1a, b, d some pictures of the prepared plates are reported.

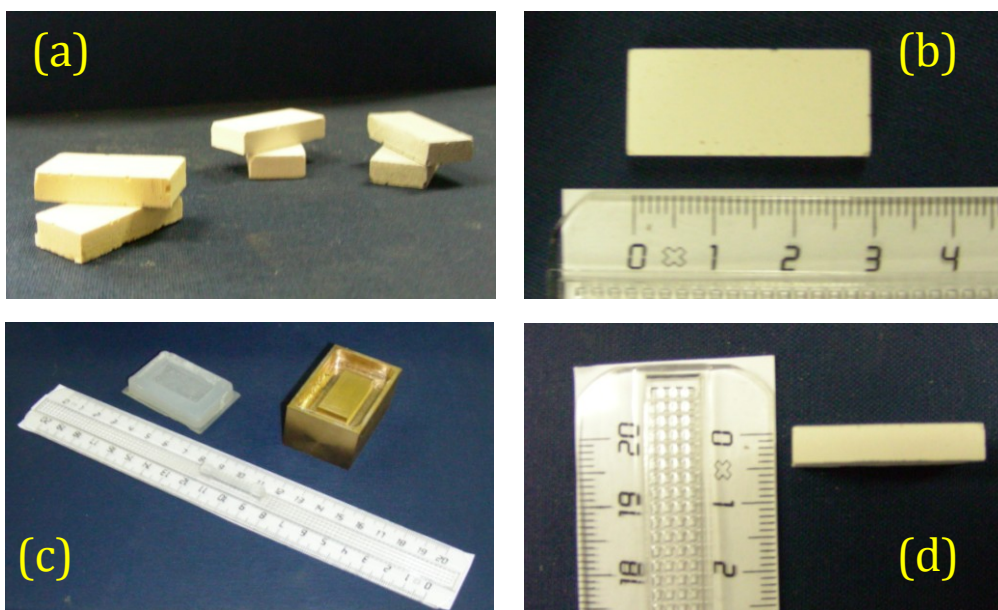


Fig. II.1.1 Preparation of the alumina platelets; (a),(b),(d): platelets shape and dimension; (c) mould used in the preparation

II.1.1.2 Catalyst powder preparation

Alumina in the powder form (CK300, Akzo) is finely ground by means of a “ball milling” machine till the mean diameter of the particles is less than 2 μm . In order to shift γ - to α -alumina transition at temperatures higher than 1000°C, a stabilization procedure is needed and carried out by inserting some amount of lanthanum oxide (5wt%) into the structure, thus inhibiting the mobility of oxygen and aluminium atoms and, as consequence, the transition to the alpha phase (Arai e Machida, 1996). After being stabilized, $\gamma\text{-Al}_2\text{O}_3$ is loaded up by the active phase.

The active phase and La_2O_3 are deposited onto alumina through an “incipient wetness impregnation” method in a rotary vapour (Laborota 4002, Heidolph). According to this method the inert alumina powder is suspended in an aqueous solution constituted by the precursors of the stabilizer or of the active phase. The precursors are added to the solution in a such amount as to have the desired load and formulation of the catalysts. The prepared suspension is fed into the rotary vapour rotating at 75 rpm and it is dried under vacuum conditions (100 mbar) at 50°C. The dried impregnated powder is consequently calcined at 800°C for 3h in air.

An impregnation solution constituted by lanthanum nitrate has been prepared in order to stabilize $\gamma\text{-Al}_2\text{O}_3$. About active phase, in the case of $\text{Pt}/\gamma\text{-Al}_2\text{O}_3$ systems an impregnation solution

constituted by a diluted chloroplatinic acid solution (Sigma Aldrich) has been prepared. A solution constituted by manganese acetate (Manganese acetate tetraydrate, Aldrich) and lanthanum nitrate (Lanthanum nitrate Hexahydrate, Fluka) has been prepared in the case of $\text{LaMnO}_3/\gamma\text{-Al}_2\text{O}_3$ based catalyst. Finally, in the case of the mixed active phase, $\text{Pt-LaMnO}_3/\gamma\text{-Al}_2\text{O}_3$ catalysts, a solution constituted at the same time by the precursors of Pt, Mn and La has been considered.

As stated above, the amount of perovskite deposited on $\gamma\text{-Al}_2\text{O}_3$ is of 20 wt% as regards the total weight of catalysts. Moreover, platinum based catalysts are characterized by a Pt amount of 1 wt % as regards the total weight of catalysts. The nominal and actual composition of catalysts powders prepared is reported in table II.1.1

Table II.1.1 Nominal and actual composition of powders catalysts

Catalyst	loading, %			
	LaMnO ₃		Pt	
	Nominal	Actual	Nominal	Actual
<i>LM20</i>	20	18.5	0	-
<i>1PtLM20</i>	20	18.5	1.00	1.04
<i>1Pt</i>	0	-	1.00	1.11

II.1.1.3 Deposition of active phase on substrates

In order to deposit the catalytic film on the alumina substrate, a “slurry” constituted by the fresh powder catalysts is prepared. At this purpose the powder samples, prepared according to the procedure as reported above, is mixed with Boehmite (Disperal, Sasol), used as binder. The solid mixture is thus suspended in an aqueous solution of nitric acid. The recipe of the slurry used for the coating of the alumina plates is reported in Table II.1.2. The slurry is spread on the plates through a paintbrush and it is, successively, dried at 120°C for 20min. It is, finally, calcined at 800°C for 3hr, in order to anchor the catalytic film on the substrate. The planar systems prepared are listed in table II.1.3

Table II.1.2 Composition of the slurry used for coating alumina platelets

	Amount [mg/(H₂Oml)]
HNO₃ (65%wt)	21.6
Boehmite	58.8
Powder catalyst	250

Table II.1.3 Active platelet prepared

Code	Amount of catalyst	Nominal active phase loading, %	
	mg	LaMnO ₃	Pt
LM20-A	26	20	01
1Pt-A	27	0	1

II.1.2 Monolith Catalysts

Cordierite honeycombed monoliths, supplied by NGK, are cut in the desired circular form (Fig.II.1.2a, b) and wash-coated with a γ -Al₂O₃ thin layer (approximately 50 μ m thick) through modified dip-coating technique (Cimino et al., 2001). According to this technique, the sample is dipped in a suspension made of diluted nitric acid and a solid content, equal to 20 wt%, constituted by a mixture of small size alumina ($d_p < 2 \mu$ m obtained by the afore mentioned grinding of CK300) and commercial boehmite (Disperal, Sasol) powder. After few minutes, enough to fill the channels with the slurry, the monolith is removed from the suspension and the excess is blown-out by means of compressed air. The sample is dried for 20 minutes at 120°C and afterwards calcined at 550°C for 2 hours. A certain number of cycles are needed in order to achieve the desired thickness of the layer and once got it the sample is calcined at 800°C for 3 hours in order to anchor the layer to the substrate. After that, the γ -Al₂O₃ has been stabilized by adding lanthanum oxide; the loaded amount of stabilizer is 5-7 wt% respect to the total washcoat weight (lanthanum and aluminium oxide

weight). Impregnation technique is used to disperse La_2O_3 in the alumina structure. At this purpose, the wash-coated sample is dipped in a solution of diluted lanthanum nitrate (Lanthanum nitrate Hexahydrate, Fluka) until the monolith channels are filled with the solution. Then the sample is thus removed from the solution, the excess of solution is blown-out and the monolith is dried at 120°C for 20 min and calcined at 800°C for 3h. This procedure is repeated until the desired loading of La_2O_3 is obtained.

Impregnation technique is also used to load the active phase. In the case of $\text{Pt}/\gamma\text{-Al}_2\text{O}_3$ catalysts, the wash-coated sample is dipped in a solution of diluted chloroplatinic acid (Sigma Aldrich), corresponding to 0.1wt% of Pt. After the sample is removed from the solution and the excess is blown-out, it is calcined at 800°C for 3hour. This procedure is repeated until the desired loading of Pt is obtained. The same procedure is followed in the case of perovskite based catalysts. In particular for preparing $\text{LaMnO}_3/\gamma\text{-Al}_2\text{O}_3$, the wash-coated monoliths are dipped in an aqueous solution made of lanthanum nitrate (Lanthanum nitrate Hexahydrate, Fluka) and manganese acetate (Manganese acetate tetraydrate, Aldrich), corresponding to 1.7 wt% of La and 0.7wt% of Mn. In the case of $\text{Pt-LaMnO}_3/\gamma\text{-Al}_2\text{O}_3$, only one solution containing both perovskite and Pt precursors is prepared. In particular the aqueous solution, made starting from lanthanum nitrate, manganese acetate and chloroplatinic acid, contains 1.7 wt% of La and 0.7wt% of Mn and 0.1wt % of Pt. The monoliths prepared and used in this PhD activity are listed in table II.1.4.

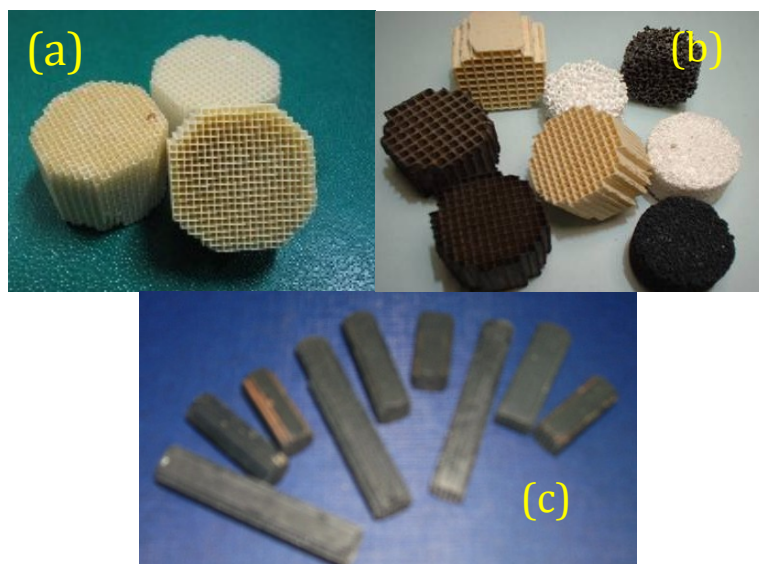


Fig II.1.2- a) and b) cordierite monolith substrates; c) some LM20-C monolith

Table II.1.4 Summary of some monolith catalysts prepared: washcoat and active phase loading in terms of nominal and measured values. the catalyst are named in base of the catalyst employed by means of the corresponding symbol (Pt, LM=LaMnO₃,Pt-LM=Pt/LaMnO₃) followed by an hyphen and the cell density. The last number refer to the monolith length.

Catalyst code	Cell density, cpsi	Dimension, mm		Catalyst Loading, g	Nominal Loading, %		Actual Pt loading, %
		<i>D</i>	<i>L</i>		<i>LaMnO₃</i>	<i>Pt</i>	
Pt-C600-10	600	9	10	0.24	-	1.00	1.06
Pt-LM-C900-12	900	17	12	1.1	20	1	1.03
LM-C900-50	900	9	50	1.41	20	1	-
LM-C600-20	600	9	20	0.54	20	-	-

II.2 Catalyst Characterization

In order to confirm that the expected elements were present in the prepared catalysts in the due amounts, actual metal contents were quantitatively determined on all the prepared samples by inductively coupled plasma spectrometry (ICP) on an Agilent 7500 ICP-MS instrument, after microwave-assisted digestion of samples in nitric/hydrochloric acid solution.

Specific surface area (SSA) of planar systems as well as monolith samples and powder catalysts were evaluated by N₂ adsorption at 77 K, according to BET method, using a Quantachromm Autosorb 1-C after degassing under vacuum at 150°C. Since, the low catalyst loadings and dimension platelets (see table II.1.3), the SSA were determined by measuring the SSA of the corresponding slurry powders calcined at 800°C for 3hr. These values were compared to those of the corresponding fresh powders catalysts employed for slurry preparation. While in the case of monolith, the fresh and used samples were opportunely cut and the SSA was assigned only to the active washcoat layer (SSA of honeycomb substrate ≤ 1 m²/g).

The redox properties of the active phases were tested by means of H₂ and CO-TPR carried out on powders samples (200-300 μm). The tests were performed in an atmospheric experimental test rig described in paragraph II.3.1. The different affinity for oxygen was thus highlighted.

The samples were loaded in a quartz reactor (9 mm internal diameter), pre-treated at 800°C under air flow for 1 h before the experiment in order to resemble the pre-treatment condition used before catalytic tests and then reduced with a 1% H₂/N₂ mixture or a 0,15% CO/ N₂ (250 cm³ min⁻¹), heating at 10°C min⁻¹ from RT up to 800°C.

Moreover, in order to evaluate the role of perovskite in enhancing the thermal stability (i.e. reducing volatilization) of Pt particles in the bi-functional 1PtLM20 catalysts, ICP analysis were carried out after different calcination temperature up to 1000°C and the Pt amounts collected were compared with the actual metal content of the dehydrated sample. The 1PtLM20 catalysts were named according to the calcination procedures as reported in table II.2.1

Table II.2.1 Denomination and calcination procedures for 1PtLM20 catalyst powders used in the stability tests.

<i>Code</i>	<i>Description</i>	<i>Period, hr</i>	<i>Calcination temperature, °C</i>
1PtLM20/D	Dehydrated	-	-
1PtLM20/C-550		3	550
1PtLM20/C-650		3	650
1PtLM20/C-800	Calcined	3	800
1PtLM20/C-1000/2		2	1000
1PtLM20/C-1000/4		4	1000

II.3 Activity Test at Atmospheric Pressure: Study of H₂-CCM under autothermal condition

II.3.1. Atmospheric Rig Description

The methane combustion and hydrogen assisted catalytic combustion of methane (H₂-CCM) tests have been carried out under autothermal conditions in the experimental apparatus reported in Figure II.3.1. Overall, it is divided into a gas feed, reactive and analysis sections, whose details are reported below. Gas is stored in high purity cylinders; specifically, methane (IP 4.5), oxygen (IP 2.7), nitrogen (IP 4.8) and H₂/N₂ mixture (2Vol% H₂) have been used. Moreover, pure hydrogen has been provided by a generator (HG2400, Claind) based on water electrolysis.

The Gas flow rates have been controlled through mass flow controllers (MFC 5850E, Brooks, working at 4 bar), communicating with a computer by means of a serial interface. The rig is equipped with a four way valve that regulates, in dependence of the valve position, the reactor bypass that is necessary to the inlet gas composition measurements.

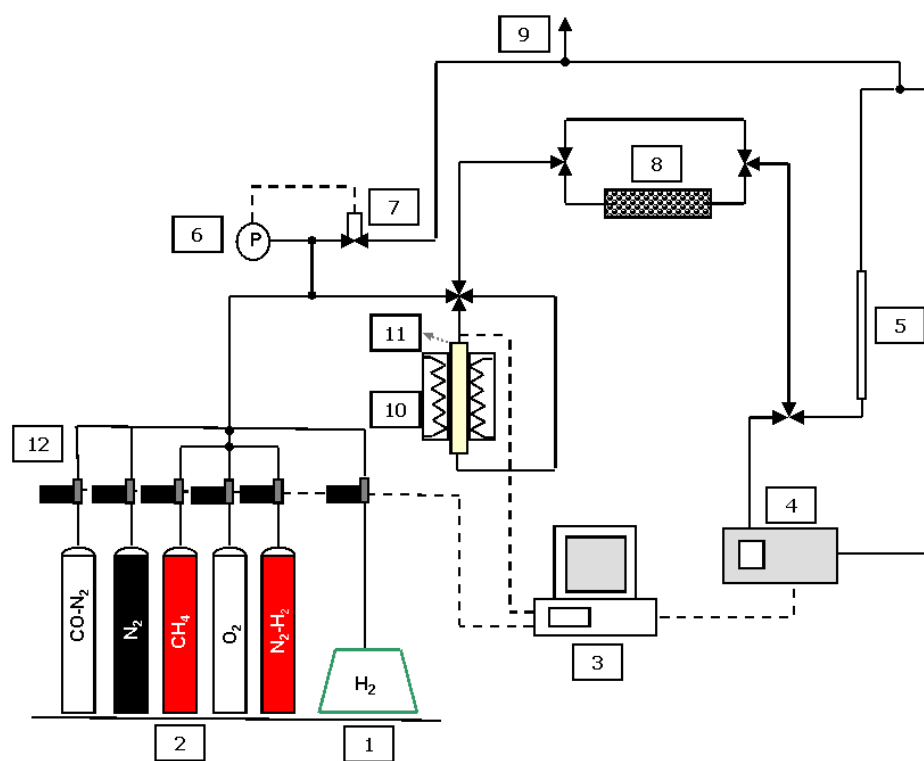
The external heating of the reactor, described in paragraphs II.3.1.1, is provided by means of a vertical furnace supplied with a PID-type controller. Moreover, the furnace could be open allowing a sudden interruption of heating limiting the influence of furnace thermal inertia.

A chemical trap, constituted by a calcium chloride bed, is placed downstream of the reactor in order to avoid the water condensation in the analyzer cells. This kind of trap is effective and selective in adsorbing water vapor while it is inert with respect to the other reaction reactants and products (particularly CO₂).

CH₄, CO, CO₂, H₂ and O₂ concentrations are measured by means of a continuous analyzer (NGA2000, Fisher-Rosemount) whose total flow rate working range is 12 -90 slph. In particular, an infrared detector is employed for CH₄, CO, CO₂ analysis, a TCD provides hydrogen measurement while a para-magnetic cell is considered in the case of O₂ analysis. A software internal to the analyzer allows a concentration measurement corrected from eventual interferences in real time; in the specific, it is needed to take into account interferences in hydrogen measurement through TCD. Finally, the experimental apparatus is supplied with a bubble flow meter.

Relative pressure is detected upstream of the reactor by means of a transducer (ROSEMOUNT 2088). In order to vent eventual over pressure, an On-Off electron valve (ASCO 8263) with a threshold value equal 0.5 bar is employed. National Instruments data acquisition board (NI PCI-6229, M series DAQ) is used to acquire signals from thermocouples, transducer and analyzer. The data are collected, visualized, recorded and elaborated by means of a PC using a home-made software developed in Lab View environment.

The above described plant was used with some minor modifications for H₂, CO-TPRs too. In particular other than 2% H₂/N₂ gas cylinder, also a gas cylinder containing a 5% CO/N₂ mixture was used. In addition the N₂ purity index was 6.0.



- | | |
|-----------------------------|-----------------------------------|
| 1. H ₂ Generator | 8. CaCl ₂ trap |
| 2. Gas cylinders | 9. Venting |
| 3. Data acquisition board | 10. Heating elements |
| 4. Analyzer | 11. Reactor |
| 5. Bubble flow meter | 12. Mass flow controller |
| 6. Pressure transducer | --- |
| 7. Electro valve | --- Data lines/electrical signals |

Fig. II.3.1 A description of the experimental apparatus for H₂-CCM

II.3.2 Reactor Configuration

A quartz reactor has been used for the study of auto-thermal combustion of methane alone and in presence of hydrogen on monolith catalysts at atmospheric condition. A reactor drawing is reported in Figure II.3.2. It consists of a cylindrical quartz tube whose external and internal diameters are respectively 2.5 and 2.4 cm. The monolith catalyst (PtLM-C900-12; length: 12mm; diameter of 17mm) is inserted inside the tube. Two ceramic foams (2.5 cm long) are placed upstream and downstream of the catalyst acting as thermal shields. In order to avoid reactants bypass through the gap between the quartz and the catalytic substrate, monolith and foams are wrapped in a thin ceramic wool blanket before being inserted in the quartz tube. A particular attention is devoted to make possible the temperature measurement inside the channels of the monolith. In particular, a second and smaller quartz tube is mounted coaxially with the previous one and is used to house thermocouples (K type). The tube has one end outside the reactor, in a cold zone, and the other in contact with the upstream foam. The thermocouples pass through the upstream foams and enter one channel of the monolith. Three thermocouples are inserted inside the catalyst monolith; specifically, temperature is detected at the inlet (approximately 3 mm far from the inlet), at the middle and at the end (approximately 3 mm far from the outlet) of the catalyst.

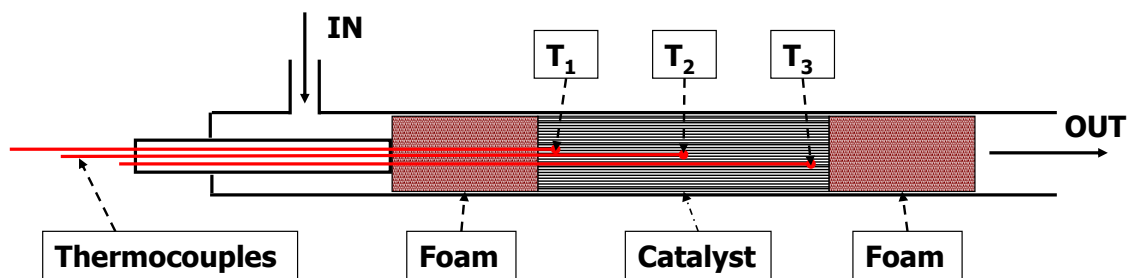


Fig. II.3.2 Quartz reactor for H₂-CCM on monolith Flow configuration. Placement of monolith catalyst and of ceramic foams. Thermocouples position.

II.3.3 Operative Conditions

The tests were carried out for the measure of the stable operation limits for catalytic combustion with respect to the pre-heating temperature. Therefore, according to the following specific procedure, the minimum ignition temperature (MIT) and the quenching temperature (QT) for a certain fuel-oxygen mixture, have been measured.

Specifically, the system is heated (reactor, catalyst, gas feeding tubes) in inert atmosphere (N_2) up to a specific set-point furnace temperature. Then the reactants mixture is fed to the reactor and temperature profile inside the catalyst as well as fuel conversion are continuously measured. If conversion does not go to about 100% and temperature is not drastically increased, temperature set point of the external electric furnace is increased with a step of $5^\circ C$ (under inert atmosphere) and the procedure is repeated till fuel ignites and reaches 100% steady-state combustion after an often long transient phase. The temperatures reported as MIT in the following chapter are those measured by a thermocouple inside the catalytic reactor; which are generally different from the actual furnace temperature. After fuel mixture ignition, steady states of methane combustion are measured by decreasing furnace set-point temperature until reaching a value of pre-heating temperature insufficient to sustain an ignited state of the system, hereafter defined as the quenching temperature QT.

As regards the ignition phenomena the considered temperature is the exit one, which is the highest in the absence of reaction; on the contrary as regards the quenching it is the entrance temperature, which corresponds to the pre-heating one.

As it can be evident in Table II.3.1, four different fuel composition are chosen. In the case of CH_4 - H_2 mixture, Mix3, it is characterized by the same overall heating value of Mix1 and a H_2/CH_4 ratio of 0.95 corresponding to a substitution of methane with hydrogen of 49% as regards the molar content or 22% considering the energetic content of H_2 with respect to the overall mixture. Mix4 has been prepared with the same hydrogen content as Mix3 and by replacing CH_4 with N_2 . Such a fuel has been considered as a reference of the thermal power supplied by hydrogen in CH_4 - H_2 combustion. Finally, total flow rate varied from 40 and 140slph corresponding to an input power in the range of 2÷50W.

Table II.3.1-Operative conditions adopted for the tests under autothermal condition at atmospheric pressure

	Fuel			
	CH₄		CH₄- H₂	H₂
	<i>Mix1</i>	<i>Mix2</i>	<i>Mix3</i>	<i>Mix4</i>
H₂, %	-	-	2.1	2.1
CH₄, %	2.8	3.8	2.2	-
O₂, %	10.0	10.0	10.0	10
N₂, %	87.2	86.2	85.7	87.9
Equivalence ratio, Φ	0.56	0.76	0.54	0.1
Heating value, KJ·NI⁻¹	0.9	1.2	0.9	0.2

Q_{TOT}=40÷140slph

GHSV, @ STP=2.2-7.7·10⁴h⁻¹

II.4 Activity Test under Pressure

II.4.1 Design and Description of High-Pressure Test Rig

The test rig, which schematically is reported in Fig. II.4.1, was designed in order to carry out the experimental measures under pressure and, therefore, to fit the following basic requirements:

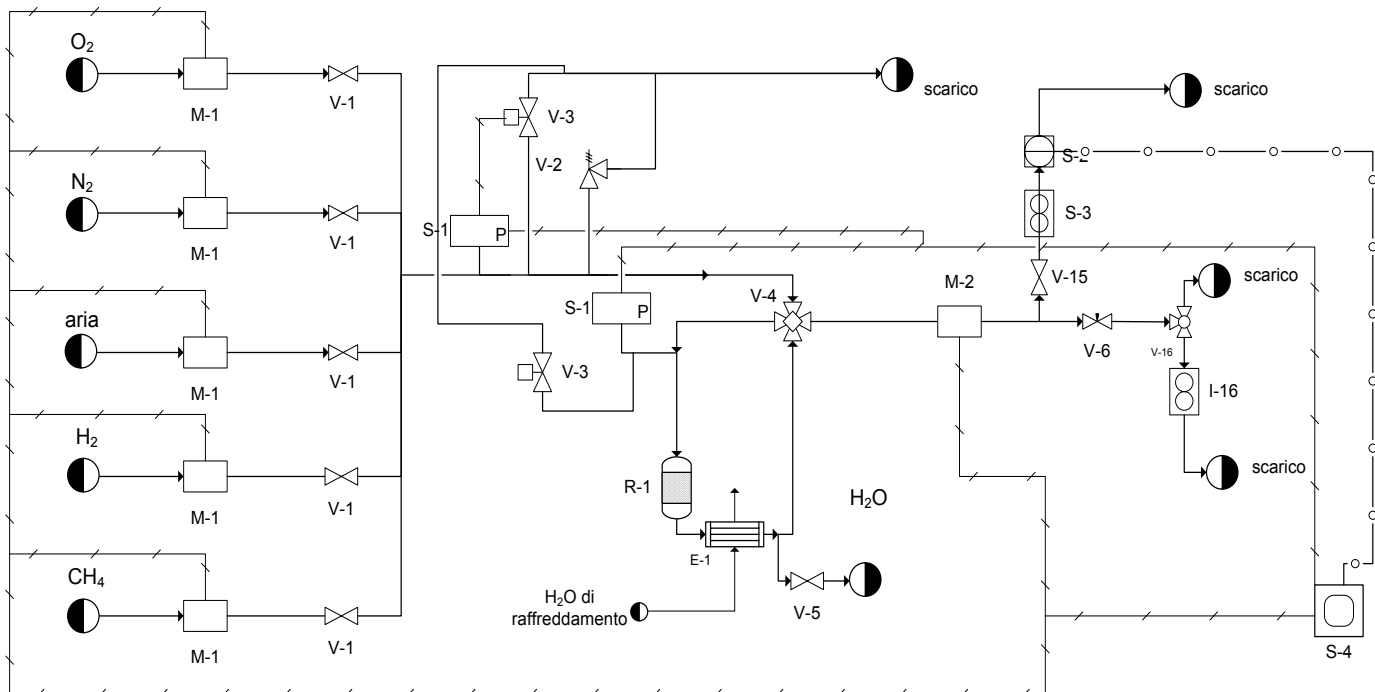
- To work at pressure between 1 and 12 bar and at temperatures up to 1000°C;
- To modify the reacting gas composition varying the relative ratio of different fuel (CH₄, CO, H₂) as well as equivalence ratio;

- To guarantee the safety of workers and equipments by means of several (mechanical and operated by remote control) safety measures
- To manage by remote control all the employed equipments
- To conduct the kinetics studies of methane, hydrogen and carbon monoxide under isothermal operation, obtained with specific reactor configuration and operative condition too;
- To study the catalysts behavior also under autothermal condition:
- Allowing the achievements of Reynolds number as high as 10^2

Also this experimental set-up is constituted by gas feed, reactive and analysis sections. The latter at atmospheric pressure.

The gas feed was designed and realized for the feeding of O₂, N₂, air, CH₄, H₂ and CO which come from gas cylinder at high purity for methane (99.995% purity), oxygen (99.7 purity) and nitrogen (99.998 purity), while in the case of hydrogen and carbon monoxide two different certified mixtures were used: 15% H₂/N₂ and 5% CO/N₂ respectively. The gas cylinders were equipped with specific regulators adjusting the delivery pressure to the MFCs at their working value (15 bar). Gas flow rates have been independently controlled through mass flow controllers Brooks (SLA5850; M-1 in Fig.II.4.1). A two-way electrovalve operated by remote control was placed downstream every MFC, with a double function: first, to block the gas flow of unused gasses and, second, to interrupt the flow of all gasses if the condition can cause safety damages. Besides, a pressure transducer (ABB 261G; S-1 in Fig.II.4.1) is placed just downstream the gasses mixing point thus allowing the on line monitoring of the pressure in the first section of the rig. A system of three two-way remote controlled electrovalves simulates a four-way valve (V-4 in Fig.II.4.1) allowing the analysis of both reacting mixture and reactor off products.

The pressure at the reactor inlet was monitored by means of a second pressure transducer (ABB 261G; S-1 of Fig. II.4.1) just upstream the reactor thus allowing the pressure measures also when the reactor is bypassed. In this way it is also possible to check quickly the absence of gas leaks in the reactor section.



- | | |
|---------------------------------------|---------------------|
| M1 Mass flow controllers | V-6 Needle-valve |
| M2 pressure controller | S-2 Analysis system |
| S-1 pressure transducers | S-3 Asameter |
| V-1 electronic valves | S-4 PC |
| V-2 Rupture disk | R-1 Reactor |
| V-3 safety electronic valves | E-1 Condenser |
| V-4 Four way valve | |
| V-5 valve for condensed water release | |

Fig II.4.1 High pressure set-up schematic.

The reactor, showed in fig. II.4.2, is a circular tube made of high thermal resistance stainless steel (AISI 310S); the outer diameter is 2.54 cm thus allowing the use of A-lock 1" tube fittings that mainly assure the absence of leaks. The cavities created in the inner of the stainless steel tube are of appropriate form and dimensions (see Fig. II.4.2b, c) in order to allocate the catalytic structured systems. In particular, in Fig. II.4.2b and c were respectively reported the cavities used for monoliths and catalytic platelets. In the latter, are also visible the one way-holes made in the upper and lower side of the cavity that were used to allocate thermocouples.

An heating jacket (Tyco Thermal Controls) (Fig. II.4.3a) equipped with a PID controller, provides for the external heating of the reactor at the desired temperature. The choice of the jacket was made

since it could be easily removed for the reactor assembly and de-assembly operation and allows the sudden interruption of external heating.

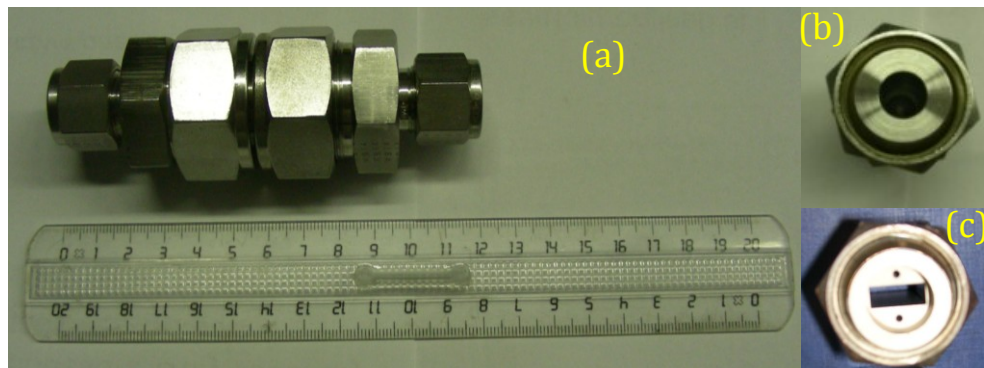


Fig II.4.2 Stainless steel reactor equipped with tube fittings: side(a) and front view (b,c)

In order to avoid undesired water condensation, especially at high pressure, the reactor exit line was maintained at 120°C till the entrance of the condenser (Fig II.4.3b). It consists of two co-axial steel tubes coils (Parker); the inner (1/4") for the gas flow and the outer (3/8") for the countercurrent cooling water flow. The condensed water is collected in a tank.

Finally, the dry gasses or the reacting mixture, on dependence of "four way" valve position, flow through the pressure controller (Brooks SLA5820; M-2 in Fig. II.4.1). This controller regulates the upstream pressure in a range between 0 and 15 bar gauge regardless of the total gas flow rate. The remainder of the plant is, then, at a pressure slightly above the atmospheric one.

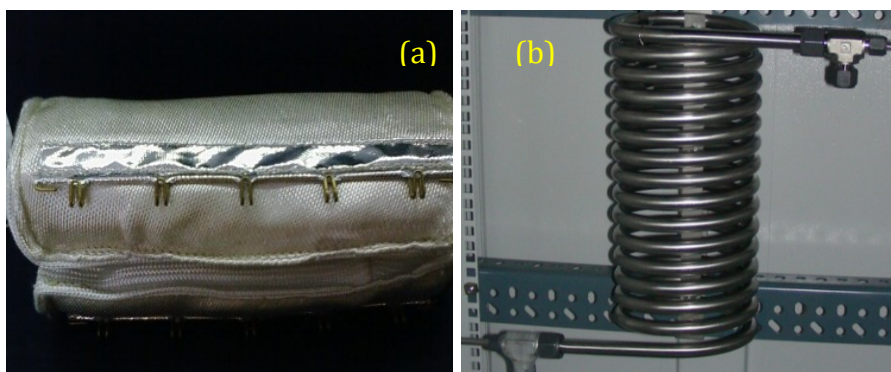


Fig II.4.3 (a) heating jacket (b) condenser

The gasses are further dried by means of a CaCl_2 chemical trap before entering into the analysis system. The latter, visible in Fig. II.4.4, operating at atmospheric pressure, is constituted by several continuous analyzers (ABB AO2000) allowing the independent measurements of several gas concentrations. An Uras measures CH_4 , CO_2 , CO contents by infrared absorption, a Magnos measures O_2 concentration by a paramagnetic detector and Caldos measures H_2 by a thermoconductibility detector, equipped with a cross sensitivity correction, and, finally a Limas measures NO , NO_2 concentration by ultraviolet adsorption. Due to the high flow rates used in order to reach the above mentioned Re numbers and incompatible with the optimal range of flow rates for analyzers, a part of the gas flow rate is directly sent to the venting. The analyzer optimal operation needs a more or less constant flow rate, for this purpose a needle valve is used for splitter regulation.

A computer interface collects the on line acquisition of all the signals (temperatures, pressures, concentrations) and is used also for the remote control of all the equipments by means of an appropriate home-made software developed in Lab View environment, whose graphic interface is partially visible also in Fig.II.4.4. In particular the temperature, pressure and valve control signals are managed by an suitable hardware(CompactDAQ, National Instrument), while a Brooks junction box, connected to the computer by means of a serial RS-232 port. is responsible for the management of MFCs. Finally, the analyzers signals are digitally acquired by means of an ethernet connection.

The choice of the remote control is fundamnetal, for example, in order to set the allarm pressure level on dependence of the actual pressure of operation (for example 2 bar higher) and as a consequence to cause the opening of safety valves when the safety level is exceeded(V-3 in Fig II.4.1). In the case of failure of this procedure, the setup is provided with a rupture disk (Oseco; V-2 in Fig II.4.1) set to break at 15 bar.

Moreover, in order to limitate the risks associated with the operation under pressure, all the setup, except analysis section and PC, is mounted in a rack equipped with Lexan door and an aspiration fan in the upper side (flow 200-300 m^3/h). The fan allows to wash the inside volume, thus avoiding the eventual formation of flammable mixtures in the case of gas leaks, and to cool the electrical part.

As stated above, the high pressure setup was used for both the kinetic and autothermal operations. Due to the different purposes, different catalytic reactor configurations and conditions were used as reported in paragraphs II.4.2. and II.4.3.



Fig.II.4.4 High pressure test rig picture

II.4.2.1 Reactor configuration

Two catalytic platelets (LM20-A; 1Pt-A), essentially differing for active phase, were used for the kinetic studies of CH₄, H₂ and CO combustion. The rectangular platelets were allocated in a specific 50 mm long reactor cavity (Fig. II.4.5 (b)) divided in three part. In the middle there is a rectangular chamber 6mm high,15 mm wide and 30 mm long realized with high precision. In this way, when the platelet is inserted, a 1 mm gap is determined above the platelet thus creating the combustion chamber.

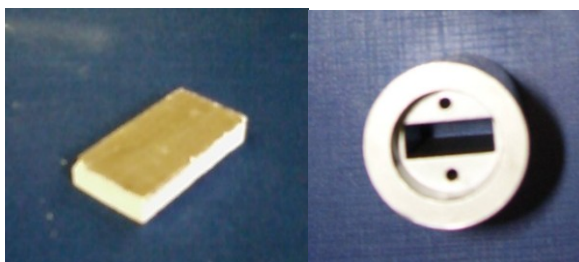


Fig II.4.5 LM-20 platelet (a) and (b) front view of the stainless steel reactor with the rectangular cavity and dead end holes for thermocouples placements.

At the two edges of the rectangular chamber, there are two circular hollows (d_i 17 mm; $l=10$ mm), that allow to insert two circular SiC foams (45 ppi) used in order to well distribute the mass flow of the gas in correspondence with the inlet and the outlet of the catalyst and, at the same time, to block the platelet in the appropriate position. The fluid dynamics of the reactor is deepened in the Appendix A.

In the first foam, moreover, two circular holes ($d < 1$ mm) are created in correspondence to the ones of the main body that are at 1 mm distant from rectangular chamber. The thermocouples are placed in this dead end holes (Fig. II.4.5), in order to limit their contribution to the reaction and do not alter the flow pattern in the chamber. In this way the thermal profile along the axial direction and the temperature difference between upside wall of the chamber and the downside (i.e. below the platelet) are detected. The 4 thermocouples were sealed thanks to a Multiple-Hole Ceramic gland provided by Conax Buffalo (MHC series; see Fig. II.4.6). The schematic picture of the thermocouples placement is reported in Fig. II.4.7. In particular, three axial temperature (T_1, T_2 and

T_3) measurements were done above the combustion chamber, while a fourth thermocouple is positioned at below the platelet in correspondence of T_2 .

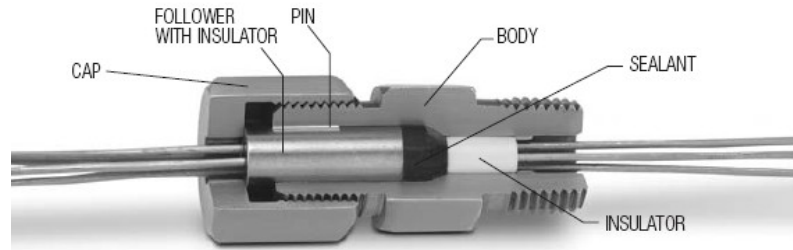


Fig. II.4.6-Section of Multiple-Hole Ceramic Feedthrough (Conax Buffalo).

During all tests, the maximum allowable difference of temperature (in any direction) was below 3°C . This degree of isothermicity was achieved thanks to the appropriate placement of the heating jacket ($L=180\text{ mm}$) and the intrinsic non adiabaticity of the stainless steel reactor.

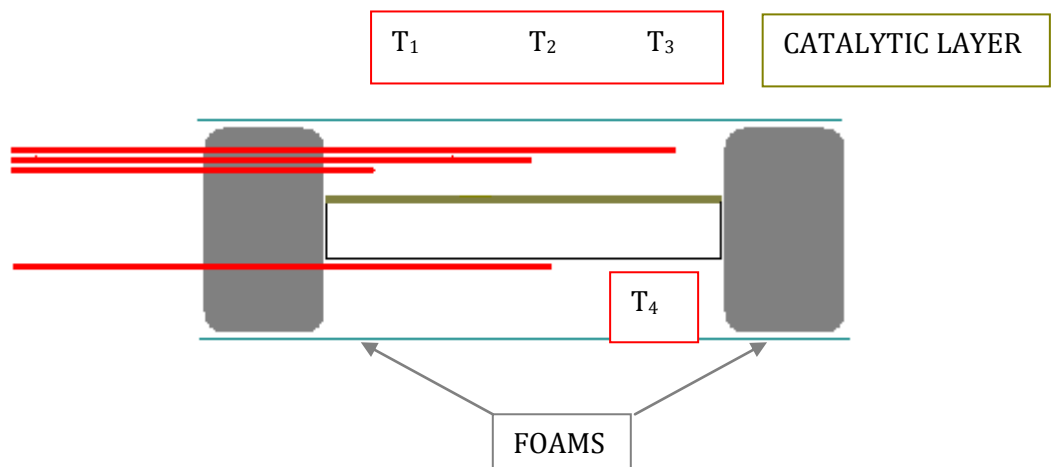


Fig II.4.7 Schematic of thermocouples placement (the measures are not in scale).

II.4.2.2 Operative condition

High diluted CH₄, H₂ and CO mixtures were used for the assessment of the more appropriate kinetic law and the temperature dependence of the kinetic parameters. Before experiment, the catalyst were aged in air at 800 °C for at least 3 hr. However the temperature was always under 620°C achieved for the LM20-A. The O₂ content in the mixtures was set at value below of 10%. Moreover some test were repeated in order to check the repeatability of experiments and the occurrence of deactivation phenomena.

The two studied active phases, Pt and LaMnO₃, are very different as regards their activity towards the different fuels therefore affecting the operative conditions (temperatures, flow rates etc) suitable to gain information on kinetics. For both catalysts a preliminary study on possible range of reaction condition was done (appendix A). In table II.4.1, the operative conditions adopted for the combustion test under pressure are summarized for the two different platelet.

Table II.4.1-Operative conditions adopted for the tests under isothermal condition

Platelet	LM20-A		
	CH₄	H₂	CO
Fuel , %	0.15-1	0.25-1	0.25-1
O₂, %	8.5	2-8.5	2-8.5
Q_{TOT}, splh	55-80	75	75
τ, g·l·s⁻¹	1.7-1.2	1.25	1.25
Platelet	1Pt-A		
Fuel , %	0.25-1	0.25-1	0.25-1
O₂, %	4.2-8.5	2-8.5	4.2-8.5
Q_{TOT}, splh	75	100	30-150
τ, g·l·s⁻¹	1.3	0.98	3.2-0.65

II.4.2.3 Reactor model and numerical methodologies

In order to gain information about the appropriate kinetics mechanism, the model discrimination was done using the criterion of the minimisation of the statistical parameter mean residual sum of squares (MRSS) defined by the following expression:

$$MRSS = \frac{\sum_{n=1}^N (x_{p,n} - x_n)^2}{N_{obs} - N_{para}} \quad \text{eq. II.4.1}$$

Where the $x_{p,n}$ and x_n are respectively the predicted and experimental conversion of the n th experiment, N_{obs} is the number of experimental observation and N_{para} are the number of parameter used in the model.

In order to express the experimental conversion functionality on temperature, pressure, reactants molar fractions and contact time, it was necessary to develop an appropriate reactor model.

Accordingly, the reactor was assimilated to a Plug Flow Reactor (PFR) in which mass transfer diffusion can be neglected and under these assumptions, that were verified in the appendix, the material balance on fuel between two consecutive reactor sections under steady state condition imposes:

$$Q_{tot} \cdot C|_z - Q_{tot} \cdot C|_{z+dz} - r \cdot dW = 0 \quad \text{eq. II.4.2}$$

where Q_{tot} is the total volumetric flow rate, C is the concentration of fuel and dW represents the weight contained in the infinitesimal element of volume $S \cdot dz$ according to eq. II.4.3

$$\rho_{cat} \cdot S \cdot dz \quad \text{eq. II.4.3}$$

where S represents the transversal section of the catalyst layer and ρ_{cat} is the apparent catalyst density.

It is well known that by introducing the fuel conversion $x = \frac{C^o - C}{C^o}$ and contact time τ defined as follows:

² for the sake of brevity the subscript fuel is omitted

$$\tau = \frac{w}{Q_{tot}} \Rightarrow d\tau = \frac{dw}{Q_{tot}}, \quad \text{eq. II.4.4}$$

with the appropriate substitutions and mathematical operations, the relation between conversion and contact time for a PFR reactor is given by eq. II.4.5:

$$-r = \frac{C^0 \cdot dx}{d\tau} \quad \text{eq. II.4.5}$$

In the case of conversion lower than 10% the reactor could be assimilated to a differential reactor and eq. n II.4.5 can be transformed in eq. II.4.6

$$r_s = \frac{Q_{tot} \cdot C^0 \cdot x}{w_{cat}} \quad \text{eq. II.4.6}$$

while in the case of conversion higher than 10%, the error performed by considering the fuel concentration constant along the reactor and equal to its initial value (C^0) is too high and the more appropriate expression is obtained by integrating the eq. II.4.5:

$$\int_0^{x_{fin}} \frac{dx}{r} = \frac{\tau}{C^0} = \frac{RT \tau}{P \cdot y^0} \quad \text{eq. II.4.7}$$

Where y^0 is the initial fuel fraction, x_{fin} is the final conversion of the experiment, τ is the contact time and P the pressure. Moreover, by means of eq. II.4.7, the final conversion is related to the above mentioned variables (temperature, pressure, contact time and so on) and, after expressing r , also to model parameters (θ). The eq. II.4.7 is valid in the overall range of conversion (0-100%) provided that the impact of mass transfer limitation is not significant.

Therefore the model parameters are identified by the fitting the experimental observed final conversion with the implicit functionality expressed in eq. II.4.7.

It is evident that the eq. II.4.7 could lead to implicit expression that are difficult to manage, even more if we consider that the fitting is non linear, often also in the parameters. Therefore the fitting was done using the least-squares fitting algorithm (Powell algorithm) implemented in the commercial program Scientist (Micromath).

This program can provide, other than evaluated parameters, several statistical output data, such as MRSS, confidence intervals and other statistics.

In the following only differences among MRSS values will be discussed in order to define the best model, F values, suggesting the same considerations.

II.4.3 Autothermal Test

II.4.3.1 Reactor configuration

The influence of several parameters, especially pressure, on methane combustion was evaluated at conditions more similar to the real ones. The catalytic systems chosen were LM-C900-50 and LMC600-20 (see table II.1.4 for catalysts specifications). Perovskite was selected since its behavior under pressure is less known respect to Pt. Moreover, a honeycomb substrate was chosen to load significant amounts of catalyst and at the same time to limit the pressure drops.

As in the case of paragraph II.3.2, the catalytic monolith was stacked between two inert foams, (Mullite, 45 ppi; L=50mm D=9mm) acting as radiation shields (fig. II.4.8), and all the elements were wrapped in ceramic wool blanket and tightly placed in the circular cavity of stainless steel reactor (Di=11mm, L =70 mm) inserted in the heating jacket used for pre-heating the reacting mixture.



fig. II.4.8- Monolith stacked between inert foams.

In Fig. II.4.9, the thermocouples placement is sketched. In particular, two thermocouples were placed in the inner of the reactor in order to monitor the pre-heating of the gasses and the temperature of the catalyst respectively at the center of the first heat shield (T_{pre}), and at the middle of the catalyst monolith (T_{cat}). The thermocouples were sealed thanks to a Multiple-Hole Ceramic

gland (supplied by Conax Buffalo). A third thermocouple was positioned outside of the reactor, contacting the stainless steel external wall, in order to evaluate the heat exchange with the outside. In order to improve gas feed pre-heating an heating tape, whose temperature in all the experiments was set to 295°C, was placed upstream the reactor.

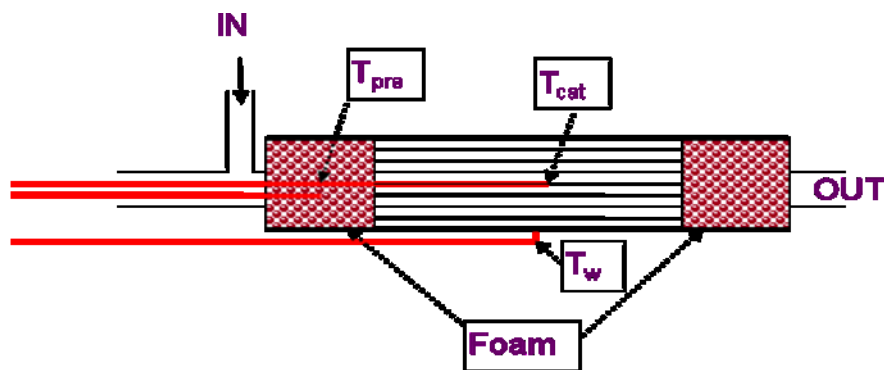


Fig. II.4.9-Schematic of thermocouple placement

II.4.3.2 Operative condition

In order to achieve pseudo-autothermal conditions, thermal power developed by mixture combustion must be high enough to sustain catalyst temperature higher than external one. As a consequence, an high overall heating value mixture is required, differently from isothermal tests where a strong reactant dilution was taken into account. However, in most cases the heat losses, especially in a lab-scale setup, are too high to allow thermal auto-sustainability through reaction heat alone; external heat is supplied in order to keep the entire system at a controlled temperature by the heating jacket. In the tests carried out, two different external heating were considered by setting the jacket temperature at 600 and 700°C which correspond to internal temperatures equal to 460 and 530°C. This temperatures could be considered as pre-heating temperatures. In this way different adiabatic degrees can be simulated.

The specific features of the considered $\text{CH}_4/\text{O}_2/\text{N}_2$ mixtures are reported in Table II.4.2 for the different pre-heating temperatures.

Table II.3.1-Operative conditions adopted for the tests under autothermal condition

	Pre-Heating Temperature, °C	
	460	530
CH₄, %	2.5-4.5	1.0-3.0
O₂, %	10.0	
N₂, %	balance	
Equivalence ratio, Φ^*	0.5-0.9	0.2-0.6
Heating value, kJ·NI⁻¹	0.8-1.4	0.3-0.9
Q_{TOT}, splh	30-90	40
Re^{IN}, @STP	11-33	14
GHSV, @ STP	1.3-6.7·10 ⁴	1.6·10 ⁴
P=1÷10 Bar		

In all the cases the oxygen content was set well below the Minimum Oxygen Content (MOC) content, moreover the maximum methane content was 4.5% that is slightly below the LFL of methane.

The effect of co-feeding hydrogen and carbon monoxide on methane ignition has also been studied. In order to stress eventual differences a shorter (20 mm long) catalyst has been used and the total flow rate was set at 100 splh. Methane ignition has been conducted by a 2% vol. mixture, while in the CH₄/CO/H₂ mixture the concentrations are respectively 1.5%, 0.6% and 0.9% vol., developing the same thermal power of the CH₄ alone mixture. The concentrations have been chosen in order to obtain a CH₄/(CO+H₂) ratio equal to 1 and a H₂/CO ratio equal to 1.5.

III CATALYSTS CHARACTERIZATION

III.1 BET Analysis on Powders Catalysts

The specific surface areas (SSA) of the catalysts, fresh and used, are reported in table II.1.1.; they are lower than those of the starting γ -alumina, generally about 200 m²/g, probably because of a partial occlusion of pores due to the deposition of active elements. As a matter of fact, the catalyst showed the following scale with respect to the SSA:

1Pt>LM20>1PtLM20, inverse respect to the active phase loading.

Tab. III.1.1 SSA measured according to the BET method. Fresh samples are those calcined at 800°C for 3 hr. Used sample are those used in the TPR experiments.

<i>Code</i>	<i>SSA m²/g</i>	
	fresh	used
La-γAl₂O₃	185	171*
LM20	103	113
1Pt	157	161
1PtLM20	75	98

* Treated at 800°C under N₂-CO (CO=1450 ppm) flow.

According with the results of Giebler et al. (2007), the SSA of the bi-functional 1PtLM20 is lower respect to the non doped catalyst due to the co-presence of both active phases.

Moreover as a consequence of the H₂/CO reduction and re-oxidation cycles, the SSA of the used catalyst are higher than those of the fresh ones. On the contrary in the case of the sample La- γ Al₂O₃ the treatment under CO-N₂ flow (1450 ppm) up to 800°C results in a decrease of SSA. These results suggest that the H₂ causes a redistribution of the active phases improving their dispersion. This findings however is in contrast with the work of Demoulin et al (2006), who studied the effect of H₂

addition to methane under reaction condition on the 10%Pd/ γ Al₂O₃. As a matter of fact they found that the Pd dispersion was drastically reduced in presence of H₂ accompanied with a slight SSA decrease.

III.2 H₂-CO Temperature Programmed Reduction

III.2.1 H₂-TPR

The figure III.2.1 shows the H₂-TPR on LM20 sample according to the procedure reported in the paragraph II.1. Moreover for the sake of clarity, in fig. II.3.1, are also reported the O₂ and CO₂ signal (μ mol/gcat·min) registered during an N₂-TPD on the same sample.

The H₂ uptake signal shows two peaks. The first at about 200°C and the second at about 350°C. Moreover the complete reduction of the sample occurs at temperature below 500°C thus indicating a great reducibility of the perovskite sample. In table III.3.1 are summarized the above mentioned peaks temperature, the total hydrogen uptake (μ mol/g) and the computed H₂/Mn ratio considering that the only reducible specie by means of hydrogen in this range of temperature is Mn.

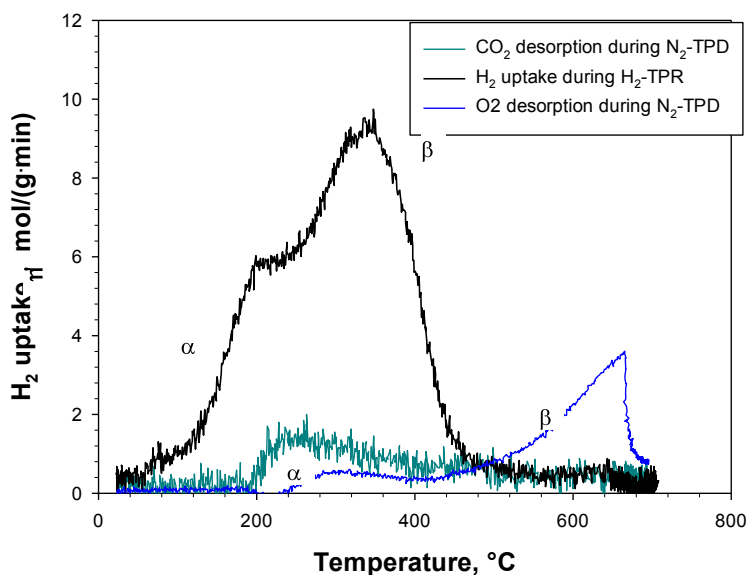


Fig. III.2.1 H₂TPR (2%vol H₂ in N₂); and N₂-TPD: heating rate 10°C/min up to 700°C. Q=15 Nl/h, LM sample pre-treated up to 700°C in air flow.

Table III.2.1 H₂TPR on LM.

H ₂ cons/g _{cat} , μmoli/g	H ₂ /Mn	Mn ⁴⁺ , %	T _α , °C	T _β , °C
413	0.56	12	200	350

The two peaks in the TPR correspond to those in the O₂ signal during TPD and, as discussed by Seyama (1992) and reported in several papers (Lisi et 1999, Rossetti and Forni, 2001; Fino et al 2003; Russo et al, 2005), correspond to the two types of chemisorbed oxygen species: a low-temperature species, generally called α , that desorbs in the 300–600 °C range, and a high-temperature one, named β , desorbed at 600–900 °C. Moreover, as pointed out by Fino et al (2006), the presence of a reducing agent (i.e hydrogen) induces the β oxygen release at temperature significantly lower than the TPD ones.

The experimental H₂/Mn ratio founded in this test is equal to 0,56, a value that is slightly higher than the theoretical one of the solely reduction of Mn³⁺ to Mn²⁺. This value suggests an initial average oxidation state of manganese between +3 and +4 and roughly 12% Mn⁴⁺; this value is lower than 30% which is typical of LaMnO₃ bulk and related to an oxygen excess of 0.18 (Lisi et al 1999; Saracco et al 1999). The lower value of Mn⁴⁺ could be related to the interaction of a part of Mn with the alumina as already reported by Cimino et al (2000) and Choudary et al 2002. Another explanation could be related to the presence of La₂O₃ used for the alumina stabilization. As a matter of fact as reported by the group of Specchia (Fino et al, 2006) in the case of La-Li-Cr perovskite, promoting the La substoichiometry with lower valence alkali metals, causes an increase of Cr⁴⁺ to maintain electroneutrality. In this sense, it could be argued that the presence of La₂O₃ reduce the tendency of Mn³⁺ to be oxidized to Mn⁴⁺.

Accordingly the two peaks could be attributed to the two step reduction of Mn⁴⁺. (Lisi et al 1999; Ciambelli et al, 2000). But, accordingly to Ciambelli et al, (2000) also in the first peak a part of Mn³⁺ is converted to Mn²⁺.

The catalytic activity of lanthanum manganate is strongly related to the presence of Mn⁴⁺. As a matter of fact when Mn³⁺ is oxidized to Mn⁴⁺, in the mean time the formation of cation vacancies

occurs accompanied with the well-known excess of oxygen compared to stoichiometric one. A similar behavior was also found with other transition metals like Cr (Fino et al, 2003).

In fig. III.2.3, the H₂ uptake obtained in the case of the 1Pt sample is reported as a function of the temperature.

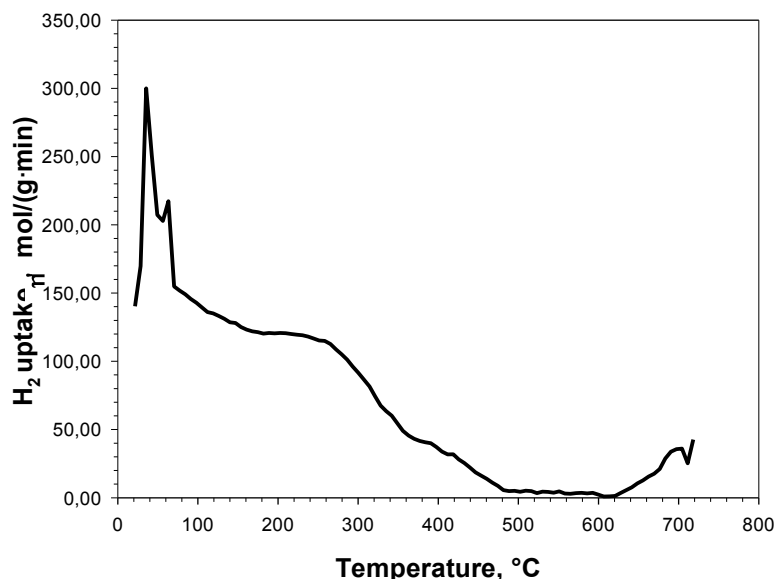


Figure III.2.3 H₂-TPR on 1Pt; pre-treated under air flow up to 700°C; Q=15 splh, H₂ (2vol%) e N₂ (balance); heating rate 10°C/min up to a 750°C.

The H₂-TPR on 1Pt sample shows that the reduction occurs at ambient temperature as the sample is exposed to the reducing mixture and the most part is reduced at temperature below 300°C. The results are summarized in Table III.2.2

Tabella III.2.2 H₂-TPR results for 1Pt.

H ₂ cons/g _{cat} , μmoli/g	H ₂ /Pt
56	1.05

The H₂/Pt ratio is compatible with the reduction of Pt from Pt⁺² to the metallic state. As expected, Pt is more reducible than LM sample under hydrogen flow.

The behavior of 1Pt-LM20 sample under reducing atmosphere is even different. As a matter of fact, the TPR signal, reported in Fig. III.2.3, is quite different from the two single phase signals.

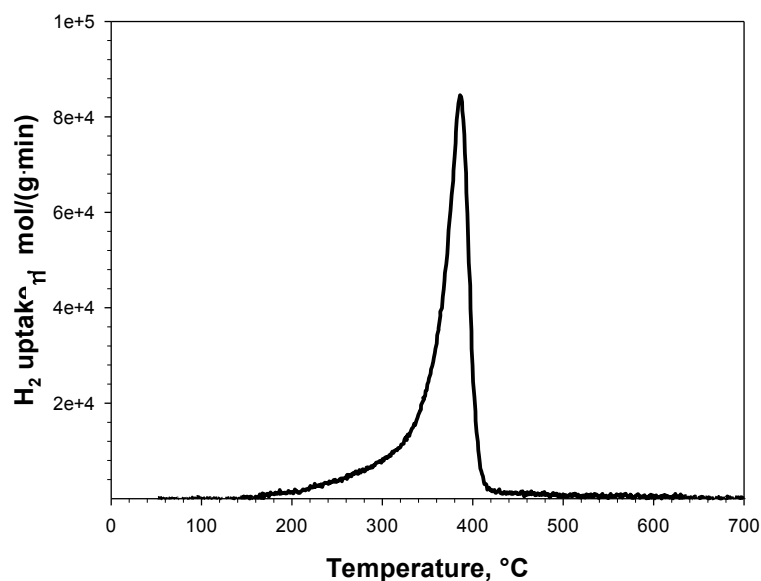


Figure III.2.3 H₂-TPR on 1PtLM; pre-treated under air flow up to 700°C; Q=15 splh, H₂ (2vol%) and N₂ (balance); heating rate 10°C/min up to a 700°C.

The sample reduction begins about at 200°C. The signal shows a narrow peak centered at 385°C with an high intensity. This behavior suggests that it is necessary a threshold temperature to allow a part of the noble metal to emerge from the perovskite structure in which it is partially included. The last statement is in agreement with the lower catalytic activity showed by the Pt dispersed on LaMnO₃ with respect to that deposited onto alumina towards hydrogen oxidation up to 250°C (Scarpa et al, 2009). This is in line with the work of Giebler et al. 2007 that found that unless a reduction pre-treatment the addition of Pt , Pd and Rh was not useful to enhance the LaMnO₃ and ascribed this fact to the incorporation of noble metals into the perovskite structure.

In table III.2.3 the results of the H₂-TPR on the bifunctional catalyst are reported

Table III.2.3 H₂ TPR on 1PtLM.

H ₂ cons/g _{cat} , μmoli/g	H ₂ /(Pt+0.5*Mn)	T, °C
462	0.99	385

In conclusion, comparing the temperature of end reduction and peak temperatures appears that the scale of reducibility by hydrogen appears to be the following: 1Pt > 1PtLM > LM.

III.2.2 CO-TPR

The affinity of the catalysts towards a different reducing agent was investigated by means of CO-TPR. It was also found that the contribute of the support in the CO-TPR of the catalyst could not be excluded. Thus, for the sake of clarity a CO-TPR on La- γ Alumina sample is first presented.

In fig. III.2.4 the CO, CO₂ and H₂ signals recorded during a CO-TPR on La- γ Al₂O₃ sample are reported.

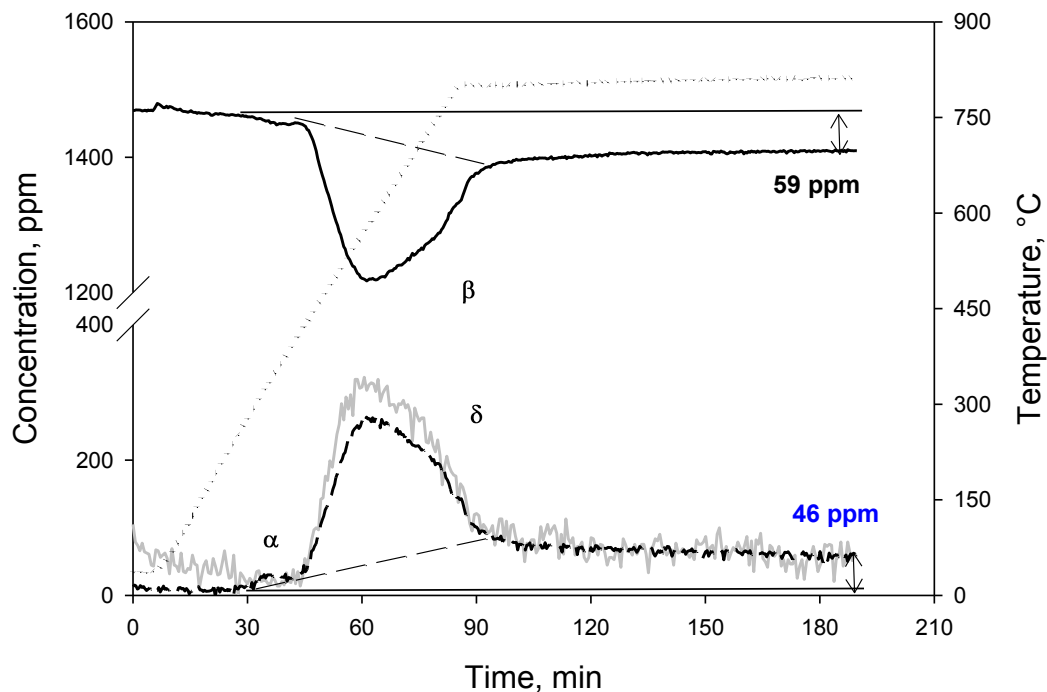


Figure III.2.4 CO-TPR on La- γ Al₂O₃; pre-treated under air flow up to 800°C; Q=15 splh, CO 1480 ppm, N₂ (balance); heating rate 10°C/min up to a 800°C;

Moreover it is evident that the CO uptake (i.e. CO₂, H₂ production) does not terminate even after one hour of exposure at 800°C under reducing atmosphere. Therefore, from these evidences it is postulated that the reaction occurs between CO and two OH groups present on the alumina surface. As a matter of fact the total amounts of CO, H₂ and CO₂ during the TPR are in good agreement with

the hydroxyl groups concentration, estimated equal to 3.56×10^{-6} mol m⁻² for γ -alumina (Caceres et al, 1990) which correspond to 608 μ mol OH g⁻¹ for the support used in this work.

In table III.2.1 are resumed the global CO consumption, CO₂ and H₂ production are reported; in order to limit the contribution of the high temperature phenomenon, also partial results were obtained integrating the curves with respect to the baseline (the dashed line in Fig.II.2.4). Such operation does not lead to expected values for the contribution of each peak(i.e. reduction phenomenon), but can provide a qualitative representation of the process.

Table III.2.1 Global and partial results obtained for the CO- TPR La- γ -Al

	<i>Global</i>	<i>α peak</i>	<i>β peak</i>	<i>γ peak</i>
CO/g_{sup}, μmol/g	191	-	91	-
CO₂/g_{sup}, μmol/g	181	1.15	-	103
H₂/g_{sup}, μmol/g	184	-	-	105
Temperature, °C	-	330	600	600

Moreover, in order to further exclude the occurrence of the Boudouard reaction causing the formation of coke on the alumina surface a TPO analysis was performed following the TPR experiment to evaluate the presence of coke through the detection of CO₂ possibly produced. In figure III.2.5 the result of TPO is reported.

The CO₂ concentration formed during the TPO experiment is orders of magnitude smaller than that possibly related to the oxidation of coke in theory produced by the reaction (eq.III.2) and the peak temperature (240°C) too low to be associated to a combustion reaction. The CO₂ detected during the TPO seems more probably attributable to CO₂ adsorbed as gas impurity in the previous treatments also taking into account that the presence of lanthanum oxide promotes surface carbonation. On the other hand, the very small peak at 550°C can be associable to coke formation, however, its negligible amount can exclude the dominance of the Boudouard reaction.

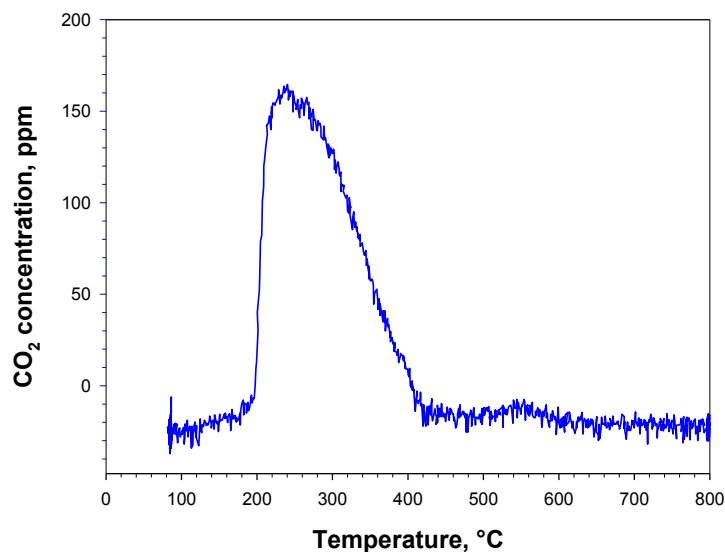


Figure III.2.5 CO₂ concentration profile during TPO in air up to 800°C after a CO-TPR on La- γ Al₂O₃; Q_{tot}=5 splh. After the CO-TPR the sample was cooled down to room temperature in the reducing CO/N₂ mixture.

Tab. III.2.2 TPO result on La- γ -Al.

<i>CO₂/g_{sup}, μmoli/g</i>	<i>T, °C</i>
18	240

Analyzing the Fig. III.2.4, it is also evident that the phenomenon occurs for at least two species of OH with different affinity towards CO. Some OH species are found to be reducible at temperature below 600°C, while other start to be reduced at 800°C. As a matter of fact, the flat profile for CO, CO₂ and H₂ at 800°C, thus indicating a very slow reduction phenomena, suggests that there are hydroxyls species less prone to be reduced by CO. This hypothesis was in agreement with the work of Morterra and Magnacca (1996) that showed that, for transition aluminas are possible three different kind of hydroxyls (linear, bridged and tri-bridged).

Since the phenomena was clearly explained in the case of the support, for the rest of the section the H₂ profile was not showed since it is like the CO₂ one except for the low temperature α peak of CO₂ that is likely attributed to the desorption of CO₂ taken as gas impurities (See Fig.III.2.4).

Figure III.2.6 reports the CO and CO₂ profiles for a CO-TPR carried out on LM20 sample according to the above mentioned procedure. The CO content on reducing mixture is of 1750 ppm and the TPR was stopped after 6 minute after the 700°C was achieved.

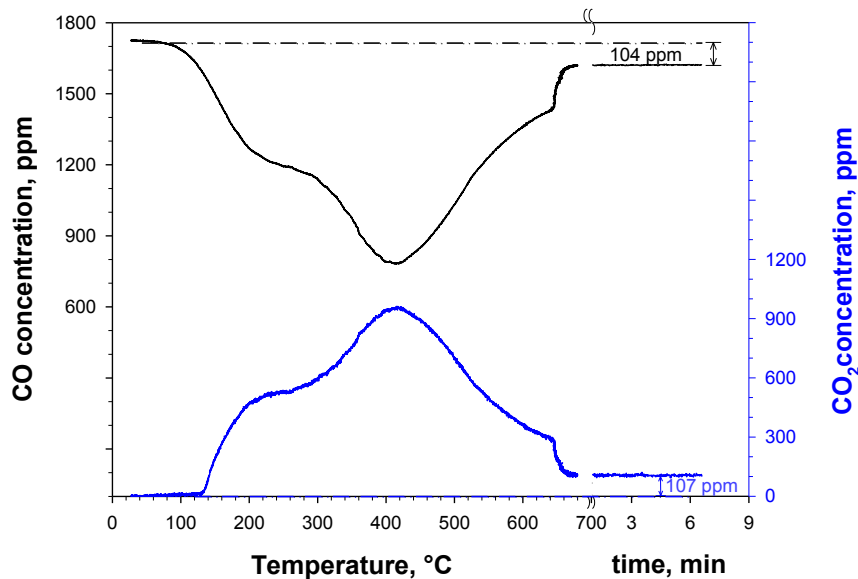


Figure III.2.6 CO-TPR on LM20; pre-treated under air flow up to 800°C; Q=15 splh, CO 1750 ppm, N₂ (balance); heating rate 10°C/min up to a 700°C;

It is evident that the CO consumption starts at temperature even below 100°C but contemporary no significant CO₂ desorption is detected up to about 150°C. It is possible that the CO reacts with an α oxygen specie at low temperature but that the CO₂ remains adsorbed and desorbs at higher temperature. Thus it is expected that at temperatures <150°C the reaction occurs but the rate limiting is the product desorption. At higher temperature it was observed that CO and CO₂ profile are specular. Maybe, in this condition the rate limiting step becomes the migration of the more bounded oxygen species β -oxygen from the perovskite structure. This behavior is hence in agreement with what reported in paragraph III.2. As a matter of fact, both the profiles show a shoulder at about 200°C and a peak centered at 420°C. These temperatures are higher compared to those of the H₂-TPR partially due to the less reducing power of the CO mixture containing only 1750 ppm. Cornering the high temperature behavior the explanation refers only to the support contribute for the reaction. As a matter of fact was evident that the difference between CO and CO₂ concentration and their initial values are respectively of 104 ppm and 107 ppm.

In Fig. II.2.7 a and b the CO and CO₂ profile recorded during a second CO-TPR on the same sample with an higher (4h) time on stream at high temperature are reported; the profiles of the first CO-TPR are also reported for comparison. Also in this case the LM20 sample was pre-treated under air flow up to 700°C in order to restore the oxidation state.

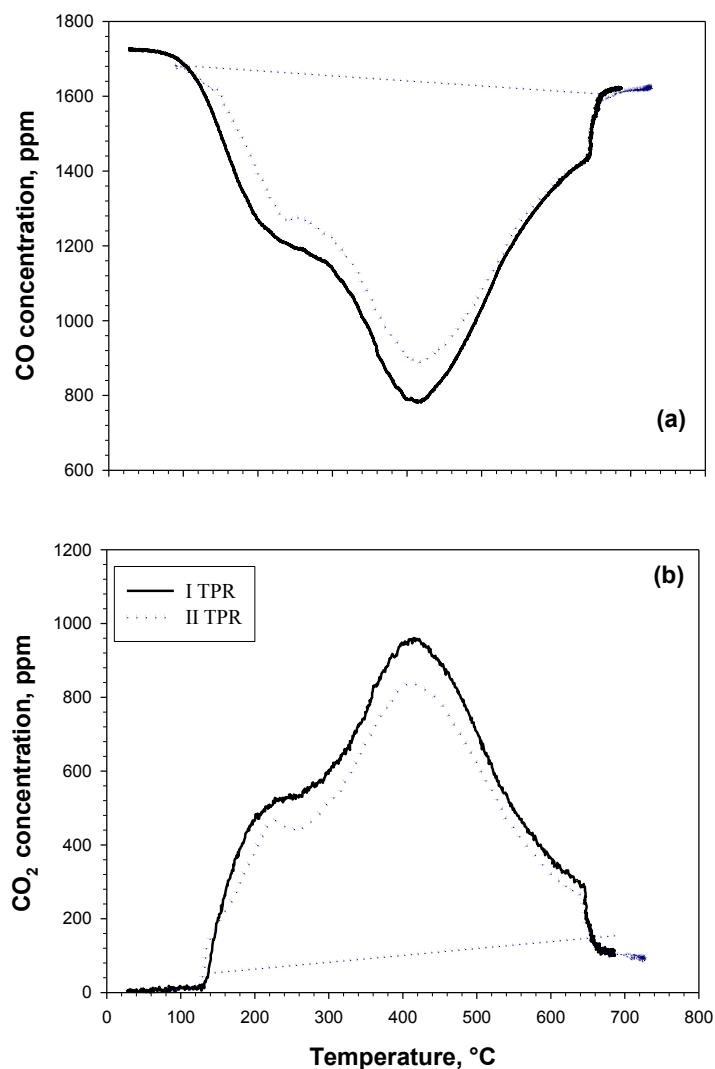


Figura III.2.7 (a)CO and (b) CO₂ profile s during CO- TPR on LM20 sample. Pre-treated in air up to 700°C; Q=15 splh, CO (1725 ppm) and N₂ (balance); heating rate of 10°C/min up to 700°C.

From Fig.III.2.7 it appears that the shapes of the two profiles are qualitatively equal each other especially in the case of the high temperature behavior, thus indicating that the support contribution does not change for the two reduction tests. On the contrary, it is evident that the peak intensities are lower in the case of the second TPR as showed in table III.3 where the peak

contribution was roughly estimated by integrating the curves with respect to dotted lines reported in Fig. III.2.7.

Tab. III.2.3 CO TPRs results on LM20

TPR di CO	CO _{cons} /g _{cat} , μmoli/g	CO/Mn
I	501	0.66
II	419	0.54

Therefore, it appears that the reducibility of the fresh catalyst is not completely restored when the catalyst was treated under reducing conditions. A possible explanation is related to the strong interaction of CO with Mn³⁺ thus forming a carbonate species with the lattice oxygen (Tejuca et al,1987). Accordingly it is possible that the reduction with CO affect the perovskite structure.

In Fig. III.2.8 shows a CO-TPR performed on the 1Pt samples with a time exposure at 800°C of 1 h.

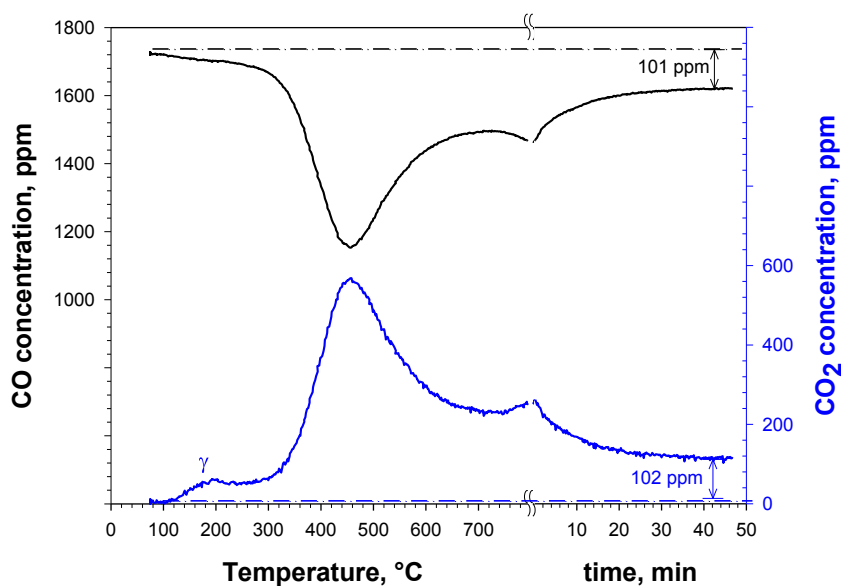


Figure III.2.8 CO-TPR on 1Pt; pre-treated under air flow up to 800°C; Q=15 splh, CO 1750 ppm, N₂ (balance); heating rate 10°C/min up to a 700C;

Also in this case the CO and CO₂ profiles are mirrored with a main peak at 460°C and a long tail at 800°C thus suggesting the possibility of a second peak at temperature above those investigated. The

latter aspect, that was not observed on LM20 sample, suggest that Pt strongly affects the alumina surface behavior in presence of CO. The CO_{cons}/g_{cat} is reported in table III.2.4 along with the calculated CO/Pt ratio.

From the data reported in Table III.2.4 appears that the Pt contribution could not be separated from those of the support, suggesting that the alumina interaction with CO is strongly mediated and promoted by the presence of the noble metal.

As a matter of fact, it was suggested by several authors that hydroxyls, present on the surface of several support like SnO_2 and alumina, could participate in the oxidation of CO chemisorbed on Pt sites. (Cominos et al. (2005)).

Tab. III.2.4 CO TPR on 1Pt

CO-TPR	CO_{cons}/g_{cat} , $\mu\text{moli/g}$	CO/Pt
I	336	6.6

Finally, in the Fig.III.2.9 the CO and CO_2 concentration registered during a CO TPR on the 1PtLM20 sample are reported.

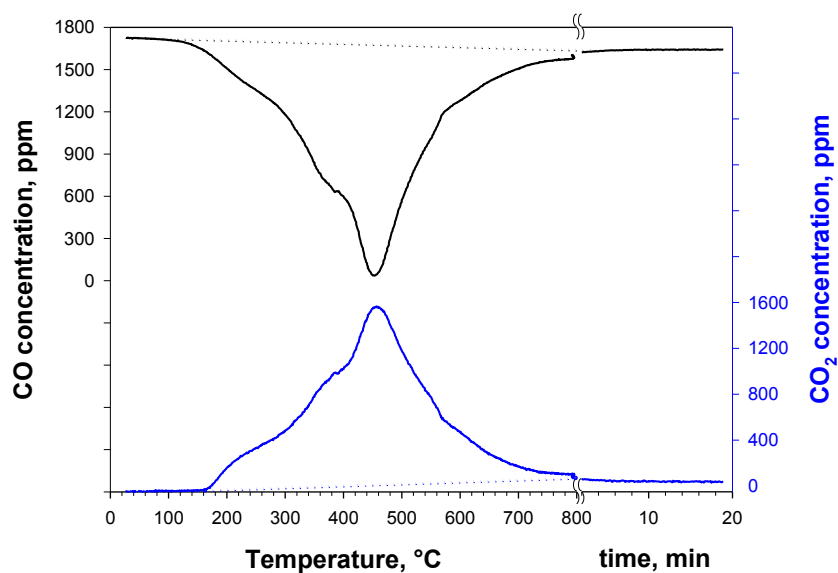


Figure III.2.9 CO-TPR on 1PtLM20; pre-treated under air flow up to 800°C; Q=15 splh, CO 1750 ppm, N_2 (balance); heating rate 10°C/min up to a 800C;

The two concentration signals show two shoulders 220°C and 340°C while the main peak is centered at 460°C. The CO consumption is reported in table III.2.5.

Tab. III.2.5 CO TPR on1PtLM.

$\text{CO}_{\text{cons}}/\text{g}_{\text{cat}}, \mu\text{moli/g}$	$\text{CO}/(\text{Pt}+0.5\cdot\text{Mn})$
640	1.4

The CO-TPR performed on the three sample are collected in Fig III.2.10. It appears that the temperature of the main peak of the bi-functional catalyst correspond to that of the 1Pt sample. As concerning the peak morphology, respect to the 1Pt it is evident the presence of the two shoulder peak at low temperature. These two shoulder peaks, roughly correspond to those of the LM20 sample, but shifted to higher temperatures.

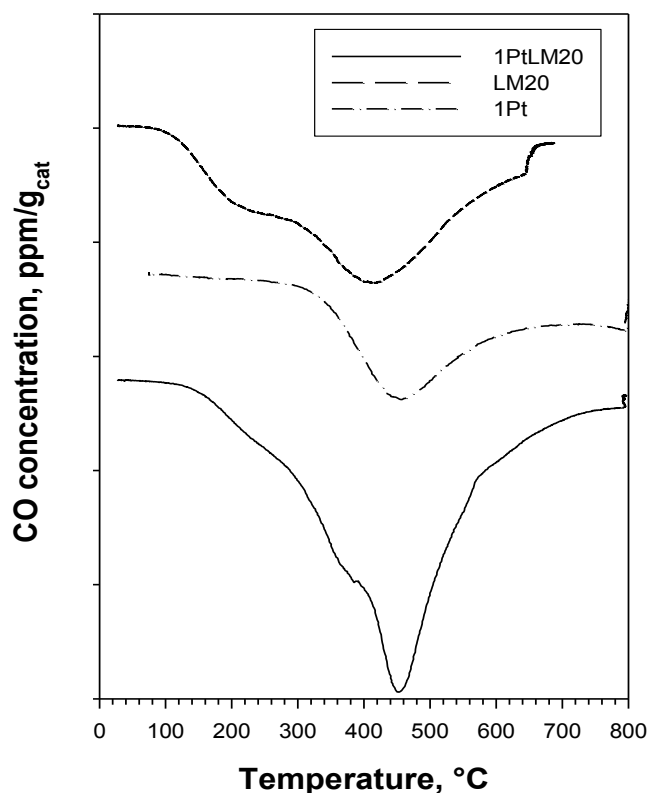


Figure III.2.10 CO concentration profile during the CO-TPR on all the three samples pre-treated under air flow up to 800°C; Q=15 splh, CO 1750 ppm, N₂ (balance); heating rate 10°C/min up to a 800C;

In conclusion, comparing the temperature of end reduction and peak temperatures appears that the scale of reducibility by CO appears to be the following: 1Pt<1PtLM<LM.

III.3 Pt volatilization study for the bi-functional 1Pt-LM20

In table III.3.1, the codes and relative calcination procedures of the bi-functional catalyst are reported; a simple dehydrated ample has been reported as reference.

Table III.3.1-Sample nomenclature according to the calcination procedure

<i>Sample denomination</i>	<i>Description</i>	<i>Period, hr</i>	<i>Calcination temperature, °C</i>
1PtLM20/D	Dehydrated	-	-
1PtLM20/C-550	Calcined	3	550
1PtLM20/C-650		3	650
1PtLM20/C-800		3	800
1PtLM20/C-1000/2		2	1000
1PtLM20/C-1000/4		4	1000

In Table III.3.2, the corresponding results of the ICP analysis are reported. Increasing the calcination temperature causes an increase of the oxygen content in the samples (i.e. samples are more oxidized) and, as a consequence, the metal content percentages of Al, Mn, La and Pt diminish.

Table III.3.2-ICP results

	D	C-550	C-650	C-800	C-1000/2	C-1000/4
Al	40	37,7	36,6	32,6	29,57	28,05
Mn	3,1	3	2,93	2,6	2,68	2,52
La	10	9,9	9,6	8,7	8,5	8,3
Pt	0,92	1	0,92	0,84	0,16	0,08
O	45,98	48,4	49,95	55,26	59,09	61,05

In order to limit this misleading effect and assess the real volatilization of Pt, the percentages are recalculated by setting the Al percentage at the value of the 1PtLM20/D for all the calcined samples. According to this procedure, the recalculated metal content are diagrammed in Fig.III.1.1.

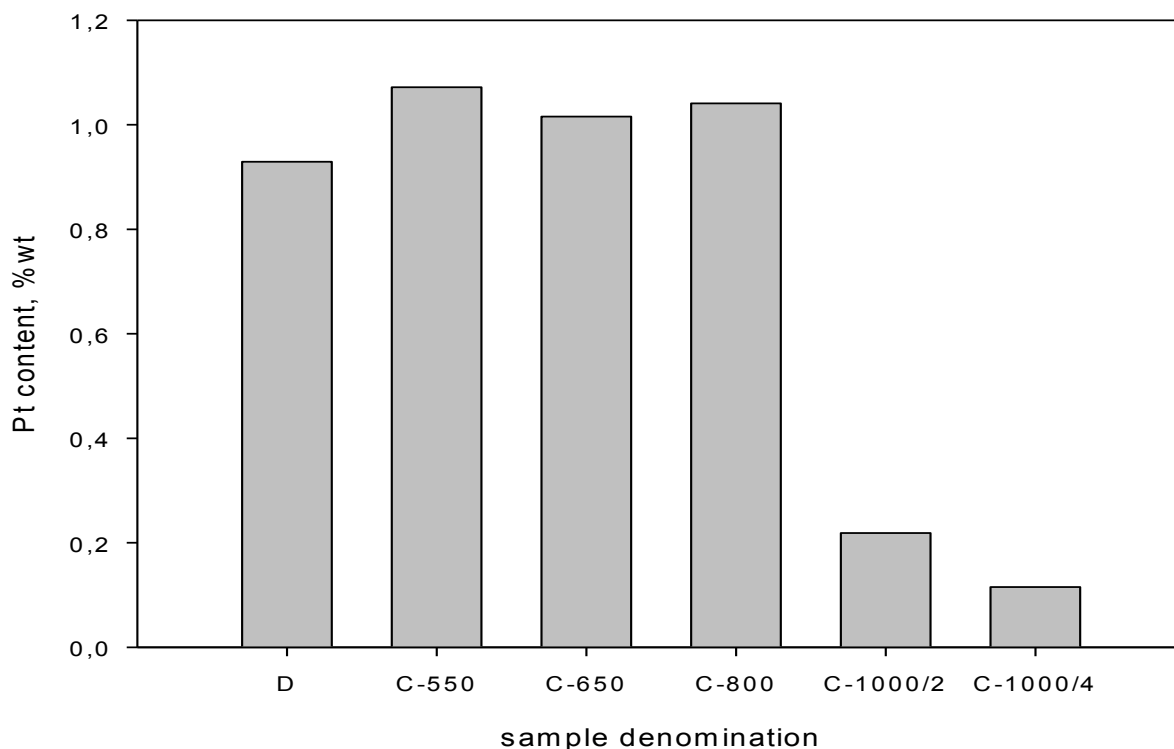


Figure III.3.1 Pt weight concentration measured by ICP for bi-functional catalysts calcined at different temperatures

It clearly appears that, up to 800°C, the Pt amount does not change (i.e. no volatilization occurs), while for a calcination temperature equal to 1000 °C the noble metal percentage drastically drops to a value of 0,02 (one fifth of the initial value). Moreover extending the time exposure to 4 hr at 1000°C, causes a further metal volatilization.

From these results, it appears that the perovskite structure allows to avoid Pt volatilization up to 800 °C, for temperatures above this threshold value, the Pt volatilization occurs.

IV-ATMOSPHERIC AUTOTHERMAL RESULTS

Before discussing the effect of pressure on the catalytic performance is helpful to elucidate some features of the autothermal response of a catalytic reactor with respect to important parameters such as the pre-heating temperature, of the total flow rate and partial fuel substitution. As previously reported this study was effectuated on a bi-functional Pt –LaMnO₃ supported catalyst that was deposited on a honeycomb substrate. More detail about reactor configuration and catalyst characteristics are reported in paragraphs II.3.2 and II.3.3.

The present study was conduct after catalyst stabilization under reaction condition for about one hour at high temperature ($\approx 1000^{\circ}\text{C}$). No further deactivation has been detected since the maximum reached temperature was 900°C .

IV.1 Methane Ignition And Quenching

The steady-state values of methane conversion as a function of the pre-heating temperature are reported in Fig.IV.1.1a for the combustion of a mixture 2.8%/10%/87,2% vol. of CH₄/O₂/N₂ (MIX1) at a total flow rate of 80slph. Increasing temperature, the conversion appears to weakly increase (low conversion branch) around low values (7-10%) up to 534°C pre-heating temperature that represents the Minimum Ignition Temperature, hereafter called MIT, under the explored conditions. At temperatures higher than MIT methane conversion becomes complete, while reducing the pre-heat starting from the ignited state the catalytic combustion of methane still remains effective, not retracing the curve exhibited during the heating up (high conversion branch); such a behavior is typical of highly exothermic reactions for which a multiplicity of steady states may result from energy and mass balance equations for any given set of inlet conditions to reactor (Hayes et al, 1997) . Decrease pre-heating temperature below 370°C corresponds to a sudden conversion drop restoring low conversion branch performance and quenching occurs. Temperature profiles reported in fig. IV.1.1b are related to the high conversion branch. As assessed above, QT is the entrance temperature measured at quenching conditions and corresponds to 330°C for this experimental set, significantly lower than MIT. Such a discrepancy points out the hysteresis of about 200°C exhibited by the cooling/heating curve.

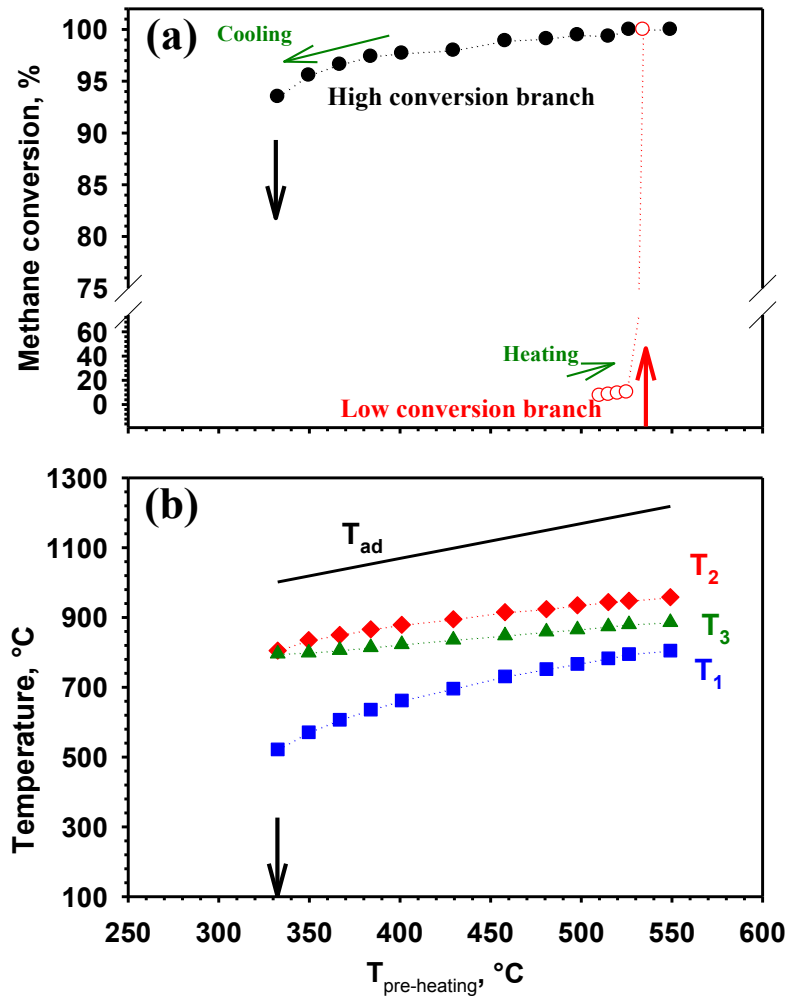


Fig.IV.1.1 (a) steady-state values of CH₄ conversion and (b) temperature profiles for the high conversion branch for the combustion of 2.8%/10%/87,2% vol. of CH₄/O₂/N₂; Q_{tot} 80slph. T_1 , T_2 and T_3 correspond to the temperatures measured respectively at the beginning, the center and the end of the monolithic reactor.

Moreover, temperature profiles (IV.1.1.b) clearly show the presence of a maximum placed in the center of the reactor; based on this result, it is possible to affirm that the reaction front is stabilized at the center of the monolith, whereas the second half of the reactor appears as a post-combustion zone, where the detected temperature decreases because of the heat losses, and the first half of the reactor provides for the gas pre-heating, through an axial heat flux from the combustion zone. The non-adiabaticity of the reactor is clearly confirmed comparing measured and adiabatic temperatures (fig. IV.1.1b), the latter resulting always higher than the others.

By decreasing the pre-heating temperature a general decrease in the temperature level is observed as a consequence of the lower adiabatic temperature, but also due to the small, even if significant decrease of methane conversion. However, a different slope is observed for the three decreasing temperatures. Concerning the entrance temperature, its drop with $T_{\text{pre-heating}}$ is consistent with T_{ad} decrease: this assumption is made clear considering that T_1 and T_{ad} decrease slopes are approximately the same, at least till methane is totally converted (Fig. IV.1.1a). In particular, in consequence of a decrease in pre-heating of about 200°C T_1 decreases of about 280°C. On the contrary, in correspondence with the same decrease in pre-heating T_2 and T_3 decrease is significantly lower and specifically 153 and 90°C respectively, thus suggesting a shift of the reaction front downstream and, as a consequence, an extension of pre-heating zone and a reduction of the post-combustion zone. The effect of the above phenomena is the reduction of the active surface available for fuel activation, leading to incomplete conversion; thus, the generated power decreases and heat losses become more and more significant in the energy balance, causing a continuous decrease of surface temperature and activity down to values incompatible with self-sustained operation (Fig. IV.1.1a).

Before analyzing the effect of a series of parameters on the MIT and QT, the behavior of the system during the ignition of methane combustion is reported in order to better elucidate the mechanisms that rule the behavior of the entire system. In Figure IV.1.2 the transient of the ignition at MIT measured feeding Mix1 at a total flow rate of 80slph is reported. It is possible to distinguish different phases indicated as Zone 1, 2, 3 and 4 in the graph. Zone 1 is characterized by the absence of methane and is useful to monitor the “blank” temperature profile of the reactor. According to the consideration reported in the previous section, the maximum temperature (in the exit section) is assumed to be MIT, corresponding to 534°C under the experimental conditions considered. When methane is added to the gas (Zone 2) a sudden temperature increase is noted due to about 10 % methane conversion.

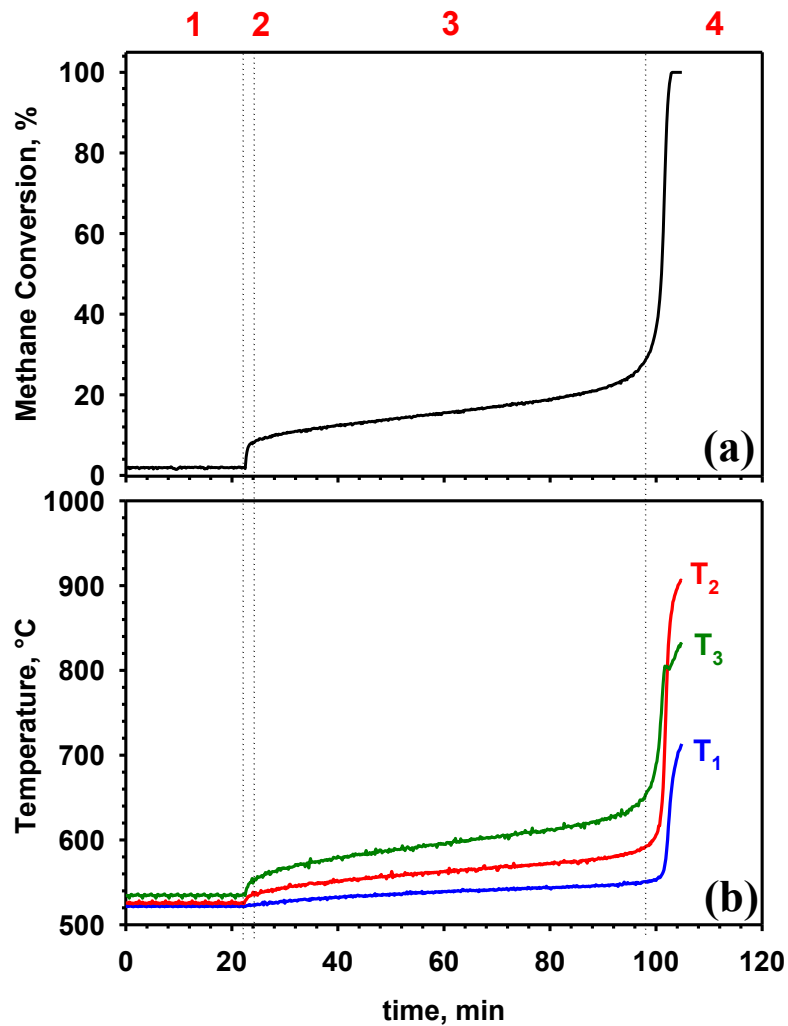


Fig.IV.1.2 (a) CH₄ conversion and (b) temperature profiles during the ignition at MIT for the 2.8%/10%/87,2% vol. of CH₄/O₂/N₂ mixture; Q_{tot} 80slph. T₁, T₂ and T₃ correspond to the temperatures measured respectively at the beginning, the center and the end of the monolithic reactor.

Temperature increases along the reactor co-ordinate according to the increase of methane conversion and consequent heat production. Such a phenomenon roughly indicates that the catalytic combustion is basically a kinetically-controlled process, in a region where convection is the most relevant heat transport mechanism. Subsequently, temperature and conversion continuously but slowly increase with time on stream (Zone 3) due to heat accumulation and progressive rise of reaction rate. A certain induction time (about 75 min) is needed in the Zone 3 to have combustion “run-away”. In the Zone 4, As a matter of fact, the temperature level reached by the system is sufficiently high to allow a sudden increase of the conversion of methane up to reach about 100%. A steep increase in the fuel converted with a negligible production of carbon monoxide is thus observed.

The total selectivity to CO₂ of the process points out that methane is converted on the heterogeneous phase, being CO one main product of homogeneous combustion in this range of operating conditions (Hayes, 1997). Moreover, the available thermal power is totally developed and, as a consequence, system temperature strongly raises, even if clearly it does not reach the value expected in the case of adiabatic temperature raise (heat losses play a relevant role).

The analysis of the three temperature values that have been monitored shows that the ignition takes place at the exit of the monolith where the temperature is higher. As already discussed, convection is the main mechanism of heat transport, so that temperature is higher and higher coming from the inlet to the exit sections of the reactor. Figure 3b clearly shows that a temperature “jump” firstly occurs for T₃ and then for T₂ and T₁. Differently from the thermal profile measured in Zone 2 and 3, in correspondence with the fuel ignition, maximum temperature shifts from the exit to the center of the reactor, suggesting that a different mechanism rules the thermal profile after the ignition, because temperatures are basically determined by the reaction kinetics and the heat losses. Actually, a temperature wave travelling from the exit to the inlet of the reactor is thus observed pointing out the reaction front propagation backwards. A similar ignition behavior has been observed by Cimino et al. (2001). However, temperature decreases with the axial co-ordinate due to the heat losses in the absence of developing reaction heat, since it is very likely that methane has been totally converted very close to the entrance of the monolithic catalyst.

In order to clarify the phenomena related to the quenching, Fig. VI.1.3 shows the transient behavior of the system during the quenching of Mix1 for a pre-heating temperature slightly lower than QT.

In particular, temperature and methane conversion measurements are reported as a function of time respectively in Fig. VI.1.3 a and b. The inlet and the centered temperatures simultaneously start to decrease while the outlet one slightly increases till to exceed T₂. Such a quenching behavior is strictly connected to the presence of important heat losses and it is due to the insufficient gas preheat or insufficient contact time in the necessary high temperature zone and results in the reaction front shift downstream and its subsequent exit from the reactor, leading to temperatures and conversion downfall.

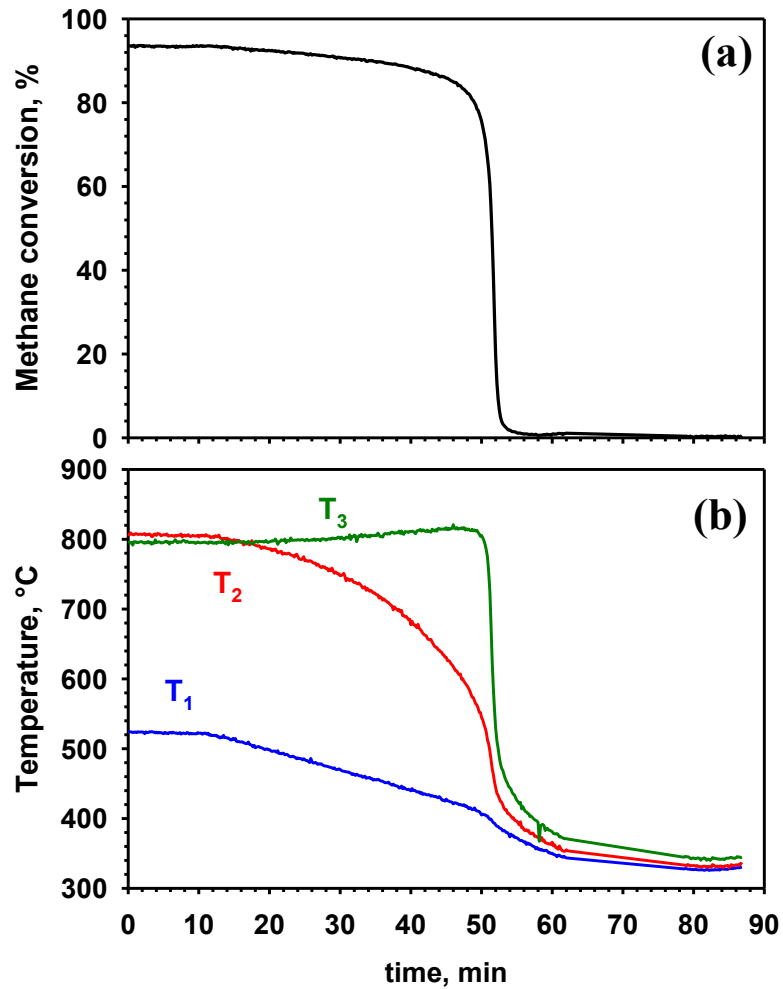


Fig.IV.1.3 (a) CH₄ conversion and (b) temperature profiles during the quenching for the 2.8%/10%/87.2% vol. of CH₄/O₂/N₂ mixture; Q_{tot} 80slph. T₁, T₂ and T₃ correspond to the temperatures measured respectively at the beginning, the center and the end of the monolithic reactor.

With changing the flow rate at fixed composition, i.e. changing the thermal power and transport coefficients, the thermal balances are modified, thus affecting quenching behavior. Fig. IV.1.4 shows the temperatures measured inside the reactor during the high conversion branch at different flow rates. As usually, the reported arrows point out the quenching temperature observed and the window of stable combustion at the different operating conditions. It is shown that the quenching temperature progressively decreases with increasing flow rate from 40 to 120slph, thus extending the limits of stable combustion. On the contrary, it starts to decrease further increasing the gas flow from 120 to 140slph, indicating a different behavior. In particular, T₁ increases by increasing the flow rate from 40 to 80slph; on the contrary, it is practically unchanged varying the gas flow from 80 to 140slph. Considering the temperature measured at the center of the reactor, T₂, it increases in

a larger flow rate range in comparison with T_1 case; particularly, T_2 progressively increases by increasing flow rate up to 120slph while it does not vary any more further increasing the flow rate up to 140slph. Finally, concerning T_3 , reactor exit temperature, it increases in all the investigated flow rate range.

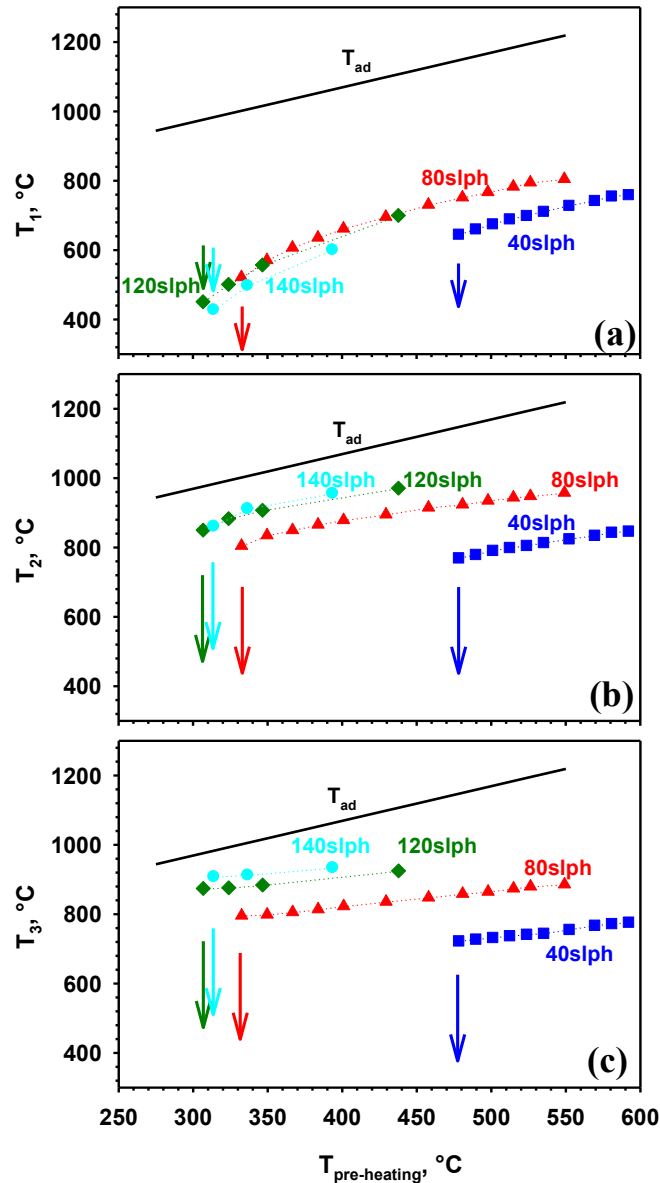


Fig.IV.1.4 Temperatures measured at different total flow rate varying the pre-heating temperature (a) T_1 (b) T_2 (c) T_3 for the 2.8%/10%/87.2% vol. of CH₄/O₂/N₂ mixture;

By increasing the flow rate a dual effect is expected on combustion stability. In particular, considering the same fuel composition, the power developed by the combustion linearly increases with total flow rate. At the steady state and for a non adiabatic reactor, the power released via

combustion is equal to the sum of the power lost through the reactor walls and in the exhausted gases. To balance the increase in the combustion power this sum has necessarily to increase linearly with the total flow rate. However, the heat losses through the reactor walls do not depend on the total flow rate and the sensible heat of exhausted only linearly. Consequently, in order to get over the higher power released via combustion at higher flow rates the system has to reach higher temperatures. In such a way, As a matter of fact, by increasing the total flow rate the power lost in the exhausted gases increases more than linearly; moreover, the heat lost through the walls increases too in consequence of the increase in the heat transfer driving force. As a result, an increase in the flow rate determines an increase in the system adiabaticity level because heat losses are a fraction less and less important of the thermal power increase developed by methane combustion. Nevertheless, an increase in the flow rate brings about a decrease in the contact time and, as a consequence, a possible worsening of fuel conversion, if contact time becomes insufficient. These considerations suggest a tradeoff behavior regarding the total flow rate. Specifically, in a range of low gas velocity, such as to guarantee a sufficient contact time, an enhancement of combustion stability is expected by increasing flow rate. Nevertheless, in a range of gas velocity not more compatible with the total fuel conversion, an increase in flow rate is detrimental for combustion stability causing blowout (Kaisare et al. 2007).

Based on these considerations, the expansion of combustion operation limits (i.e., the decrease in QT) observed by increasing the flow rate from 40 to 120slph is consistent with an enhanced system adiabaticity. Assuming T_3 as the temperature of the exhausted gas, from experimental data one can calculate the power lost in the exhausted gas and comparing it to the total power generated it is possible to evaluate the heat lost through the reactor walls. At a $T_{\text{pre-heating}} \approx 500^\circ\text{C}$, for example, considering a $Q_{\text{TOT}}=40\text{slph}$ the power released via combustion is about 10W and the sensible power of exiting gases is about 3.5W. As a result, the power lost trough the reactor walls is approximately 6,5 W that correspond to a 65% of the total power confirming the pronounced thermal dissipation of the combustor. By increasing the total flow rate and specifically at $Q_{\text{TOT}}=80\text{slph}$ but maintaining the same $T_{\text{pre-heating}} \approx 500^\circ\text{C}$, the power released via combustion is about 20W, the sensible power of exiting gases is about 11W; the power lost trough the reactor walls is thus about 9W that correspond to a 45% of the total power confirming the enhanced adiabaticity of the system. Further increasing the total flow rate from $Q_{\text{TOT}}=80\text{slph}$ to $Q_{\text{TOT}}=120\text{slph}$, at $T_{\text{pre-heating}} \approx 345^\circ\text{C}$ the percentage of heat lost through the reactor walls still decreases from 28 to 17%. As a result, under these conditions loss in combustion stability observed at a pre-heating temperature lower than QT is ascribed to the low power input compared to heat losses through the reactor wall. This particular instability mode occurs at nearly complete fuel conversion and is described as extinction (Kaisare et

al, 2008). By analyzing the thermal profiles reported in Figure IV.1.4, for $Q_{TOT}=40\div 120$ slph a maximum temperature is detected in correspondence with the center of the reactor. Such a maximum increases by increasing the flow rate confirming the enhanced adiabaticity of the system. Moreover, the increase in the flow rate in the specified range brings about an increase in the fuel conversion (not reported) despite of the decrease in the contact time, due to the faster catalytic combustion kinetics consequent to the increased temperature. The dynamics of quenching via extinction has been already discussed and pointed out in Figure 4 at $Q_{TOT}=80$ slph. Such a behavior confirms that combustion stability in those range of flow rate is not limited by fuel conversion but it only depends on the heat losses.

Nevertheless, the worsening in stability observed by further increasing flow rate from 120 to 140slph points out a change of the combustion quenching mode from extinction to blowout. Under these conditions, the increase in the gas velocity brings about a decrease in the residence time in the high temperature zone, due to the drift of the heat wave downstream. Actually, differently from what already found at lower flow rates, a shift in the position of the maximum temperature from the center to the exit of the monolith is observed at $T_{pre-heating}=336^{\circ}\text{C}$. Specifically, at the quenching temperature, T_3 is higher than T_2 . Convection, hence, at a so large flow-rate plays a major role. In addition, an increased flow velocity reduces gas pre-heating, which is critical for light-off. The result is ignition further away from the entrance. As a confirm, at the same pre-heating temperature and close to the quenching point, entrance temperature detected at $Q_{TOT}=140$ slph is about 50°C less than that obtained in the case of $Q_{TOT}=120$ slph. Concerning T_2 , only a little discrepancy is observed in the case of the two different flow rates. On the contrary, the exit of the reactor is about 50°C warmer at $Q_{TOT}=140$ slph, thus evidencing a reaction front closer to the exit when an higher flow rate is considered.

Increasing the equivalence ratio of the fuel mixture could be an effective tool to expand autothermal combustion operation involving an increase in the input power without affecting gas velocity and, as a consequence, gas residence time and fuel conversion. So, by feeding more methane it could be also possible to shift the transition from extinction to blowout quenching mode to higher flow rates. A comparison between QT values of Mix1 and of a mixture with an methane content of 3,8% vol. hereafter called Mix2, combustion is reported in Fig. IV.1.5 as a function of the flow rate. Quenching temperature of Mix2 monotonically decreases with increasing flow rate from 40 to 120slph down to near ambient temperature and results lower than the corresponding value of Mix1, thus extending the limits of stable combustion. It is worth noting that when external preheating is too low it is technically difficult to control set-point temperature of the oven; as a result, critical temperature measurements are not reliable at the highest flow rate, thus suggesting us to avoid investigation at

higher flow rates. The increased combustion stability is due to the higher temperature level developed inside the reactor and related to the higher thermal power developed by the richest mixture, as suggested before. By analyzing the trend of Mix2 quenching temperature with Q_{TOT} , its decrease shows a tendency to level off at the highest investigated flow rates. Such a behavior may suggest a transition from an extinction to a blowout quenching regime by further increasing the flow rate above $Q_{TOT}=120\text{sph}$. If so, the use of richer mixture enlarged the operability limits in terms of pre-heating temperatures, but not in terms of flow rates, quenched via blowout occurring at roughly the same flow rate independently on the fuel mixture equivalence ratio.

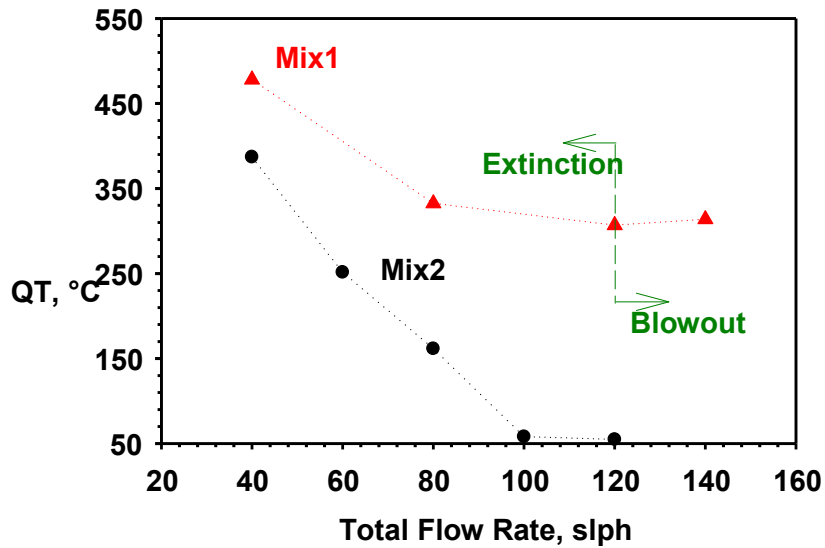


Fig.IV.1.5 QT as a function of total flow rate for the Mix1 and Mix2.

IV.2 H₂ assisted ignition and quenching of methane

In Fig. IV.2.1 the ignition transient of the equimolar CH₄/H₂ mixture hereafter called Mix3, at its MIT is reported. The experiment has been carried out at the same flow rate, $Q_{TOT}=80\text{sph}$ considered in the Mix1 ignition test. In particular, thermal profile inside the monolith (Fig.IV.2.1a) as well as CH₄ and H₂ conversion measurements (Fig. IV.2.1b) are reported as a function of time on stream. As it was shown for the experiment of Mix1 light-off (Fig. IV.1.2), in Figure IV.2.1 it is possible to distinguish four regions, Zone 1, 2, 3 and 4. Zone 5 corresponds to stable operation suspending CH₄ feeding, i.e. feeding alone H₂ (Mix4). As stated in the experimental section, the temperatures measured in Zone 1 correspond to thermal profile at MIT in the absence of the fuel, i.e. in the

absence of combustion. MIT measured under CH₄-H₂ co-feeding is 450°C, approximately 80°C lower than that obtained in the case of Mix1 combustion. As a result, by substituting part of CH₄ with H₂, maintaining the same input power to the reactor, enhances the fuel reactivity. In Zone 2 Mix3 is sent to the reactor. Due to the relatively high temperature and the presence of platinum, hydrogen is totally converted; H₂ conversion, As a matter of fact, shows a steep increase from 0 to 100% as soon as hydrogen is fed to the reactor, while CH₄ conversion is low (Fig. IV.2.1b). The heat developed by H₂ combustion produces an increase of the catalyst temperature to a level high enough to start the (heat accumulation)/(reaction rate rise) mechanism (Zone 3) previously described for CH₄ ignition, but in this case the phenomenon appears slower, induction time for light-off (Zone 4) being about 2 h. About temperature profile in Zone 2, a maximum temperature is observed at the center of the reactor, very different to that observed during CH₄ ignition (Fig.IV.1.1). However, as the time on stream increases, T₃ increases faster than T₂ until at t=80 min, in the Zone 3, they are practically equal; afterwards, T₃ results higher than T₂ until light-off occurrence.

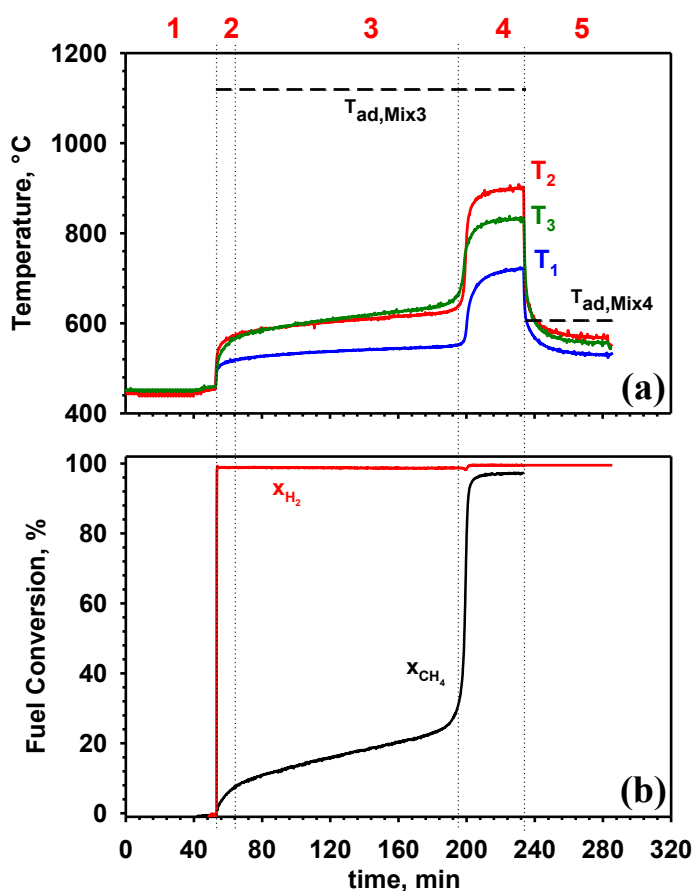


Fig.IV.2.1 (a)temperature profiles and (b) CH₄ and H₂ conversion during the ignition at MIT for the 2,1/2.2/10/85.7 CH₄/H₂/O₂/N₂ mixture; Q_{tot} 80slph. T₁, T₂ and T₃ correspond to the temperatures measured respectively at the beginning, the center and the end of the monolithic reactor.

The above results strongly suggest that H₂ and CH₄ combustions occurs separately during ignition, the former in the first part of the reactor, the latter downstream. Specifically, hydrogen is totally burnt and shows a totally developed reaction front that, as it is expected, is placed at the center of the reactor. On the contrary, in Zone 2 and 3 methane combustion proceeds very slowly and is responsible for a gradual temperature increase at the exit of the reactor. As a consequence, the increased reactivity, i.e. the lower MIT, is due to a thermal more than chemical hydrogen assistance to methane combustion, related to the higher temperature level generated by H₂ combustion.

Once Mix3 fuel mixture is ignited, Mix4 is fed to the combustor (Zone 5 in FigureIV.2.1). As it is expected, H₂ is still totally converted (Fig. IV.2.1). Moreover, in agreement with the lower overall heating value of hydrogen fuel mixture compared to that of Mix3, temperatures strongly decrease (Fig.IV.2.1). In particular, at the steady state T₁, T₂ and T₃ are respectively 529, 566 and 549°C. Mix4 fuel combustion actually produces the same thermal power developed by hydrogen in Mix3 combustion. As a consequence, the thermal profile resulting in Mix 4 combustion at a preheating temperature equals to Mix3 minimum ignition temperature, represents the effective MIT of methane in CH₄-H₂ mixture and it is consistent with the minimum ignition temperature of methane measured on the same catalyst and at the same flow rate in absence of hydrogen (Fig.IV.1.2). These results confirm the role of H₂ in thermally assisting CH₄ combustion thus decreasing its MIT. Moreover, temperatures detected in Mix4 combustion, i.e. the temperatures developed by the co-burnt hydrogen at Mix3 MIT, are higher than those found for CH₄ ignition (30°C higher). This result can be explained considering that, with respect to CH₄ ignition in Mix1, in Mix3 case methane concentrations is lower, being partially substituted with H₂. Actually, because of the first order approximation of methane combustion reaction at atmospheric pressure, the conversion does not change with CH₄ concentration and in the case of the minor equivalence ratio mixture, fixed the reactor temperature, combustion releases a lower power. As a result, in order to ignite methane in Mix3 an higher reactor temperature and a longer induction time are needed.

In Figure IV.2.2 MIT for Mix1 and Mix3 are reported as a function of the total flow rate. In the case of Mix1, MIT is practically independent on the flow rate in the limit of the experimental errors. Consistently with the MIT reported previously in the case of Q_{TOT}=80slph, MIT is around 530°C in all the investigated cases. This result is ascribed to the dual effect of the flow rate on the fuel ignition. From one side by increasing the flow rate contact time decreases and as consequence fuel conversion decreases too. However, by increasing the flow rate the input power increases too and, as a consequence, the developed power. According to the experimental results, these two effects are

balanced and increasing the flow rate the same preheating temperature is required for ignition despite of the lower fuel conversion.

Differently from the case of methane combustion, MIT of CH₄-H₂ fuel strongly depends on the flow rate, as it is shown in Figure IV.2.2, and, in particular, decreases increasing the flow rate, hydrogen addition resulting more and more effective. This behavior is related to the increased thermal power generated at high flow rate by hydrogen combustion, which is unaffected by contact time at the investigate temperatures, resulting in a higher and higher catalyst temperature increase due to H₂ combustion heat release.

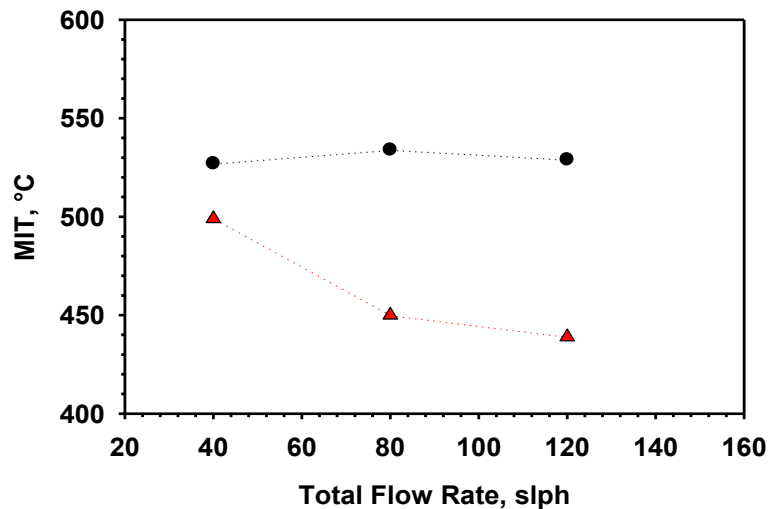


Fig.IV.2.2 Comparison of the MIT for the MiX1 and MIX3 varying the total flow rate.

On the contrary, no significant beneficial effect is detected on stability limits, i.e. on QT, as shown in Figure IV.2.3. This result strongly suggests that quenching phenomena are ruled by the ratio between the developed power via combustion and the power lost, independently on the chemical composition of the fuel. As a matter of fact, once the fuel is ignited, the thermal balance, which regulates the self-sustainability of the reactor, exclusively depends on the ratio between the generated power and heat losses, both of them unaffected by fuel composition in our experiments, thus explaining the undetectable effect of hydrogen addition on quenching temperature.

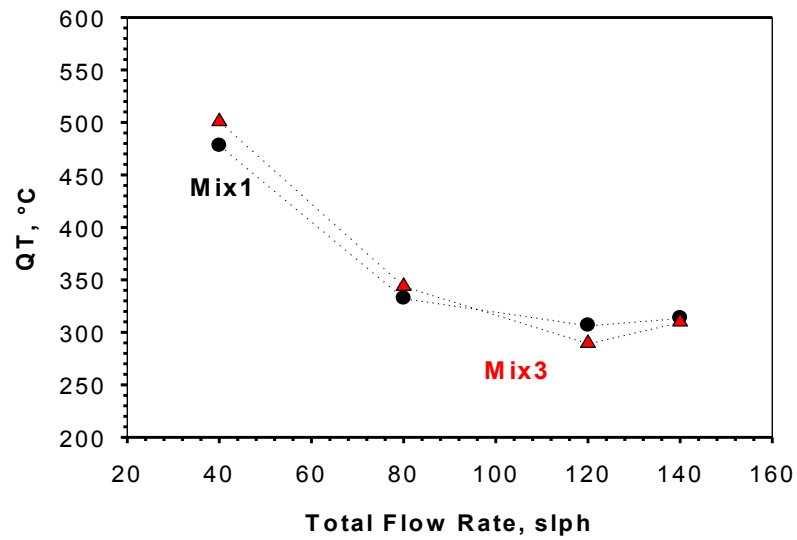


Fig.IV.2.3 Comparison of the QT for the MiX1 and MIX3 varying the total flow rate.

In conclusion this study allowed to elucidate two different quenching behavior: extinction and blow out. Moreover it was demonstrated that adding a more reactive fuel like hydrogen decreases the MIT of methane due to a thermal effect. As a matter of fact, it has emerged that the hydrogen and methane combustion occur separately. Moreover it was verified that regardless of the kind of fuel, the quenching behavior is regulated by the heat balance.

V KINETIC STUDY UNDER PRESSURE

V.1 CH₄ Combustion

V.1.1 CH₄ combustion on supported LaMnO₃

Fig.V.1.1. and V.1.2 show methane conversion as a function of the pressure parametric in the inlet methane concentration $y^{\circ}_{CH_4}$ and as a function of $y^{\circ}_{CH_4}$ parametric in the pressure at a fixed O₂ content equal to 8.5% for some selected test carried out at 555°C, 595 °C and 620°C.

It clearly appears that the conversion increases by increasing the pressure but decreases at higher methane content. As a matter of fact, plotting the conversion as a function of the $y^{\circ}_{CH_4}$, it is evident that the conversion decreases increasing the fuel content in the mixtures and that at high pressure this effect is more pronounced.

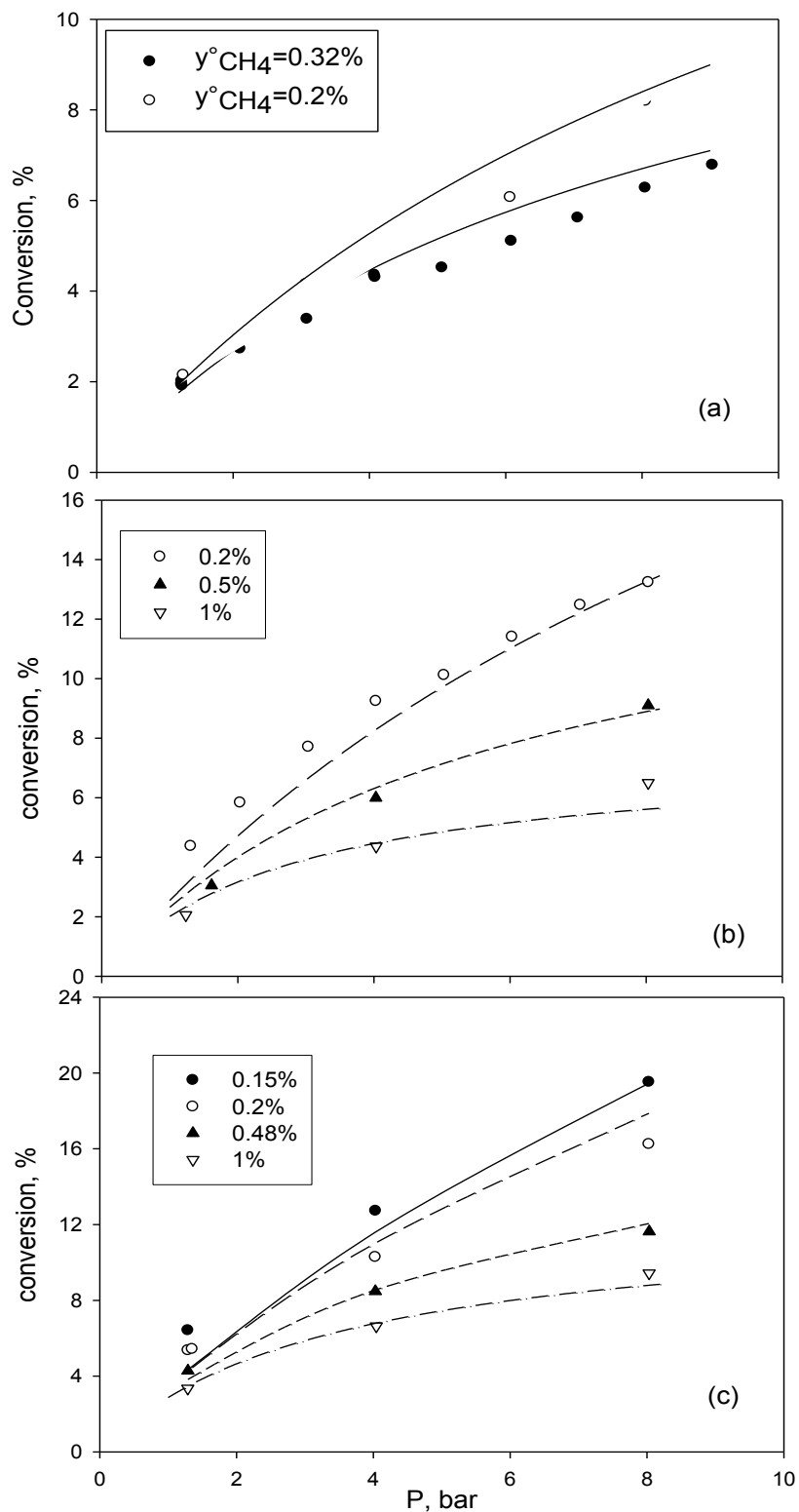


Fig.V.1.1.CH₄ conversion as a function of total pressure on LM20-A platelet. (a) T=555°C, total flow rate=55 splh; (b)T=595°C; total flow rate=80splh; (c)T=620°C; total flow rate=80splh. Symbols: experimental data; lines: predicted conversion according to model.

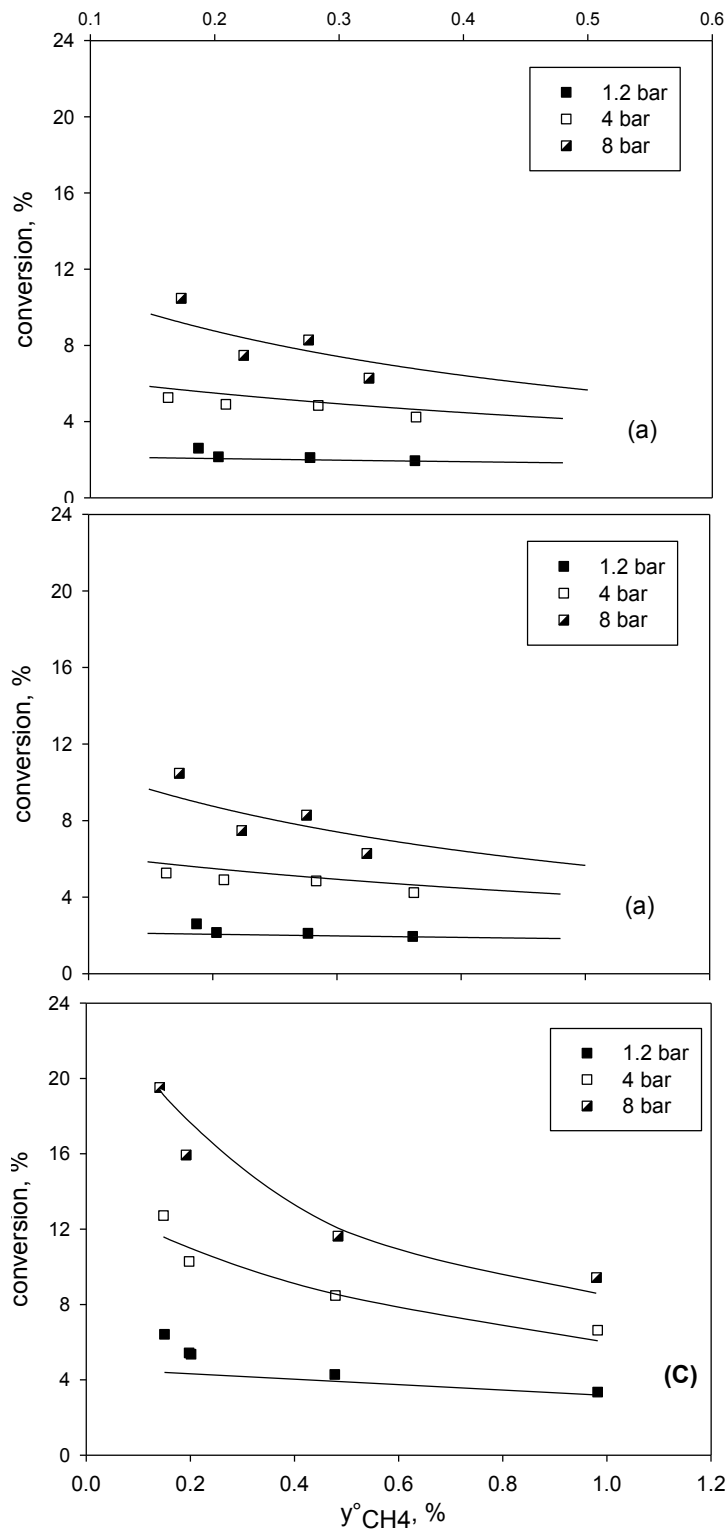


Fig.V.1.2.CH₄ conversion as a function of the initial methane fraction y_{CH_4} and parametric in the pressure on LM20-A platelet. (a)T=555°C; Total flow rate=55 splh; (b)T=595°C; total flow rate=80splh; (c)T=620°C ; Total flow rate=80 splh. Symbols: experimental data; lines: predicted conversion according to model.

The data whose conversion resulted lower than 10%, were firstly analyzed by estimating the reaction rate calculated according to the following expression:

$$r = \frac{Q_{tot} \cdot C^0 \cdot x_{fin}}{w_{cat}} \text{ mol}/(\text{g} \cdot \text{s}) \quad \text{eq. V.1.1}$$

where C^0 is the initial fuel concentration (mol/Nl), x_{fin} the conversion, Q_{tot} the total volumetric flow rate (Nl/s) and w_{cat} the catalyst weight.

The reaction rates were first fitted by simple kinetic power laws in order to gain information about the apparent reaction order with respect to total pressure and methane.

The apparent reaction orders either respect to total pressure for the data at 555°C at different inlet methane fraction are reported in table V.1 and were estimated according to the following expression rate:

$$r = k \cdot P^p \quad \text{eq. V.1.2}$$

Table V.1.1-Apparent reaction order with respect to pressure for CH₄ combustion on LM20-A platelet: data collected at T=555°C (eq.V.1.2)

T _{cat} , °C	y ^o _{CH₄}	p	k, μmol/g*s*bar ^m	R ²
555	0.2	0.78 ±0,0163	359±10,6	0,999
	0.32	0.64 ±0,0157	428±12,17	0,996

The reaction order estimated are lower than unity and equal to 0.78 and 0.64 respectively for 0.2 % and 0.32% y_{CH₄}^o.

Similarly also Reinke et al (2004) studying the methane combustion up to 16 bar on a Pt-based catalyst found that the apparent reaction order with respect to pressure was less than 1 and equal to 0.53. These authors attributed this less than linear behaviour to the reduction in surface free-site coverage caused by the corresponding increase in oxygen coverage with increasing pressure.

On the contrary, the data reported in table V.1.1 reveal that the increase of reaction rate is less than linear especially for the higher methane molar fraction thus indicating the presence of an inhibiting effect likely to be associated to methane. As a matter of fact, it is evident that the apparent reaction order of pressure cannot be independent on methane molar fraction.

Similarly the apparent reaction orders with respect to reactant were estimated at different pressure for the data at 555°C according to the following power rate law:

$$r = k' \cdot y^n \quad \text{eq. V.1.3}$$

the results of this regression are reported in table V.1.2 and in fig.V.1.3.

Table V.1.2-Apparent reaction order with respect to methane for the CH₄ combustion on LM20-A platelet : data collected at T=555°C (eq. V.1.3)

Tcat, °C	P, Bar	R ²	k', mol/(g·s·Bar ⁿ)	n
555	1,2	0,975	5.2·10 ⁻⁶	1
	4	0,979	7.3·10 ⁻⁴	0.73
	8	0,89	1.1·10 ⁻⁵	0.56

The obtained results have shown that the reaction order with respect to methane is 1 with good approximation only at atmospheric pressure, according to several authors that studied methane combustion at atmospheric pressure on both supported and unsupported perovskite catalysts (Seyama, 1992; Martinez-Ortega et al, 2001; Batiot-Dupeyrat et al, 2001), but at higher pressures the reaction order with respect to methane decreases by increasing the pressure from the unity to 0.56 at 8 bar (Table V.1.2).

Similar results were obtained also by estimating the apparent reaction order with respect to pressure and fuel at temperatures above 555°C. The results reported in table V.1.3 were estimated by substituting the kinetic expression reported in equation V.2 in the equation II.4.4, that express the final conversion as a function of the variables (contact time, pressure and so on) and model parameters, thus obtaining the following equation V.1.4:

$$x = 1 - \exp(- RT \tau^{p-1}) \quad \text{eq. V.1.4.}$$

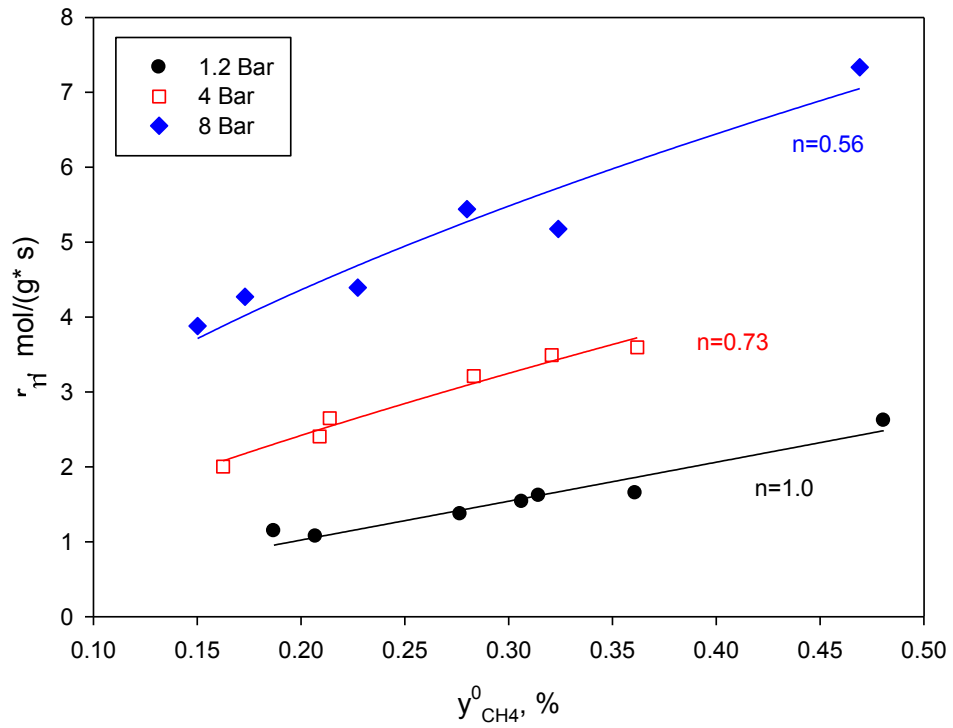


Fig.V.1.3.CH₄ reaction rates as a function of the initial methane fraction $y_{CH_4}^0$ parametric in the pressure on LM20-A platelet. T=555°C; Total flow rate=55-80 splh.

Table V.1.3-Apparent reaction order with respect to pressure for CH₄ combustion on LM20-A platelet at different temperatures and methane molar fractions estimated according to eq. V.1.4

$y_{CH_4}^0$, %	T=555°C			T=595°C			T=620°C		
	k	m	R ²	k	m	R ²	k	m	R ²
0.2	$5 \cdot 10^{-4}$	0.71	0.999	$1.4 \cdot 10^{-3}$	0.68	0.996	$1.6 \cdot 10^{-3}$	0.63	0.998
0.32	$4 \cdot 10^{-4}$	0.63	0.996	-	-	-	-	-	-
0.5	-	-	-	$8.3 \cdot 10^{-4}$	0.62	0.979	$1.4 \cdot 10^{-3}$	0.57	0.995
1	-	-	-	$6.7 \cdot 10^{-4}$	0.61	0.999	$1.0 \cdot 10^{-3}$	0.55	0.998

Comparing the data reported in table V.1.3 with the analogous ones of table V.1.1 it appears that the differential evaluation are slightly different from those carried out with eq. V.1.4. Moreover for the sets at the same temperature it appears that the values of the kinetic constant and apparent order with respect pressure decrease increasing the methane content in the mixture. In the case of the mixture $y^{\circ}_{CH_4}=0.2\%$, it appears that increasing the temperature causes a decrease of m and an increase of k .

The apparent reaction order with respect to methane for the different temperatures was estimated for the set at constant pressure by employing the kinetic expression reported in equation V.1.3. The following equation was obtained:

$$x = 1 - \left[1 - (1 - n) k' \frac{RT}{P} r(y^{\circ})^{n-1} \right]^{\frac{1}{(1-n)}} \quad \text{eq. V.1.5.}$$

The results of the fitting using eq. V.1.5 are summarized in table V.1.4.

Table V.1.4-Apparent reaction order with respect to fuel for CH₄ combustion on LM20-A platelet at different temperatures and P estimated according to eq. V.1.4

P, bar	T=555°C			T=595°C			T=620°C		
	k	n	R ²	k	n	R ²	k	n	R ²
1.2	Did not converge			9.0·10 ⁻⁵	0.53	0.994	2.6·10 ⁻⁴	0.67	0.968
4	3·10 ⁻⁵	0.76	0.825	1.7·10 ⁻⁴	0.52	0.998	5.1·10 ⁻⁴	0.66	0.998
8	4.5·10 ⁻³	0.48	0.928	2.9·10 ⁻⁴	0.54	0.999	5.3·10 ⁻⁴	0.60	0.976

For data at 595°C the n values are similar for all the pressure and equal to 0.5 while at 620°C the n slightly decreases by increasing the pressure and is estimated about 0.6. The major uncertainty in the case of data at 595°C and 620°C is associated with the lower number of experimental data compared to those at 555°C. For this reason the research for the best kinetic model was first done fitting the data at 555°C and then extending the results at the higher temperatures.

For the case of data at 555°C, the plot of reaction rate as a function of the methane partial pressure P_{CH_4} , reported in Fig V.1.4, reveals that an overall single correlation can be found independently on the overall pressure.

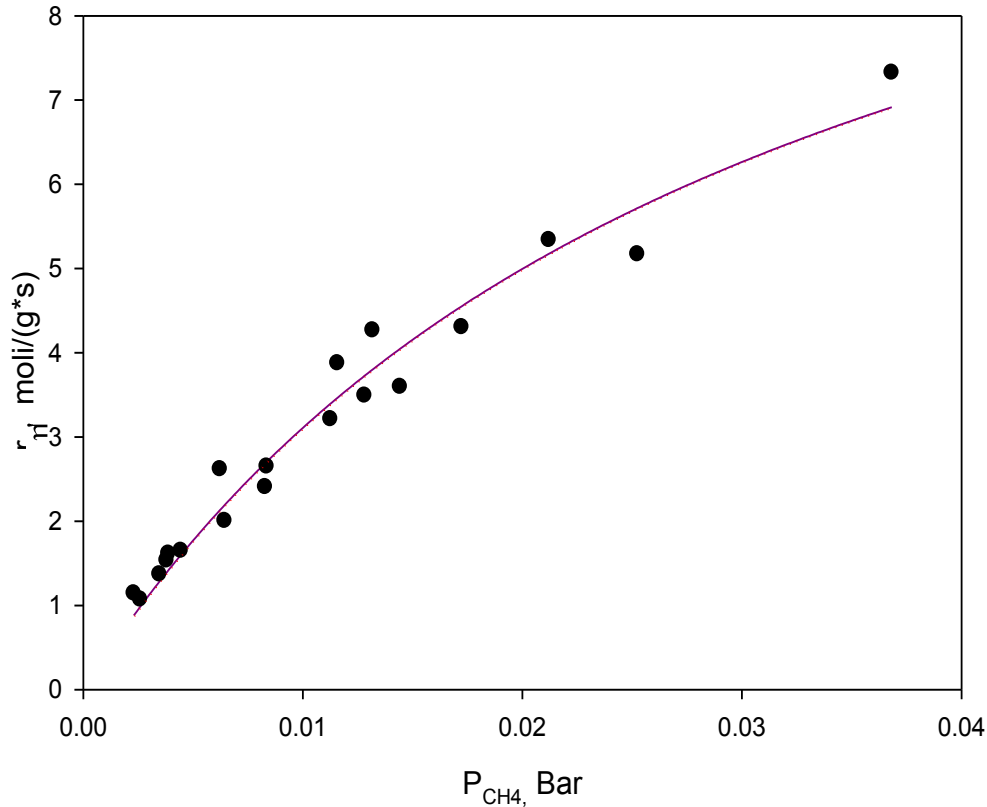


Fig.V.1.4. CH_4 reaction rates a function of the methane partial pressure P_{CH_4} on LM20-A platelet. $T=555^\circ C$; Total flow rate=55 splh. Symbols: experimental data. Line: reaction rate predicted according to model of eq. V.1.6 and parameters reported in table V.1.6.

The shape of r versus P_{CH_4} suggests that a kinetic expression with a two parameter like that reported in eq. V.1.6 is able to fit the experimental data.

$$r = \frac{kP_{CH_4}}{1 + KP_{CH_4}} \quad \text{eq.V.1.6}$$

A preliminary estimation of the parameters have been performed on sets at different pressures. The values of k and K s estimated by fitting the values of reaction rate with the model of equation V.1.6, are reported both in table V.1.5 and in fig. V.1.5.

Table V.1.5. results of the fitting of reaction rates with model of eq.V.1.6 at different pressure at 555°C for methane combustion over LM20-A platelet

modello	P, Bar	R ²	k, moli/(g·s·Bar)	K, Bar ⁻¹
$r = \frac{kP_{CH_4}}{1 + KP_{CH_4}}$	1,2	0,951	$4 \cdot 10^{-4}$	0,74
	4	0,975	$4 \cdot 10^{-4}$	40
	8	0,89	$4 \cdot 10^{-4}$	36

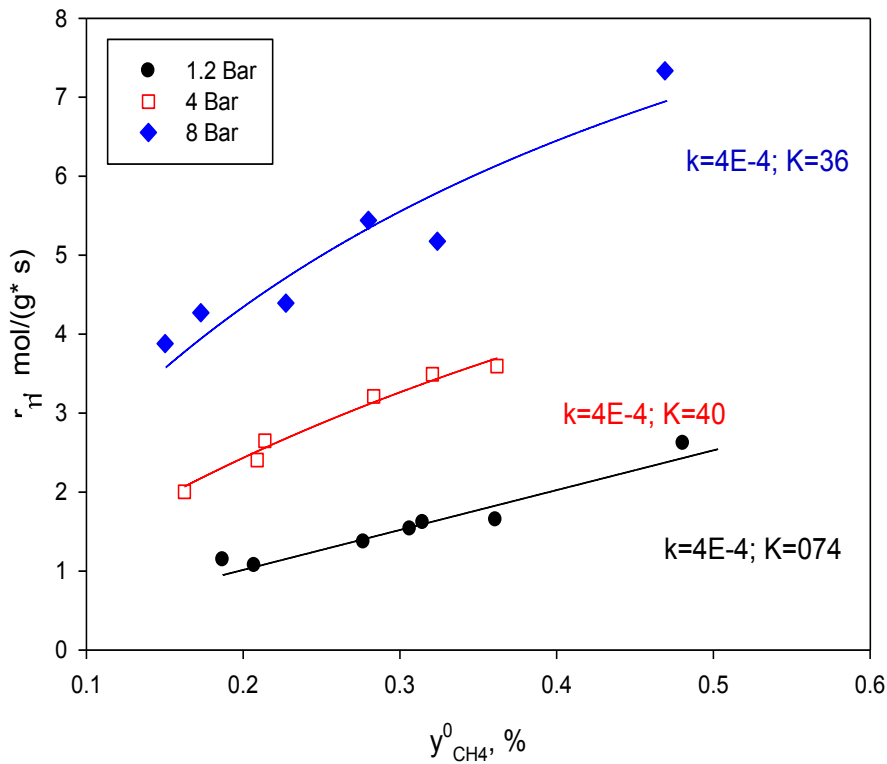


Fig.V.1.5: reaction rates as a function of $y^0_{CH_4}$ on LM20-A platelet. Symbols: experimental data: (●) P=1,2 bar; Qtot= 55splh; O₂=8,5%; Tcat=555°C; (□) P=4 bar Qtot= 55splh-65splh($y^0 = 0,15\%$); O₂=8,5%; Tcat =555°C; (◆) P=8 bar Qtot= 55splh -65splh($y^0 = 0,15\%$); O₂=8,5%; Tcat =555°C; Lines: predicted according to model of eq. V.1.6.

It appears that the value of K at atmospheric pressure is lower than those estimated at higher pressure but shows a larger confidence interval. On the other hand, the value of K at 4 and 8 bar are very similar. The comparison between experimental and predicted values of reaction rate demonstrates that the model of equation V.1.6 is able to fit the experimental data at 555°C.

On the other hand, if a fitting of the data is performed it is possible to obtain single k and K values with a good estimation of the experimental data. The values of k and K thus obtained are reported in table V.1.6 and the predicted reaction rate are reported in fig. V.1.4.

Table V.1.6. results of the fitting of reaction rates for CH₄ combustion on LM20-A platelet with model of eq.V.1.6 at 555°C

modello	R ²	k, moli/(g*s*Bar)	K, Bar ⁻¹	MRSS
$r = \frac{kP_{CH_4}}{1 + KP_{CH_4}}$	0,966	4·10 ⁻⁴	32,3±5.5	1.0·10 ⁻¹³

The research for the best kinetic model was extended also to other fractional model similar to that of eq. V.1.6. In particular the following models were considered:

$$r = \frac{k'_{CH_4}}{1 + \zeta_2 P_{O_2}} \quad \text{eq. V.1.7}$$

$$r = \frac{kP_{CH_4}}{1 + \zeta P_{CH_4} + \zeta_2 P_{O_2}^{0.5}} \quad \text{eq. V.1.8}$$

$$r = \frac{k'_{CH_4}}{1 + \zeta_3 P_{CO_2}} \quad \text{eq. V.1.9}$$

The results of the reaction rate fitting with the model of eq. V.1.7, where the inhibiting effect of oxygen was considered, are reported in table V.1.7 and the fig. V.1.6.

Tab.V.1.7. results of the fitting of experimental data for CH₄ combustion on LM20-A by the model of eq. V.1.7.

model	P	R ²	k	K ₂
$r = \frac{k' y_{CH_4}}{1 + K_2 P_{O_2}}$	1,2	0,9516	5*10 ⁻⁴	1.36
	4	0,8544	5*10 ⁻⁴	2.33
	8	0,61	5*10 ⁻⁵	-1.27

From Fig. V.1.7 it appears that the model of eq. V.1.7 is able to well fit the data only at atmospheric pressure where is valid the linear dependence on methane partial pressure. While for pressures above the atmospheric one the model gives worse prediction of experimental data. Moreover the estimates parameter at 8 bar has a negative value, thus losing its physical meaning because kinetic constant of surface reaction and adsorption constants and their product are positive. For this reason the model of eq. V.1.7 was rejected.

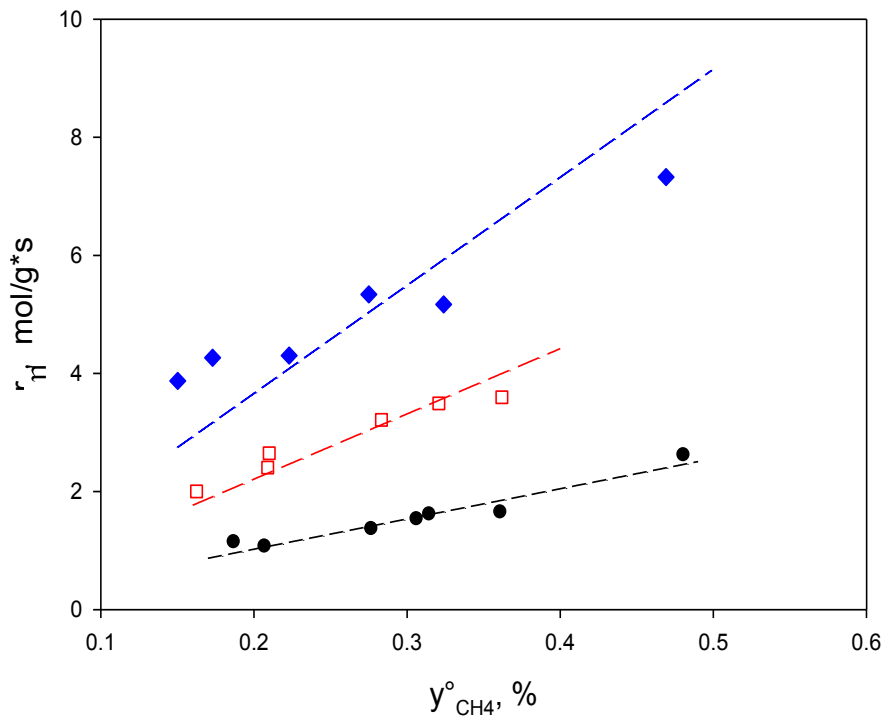


Fig.V.1.7: Reaction rates as a function of $y_{CH_4}^0$ on LM20-A platelet. Symbols: experimental data: (●) P=1,2 bar; Q_{tot}= 55splh; O₂=8,5%; T_{cat}=555°C; (□) P=4 bar Q_{tot}= 55splh-65splh($y^0 = 0,15\%$); O₂=8,5%; T_{cat} =555°C; (◆) P=8 bar Q_{tot}= 55splh -65splh($y^0 = 0,15\%$); O₂=8,5%; T_{cat} =555°C; Lines: predicted according to model of eq. V.1.7.

The model of eq. VI.8 considers a further inhibiting oxygen partial pressure added to the one of methane. With respect to model of eq. V.1.6, the effect of total pressure is no more strictly connect to that of methane but the inhibiting effect of methane is still considered. The results of the fitting of all data with the model of eq. V.1.8 are reported in table V.1.8 while in figure V.1.8 the comparison with experimental data is reported.

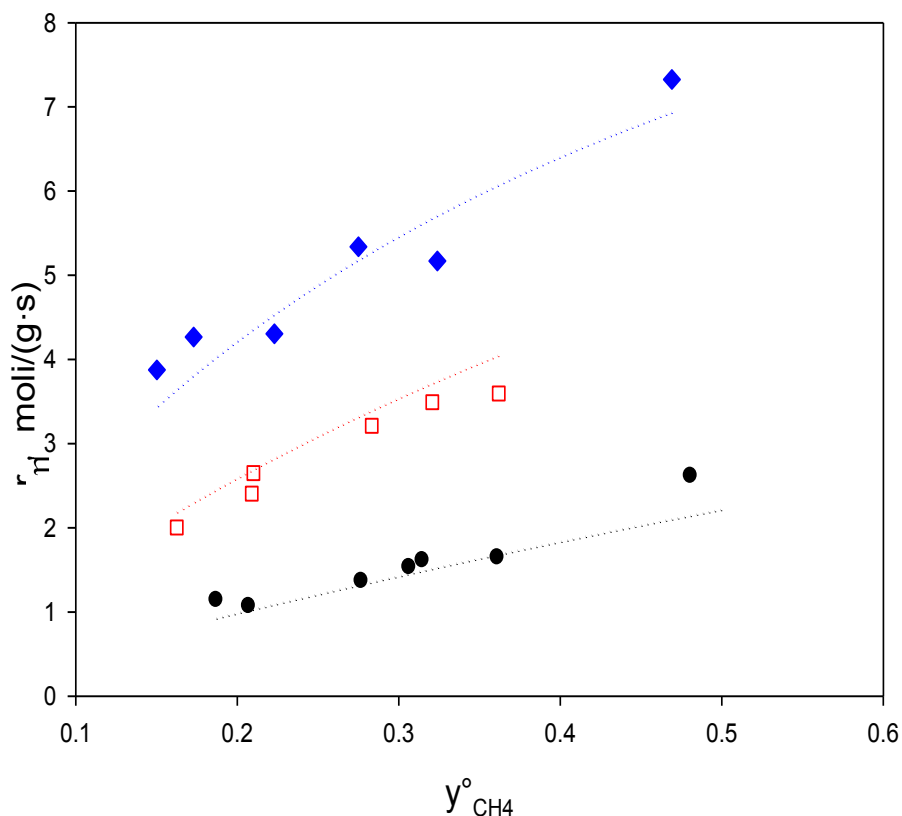


Fig.V.1.8: Reaction rates as a function of $y_{CH_4}^0$ on LM20-A platelet. Symbols: experimental data: (●) P=1,2 bar; Q_{tot} = 55splh; O_2 =8,5%; T_{cat} =555°C; (□) P=4 bar Q_{tot} = 55splh-65splh(y^0 =0,15%); O_2 =8,5%; T_{cat} =555°C; (◆) P=8 bar Q_{tot} = 55splh -65splh(y^0 =0,15%); O_2 =8,5%; T_{cat} =555°C; Lines: predicted according to model of eq. V.1.8.

With respect to the results of model V.1.6, the improvement in MRSS is only marginal, especially considering the adding of a further parameter (i.e. K2) (see tables V.1.6 and V.1.8). Moreover this parameter is badly estimated, its standard error being higher than the estimated value.

Tab.V.1.8 - results of the fitting of experimental data for CH₄ combustion on LM20-A platelet by the model of eq. V.1.8.

Model	R ²	k, mol/(g*s*Bar)	K, Bar ⁻¹	K ₂ ,	MRSS
$r = \frac{kP_{CH_4}}{1 + \zeta_1 P_{CH_4} + \zeta_2 P_{O_2}^{0.5}}$	0,967	4*10 ⁻⁴	32±5.7	0,0252±0.27	1.08·10 ⁻¹³

Another possibility is contemplated in the last model of eq. V.1.9 that considers the inhibiting effect of the produced carbon dioxide that can remain adsorbed on the perovskite catalyst. The results obtained by fitting the reaction rates with the model of eq. V.1.9 are reported in table V.1.9.

Tab.V.1.9 - results of the fitting of experimental data for CH₄ combustion on LM20-A platelet by the model of eq. V.1.9

model	R ²	k, moli/(g*s*Bar)	K ₃ , Bar ⁻¹	MRSS
$r = \frac{k' P_{CH_4}}{1 + \zeta_3 P_{CO_2}}$	0,918	4·10 ⁻⁴	358.2±93	2.4·10 ⁻¹³

It appears that the MRSS is higher respect to the model of eq. V.1.6. The comparison between the model of eq. V.1.6 and V.1.9 is reported in fig.V.1.9 where the predicted reaction rates according to the two model are plotted against the experimental reaction rates. It appears that the model of equation V.1.6 gives slightly better prediction of the data especially for reaction rates higher than 4 μmol/(g·s).

The kinetic expression of eq. V.1.6 was used to fit the conversion at the different temperatures. In table V.1.10. the estimated parameters are reported with also their respective 95% range of confidence.

The fit goodness is shown by the fig V.1.1 and V.1.2 were the predicted conversions are plotted in comparison with the experimental conversion as a function of the pressure and of initial methane molar fraction respectively.

Table V.1.10-Result of the integral data for CH₄ combustion on LM20-A platelet regressed for the different temperature according to the model of eq. 2.

T, °C	k	K ₁	MSSR
555	4.1±0.7·10 ⁻⁴	41.7±18	4.9·10 ⁻⁵
595	9.5±0.5·10 ⁻⁴	31.1±7	6.7·10 ⁻⁵
20	1.2±0.3·10 ⁻⁴	23.4±10.75	1.6·10 ⁻⁵

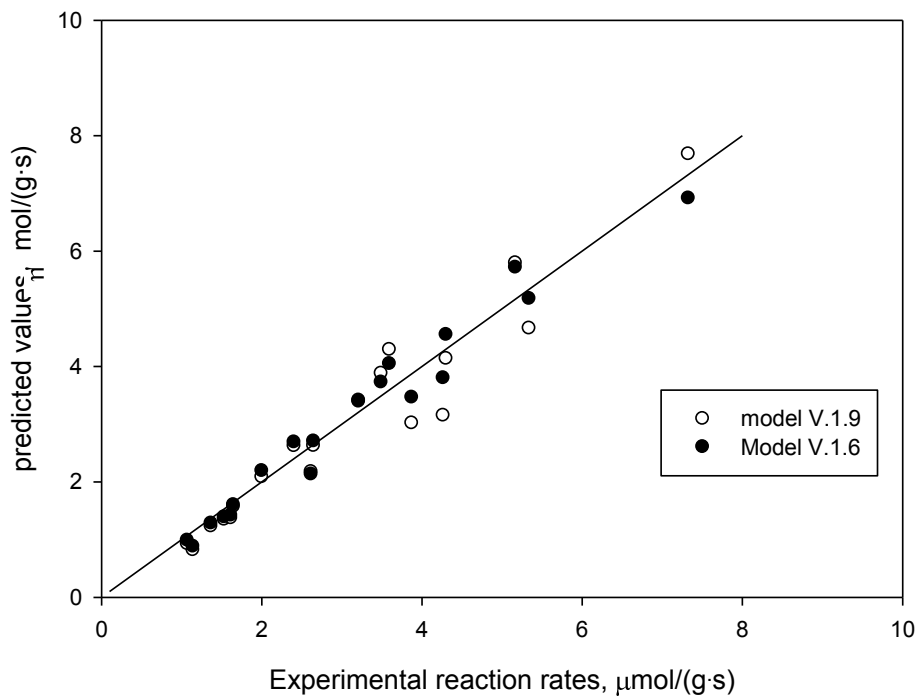


Fig.V.1.9: Predicted reaction rates versus experimental reaction rates on LM20-A platelet. Black full circles: model V.1.6; white circles: model V.1.9.

It is noteworthy that the model was able to regress the data in a wide range of oxygen partial pressure: (0.08-0.68 bar) and O₂/CH₄ ratio (8.5: 57). As a matter of fact, as also reported by Zhi Bang Chen and co-workers (1997), in some condition the methane combustion is zero order with respect to oxygen, being the surface saturated by the oxygen that comes from the lattice of the perovskite structure, due to the oxygen surface saturation related to high lattice oxygen mobility at high temperature.

Fig. V.1.10.(a, b) shows CH₄ conversion as a function of pressure and parametric in the inlet methane fraction at two different oxygen fractions respectively equal to 8.5% and 4.25% at 555°C and for a total flow rate equal to 75 splh.

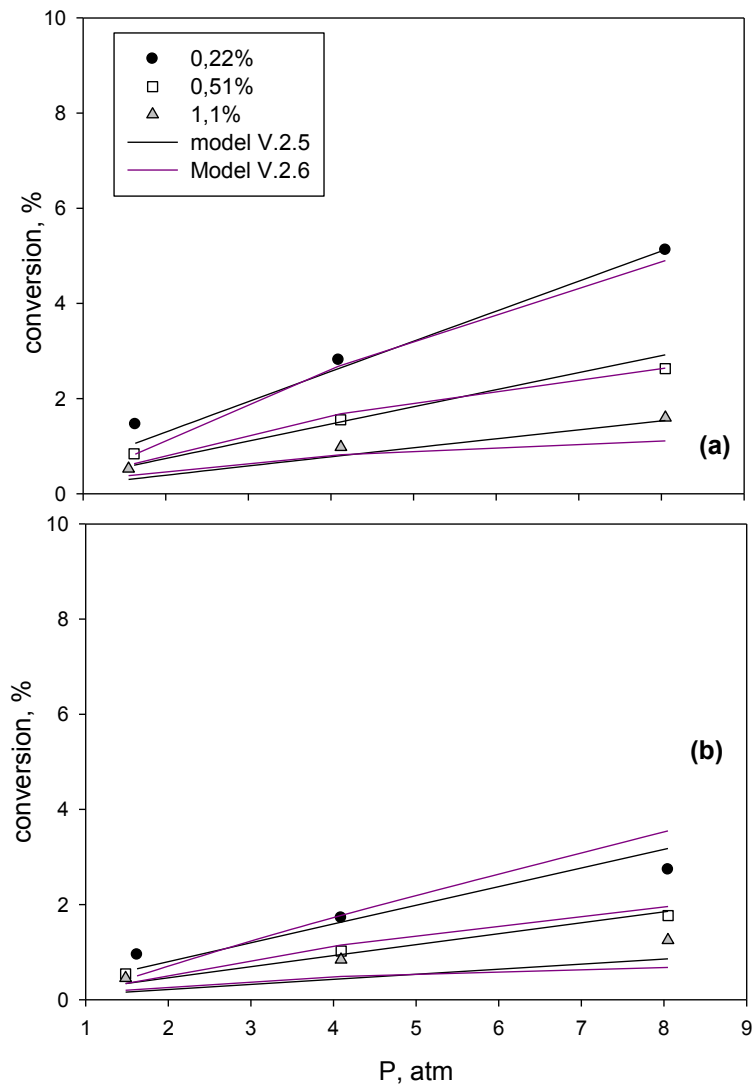


Fig. V.1.10 CH₄ conversion as a function of the pressure and parametric in the inlet CH₄ fraction over 1Pt-A platelet. Experimental data (symbols) and model prediction (lines) according to eq. V.1.13. Q_{tot}=75 splh, T=555°C. (a) y_{O₂}=8.5%; (b) y_{O₂}=4.25%.

From fig.V.1.10 it appears that methane conversion increases by increasing the pressure and that oxygen has a beneficial effect on conversion. On the contrary the mixtures that are characterized by an higher fuel content show lower conversion. These findings suggest that reaction rate is less than linear with respect to methane. Similar results were also found at higher temperature as reported in Fig.V.1.11-13 respectively showing the results for $T=585^{\circ}\text{C}$; $T=615^{\circ}\text{C}$ and $T=670^{\circ}\text{C}$.

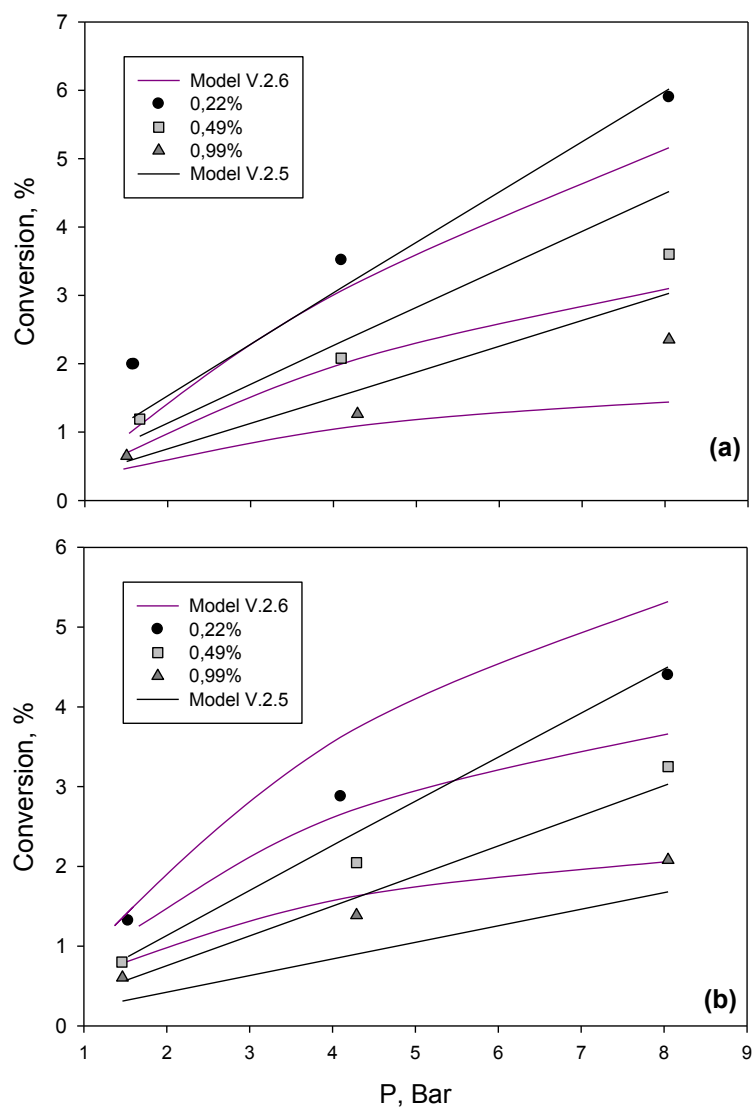


Fig. V.1.11 CH₄ conversion as a function of the pressure and parametric in the inlet CH₄ fraction over 1Pt-A platelet. Experimental data (symbols) and model prediction (lines) according to eq. V.1.13 and eq.V.2.6. Q_{tot}=75 splh, T=585°C. (a) y_{O₂}=8.5%; (b) y_{O₂}=4.25%.

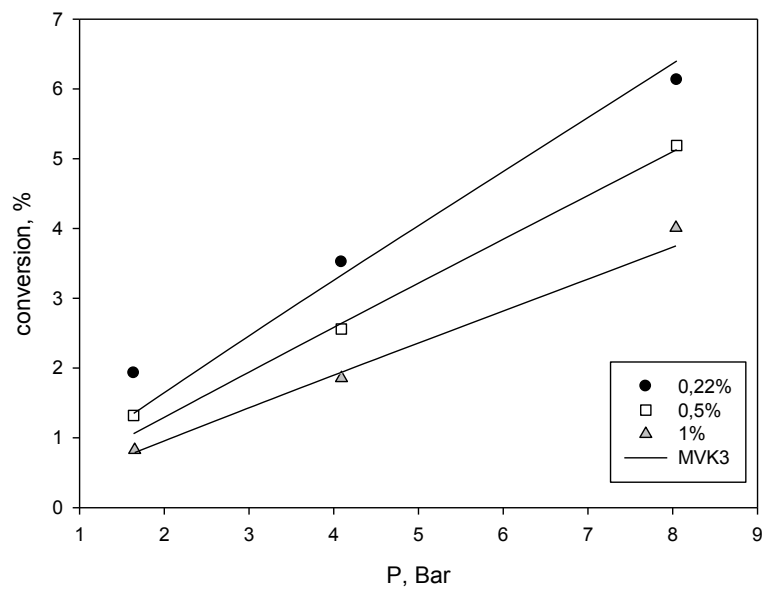


Fig. V.1.12 CH₄ conversion as a function of the pressure and parametric in the inlet CH₄ fraction over 1Pt-A platelet Experimental data (symbols) and model prediction (lines) according to eq. V.1.13. $Q_{tot}=75$ splh, $T=615^{\circ}C$. $y_{O_2}=4.25\%$.

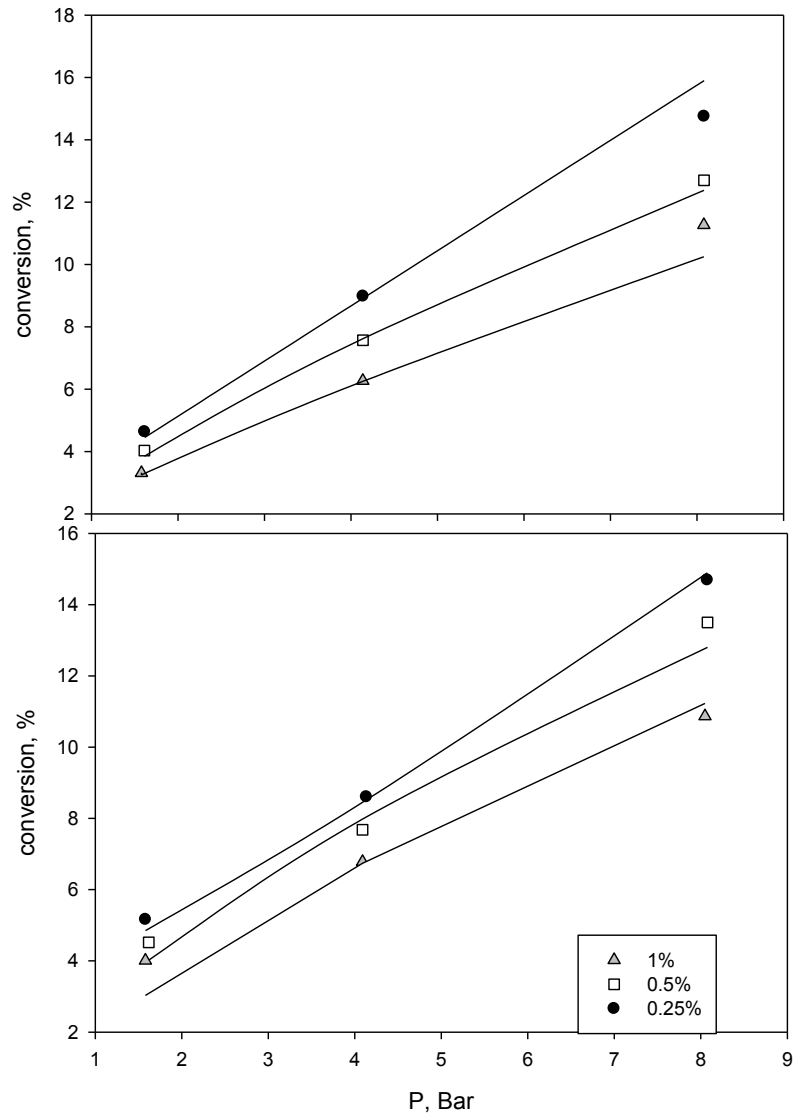


Fig. V.1.13 CH₄ conversion as a function of the pressure and parametric in the inlet CH₄ fraction over 1Pt-A platelet Experimental data (symbols) and model prediction (lines) according to eq. V.1.13. Q_{tot}=75 splh, T=670°C. (a) y_{O₂}=8.5%; (b) y_{O₂}=4.25%.

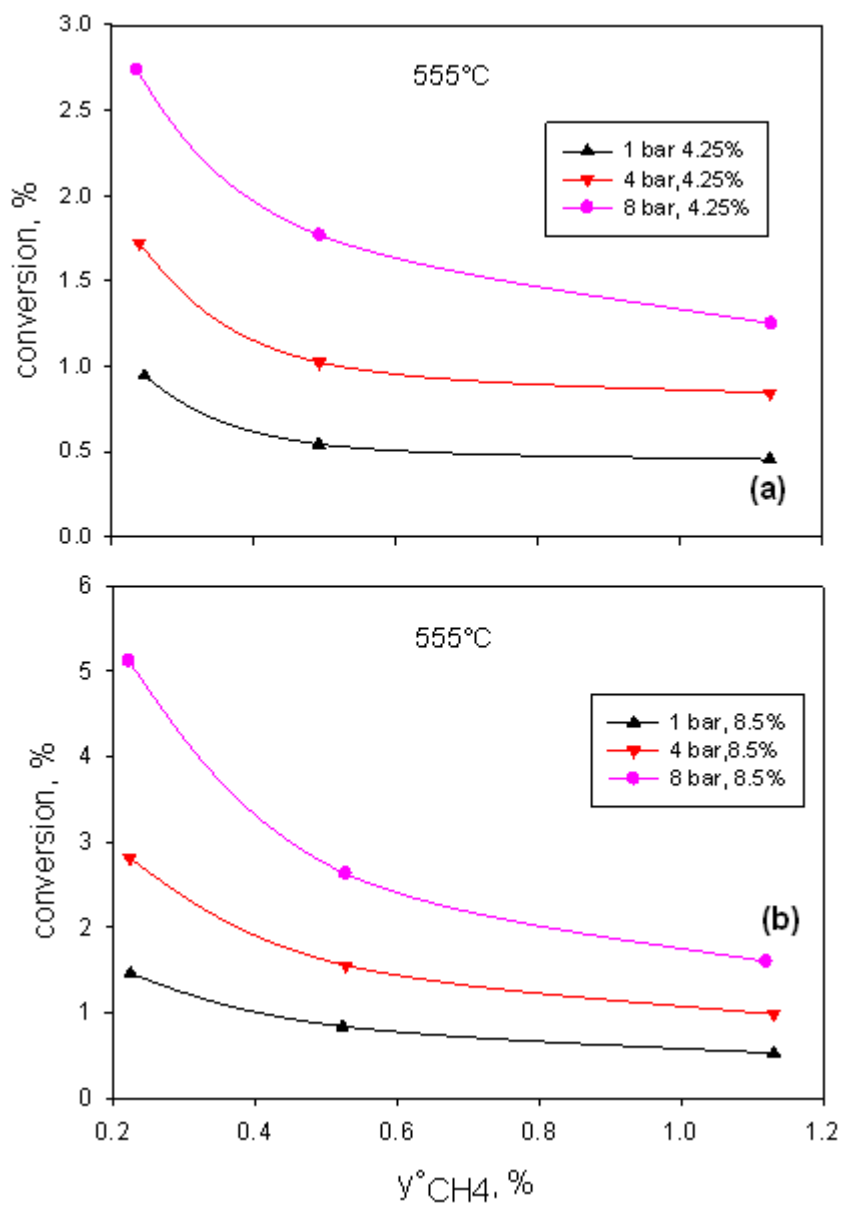


Fig. V.1.14 CH₄ conversion as a function of the inlet CH₄ fraction and parametric in pressure over 1Pt-A platelet. Q_{tot}=75 splh, T=555°C. (a) y_{O₂}=8.5%; (b) y_{O₂}=4.25%.

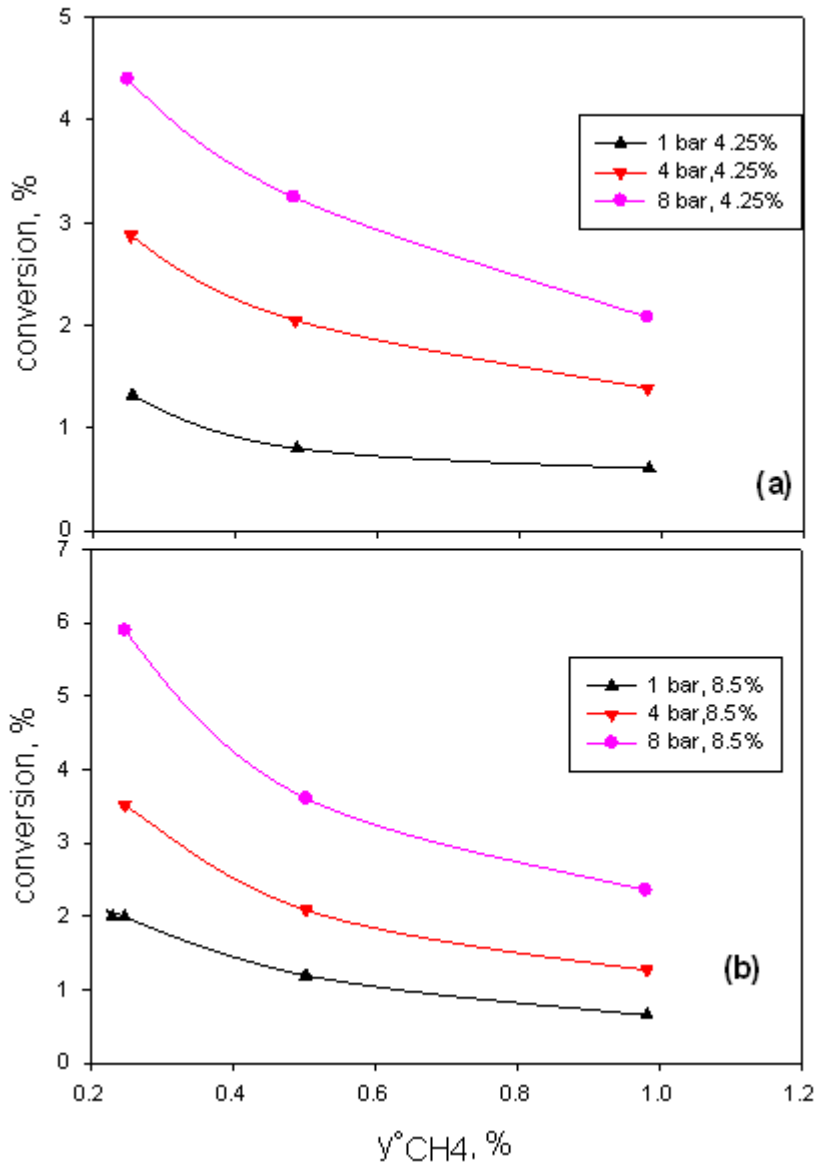


Fig. V.1.15 CH₄ conversion as a function of the inlet CH₄ fraction and parametric in pressure over 1Pt-A platelet. Q_{tot}=75 splh, T=585°C. (a) y_{O₂}=8.5%; (b) y_{O₂}=4.25%.

Similarly to the case of methane combustion on perovskite data whose conversion was lower than 10% were first analyzed by simply fitting the reaction rates with kinetic power law. As a matter of fact the data at constant oxygen inlet fraction (see Fig. V.1.14 and Fig. V.1.15) were fitted with the following rate expression:

$$r = k \cdot P^p \cdot y_{CH_4}^n \quad \text{eq. V.1.10}$$

thus obtaining the apparent reaction orders with respect to methane (n) and pressure (p) reported in table V.1.11.

Table V.1.11-Apparent reaction orders with respect to fuel and pressure for CH₄ combustion over 1Pt-A: set at different y^o₀₂ at 555°C and 585°C estimated according to the kinetic expression of eq. V.1.10.

y ^o ₀₂ , %	T=555°C					T=585°C				
	k, $\frac{\mu \text{ mol}}{\text{g} \cdot \text{s}}$	n	p	R ²	MRSS	k, $\frac{\mu \text{ mol}}{\text{g} \cdot \text{s}}$	n	p	R ²	MRSS
4.25	1.1	0.56±.04	0.63±.03	0.987	2.2·10 ⁻¹⁴	1.8	0.47±.04	0.60±.05	0.981	6.0·10 ⁻¹⁴
8.5	1.2	0.33±.02	0.72±.03	0.993	2.0·10 ⁻¹⁴	1.4	0.32±.03	0.77±.04	0.989	5.3·10 ⁻¹⁴

The apparent reaction order with respect to the pressure was about 0.7 while that of methane was about equal to 0.5, in agreement with those reported by Muto and co-workers (1996) for noble metal catalyst supported on silica and/or alumina. Moreover the same authors reported that the reaction order with respect to methane and oxygen were respectively of 0.53 and 0.18 for the alumina supported catalyst, thus obtaining an overall reaction order with pressure of about 0.7, is in agreement with the data reported in table V.1.11 too.

The higher reaction order of pressure with respect to that of methane indicates that the order of oxygen has a positive value. However, the reaction orders may depend on the experimental conditions such as temperature, pressure and the ratio of O₂ to CH₄ as pointed out by many authors (Trimm and Lam., 1980; Niwa et al. 1983) and also demonstrated by the values of table V.1.11. As a matter of fact Niwa et al. (1983) found that methane oxidation over Pt/Al₂O₃ was zero order with respect to oxygen partial pressure while Trimm et al. (1980) obtained a high reaction order with respect to the oxygen partial pressure (0.75-1).

Moreover from table V.1.11 appears that the reaction order with respect to methane slightly decreases increasing pressure for the set of data at 4.25% while for data at higher oxygen content the methane reaction order is quite the same.

The sets at constant pressure were fitted by the following apparent kinetic expression:

$$r = k' \cdot y^{n}_{CH_4} \cdot y^m_{O_2} \quad \text{eq. V.1.11}$$

Thus the apparent reaction order with respect to methane and oxygen, and as a consequence of pressure, were estimated at constant pressure and temperature and reported in table V.1.12-13 respectively for the temperature of 555°C and 585°C .

Table V.1.12-Apparent reaction orders with respect to fuel and oxygen for CH₄ combustion over 1Pt-A: set at different pressure at 555°C estimated according to the kinetic expression of eq. V.1.11.

P, bar	T=555°C					
	k',moli/(g·s)	n	m	(n+m)	R ²	MRSS
1.2	3.95·10 ⁻⁵	0.46±0.08	0.40±0.14	0.86	0.935	2.24·10 ⁻¹⁴
4	7.28·10 ⁻⁵	0.45±0.08	0.45±0.15	0.90	0.933	8.14·10 ⁻¹⁴
8	1.15·10 ⁻⁴	0.37±0.07	0.55±0.13	0.92	0.948	1.47·10 ⁻¹³

Table V.1.13-Apparent reaction orders with respect to fuel and oxygen for CH₄ combustion over 1Pt-A : set at different pressure at 585°C estimated according to the kinetic expression of eq. V.1.11.

P, bar	T=585°C					
	k',moli/(g·s)	n	m	(n+m)	R ²	MRSS
1.2	2.27·10 ⁻⁵	0.47±0.06	0.20±0.08	0.67	0.945	9.4·10 ⁻¹⁵
4	8.01·10 ⁻⁵	0.47±0.02	0.24±0.04	0.71	0.998	2.5·10 ⁻¹⁴
8	9.88·10 ⁻⁵	0.51±0.06	0.27±0.08	0.78	0.953	1.72·10 ⁻¹³

The value of the apparent kinetic constant increases by increasing the pressure. This finding is explainable by taking into account that the pseudo kinetic constant englobes the pressure:

$$k^* = k \cdot P^{(n+m)} \quad \text{eq.V.1.12}$$

On the contrary, the trends of apparent reaction orders with respect to methane and oxygen are opposite. As a matter of fact n slightly decreases by increasing the pressure while m increases. Comparing the data at different temperature shows that the overall reaction order decreases with the temperature.

In conclusion the analysis of apparent reaction orders shows that the reaction is not zero order with respect to oxygen being its apparent reaction order ranging, on dependence of pressure and temperature, from 0.2 to 0.6. On the other hand the apparent order of methane is with good approximation equal to 0.5.

These finding strongly suggest that, between the different models discriminated for the methane reaction on platinum (some of them discussed hereafter) a Mars van Krevelen model which takes into account the O₂ molecular concentration on platinum surface and its dissociation could be appropriate to explain the complex behavior of oxygen and thus to fit the experimental data. The kinetic expression of this mechanism is reported in eq. V.1.13.

$$r = \frac{k_1 \cdot P_{O_2} \cdot k_2 P_{CH_4}}{(k_1 P_{O_2} + 2k_2 P_{CH_4})} \cdot \left(1 - \frac{k_1 \cdot P_{O_2}}{k_1^*} \right) \quad \text{eq V.1.13}$$

were k₁, k₁^{*} and k₂ represent the kinetic constants respectively of the oxygen non-dissociative adsorption, the dissociation of adsorbed molecular oxygen and the reaction of adsorbed methane according to the reaction scheme reported in Fig. V.1.16.

The parameters estimated by regressing the conversion with the model of equation V.1.13 are reported in table V.1.14., while in Fig.V.1.10-12 the predicted conversion are compared with the experimental data.

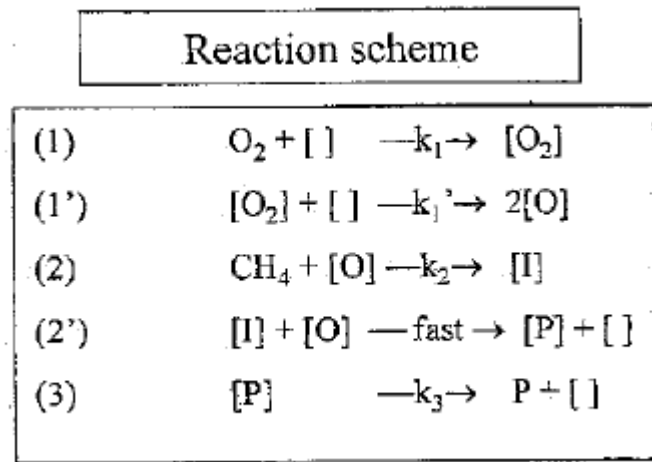


Fig. V.1.16 Reaction scheme for MvK mechanisms. (Auer et al.,2001)

Table V.1.14 Estimated parameters for the model of equation V.1.13

T, °C	k_1 , moli/(g·s·bar)	k_2 , moli/(g·s·bar)	k_1^* , moli/(g·s)	R ²	MRSS
555	$1.5 \cdot 10^{-5}$	$4.0 \cdot 10^{-4}$	$3.6 \cdot 10^{-3}$	0.947	$1.06 \cdot 10^{-3}$
585	$3.0 \cdot 10^{-5}$	$5.0 \cdot 10^{-4}$	$4.8 \cdot 10^{-3}$	0.869	$4.48 \cdot 10^{-3}$
615	$5.7 \cdot 10^{-5}$	$6.2 \cdot 10^{-4}$	$6.3 \cdot 10^{-3}$	0.978	$1.22 \cdot 10^{-3}$
670	$1.22 \cdot 10^{-4}$	$9.0 \cdot 10^{-4}$	$8.03 \cdot 10^{-3}$	0.871	$1.03 \cdot 10^{-2}$

Recently this model was also proposed in literature for Pd catalysts (Specchia et al, 2010), suggesting that in this temperature range the mechanism of methane combustion on noble metal is the same.

For the sake of completeness other models proposed in literature for the methane deep oxidation on platinum were also tested:

$$r = \frac{k \cdot P_{CH_4} \cdot P_{O_2}}{(1 + \zeta_C \cdot P_{CH_4} + \zeta_O \cdot P_{O_2})^2} \quad \text{eq. V.1.14}$$

$$r = \frac{k_1 \cdot k_2 \cdot P_{CH_4} \cdot P_{O_2}}{(k_1 \cdot P_{O_2} + \beta \cdot k_2 \cdot P_{CH_4} + k_1 \cdot k_2 / k_3) P_{CH_4} \cdot P_{O_2}} \quad \text{eq. V.1.15}$$

The first model, proposed by Trimm and Lam (1980) , is a LH type that was based on a model involving reaction between adsorbed methane and diatomically adsorbed oxygen, competing for a single site.

The second model, proposed by Hurtado et al. (2004) over 0.5%Pd γ -Al₂O₃ represent a Mars van Krevelen model in which the limiting step is the desorption of the product.

Table V.1.15 shows the results of the parametric inference of the model of equation V.2.6.

Table V.1.15 Estimated parameters for the model of equation (V.1.14) for CH₄ combustion over 1Pt-A.

T, °C	K _c , moli/(g·s·bar)	K _o , moli/(g·s·bar)	k, moli/(g·s)	R ²	MRSS
555	41.9	1.4	6.8·10 ⁻³	0.897	9.99·10 ⁻⁴
585	46.4	3.8	2.0·10 ⁻²	0.920	1.57·10 ⁻³
615	21.7	5.16	2.4·10 ⁻²	0.961	1.2·10 ⁻³
670	14.2	5.56	6.7·10 ⁻²	0.850	1.01·10 ⁻²

From table V.1.15 it appears that the model is able to well fit the data as also shown in fig. V.1.10-11, but the values of adsorption constants, especially those of oxygen, increase increasing the temperatures inconsistently with the thermodynamic requirements.

The results of the fitting with model of eq. V.1.15. are not presented since two of the three kinetic constants assume negative values.

V.2 H₂ combustion

V.2.1 H₂ combustion on supported LaMnO₃

Fig.V.2.1 shows the H₂ conversion as a function of pressure for three different temperatures and parametric in the H₂ inlet fraction for a total gas flow rate equal to 100 splh and for y_{O₂}=8.5%.

The conversion at different H₂ initial content in the mixtures are very similar suggesting a linear dependence with respect to H₂, while the effect of the pressure is quite different. As a matter of fact, the conversion increase is more pronounced at low pressure while raising pressure from 8 to 12 bar a less conversion increase was noted.

In order to roughly estimate the reaction orders, a power law expression was used with apparent hydrogen and oxygen reaction order α and β respectively.

The results have been reported in tables V.2.1-V.2.3 together with the results of some tested models. In particular the apparent hydrogen reaction order is equal to 1 in all the range of temperature investigated, while oxygen has an apparent negative reaction order that is estimated at about constant values around -0.5.

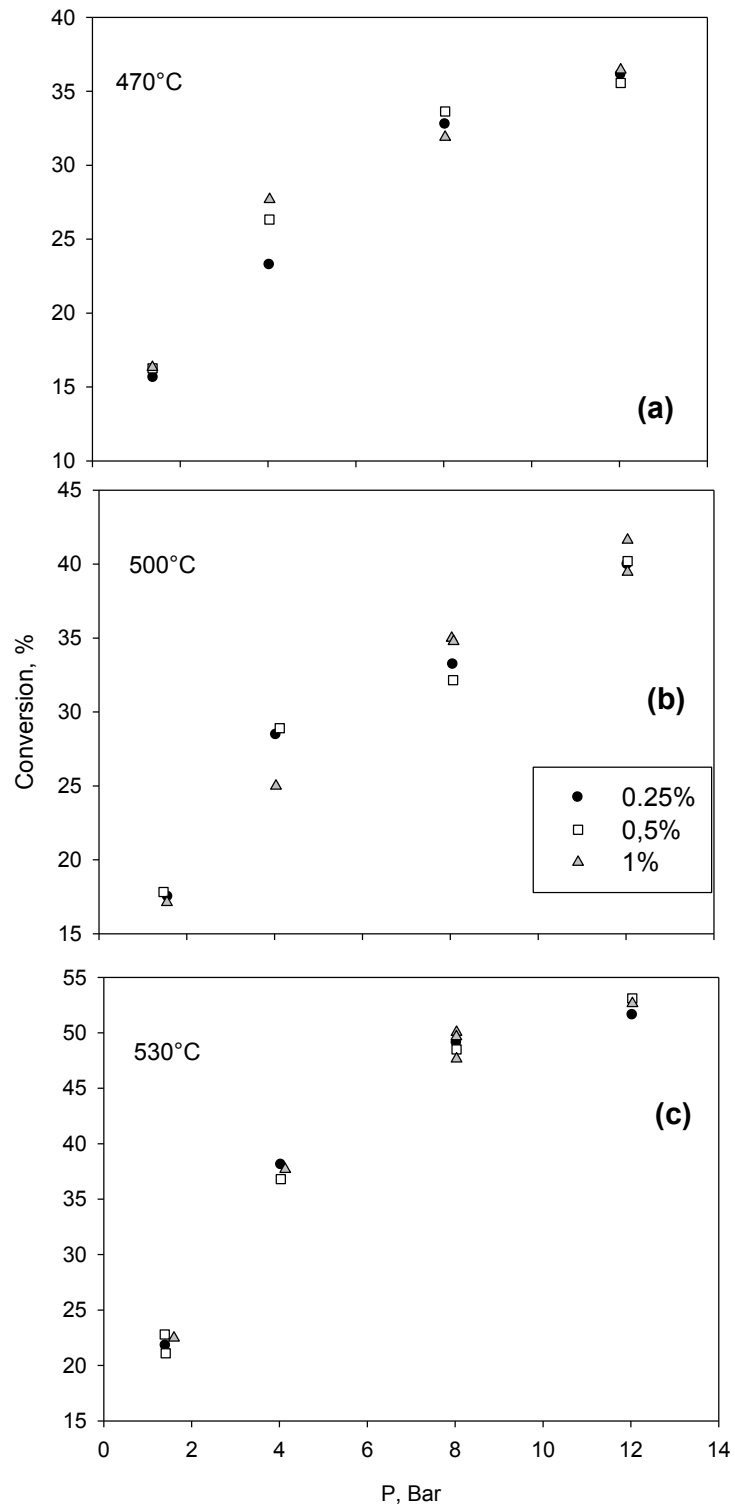


Fig.V.2.1 H₂ conversion as a function of pressure and parametric in the H₂ inlet fraction for LM20-A platelet. T=(a)470°C, (b)=500°C and (C) 530°C. Q_{tot}= 100 splh

Table V.2.1.-Regression results for several reaction models for the experimental set at 470°C for H₂ combustion over LM20-A

470°C	k	α	β	R ²	MSSR	F
1. $r = k \cdot P_{H_2}^\alpha \cdot P_{O_2}^\beta$	5.6·10 ⁻³	0.996	-0.56	0.984	1.82·10 ⁻⁴	611

470°C	kRT	K_{H_2}	K_{O_2}	R ²	MSSR	F
2. $r = \frac{k \cdot P_{H_2} \cdot \sqrt{K_{O_2} \cdot P_{O_2}}}{(1 + \sqrt{K_{O_2} \cdot P_{O_2}})}$	-	-	-	-	-	-
3. $r = \frac{k \cdot P_{H_2} \cdot K_{O_2} \cdot P_{O_2}}{(1 + K_{O_2} \cdot P_{O_2})}$	-	-	-	-	-	-
4. $r = \frac{k \cdot P_{H_2} \cdot K_{O_2} \cdot P_{O_2}}{(1 + \sqrt{K_{O_2} \cdot P_{O_2}})^2}$	-	-	-	-	-	-
5. $r = \frac{k \cdot K_{H_2} \cdot P_{H_2} \cdot \sqrt{K_{O_2} \cdot P_{O_2}}}{(1 + \sqrt{K_{H_2} \cdot P_{H_2}} + \sqrt{K_{O_2} \cdot P_{O_2}})^2}$	10.17	0.0182	17.63	0.994	1.24·10 ⁻⁴	1881
6. $r = \frac{k \cdot K_{H_2} \cdot P_{H_2} \cdot K_{O_2} \cdot P_{O_2}}{(1 + K_{H_2} \cdot P_{H_2} + K_{O_2} \cdot P_{O_2})^2}$	0.4943	0.1410	11.12	0.964	2.6·10 ⁻⁴	862
7. $r = \frac{k \cdot \sqrt{K_{H_2} \cdot P_{H_2}} \cdot \sqrt{K_{O_2} \cdot P_{O_2}}}{(1 + \sqrt{K_{H_2} \cdot P_{H_2}} + \sqrt{K_{O_2} \cdot P_{O_2}})^2}$	-	-	-	-	-	-
8. $r = \frac{k \cdot K_{H_2} \cdot P_{H_2} \cdot \sqrt{K_{O_2} \cdot P_{O_2}}}{(1 + \sqrt{K_{H_2} \cdot P_{H_2}} + \sqrt{K_{O_2} \cdot P_{O_2}})^2}$	-	-	-	-	-	-
9. $r = \frac{k \cdot P_{H_2} \cdot \sqrt{K_{O_2} \cdot P_{O_2}}}{(1 + \sqrt{K_{O_2} \cdot P_{O_2}})^2}$	0.1828	-	17.74	0.995	1.17·10 ⁻⁴	1990
10. $r = \frac{k \cdot P_{H_2} \cdot \sqrt{K_{O_2} \cdot P_{O_2}}}{(1 + \sqrt{K_{O_2} \cdot P_{O_2}})^2}$	-	-	-	-	-	-
11. $r = \frac{k \cdot P_{H_2} \cdot K_{O_2} \cdot P_{O_2}}{(1 + K_{O_2} \cdot P_{O_2})^2}$	0.070	-	11.12	0.965	2.6·10 ⁻⁴	865

Table V.2.2.-Regression results for several reaction models for the experimental set at 500°C for H₂ combustion over LM20-A

500°C	k	α	β	R ²	MSSR	F
1. $r = k \cdot P_{H_2}^\alpha \cdot P_{O_2}^\beta$	7.2·10 ⁻³	0.99	-0.4	0.983	4.7·10 ⁻⁴	604

500°C	k	K_{H_2}	K_{O_2}	R ²	MSSR	F
2. $r = \frac{k \cdot P_{H_2} \cdot \sqrt{K_{O_2} \cdot P_{O_2}}}{(1 + \sqrt{K_{O_2} \cdot P_{O_2}})}$	-	-	-	-	-	-
3. $r = \frac{k \cdot P_{H_2} \cdot K_{O_2} \cdot P_{O_2}}{(1 + K_{O_2} \cdot P_{O_2})}$	-	-	-	-	-	-
4. $r = \frac{k \cdot P_{H_2} \cdot K_{O_2} \cdot P_{O_2}}{(1 + \sqrt{K_{O_2} \cdot P_{O_2}})^2}$	-	-	-	-	-	-
5. $r = \frac{k \cdot K_{H_2} \cdot P_{H_2} \cdot \sqrt{K_{O_2} \cdot P_{O_2}}}{(1 + \sqrt{K_{H_2} \cdot P_{H_2}} + \sqrt{K_{O_2} \cdot P_{O_2}})^3}$	1.79	0.12	13.33	0.999	9·10 ⁻⁵	506
6. $r = \frac{k \cdot K_{H_2} \cdot P_{H_2} \cdot K_{O_2} \cdot P_{O_2}}{(1 + K_{H_2} \cdot P_{H_2} + K_{O_2} \cdot P_{O_2})^2}$	0.32	0.253	9.52	0.977	2.1·10 ⁻⁴	424
7. $r = \frac{k \cdot \sqrt{K_{H_2} \cdot P_{H_2}} \cdot \sqrt{K_{O_2} \cdot P_{O_2}}}{(1 + \sqrt{K_{H_2} \cdot P_{H_2}} + \sqrt{K_{O_2} \cdot P_{O_2}})^2}$	-	-	-	-	-	-
8. $r = \frac{k \cdot K_{H_2} \cdot P_{H_2} \cdot \sqrt{K_{O_2} \cdot P_{O_2}}}{(1 + \sqrt{K_{H_2} \cdot P_{H_2}} + \sqrt{K_{O_2} \cdot P_{O_2}})^2}$	-	-	-	-	-	-
9. $r = \frac{k \cdot P_{H_2} \cdot \sqrt{K_{O_2} \cdot P_{O_2}}}{(1 + \sqrt{K_{O_2} \cdot P_{O_2}})^3}$	0.20	-	14.1	0.989	4.9·10 ⁻⁵	946
10. $r = \frac{k \cdot P_{H_2} \cdot \sqrt{K_{O_2} \cdot P_{O_2}}}{(1 + \sqrt{K_{O_2} \cdot P_{O_2}})^2}$	-	-	-	-	-	-
11. $r = \frac{k \cdot P_{H_2} \cdot K_{O_2} \cdot P_{O_2}}{(1 + K_{O_2} \cdot P_{O_2})^2}$	0.081	-	9.57	0.977	2.2·10 ⁻⁴	424

Table V.2.3.-Regression results for several reaction models for the experimental set at 530°C for H₂ combustion over LM20-A

530°C	k	α	β	R ²	MSSR	F
1. $r = k \cdot P_{H_2}^\alpha \cdot P_{O_2}^\beta$	0.01	1.0	-0.49	0.98	3.4·10 ⁻⁴	315

530°C	k	K_{H_2}	K_{O_2}	R ²	MSSR	F
2. $r = \frac{k \cdot P_{H_2} \cdot \sqrt{K_{O_2} \cdot P_{O_2}}}{(1 + \sqrt{K_{O_2} \cdot P_{O_2}})}$	0.012	-	1·10 ¹ ₂	0.52	0.081	13.8
3. $r = \frac{k \cdot P_{H_2} \cdot K_{O_2} \cdot P_{O_2}}{(1 + K_{O_2} \cdot P_{O_2})}$	0.012	-	1·10 ¹ ₅	0.52	0.081	13.8
4. $r = \frac{k \cdot P_{H_2} \cdot K_{O_2} \cdot P_{O_2}}{(1 + \sqrt{K_{O_2} \cdot P_{O_2}})^2}$	0.012	-	6·10 ¹ ₄	0.52	0.081	13.84
5. $r = \frac{k \cdot K_{H_2} \cdot P_{H_2} \cdot \sqrt{K_{O_2} \cdot P_{O_2}}}{(1 + \sqrt{K_{H_2} \cdot P_{H_2}} + \sqrt{K_{O_2} \cdot P_{O_2}})^3}$	0.202	1.053	9.86	0.99	1.5·10 ⁻⁴	708.4
6. $r = \frac{k \cdot K_{H_2} \cdot P_{H_2} \cdot K_{O_2} \cdot P_{O_2}}{(1 + K_{H_2} \cdot P_{H_2} + K_{O_2} \cdot P_{O_2})^2}$	0.081	1.18	8.43	0.98	2.52·10 ⁻⁴	427.5
7. $r = \frac{k \cdot \sqrt{K_{H_2} \cdot P_{H_2}} \cdot \sqrt{K_{O_2} \cdot P_{O_2}}}{(1 + \sqrt{K_{H_2} \cdot P_{H_2}} + \sqrt{K_{O_2} \cdot P_{O_2}})^2}$	0.424	0.0004	3.02	0.6	0.37	0.125
8. $r = \frac{k \cdot K_{H_2} \cdot P_{H_2} \cdot \sqrt{K_{O_2} \cdot P_{O_2}}}{(1 + \sqrt{K_{H_2} \cdot P_{H_2}} + \sqrt{K_{O_2} \cdot P_{O_2}})^2}$	97.2	0.0065	4·10 ³	0.98	3.5·10 ⁻⁴	612
9. $r = \frac{k \cdot P_{H_2} \cdot \sqrt{K_{O_2} \cdot P_{O_2}}}{(1 + \sqrt{K_{O_2} \cdot P_{O_2}})^3}$	0.213	-	10	0.99	1.4·10 ⁻⁴	1555
10. $r = \frac{k \cdot P_{H_2} \cdot \sqrt{K_{O_2} \cdot P_{O_2}}}{(1 + \sqrt{K_{O_2} \cdot P_{O_2}})^2}$	0.635	-	4·10 ³	0.98	3.5·10 ⁻⁴	611
11. $r = \frac{k \cdot P_{H_2} \cdot K_{O_2} \cdot P_{O_2}}{(1 + K_{O_2} \cdot P_{O_2})^2}$	0.095	-	8.49	0.98	2.3·10 ⁻⁴	915

According to this apparent reaction orders several models were examined, some of them are reported in the tables V.2.1-V.2.3.

In particular, three Eley-Rideal model (ER) were considered (model 2, 3 and 4). In these models the limiting step is the reaction between gaseous H₂ and adsorbed, dissociatively (model 1) and not (eq. V.3.2) oxygen. Moreover, the model 4 considers that are involved two active sites.

$$r = \frac{k \cdot P_{H_2} \cdot \sqrt{K_{O_2} \cdot P_{O_2}}}{(1 + \sqrt{K_{O_2} \cdot P_{O_2}})} \quad \text{model 2}$$

$$r = \frac{k \cdot P_{H_2} \cdot K_{O_2} \cdot P_{O_2}}{(1 + K_{O_2} \cdot P_{O_2})} \quad \text{model 3}$$

$$r = \frac{k \cdot P_{H_2} \cdot K_{O_2} \cdot P_{O_2}}{(1 + \sqrt{K_{O_2} \cdot P_{O_2}})^2} \quad \text{model 4}$$

The ER models provided poor fitting of experimental data, with also estimated adsorption constant of the order of 10¹⁴ bar⁻¹ and for these reasons were rejected.

As concerns the LH models, it is visible that in all the condition the estimated value of K_{H₂} and K_{O₂} are very small and badly estimated, thus suggesting that the dependence of the conversion, i.e. the reaction rate, on these parameters has low significance.

For these reason modified LH models were also considered. In particular according to the apparent reaction order, two of the three modified models were found to well fit the experimental data and reported below:

$$r = \frac{k \cdot P_{H_2} \cdot \sqrt{K_{O_2} \cdot P_{O_2}}}{(1 + \sqrt{K_{O_2} \cdot P_{O_2}})^3} \quad \text{model 9}$$

$$r = \frac{k \cdot P_{H_2} \cdot K_{O_2} \cdot P_{O_2}}{(1 + K_{O_2} \cdot P_{O_2})^2} \quad \text{model 11}$$

The model 9 usually gives a better fit of the data being the MSSR the lowest for all the temperatures. However the improvements in data fitting, i.e. the difference in MSSRs is of the same order of the standard error and thus, the two models are not statistically different. As a consequence, the model

11 has been considered to give the best fitting, because it is related to a reaction mechanism involving two (and not three) sites.

In table V.2.4 the coefficient with their own 95% confidence interval are summarized for the model 11, while the fig. V.2.2 reports the data fitting by the model 11. Calculated activation energy for k and ΔH_{O_2} for K_{O_2} are 25 kJ/mol and 22 kJ/mol. Even if the activation energy appears low, this value is not so far from those previously reported (Scarpa et al. 2009), suggesting that the limiting step is slightly activated by the temperature. As suggested by the very low MSSR values, the model lines show a good agreement with experimental data in the whole range of pressures, temperatures and compositions investigated.

Table V.2.4. Regression results at different temperatures according to model eq. V.2.5.

T, °C	k	K_{O₂}	MSSR
470	$7 \pm 1 \cdot 10^{-2}$	11.13 ± 2	$2.6 \cdot 10^{-4}$
500	$8 \pm 1 \cdot 10^{-2}$	9.57 ± 1.1	$4.9 \cdot 10^{-5}$
530	$9.5 \pm 0.8 \cdot 10^{-2}$	8.5 ± 1.0	$2.3 \cdot 10^{-4}$

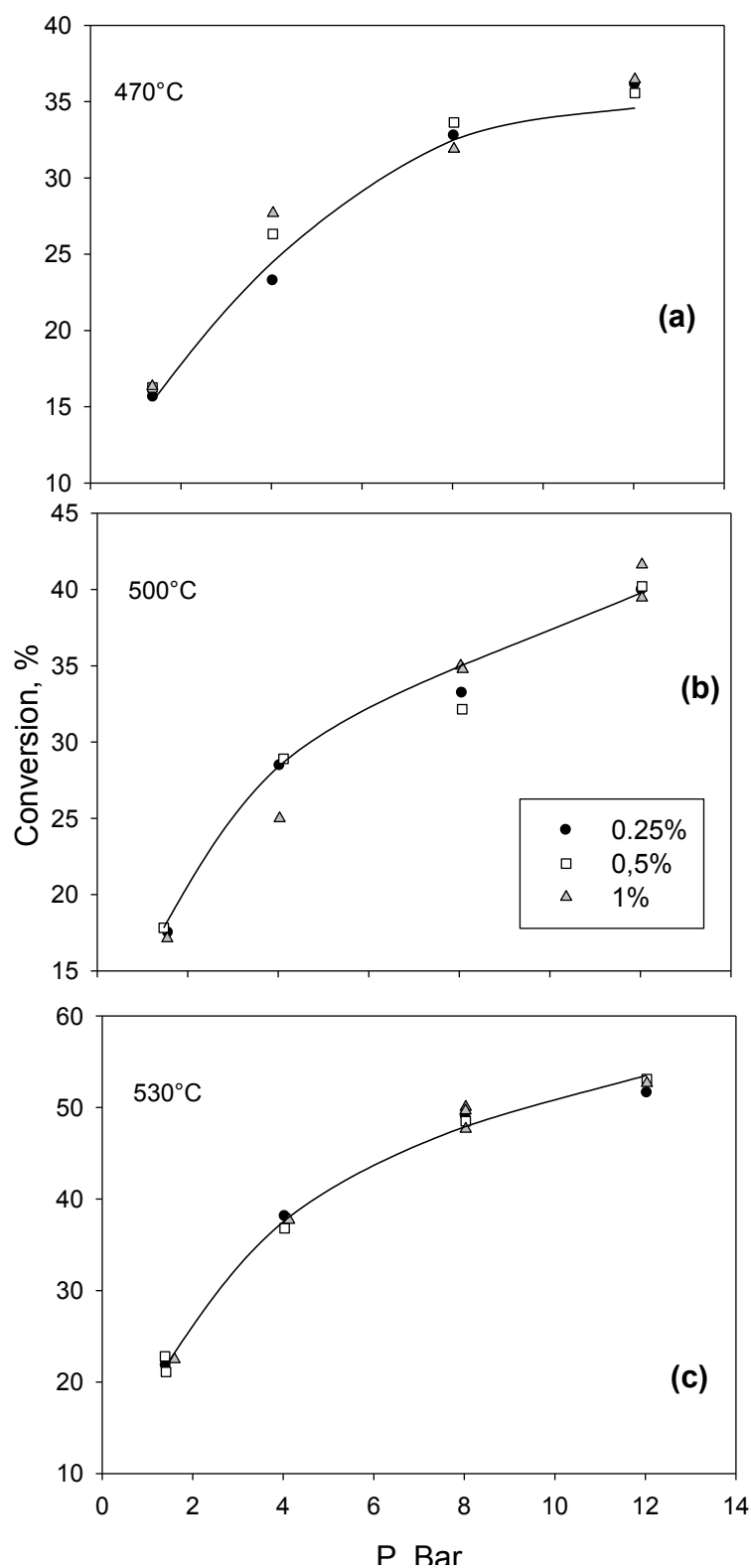


Fig.V.2.2 H₂ conversion as a function of pressure and parametric in the H₂ inlet fraction for LM20-A platelet. T=(a)470°C, (b)=500°C and (c) 530°C. Q_{tot}= 100 splh; Symbols: experimental data; solid lines: model 11 predicted conversions.

The fig.V.2.3 shows the hydrogen conversions as a function of the pressure and parametric in the inlet H₂ fraction at different oxygen concentration (a: 8.5%vol.; b: 4,25% vol.). The temperature of the experiments is set at 70°C and the total flow rate was equal to 100splh.

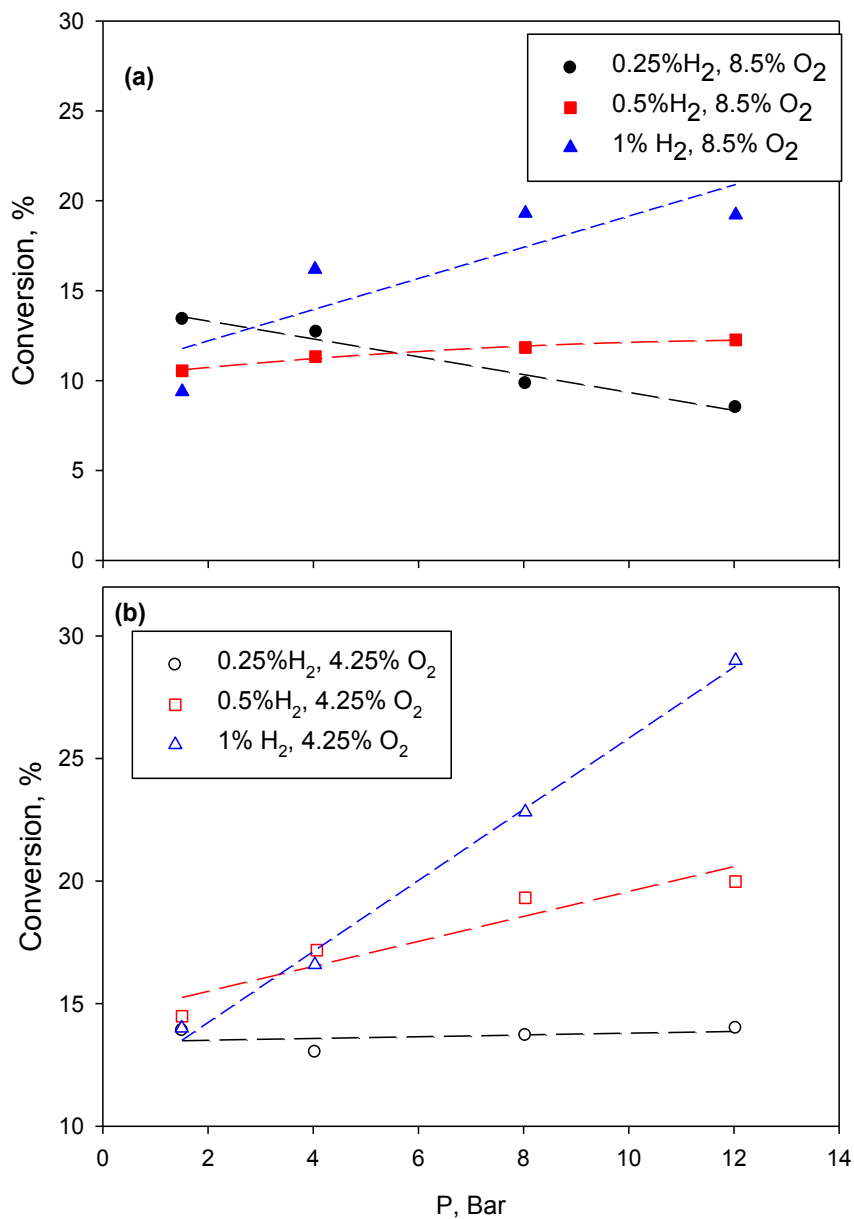


Fig. V.2.3 H₂ conversion as a function of the pressure and parametric in the inlet H₂ fraction over 1Pt-A. Q_{tot}=100 splh, T=70°C. (a) y_{O2}=8.5%; (b) y_{O2}=4.25%.

From Fig.V.2.3 it appears that very different conversion behavior are encountered not only at different y_{H_2} but also at different oxygen content. Also plotting the conversion as a function of the inlet y_{H_2} and parametric with the temperature (fig. V.2.4) it appears that the effect of the pressure, in the case of the higher oxygen content, is not monotone with the y_{H_2} . As a matter of fact, for the low y_{H_2} , the pressure has a negative effect on conversion, while at higher oxygen content a pressure increase is associated with a conversion increase. On the contrary, in the case of the tests carried out at 4.25% O_2 , the effect of the pressure is trivial (i.e conversion increases by increasing the pressure).

In order to elucidate the effect of O_2 and H_2 the apparent reaction orders have been also estimated from data at constant pressure (see table V.2.5). From these data it appears that the apparent hydrogen reaction order increases by increasing the pressure, while an opposite behavior was found for the oxygen whose reaction order is negative and even lower at high pressure. The opposite trend of fuel and oxidizer reaction order causes a maximum of apparent reaction order at 4 bar.

TabV.2.5- Apparent O_2 and H_2 reaction order estimated for the experimental sets at constant pressure for H_2 combustion over 1Pt-A

$r = \tau \cdot P^{(\alpha + \beta)} \cdot y_{H_2}^\alpha \cdot y_{O_2}^\beta$				
P, bar	k, mol/(g·s·bar ^{-($\alpha+\beta$)})	α	β	($\alpha+\beta$)
1.5	0.0093	1.0445	-0.2111	0.8334
4		1.2372	-0.2665	0.9707
8		1.4761	-0.5753	0.9008
12		1.6183	-0.8879	0.7304

The predicted conversion of the power law model were also plotted in comparison with the experimental ones as a function of the inlet hydrogen fraction for the different pressures (Fig.V.2.5).

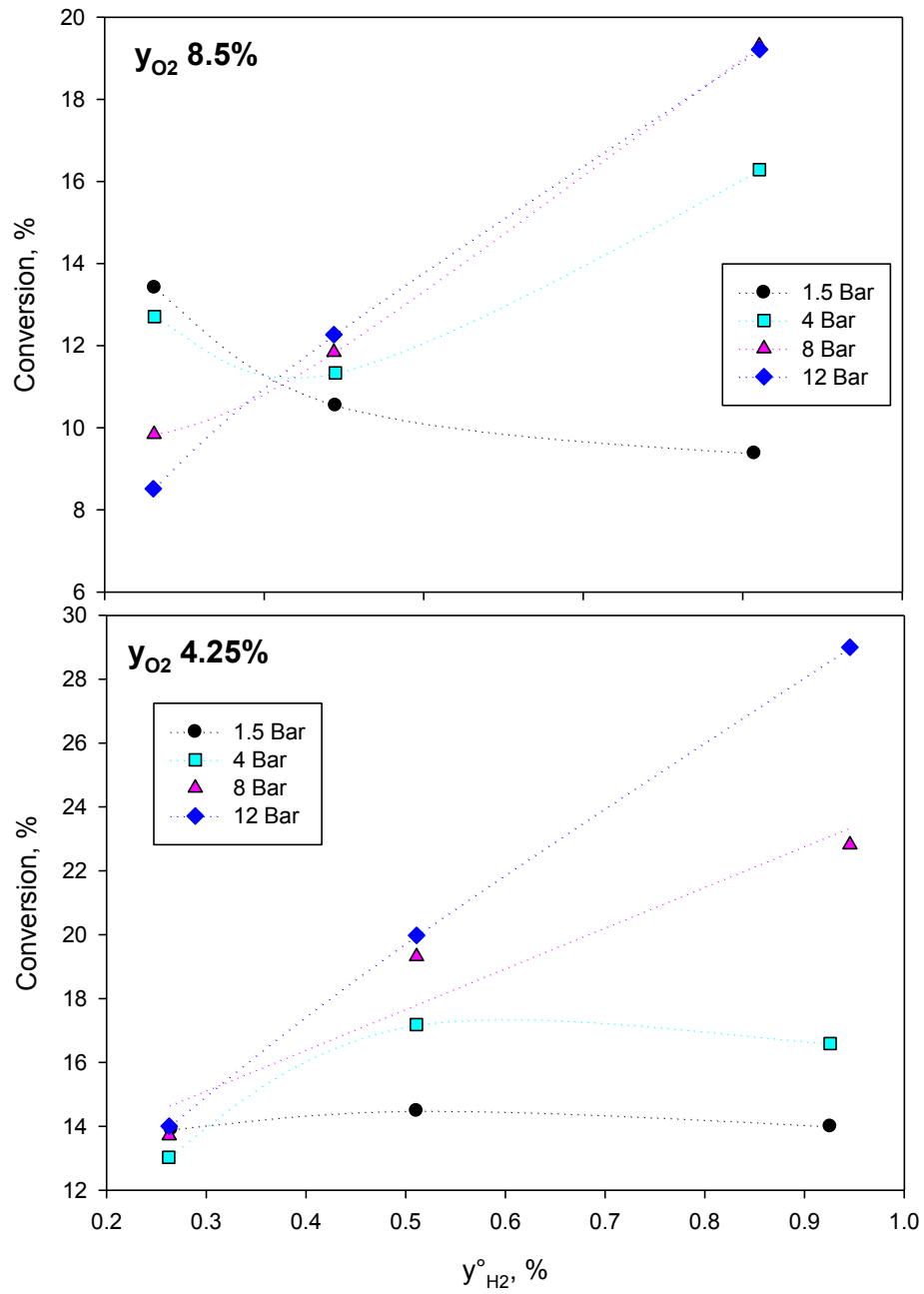


Fig. V.2.4 H₂ conversion as a function of the inlet $y_{H_2}^o$ and parametric in the pressure over 1Pt-A. $Q_{tot}=100$ splh; (a) $y_{O_2}=8.5\%$; (b) $y_{O_2}=4.25\%$.

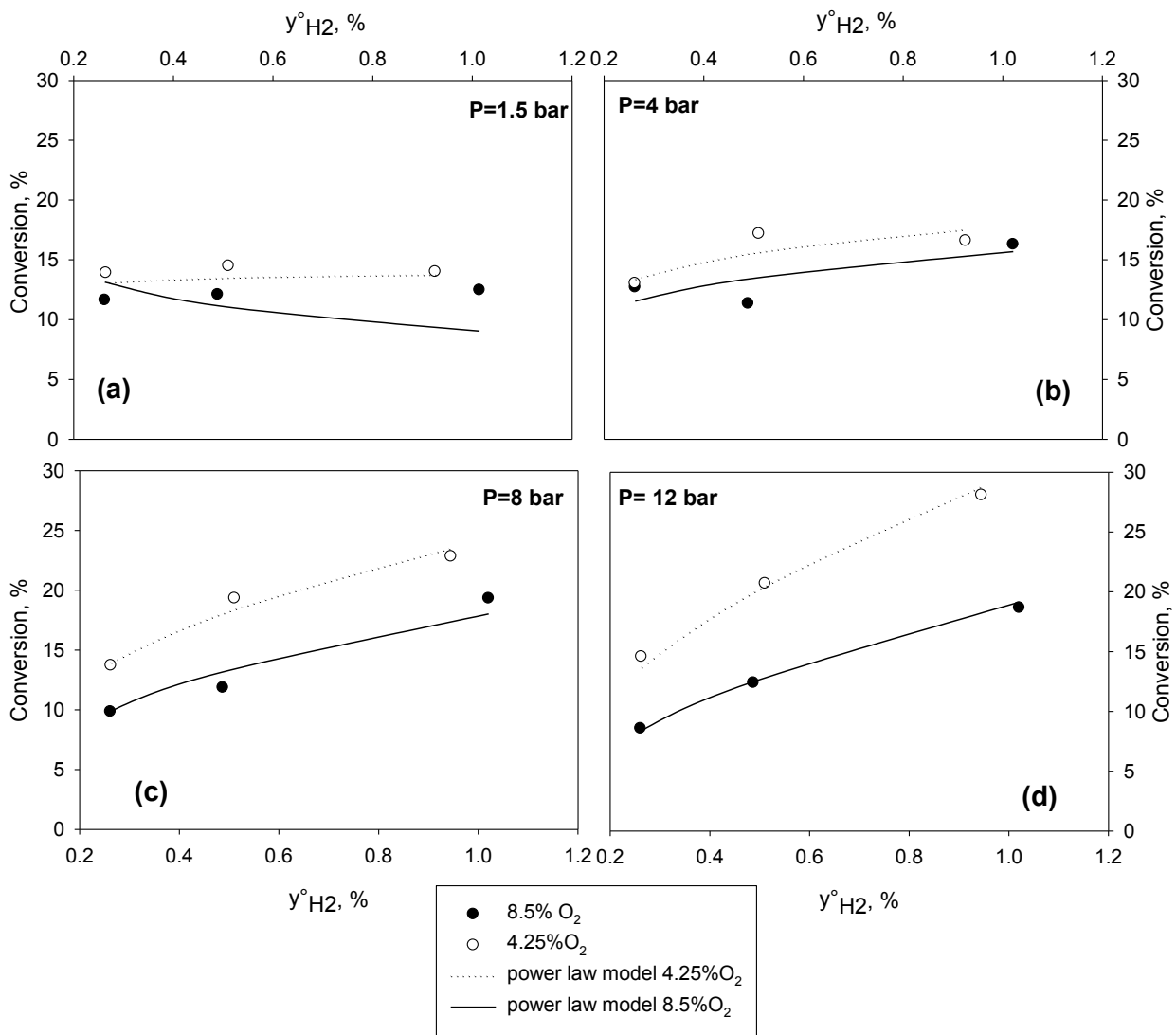


Fig. V.2.5 H₂ conversion as a function of the inlet y^oH₂ and parametric in the y^oO₂ over 1Pt-A platelet. Comparison between experimental data (symbols) and model prediction (lines). T=70°C; Q_{tot}=100 splh; (a) P=1.5 bar (b) P= 4bar (c) P=8 bar and (d) P=12 bar.

Hydrogen combustion was also investigated at 110°C. The corresponding results are reported in fig.V.2.6 showing the hydrogen conversions as a function of the pressure and parametric in the inlet H₂ fraction at different oxygen concentrations (a: 8.5% vol.; b: 4,25% vol.), while the flow rate was set at 100splh.

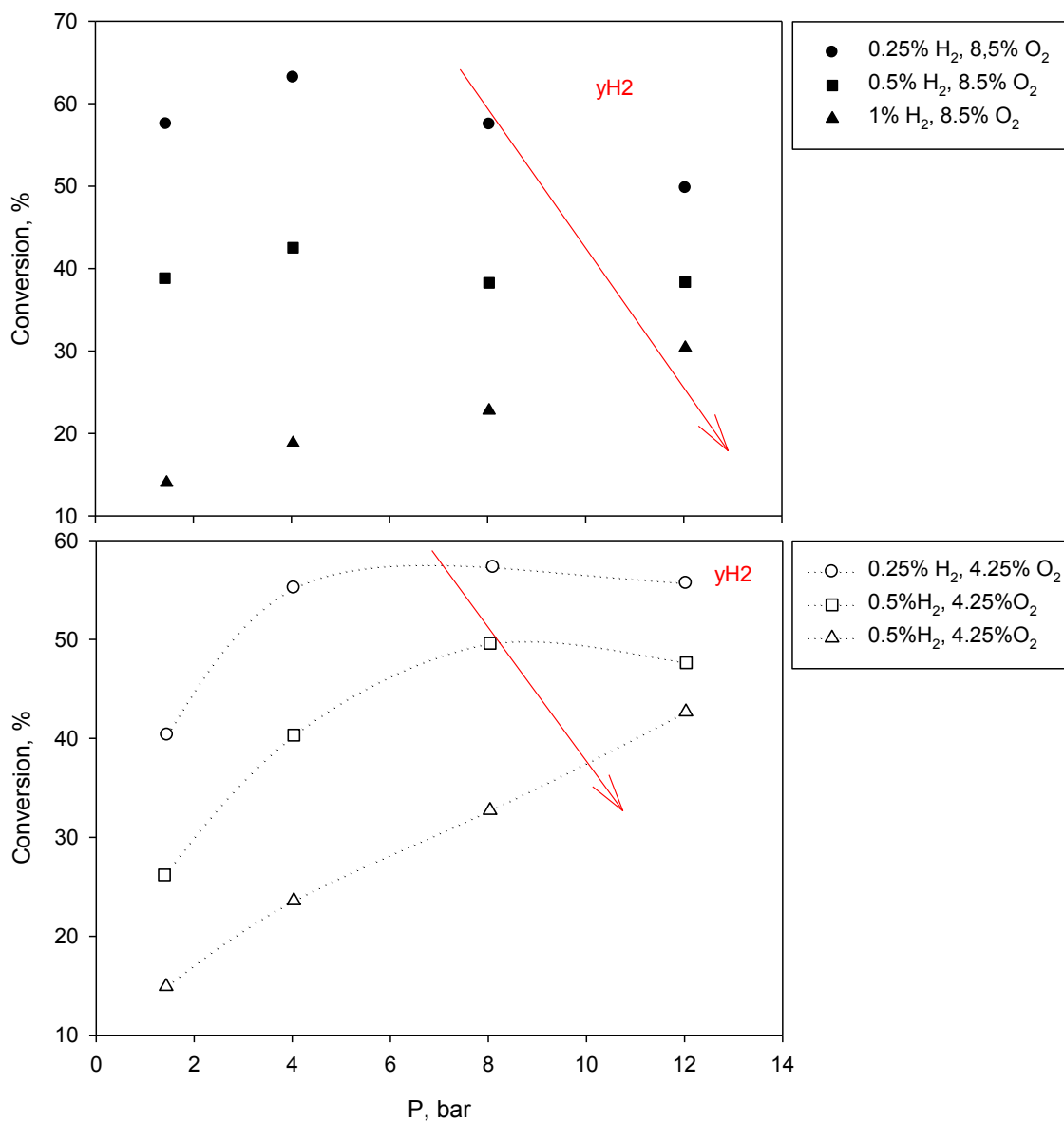


Fig. V.2.6 H₂ conversion as a function of the pressure and parametric in the inlet $y^{\circ}_{H_2}$ over 1Pt-A platelet. $Q_{tot}=100$ splh; $T=110^{\circ}C$. (a) $y_{O_2}=8.5\%$; (b) $y_{O_2}=4.25\%$.

With respect to the analogous experiments carried out at lower temperature, an opposite trend with hydrogen content is observed. As a matter of fact the conversion decrease by increasing the fuel content in the mixture, thus suggesting a reaction apparent order less than unity. The effect of oxygen is more highlighted in Fig.V.2.7 were the conversion obtained with the different oxygen content are compared and plotted as a function of the inlet $y^{\circ}_{H_2}$ and for different pressures.

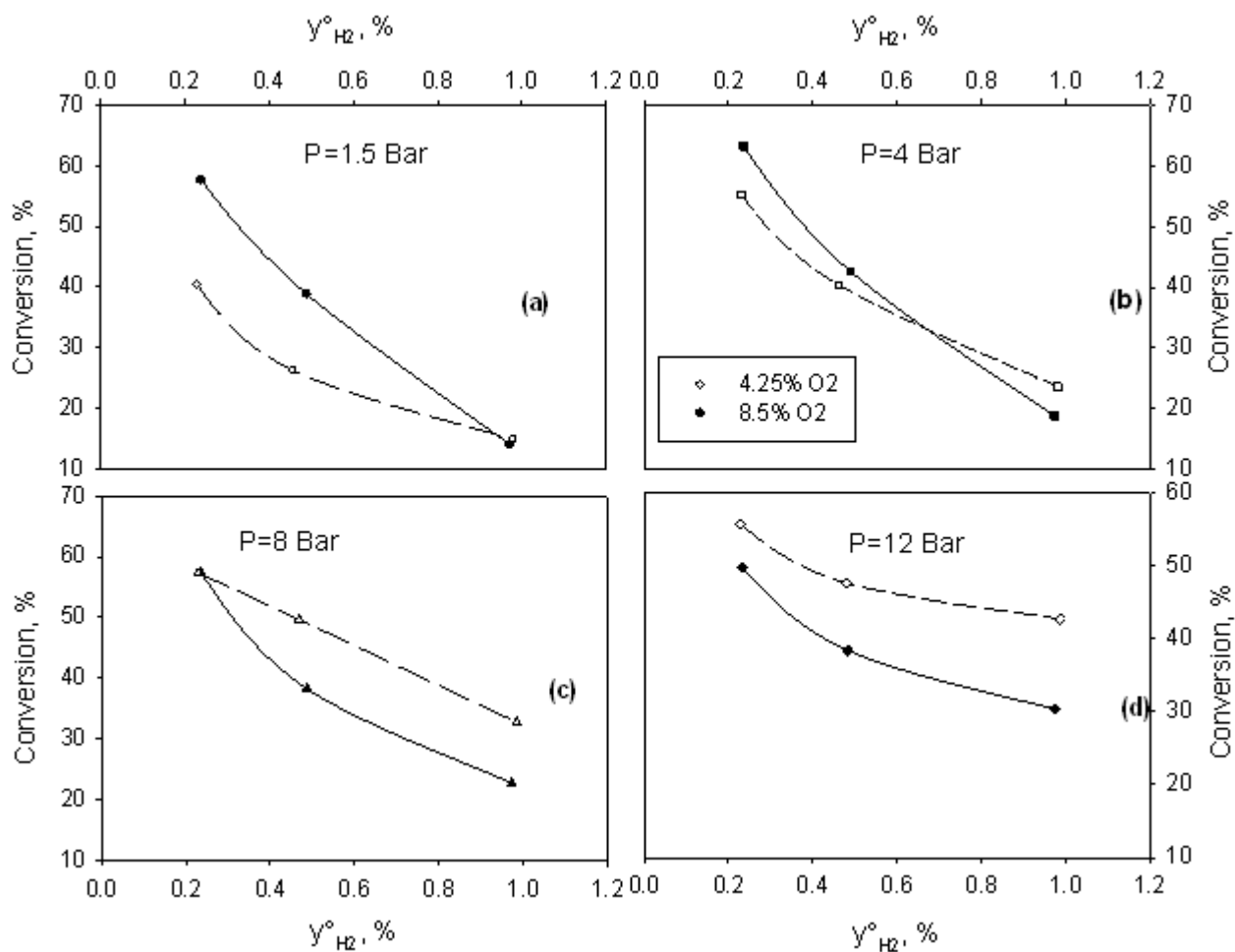


Fig. V.2.7 H₂ conversion as a function of the inlet $y^{\circ}_{H_2}$ and parametric in the $y^{\circ}_{O_2}$ over 1Pt-A platelet. $Q_{tot}=100$ splh; (a) P=1.5 bar; (b) P= 4bar; (c) P=8 bar; (d)P=12 bar. T=110°C.

The effect of oxygen on conversion is different on dependence of the pressure. As a matter of fact, at low pressure ($P \leq 4$) the oxygen has a beneficial effect on conversion, but at higher pressure, the mixture containing less oxygen shows the higher conversion. This change of the behavior is typical of the competitive adsorption systems. Accordingly the reaction order of O₂ seems to continuously decrease from positive to negative values by raising the pressure.

The apparent reaction order of H₂ and O₂ were estimated by regressing the experimental conversions using a power law as reaction rate and the results were reported in Table V.2.6.

TabV.2.6 Apparent reaction O₂ and H₂ order estimated for the H₂ combustion over 1Pt-A platelet: sets at constant pressure and 110°C.

$r = k \cdot P^{(\alpha+\beta)} \cdot y_{H_2}^\alpha \cdot y_{O_2}^\beta$				
P, bar	k, mol/(g·s·bar ⁻¹)	α	β	$(\alpha+\beta)$
1.5	0.0015	0.1610	0.5051	0.6661
4		0.3489	0.2059	0.5548
8		0.5146	-0.1856	0.3290
12		0.5812	-0.3848	0.1964

It is evident that O₂ reaction order changes significantly decreasing from 0.5 to -0.38, while also in this case the hydrogen reaction order increases with the pressure. The calculated conversion associated with the power law are also reported in comparison with experimental data in Fig. V.2.8.

For the results obtained at 110°C an attempt to use a simple reaction model was made. Among the different discriminated models, not reported, a triple site model reaction (reaction rate in eq. V.2.6) was found to give, even if poor, a fitting of the data. The corresponding parameters are reported in table V.2.7. In addition the conversion predicted by the triple site model were compared with experimental results in Fig V.2.9.

$$r = \frac{k_{SR} K_1 P_{H_2} \sqrt{K_2 P_{O_2}}}{(1 + \sqrt{K_1 P_{H_2}} + \sqrt{K_2 P_{O_2}})^3} \quad \text{eq.V.2.6}$$

TabV.2.7 Estimated parameters for the model of eq. V.2.6 at 110°C.

110°C	k _{SR} , NI/(g·s)	K ₁	K ₂	R ²
$r = \frac{k_{SR} K_1 P_{H_2} \sqrt{K_2 P_{O_2}}}{(1 + \sqrt{K_1 P_{H_2}} + \sqrt{K_2 P_{O_2}})^3}$	0.0049	264.6	46	0.832

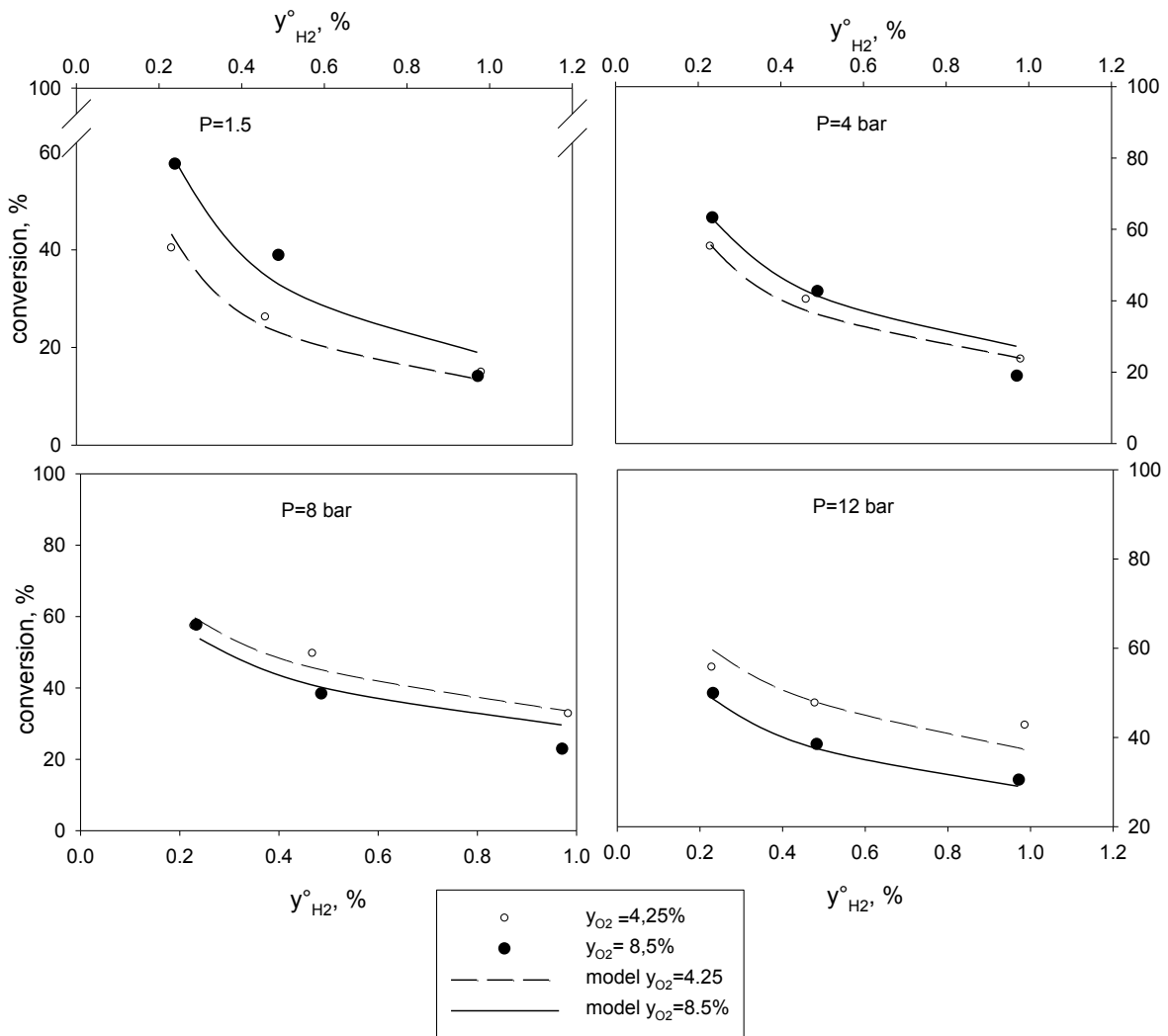


Fig. V.2.8 H₂ conversion as a function of the inlet y_{H₂} and parametric in the y_{O₂}. Comparison between experimental data (symbols) and model prediction (lines). T=110°C; Q_{tot}=100 splh; (a) P=1.5 bar; (b) P= 4bar; (c) P=8 bar; (d) P=12 bar.

The model that was found at 110°C, it could be not extended to the results obtained at lower temperature. This is in agreement with the general finding that hydrogen combustion on platinum is a complex reaction. As a matter of fact, although this reaction is well known and studied, in the literature an unified description of the water formation covering all the range of temperatures is not reported. The widespread range of activation energies for the reaction, ranging from 2 and 20 kcal/mol confirms the disagreement of the literature data.

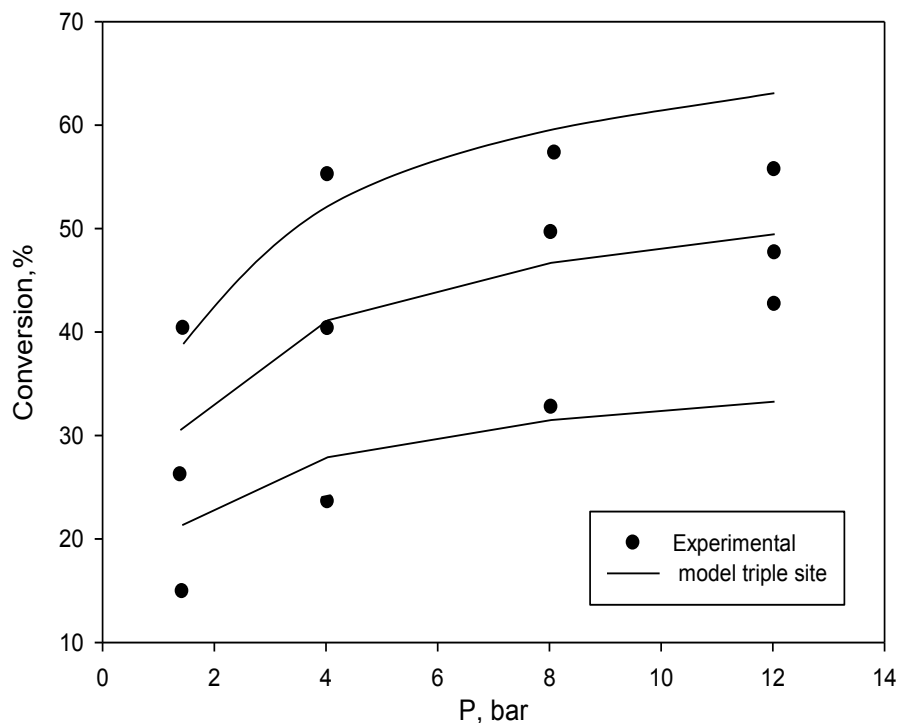


Fig. V.2.9 H₂ conversion as a function of the pressure and parametric with the inlet y_{H2}. Experimental data (symbols) and model prediction (lines). T=110°C Q_{tot}=100 splh; y_{O2}=4,25%

As a matter of fact, even if it is generally accepted that the reaction occurs either by sequential addition of H ($O+H\leftrightarrow OH$, $OH+H\leftrightarrow H_2O$) either by OH disproportionation ($OH+OH\leftrightarrow H_2O+O$), the literature is discordant in which one route is dominant. Partially this disagreement is explained, as stated by Hellsing et al (1991), by the very different magnitude orders of activation energies of various steps, probably leading to the dominance of a particular step at low temperature, while another one is limiting at higher temperatures. Analogously different steps can be limiting under hydrogen or oxygen excess.

In addition, many authors reveal some inconsistencies of their models with experimental data and consequently many theories were adducted. For example Hellsing et al (1991), studying the OH and H₂O desorption at high T, postulated that, due to repulsive lateral interactions between hydroxyls and oxygen, some activation energies may strongly depend on the surface coverage (θ).

Moreover it has been proposed that water is formed via a non homogenous surface reaction proceedings at the perimeters of O islands present on the Pt surface at low T (Gland et al 1982, Hellsing et al 1991).

Another aspect that is addressed is the role of steps on the surface that, at high oxygen coverage slow down the reaction while at low oxygen coverage causes a “branching” of the reaction (Verheij et al 1990, 1991). Verheij et al (1998 and 1997), investigating the reaction with molecular beam relaxation spectroscopy (300 K < T < 1200 K), proposed the so called *reactive site model* assuming that only few special Pt sites are catalytically active. The model consists in several reactions (about 12 reversible reactions) including the transport by means of slow diffusion of O and OH and some exchange reactions. In particular authors claim that at T below 800 K and in hydrogen excess, the O diffusion from terrace sites to reactive sites is the rate limiting step (Verheij et al 1998), while at high oxygen coverage and low T an exchange reaction $H_2O + OH \leftrightarrow OH + H_2O$ is responsible of the H transport from reactive sites to O adatoms on terrace sites (Verheij et al 1997).

In conclusion, it is not possible to derive a simple model reaction rate for H₂ combustion on Pt which covers a wide range of pressures, temperatures and reagents concentrations, as obtained in the previous and following cases.

V.3 CO combustion

V.3.1 CO combustion on supported LaMnO₃

The fig. V.3.1.1 shows the conversion for CO combustion as a function of the pressure and parametric in the inlet y°_{CO} in the case of high excess of O₂ (8.5%) and a total flow rate of 75 splh. It clearly appears that, for all the investigated temperatures, the conversion decreases by increasing the CO content, while a pressure increase causes an conversion increase principally due to the increasing of the time contact. This is also visible in Fig. V.3.1.2 where the same tests are reported as a function of the y°_{CO} parametric in the pressure.

Moreover from Fig.V.3.1.2 it appears that the conversion increasing with the pressure is higher by increasing the temperature from 470°C to 500 °C, suggesting that the apparent order with pressure increases in this range of temperature, while the data 500°C and 530°C show very similar trends with pressure thus indicating a similar value of the apparent reaction order with pressure.

In order to support this indication the computed reaction order with respect to CO and total pressure Π were obtained using a power law rate expression as follows:

$$r = k P^m y_{CO}^n \quad \text{eq. V.3.1}$$

while the corresponding reaction order at different temperatures are reported in table V.3.1

TabV.3.1 Apparent reaction order at different temperatures for the CO combustion over LM20-A platelet

T°C	m	n	K	R²
470	0.622±0.0421	0.26±0.0315	3.8·10 ⁻⁴	0.988
500	0.77±0.0184	0.56±0.0139	9.1·10 ⁻⁴	0.996
530	0.66±0.0227	0.72±0.0164	1.7·10 ⁻³	0.992

The reaction order with CO monotonously increases with the temperature; on the contrary the reaction order of pressure with temperature hasn't a monotone trend, thus suggesting a different reaction order trend with respect to oxygen.

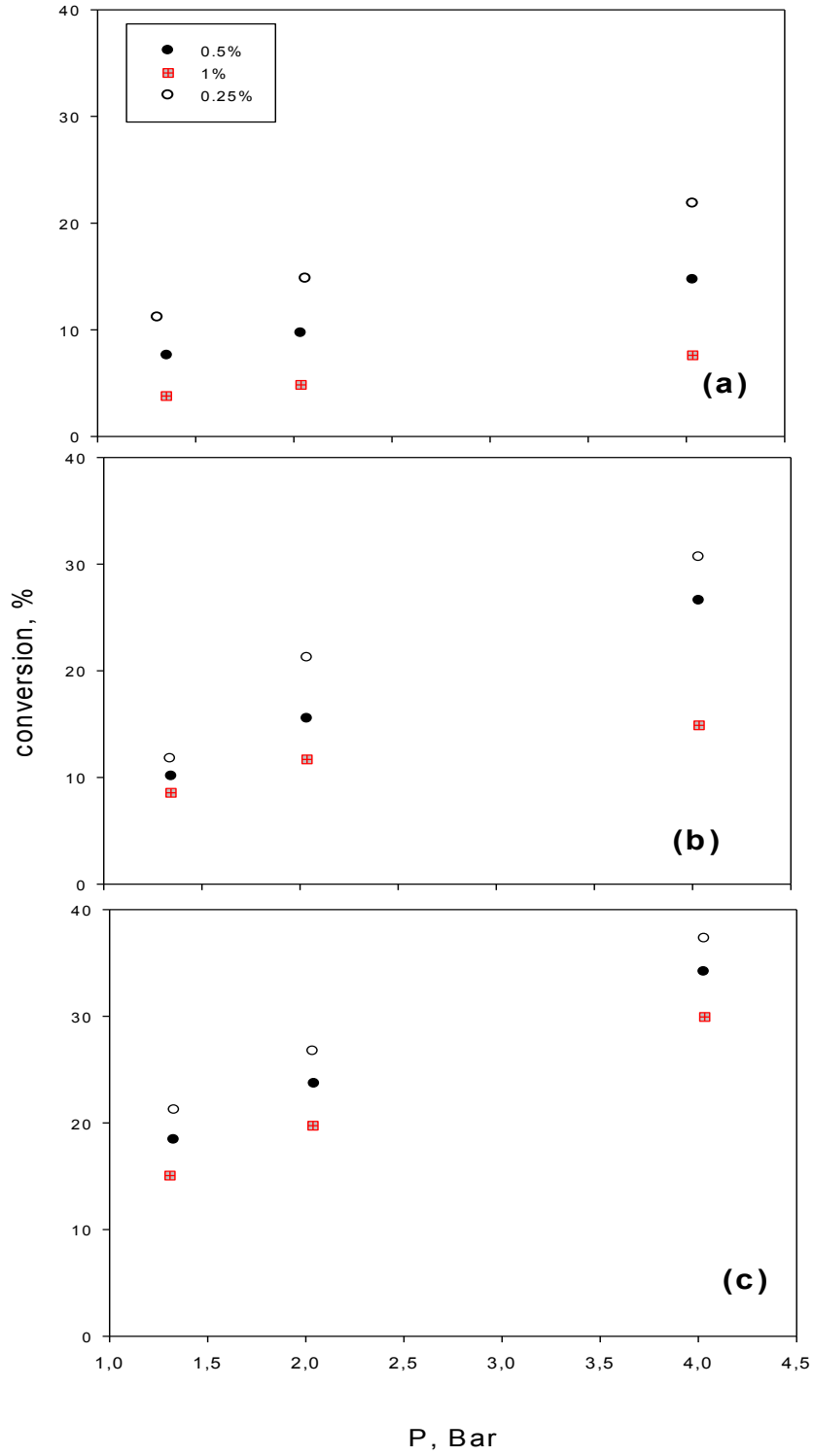


Fig.V.3.1.1.- CO conversion as a function of the pressure and parametric in the inlet y_{CO}^o over LM20-A platelet. Total flow rate 75 splh; $y_{O_2}=8,5\%$; T:(a)470°, (b) 500°C, (c) 530°C.

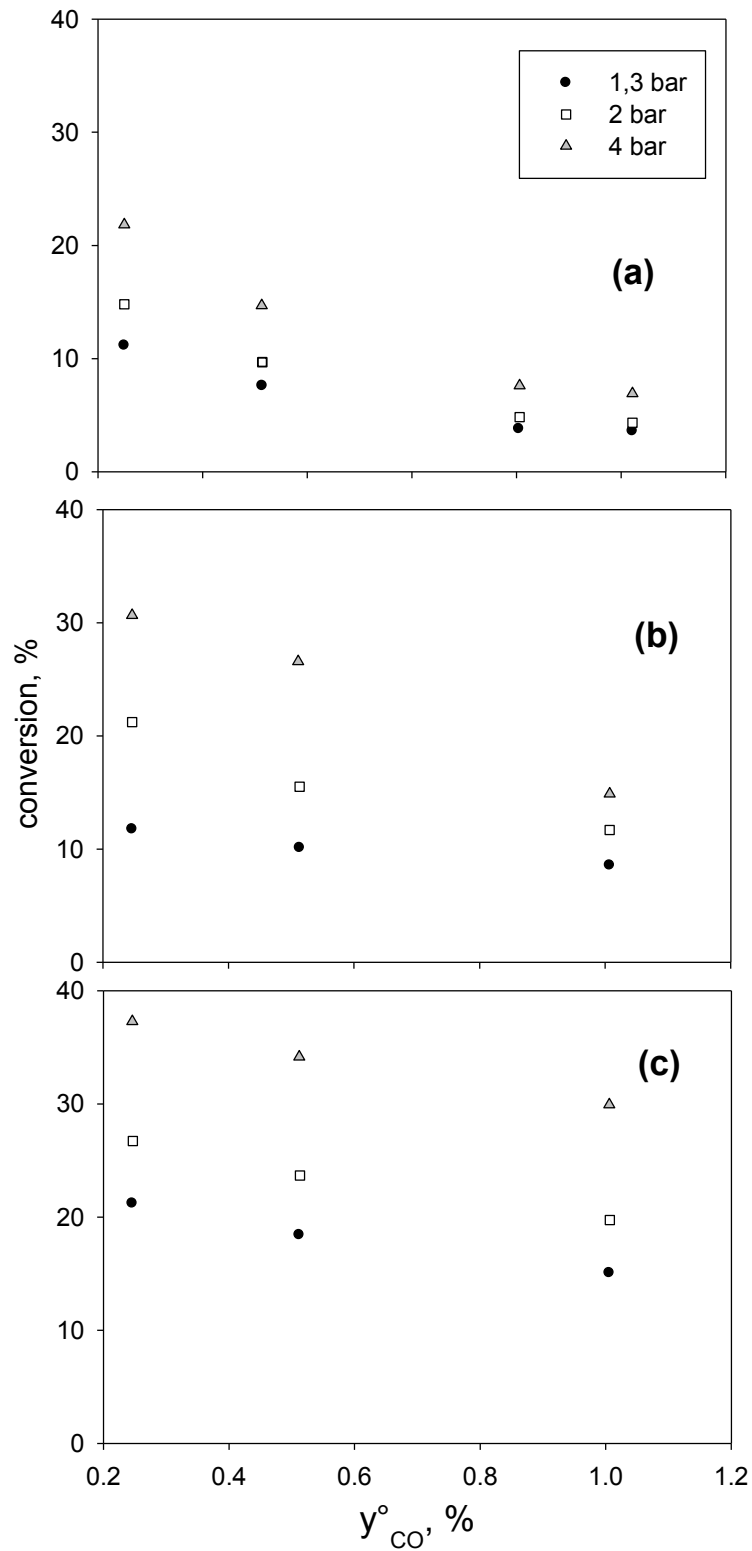


Fig.V.3.1.2.- CO conversion as a function of the inlet y°_{CO} and parametric in the pressure over LM20-A platelet. Total flow rate 75 splh; $y_{O_2}=8,5\%$; T:(a)470°, (b) 500°C, (c) 530°C.

In order to assess the role of oxygen, tests with different O₂ content were carried out too. These tests are reported in Fig. V.3.1.3. in comparison with the previous reported results.

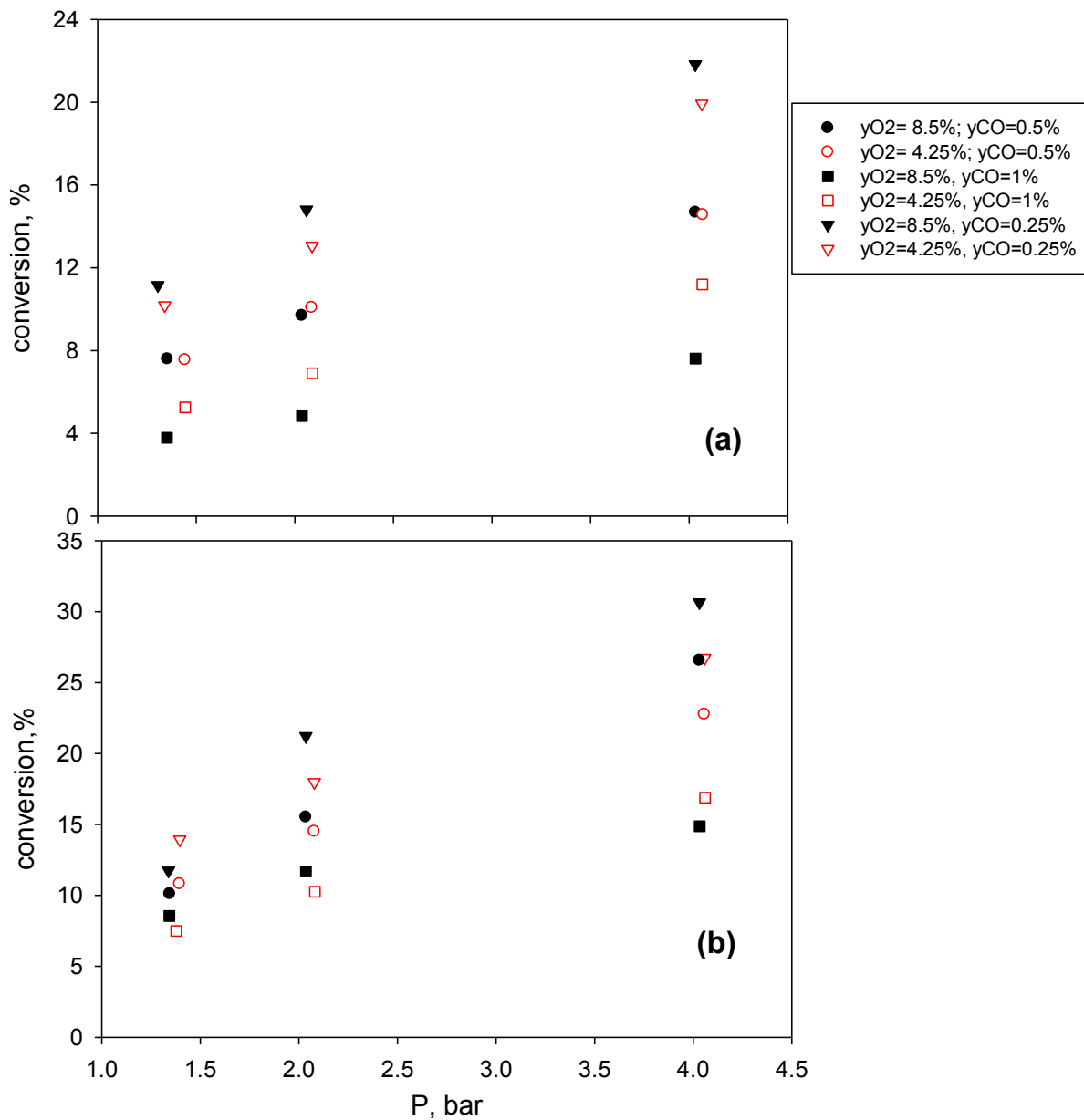


Fig.V.3.1.3.- CO conversion as a function of the pressure parametric in the y^o_{CO} over LM20-A platelet. Total flow rate 75 splh; Empty symbols:y^o_{O₂}=4,25%; Full symbols y^o_{O₂}=8,25%and T:(a)470°, (b) 500°C,

The oxygen effect is not directly highlighted. As a matter of fact it appears that on dependence of temperature and CO fraction the conversion results lower or higher of the analogous with different oxygen content.

Therefore further tests were carried out at 530°C setting the O₂/CO ratio at constant value equal to 2 and 4,25 that correspond to fed ratio of 4 and 8,5, according to the reaction stoichiometry, reported in Fig. V.3.1.4.

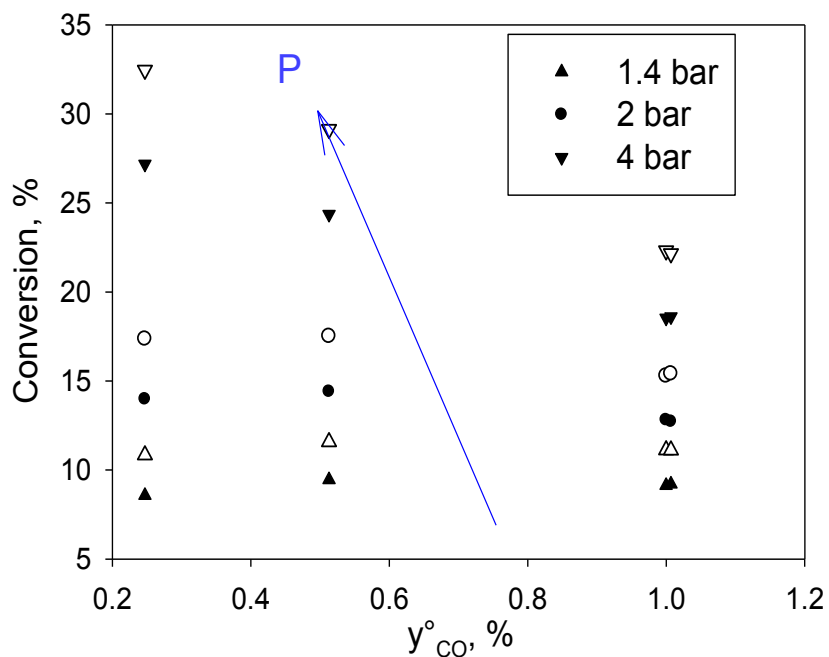


Fig.V.3.1.4.- CO conversion as a function of the pressure and parametric in the fed ratio M over LM20-A platelet. Total flow rate 75 splh; Empty symbol :M=8.5; Full symbol: M=4.5 T=530°C,

It appears that the conversion obtained with the highest fed ratio are always higher than the corresponding ones at lower ratio.

All data collected were firstly roughly regressed with a power law with exponents α and β as apparent reaction order with respect to CO and O₂. Then many fractional kinetic models, that could were tested.

The results of these regressions are reported in table V.3.1.1-3.

TabV.3.1.1 Kinetic parameters obtained for different models at 470°C for CO combustion over LM20-A platelet

470°C	Model	k	α	β	R ²	MSSR	F
Power law	$r = k \cdot P_{CO}^{\alpha} \cdot P_{O_2}^{\beta}$	8·10 ⁻⁴	0.51	0.27	0.92	4.8·10 ⁻⁶	249

470°C	Model	k	K_{CO}	K_{O_2}	R ²	MSSR	F
Eley rideal	$r = \frac{k \cdot P_{CO} \cdot K_{O_2} \cdot P_{O_2}}{(1 + K_{CO} \cdot P_{CO})}$	2.7·10 ⁻⁴	1.16·10 ³	-	0.09	7.1·10 ⁻⁵	3.49
Langmuir Hinshelwod	$r = \frac{k \cdot K_{CO} \cdot P_{CO} \cdot K_{O_2} \cdot P_{O_2}}{(1 + K_{CO} \cdot P_{CO} + K_{O_2} \cdot P_{O_2})^2}$	5·10 ⁻⁴	95.17	13.18	0.82	1.15·10 ⁻⁵	95.1
	$r = \frac{k \cdot K_{CO} \cdot P_{CO} \cdot \sqrt{K_{O_2} \cdot P_{O_2}}}{(1 + K_{CO} \cdot P_{CO} + \sqrt{K_{O_2} \cdot P_{O_2}})^2}$	7·10 ⁻⁴	58.63	3.43	0.91	5.9·10 ⁻⁶	206
LH different sites	$r = \frac{k \cdot K_{CO} \cdot P_{CO} \cdot K_{O_2} \cdot P_{O_2}}{(1 + K_{CO} \cdot P_{CO}) + (1 + K_{O_2} \cdot P_{O_2})}$	1·10 ⁻⁴	108.56	65.43	0.89	7.0·10 ⁻⁶	168
	$r = \frac{k \cdot K_{CO} \cdot P_{CO} \cdot \sqrt{K_{O_2} \cdot P_{O_2}}}{(1 + K_{CO} \cdot P_{CO}) + (1 + \sqrt{K_{O_2} \cdot P_{O_2}})}$	2·10 ⁻⁴	120.23	15.85	$\frac{0.92}{2}$	5.2·10 ⁻⁶	236
modif ied	$r = \frac{k \cdot K_{CO} \cdot P_{CO} \cdot \sqrt{K_{O_2} \cdot P_{O_2}}}{(1 + K_{CO} \cdot P_{CO})^2}$	6·10 ⁻⁴	52.56	-	0.69	2.0·10 ⁻⁵	90

TabV.3.1.2 Kinetic parameters obtained for different models at 500°C for CO combustion over LM20-A platelet

500°C	Model	k	α	β	R ²	MSSR	F
Power law	$r = k \cdot P_{CO}^{\alpha} \cdot P_{O_2}^{\beta}$	1.9·10 ⁻³	$\alpha=0.60$	$\beta=0.23$	0.92	3.5·10 ⁻⁵	97

500°C	Model	k	K_{CO}	K_{O_2}	R ²	MSRR	F
Eley rideal	$r = \frac{k \cdot P_{CO} \cdot K_{O_2} \cdot P_{O_2}}{(1 + K_{CO} \cdot P_{CO})}$	6·10 ⁻⁴	1.2·10 ³	-	0.44	2.4·10 ⁻⁴	15
Langmuir Hinshelwood	$r = \frac{k \cdot K_{CO} \cdot P_{CO} \cdot K_{O_2} \cdot P_{O_2}}{(1 + K_{CO} \cdot P_{CO} + K_{O_2} \cdot P_{O_2})^2}$	1.0·10 ⁻³	58.76	6.69	0.96	1.5·10 ⁻⁵	231
	$r = \frac{k \cdot K_{CO} \cdot P_{CO} \cdot \sqrt{K_{O_2} \cdot P_{O_2}}}{(1 + K_{CO} \cdot P_{CO} + \sqrt{K_{O_2} \cdot P_{O_2}})^2}$	1.3·10 ⁻³	46	3.13	0.97	1.2·10 ⁻⁵	324
LH different sites	$r = \frac{k \cdot K_{CO} \cdot P_{CO} \cdot K_{O_2} \cdot P_{O_2}}{(1 + K_{CO} \cdot P_{CO}) + (1 + K_{O_2} \cdot P_{O_2})}$	2·10 ⁻⁴	76.35	35.2	0.96	1.5·10 ⁻⁵	252
	$r = \frac{k \cdot K_{CO} \cdot P_{CO} \cdot \sqrt{K_{O_2} \cdot P_{O_2}}}{(1 + K_{CO} \cdot P_{CO}) + (1 + \sqrt{K_{O_2} \cdot P_{O_2}})}$	3·10 ⁻⁴	77.30	23.16	0.97	1.4·10 ⁻⁵	262
modified	$r = \frac{k \cdot K_{CO} \cdot P_{CO} \cdot \sqrt{K_{O_2} \cdot P_{O_2}}}{(1 + K_{CO} \cdot P_{CO})^2}$	1.1·10 ⁻³	35	-	0.86	5.8·10 ⁻⁵	118

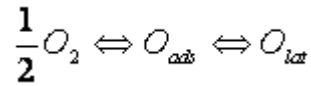
TabV.3.1.3 Kinetic parameters obtained for different models at 530°C for CO combustion over LM20-A platelet

530°C	Model	k	α	β	R ²	MSSR	F
Power law	$r = k \cdot P_{CO}^{\alpha} \cdot P_{O_2}^{\beta}$	3.8·10 ⁻²	$\alpha=0.67$	$\beta=0.22$	0.91	1.910 ⁻⁵	151

530°C	Model	k	K_{CO}	K_{O_2}	R ²	MSE	F
Eley rideal	$r = \frac{k \cdot P_{CO} \cdot K_{O_2} \cdot P_{O_2}}{(1 + K_{CO} \cdot P_{CO})}$	0.0013	93	-	-1.66	5.5·10 ⁻⁴	-2
Langmuir Hinshelwood	$r = \frac{k \cdot K_{CO} \cdot P_{CO} \cdot K_{O_2} \cdot P_{O_2}}{(1 + K_{CO} \cdot P_{CO} + K_{O_2} \cdot P_{O_2})^2}$	2.9·10 ⁻⁶	3.36	7.8·10 ⁻⁶	-3.43	2.8·10 ⁻⁴	-3.5
	$r = \frac{k \cdot K_{CO} \cdot P_{CO} \cdot \sqrt{K_{O_2} \cdot P_{O_2}}}{(1 + K_{CO} \cdot P_{CO} + \sqrt{K_{O_2} \cdot P_{O_2}})^2}$	2.2·10 ⁻³	32.48	4.06	0.96	9.3·10 ⁻⁶	338
LH different sites	$r = \frac{k \cdot K_{CO} \cdot P_{CO} \cdot K_{O_2} \cdot P_{O_2}}{(1 + K_{CO} \cdot P_{CO}) + (1 + K_{O_2} \cdot P_{O_2})}$	4·10 ⁻⁴	55.51	82.02	0.92	1.6·10 ⁻⁵	184
	$r = \frac{k \cdot K_{CO} \cdot P_{CO} \cdot \sqrt{K_{O_2} \cdot P_{O_2}}}{(1 + K_{CO} \cdot P_{CO}) + (1 + \sqrt{K_{O_2} \cdot P_{O_2}})}$	5·10 ⁻⁴	51.37	33.34	0.95	1·10 ⁻⁵	294
modified	$r = \frac{k \cdot K_{CO} \cdot P_{CO} \cdot \sqrt{K_{O_2} \cdot P_{O_2}}}{(1 + K_{CO} \cdot P_{CO})^2}$	2.0·10 ⁻³	30.4563	-	0.35	1.3·10 ⁻⁴	17.5

From the power law regression, it appears that the reaction order with CO increases by increasing the temperature while the one of the partial pressure of oxygen slightly decreases increasing the temperature. As a matter of fact, this trend of oxygen reaction order was also reported by other authors on bulk perovskite(Seyama et al(1992); Zhi-Bang Chen 1997). As a matter of fact according to Seyama and co-workers this trend of reaction order of oxygen with temperature was explained taking into account the presence of the two oxygen species, α -oxygen and β -oxygen mentioned in Chapter III. As a matter of fact, with a rise in reaction temperature, not only α -oxygen decreases but β -oxygen becomes reactive. As a matter of fact, the temperature promotes the diffusion of β -oxygen

from the lattice to the surface. Accordingly, in order to explain the oxygen state the following reaction steps could also be taken into account.



Evidently these step have an opposite trend with temperature.

When only β -oxygen is involved in the high temperature reaction the order of oxygen approaches zero, becoming the reaction independent on the oxygen partial pressure.

Concerning the fractional kinetic models, it appears that the best model were the following:

$$r = \frac{k \cdot K_{CO} P_{CO} \sqrt{K_{O_2} P_{O_2}}}{\left(1 + K_{CO} P_{CO} + \sqrt{K_{O_2} P_{O_2}}\right)^2} \quad \text{model 1}$$

$$r = \frac{k \cdot K_{CO} \cdot P_{CO} \cdot \sqrt{K_{O_2} \cdot P_{O_2}}}{\left(1 + K_{CO} P_{CO}\right) \cdot \left(1 + \sqrt{K_{O_2} \cdot P_{O_2}}\right)} \quad \text{model 2}$$

The model 1 is a typical Langmuir-Hinshelwood model which takes into account the dissociately adsorption of oxygen and is derived under the assumption that the rate limiting step is the reaction between adsorbed CO and O. Model 2 differs from model 1 only for the assumptions that there were two different kinds of sites. Both model minimize the objective function for all the investigated temperatures. Even if it appears that model 2 gives a lower value of MRSS, the difference of the MRSS is in the range of the experimental error, thus is not possible to discriminate between the two models on this basis. Moreover, reporting the conversion predicted by the two models and comparing them with experimental one, it is evident that predicted value are equivalent (Fig. V.3.1.5). According to the trend of the apparent reaction order of oxygen the estimated values of K_{O_2} increases by increasing the temperature. This fact is more pronounced in model 2 while model one gives a lower value of this coefficient with a less variation of K_{O_2} with temperature.

Concerning the ΔH_{CO} in the case of model 1 it is equal to 48kJ/mol while for model 2 this value is higher and equal to 70 kJ/mol. The calculated conversion according the two models are reported in Fig. V.3.1.5.

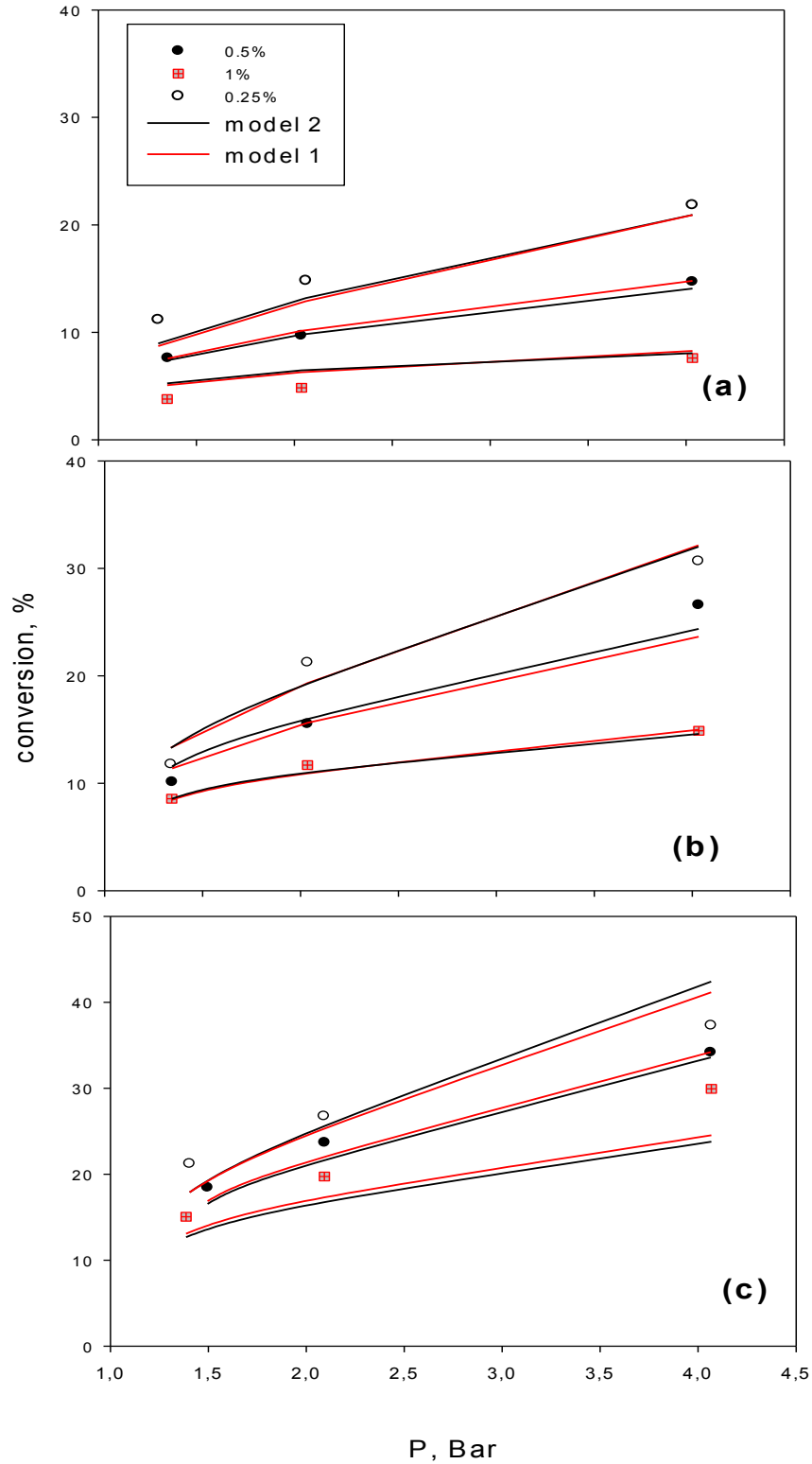


Fig.V.3.1.5.- CO conversion as a function of the pressure and parametric in the inlet y_{CO}^o over 1Pt-A platelet. Symbols experimental data; red lines: conversion predicted according model 1; black lines conversion predicted by model 2. Total flow rate 75 splh; $y_{O_2}^o=8,5\%$; T:(a)470°, (b) 500°C, (c) 530°C.

Fig.V.3.2.1 shows the CO conversion as a function of the temperature and parametric in the total flow rate for a mixture of 1/8.5/90.5% vol. CO/O₂/N₂ at atmospheric pressure. These conversions were collected heating up the reactor at 2°C/min under reaction conditions in order to preliminarily verify the conditions leading to a kinetic control.

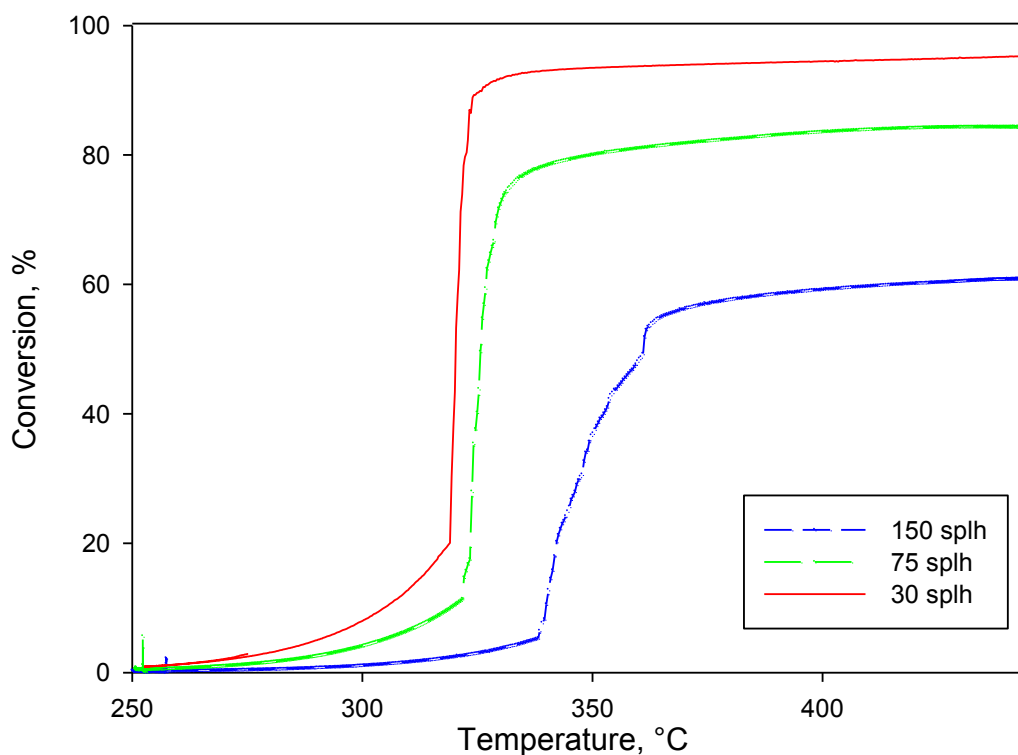


Fig.V.3.2.1- CO conversion as a function of the temperature and parametric in the total flow rate over 1Pt-A platelet. CO/O₂/N₂ = 1/8.5/90.5% vol. at atmospheric pressure. heating rate: 2°C/min.

It is evident that the increase of conversion is steeply at a temperature of about 300-340°C (depending on total flow rate), and that in few degrees, the mass transfer limitation is achieved and depends on total flow rate according to the follow eq. V.3.2 :

$$x=1-\exp(-K_D \cdot \tau') \quad \text{eq. V.3.2}$$

The same procedure was applied also for 0.25/8.5/91.25% vol. CO/O₂/N₂ and results were reported in Fig.V.3.2.2.

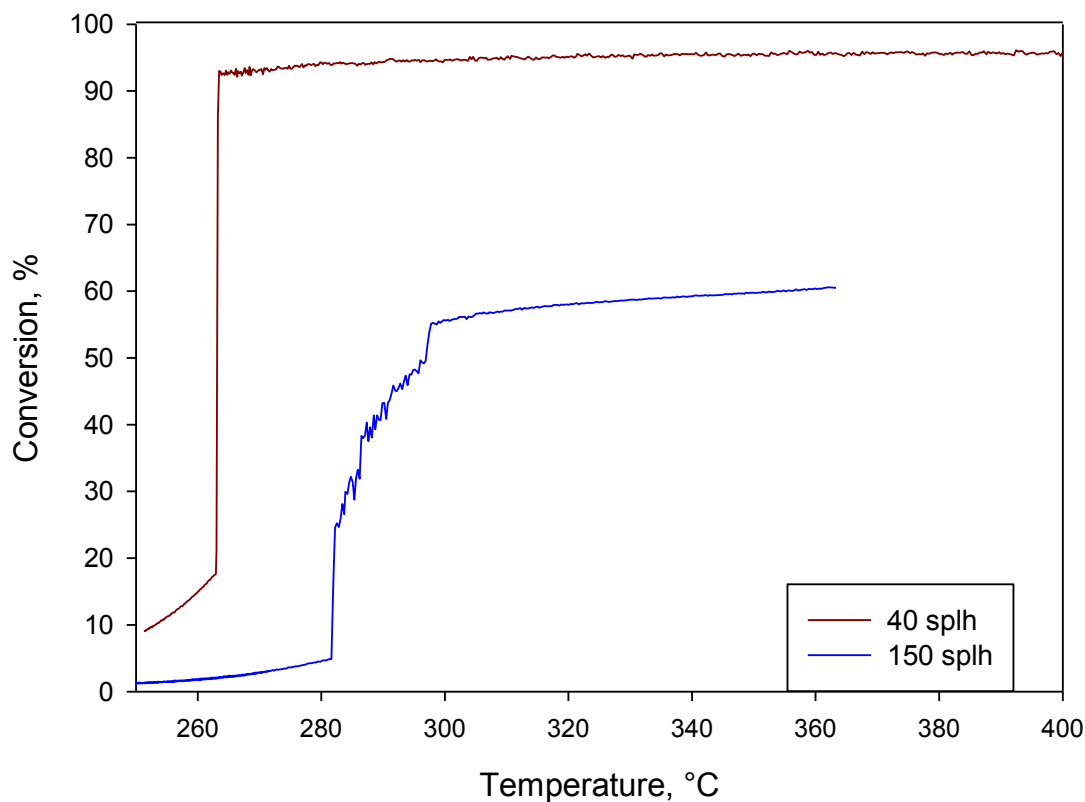


Fig.V.3.2.2- CO conversion as a function of the temperature and parametric in the total flow rate over 1Pt-A platelet. CO/O₂/N₂ = 0.25/8.5/91.25% vol. at atmospheric pressure. heating rate of 2°C/min.

The behavior of the 0.25% mixture is the qualitatively the same of the richer mixture, but the temperatures of transition to the diffusion limit are lower.

It appears that the range of temperature suitable to conduct the kinetic study is very narrow. Moreover there were regions for which small temperature variation ($\pm 2^\circ\text{C}$) can cause large conversion variation leading to significant errors in evaluation of the proper kinetic model.

Starting from this consideration it seems necessary to work at a temperature of 250°C and 280°C and with different total flow rates in order to work at steady-state condition under kinetic control. As a consequence in the following reaction rates will be reported.

Fig.V.3.2.3 (a,b,c) shows the reaction rates parametric in the O₂ concentration as a function of the CO inlet fraction. The corresponding conversion are all below 10%, and as a consequence, the reported rates have been calculated under hypothesis of differential reactor according to expression.

It is evident that the CO effect on reaction rates is negative, according to literature data that reports a negative reaction order for CO (Zhadanov and Kasemo, 1994). Evidently the CO strongly interacts with the surface and remains adsorbed, on the other hand, the O₂ effect appears positive on kinetics.

The data with a 4.25 and 6.6% of oxygen were also regressed with a power law reported below:

$$r = k \cdot P^{(\alpha+\beta)} \cdot y_{CO}^{\alpha} \cdot y_{O_2}^{\beta} \quad \text{eq. V.3.3}$$

The values of k, α and β that minimizes the mean square error, are reported in table V.3.2.1. The order with respect to CO was negative and is about -0.5 while the order with respect to O₂ is positive and slightly higher than 0.5, as a consequence the order with respect to pressure is slightly higher than zero.

In Fig. V.3.2.4, the calculated rates (lines) are compared with the experimental ones (symbols).

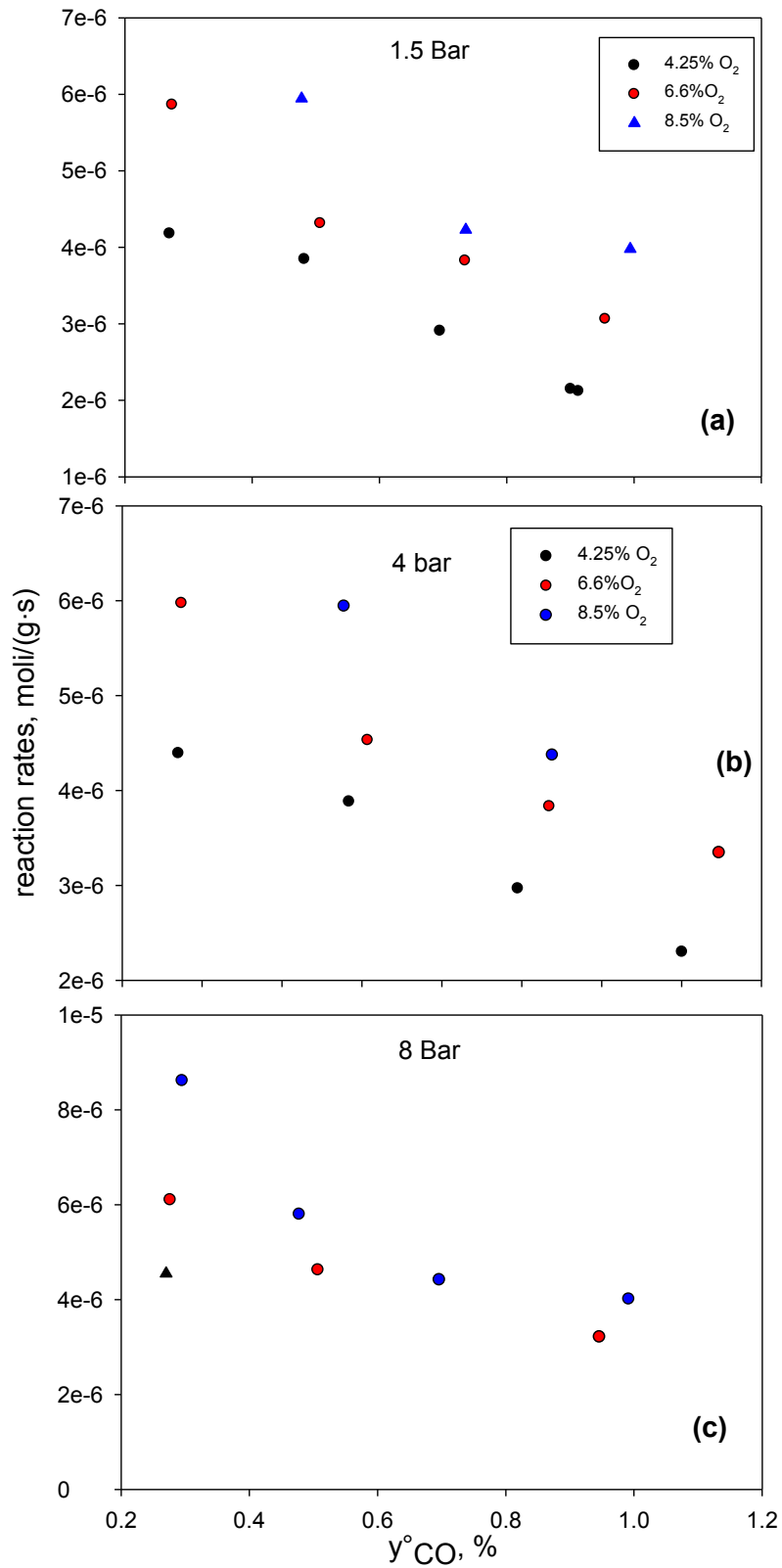


Fig. V.3.2.3 Reaction rates as a function of the $y^{\circ}CO$ and parametric in the $y^{\circ}O_2$ over 1Pt-A platelet. T=280°C (a) P=1.5 (b) 4 bar (c) 8 bar.

Table V.3.2.1-Parameters estimated regressing the reaction rate of CO consumption over 1Pt-A platelet at 280°C.

280 °C Model	k	K_{CO}	K_{O_2}	R ²	MRSS	F
$r = k \cdot P_{CO}^\alpha \cdot P_{O_2}^\beta$	1.31e-6	-0.49	0.54	0.96	3.3·10 ⁻¹⁵	212
$r = \frac{k \cdot P_{CO} \cdot P_{O_2}^{1/2}}{(1 + K_{CO} \cdot P_{CO} + (K_{O_2} \cdot P_{O_2})^{1/2})}$	0.013	219	0.0008	0.84	1.3·10 ⁻¹⁴	47.7
$r = \frac{k \cdot P_{CO} \cdot P_{O_2}^{1/2}}{(1 + K_{CO} \cdot P_{CO})^2}$	0.0129	218	-	0.84	1.16·10 ⁻¹⁴	100
$r = \frac{k \cdot P_{CO} \cdot P_{O_2}}{(1 + K_{CO} \cdot P_{CO})^2}$	0.4842	1175		0.38	4.6·10 ⁻¹⁴	11

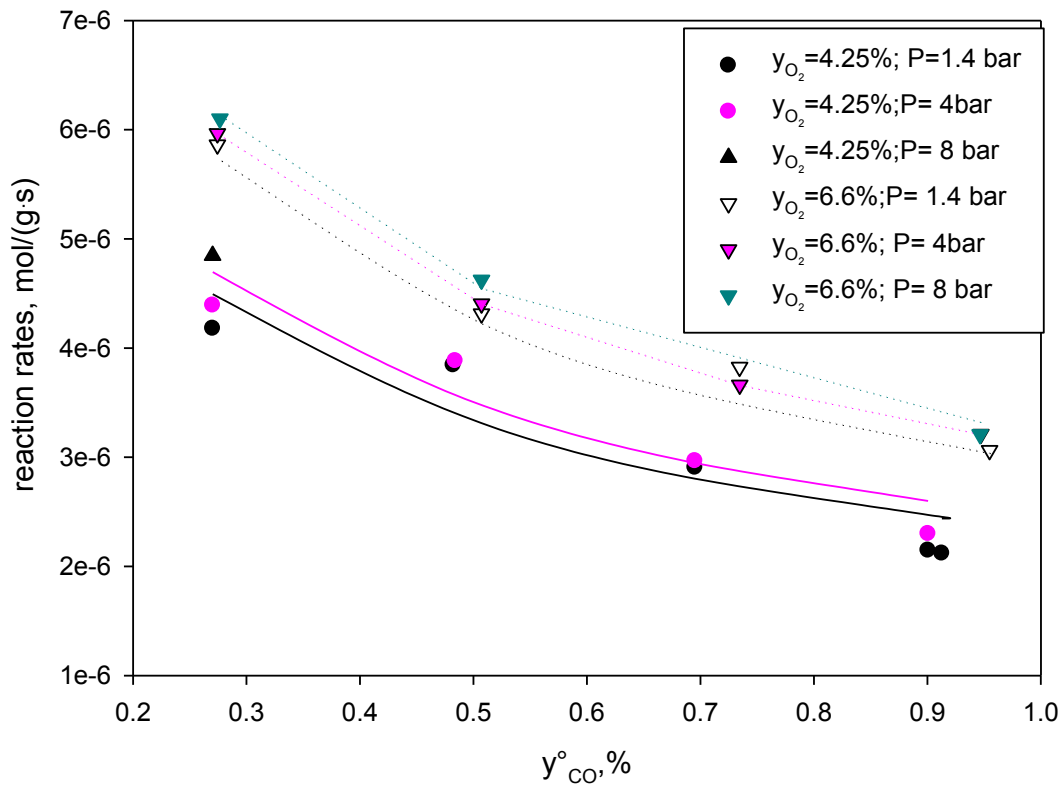


Fig. V.3.2.4 reaction rates calculated according to the power law (lines) compared with the experimental ones (symbols) for different pressures and y_{O_2} over 1Pt-A platelet. T=280°C.

Several reaction model, also those proposed in literature (Zhadanov and Kasem,1994), were analyzed and some of them are reported in table V.3.2.1.

According to the data reported in tableV.3.2.1, the best model is the following:

$$r = \frac{k_{sr} \cdot P_{CO} \cdot \sqrt{P_o}}{(1 + K_{CO} P_{CO})^2} \quad \text{eq. V.3.4}$$

Showing the overall and partial reaction orders similar to those obtained with the power law.

Moreover, the addition of a third parameter as in the case of

$$r = \frac{k_{sr} \cdot P_{CO} \cdot \sqrt{P_o}}{(1 + K_{CO} P_{CO} + \sqrt{K_o P_o})^2} \quad \text{eq. V.3.5}$$

does not decrease the MRSS suggesting that the value of K_{O_2} is not significant, as the standard error related to the coefficient of the same order of its value reveals. Accordingly this dependence was no necessary for the explanation of the predicted reaction rates. The other models provide very poor agreement with experimental data compared to the previous one.

In Fig.V.3.2.5(a,b,c) the predicted reaction rates were compared with experimental ones for the different pressure and as a function of y_{CO} parametric in the y_{O_2} .

From Fig. V.3.2.5 it appears that an overall good prediction was found. In addition, the parameters with their range of 95% confidence are summarized in table V.3.2.2..

The model was used also for the prediction of the reaction rate at 250°C. However since the lower conversions and the minor number of experiment the parameter confidence intervals are wider.

Table V.3.2.2.-Model estimates and confidence intervals at 95%

model	T, °C	k, mol/(g·s)	K_{CO} , Bar ⁻¹
$r = \frac{k \cdot P_{CO} \cdot P_{O_2}^{1/2}}{(1 + K_{CO} \cdot P_{CO})^2}$	280	0.0129±0.0036	218±40
	250	0.0100±0.0075	425±108

The calculated value of E_{att} and ΔH_{CO} are respectively of 20.3 kJ/mol and 26.9 kJ/mol.

Moreover it is interesting to note that the best model proposed has been also reported in the literature for noble metal catalyst (Voltz et al (1973), Dubien et al, 1998; Groppi et al., 2001), suggesting that in this type of catalysts CO oxidation occurs through the same reaction mechanism

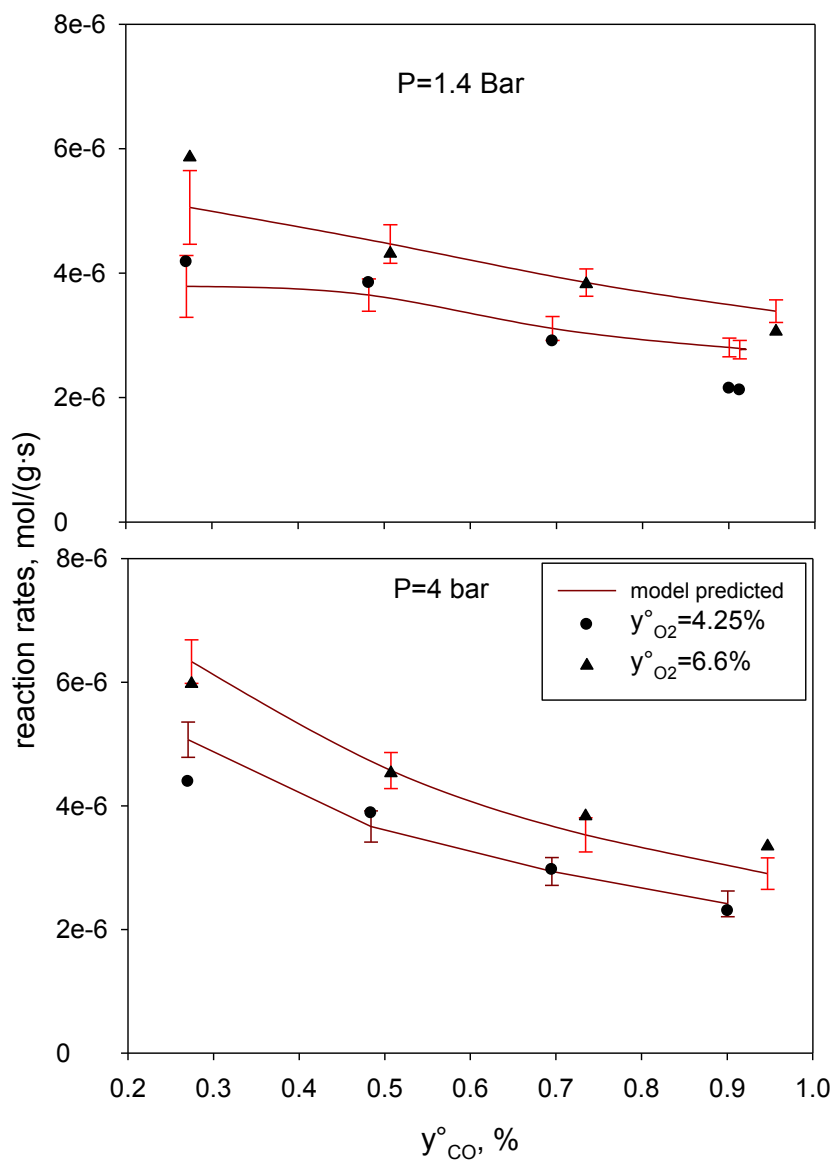


Fig. V.3.2.5 reaction rates as a function of the y_{CO} parametric in the y_{O_2} . $T=280^{\circ}C$ (a) $P=1.5$ (b) 4 bar. Symbols: experimental data; lines: predicted value, error bars represent the range of predicted reaction rates at 95% of confidence.

VI AUTHO-THERMAL TEST UNDER PRESSURE

In this Chapter the results of the combustion tests under pseudo-autothermal condition are reported. In particular, tests were carried out on the perovskite catalyst, whose behaviour has been less investigated in the open literature.

Experiments performed at low pre-heating temperature are first reported in order to elucidate the effect of the pressure on the fuel ignition. Methane has been chosen as fuel and results have been related to those reported in the chapter 4. Then tests conducted at higher pre-heating temperature are reported, showing the effect of the pressure on the steady-state methane combustion. Finally, the effect of co-feeding CO and H₂, thus partially simulating co-feeding a syn-gas, on CH₄ ignition has been described.

VI.1 Effect of pressure on CH₄ ignition

The results of the combustion of a 3.7% CH₄ mixture at a total flow rate of 31 splh are reported in Fig VI.1.1 in terms of methane conversion and temperature profiles both as a function of the pressure.

As discussed in the chapter IV, ignition occurs when the heat produced by the reaction is higher than the exchanged one and heat accumulation on the catalyst surface takes place. At fixed pressure, as in the experiments described in the chapter IV, the main way to induce ignition, i.e. to enhance heat production, is to increase the pre-heating temperature. On the other hand, by changing the pressure at fixed mass flow rate it is possible to enhance fuel conversion, due to longer contact times and faster reaction rates, as reported in the previous chapter, and consequently to induce ignition at fixed pre-heating temperature.

As expected, at low pressure a progressive increase of methane conversion is observed; on the contrary, between 4 and 5 bar a steep conversion increase up to 100% is detected, associated with the ignition occurrence. As a matter of fact, in the mean while, the T_w (i.e. the temperature of the external steel wall) increases from 517°C up to 550°C, suggesting a trend for the exchanged thermal power, related to this temperature, similar to the conversion one. In the same way, also T_{pre}, i.e. the temperature in the first thermal shield, increases from 450°C up to 490°C. The behaviour of T_{cat} is

slightly different and will be discussed afterward, but, from a general point of view, once the system is ignited, the temperature in the catalytic zones turns out to be higher than the external one ($T_{cat} > T_w$), thus indicating that the heat transfer is directed from the catalyst to the surroundings.

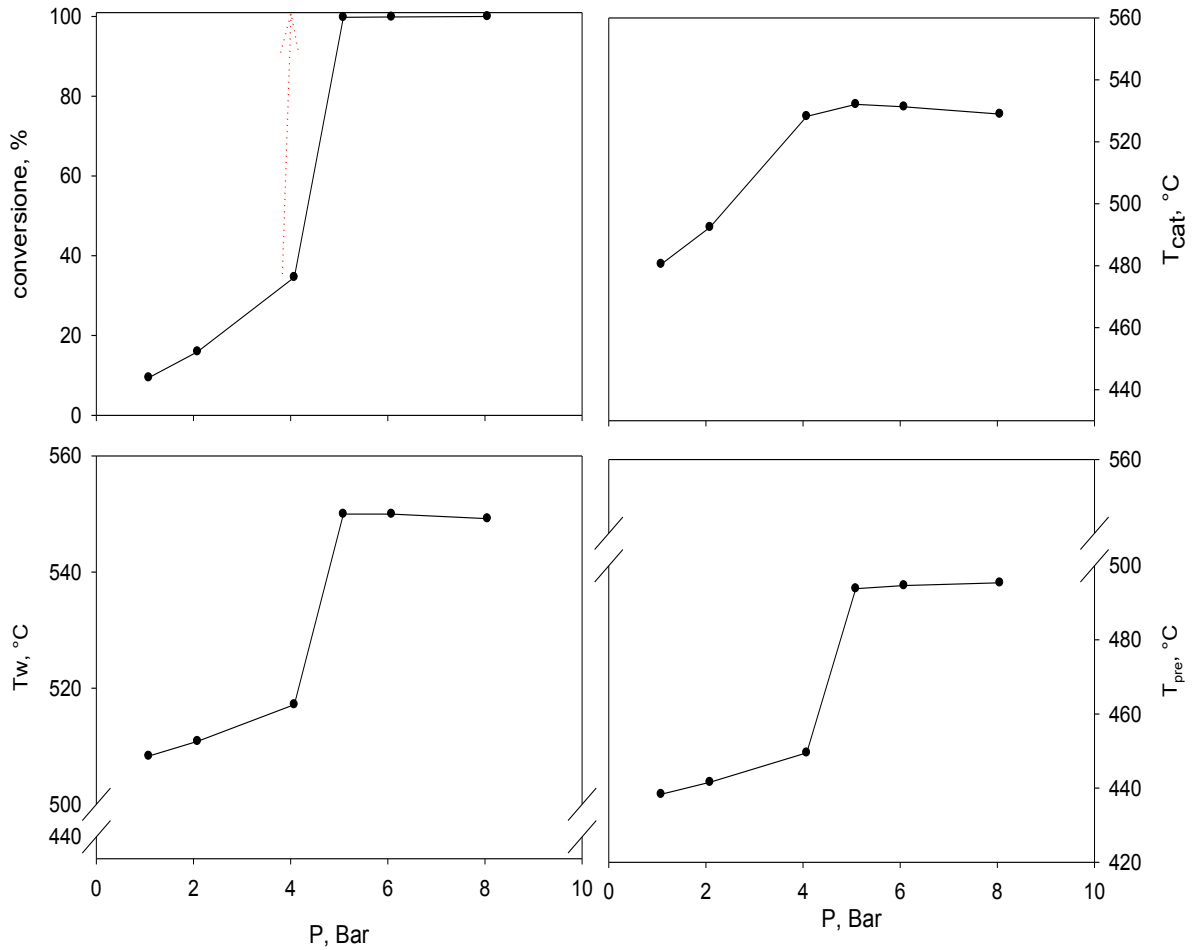


Fig. VI.1.1.: Conversion and temperatures as a function of the pressure during methane combustion over LM-C900-50 monolith; total flow rate = 31Slph; $O_2 = 10\%$; $CH_4 = 3,7\%$ $N_2 = \text{balance}$; $T_{jacket} = 600^\circ\text{C}$;

In fig. VI.1.2 the temperature profiles and calculated conversion recorded during the ignition at 5 bar are reported as a function of time on stream.

In particular it appears that when fuel is fed to the reactor after thermal equilibration of the system under N_2+O_2 flow the conversion is equal to about 25% with a corresponding increase of the catalyst temperature of 30°C . The conversion and temperatures continue to increase until the ignition occurs. In correspondence of this phenomenon it is visible in the T_{cat} profile a maximum of

about 650°C; as already reported, the peak is related to the reaction front movement from the end of the catalyst, where the temperature are expected to be higher, to the reactant inlet thanks to the retrodiffusion of the heat. At higher pressures, the position of the reaction front can change, as occurs by changing other parameters such as temperature, flow rate and fuel fraction, as demonstrated in chapter IV.

Since the 100% conversion is achieved in an internal section of the catalyst, the post reaction section of the reactor do not contribute to the heat generation and as a consequence the temperature is lower duo to the heat transfer towards the surroundings.

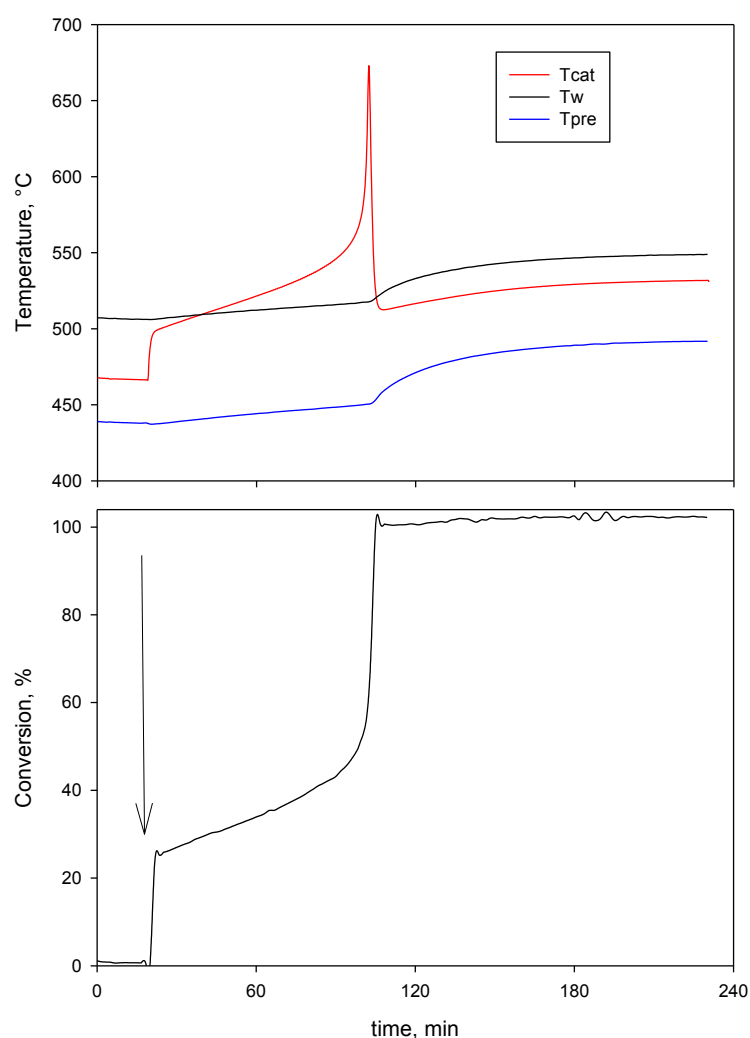


Fig. VI.1.2: Temperatures (a) and CH₄ conversion (b) as a function of the time on stream during ignition over LM-C900-50 catalysts at 5 bar. Q_{tot}=31Slph; CH₄ = 3.7%; O₂=11%; N₂=balance; T_{jacket}=600°C. The vertical arrow indicates fuel feeding.

As suggested above and according to fig. VI.1.1, ignition is promoted by the pressure; this phenomenology is related with the occurrence of two distinct effects that are associated with the pressure increase. In a monolithic reactor that is operated at constant mass flow rate, the local temperature depends, a part from the pre-heating temperature, also by the heat generated by means of the combustion reaction, the latter being a linear function of conversion, and by the heat exchanged with the surroundings. As discussed before, the pressure increase is responsible of enhanced surface kinetics and of contact time increase between gasses and catalytic surface, both providing beneficial effects on conversion and, thus, on catalyst temperature.

Similar results were obtained for different methane concentration (fig. VI.1.3). In particular for concentrations ranging from 3 to 4,5% , it was found that ignition occurs always between 4 and 6 atm. On the other hand for the mixture containing 2.5% methane, the conversion steadily increases up to 80% by increasing pressure without showing the occurrence of ignition phenomenon. Evidently, the heat losses, especially the irradiative ones more significant due to the relative high surface to volume ratio of lab-scale monolithic reactor, result higher than the heat produced by the leanest mixture not allowing the heat accumulation mechanism and, as a consequence, the ignition occurrence.

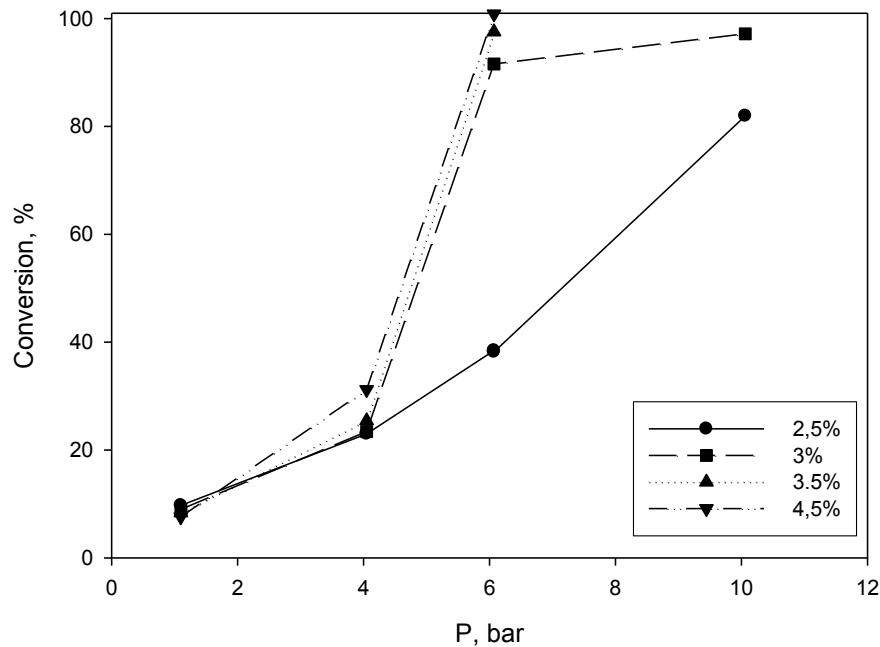


Fig. VI.1.3: CH₄ conversion as a function of the pressure at different fuel concentrations during methane combustion over LM-C900-50 monolith. Q_{tot}=31Slph; O₂=10%; N₂=balance; T_{jacket}=600°C.

At atmospheric pressure the conversions are similar independently on the CH₄ inlet fraction, thus indicating that the reaction rate is linear with respect to methane concentration, as reported in the previous chapter. For pressure higher than the atmospheric one, richer mixtures show higher conversion, contrary to what predictable under isothermal conditions. This discrepancy is attributable to the no negligible heat generated by the combustion. As a matter of fact, feeding richer mixtures the mean temperature of the reactor is higher due to larger produced heat thus showing higher reaction rates and, as a consequence, conversion. However these differences seem to only slightly affect methane ignition, occurring in a limited pressure range (i.e. 4-6 bar).

In fig VI.1.4 (a,b,c) and (d,e,f) the temperature profiles respectively as a function of pressure and $y_{CH_4}^{IN}$ are reported.

At 4 atm, i.e. in the absence of ignition, the measured catalyst temperature increases by increasing methane concentration, due to the higher thermal power developed (Fig. VI.1.5 (e)). This behaviour is typical of the condition before ignition.

On the contrary, when a reaction front is established, the thermal profile is not univocally determined by conversion. For instance, it is noteworthy that a 10 atm the T_{cat} profile as a function

of $y_{CH_4}^o$ is mirrored by the T_{pre} profile (Fig.VI.1.5 (d) and (e)). This behaviour is associated with the shift of the reaction front towards the gas inlet due to an higher amount of fuel converted in the first part of the catalyst (i.e. upstream to the reaction front) leading to a shorted pre-heating zone.

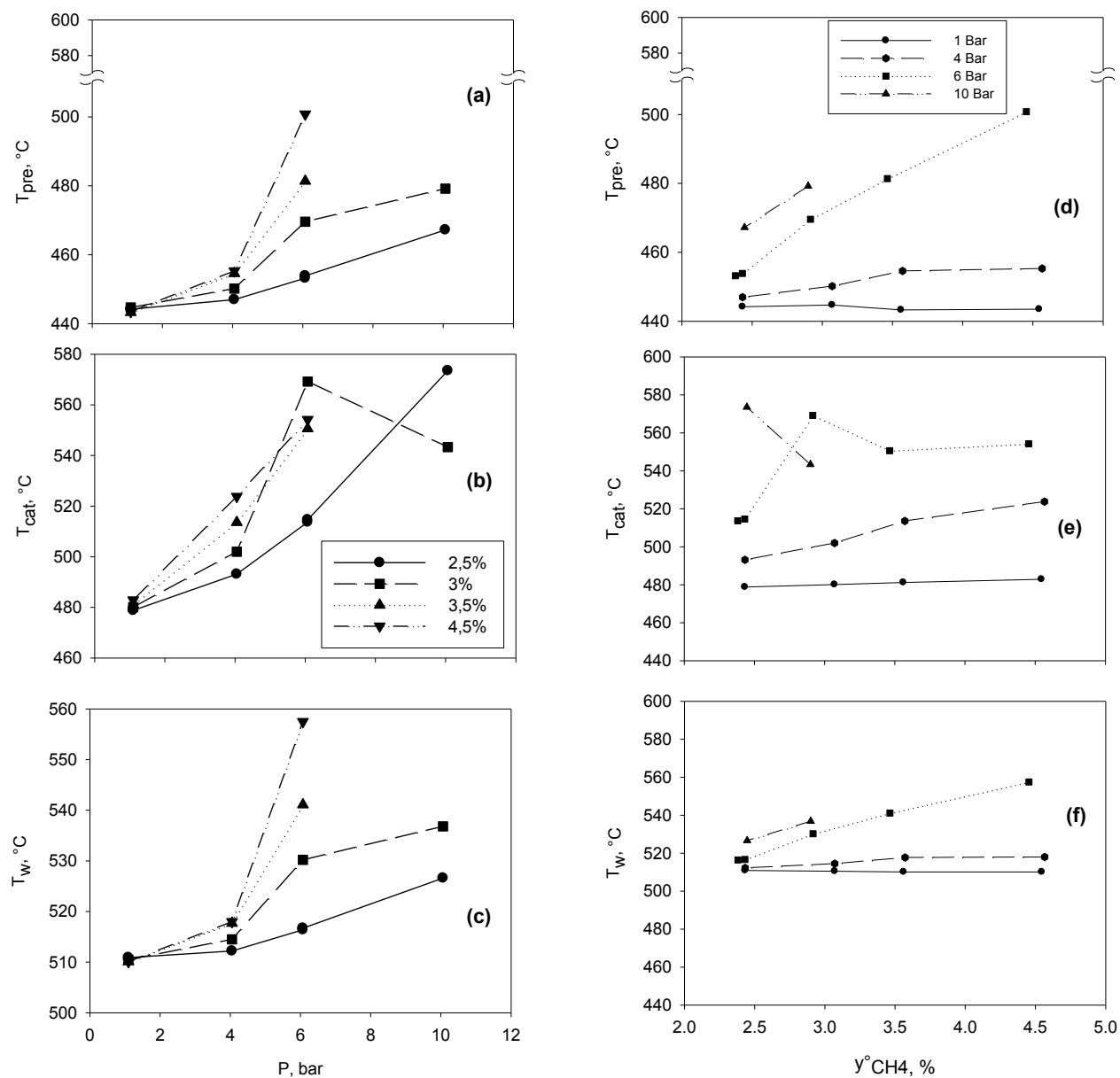


Fig. VI.1.4 (a), (b),(c): temperature profile of T_{pre} , T_{cat} , T_w as a function of the pressure; and **(e), (d), (f)** of $y_{CH_4}^o$; $Q_{tot}=31$ splh; $O_2=10\%$; $N_2=balance$; $T_{jacket}=600^\circ C$;

VI.2 Pressure ignition: total flow rate effect

Fig. VI.2.1. shows the conversion and temperature profiles as a function of the pressure for two different values of the total flow rate (31 e 88 splh) and for the combustion of the mixtures with the following composition $\text{CH}_4/\text{O}_2/\text{N}_2=3,7\%/10\%/86,3\%$.

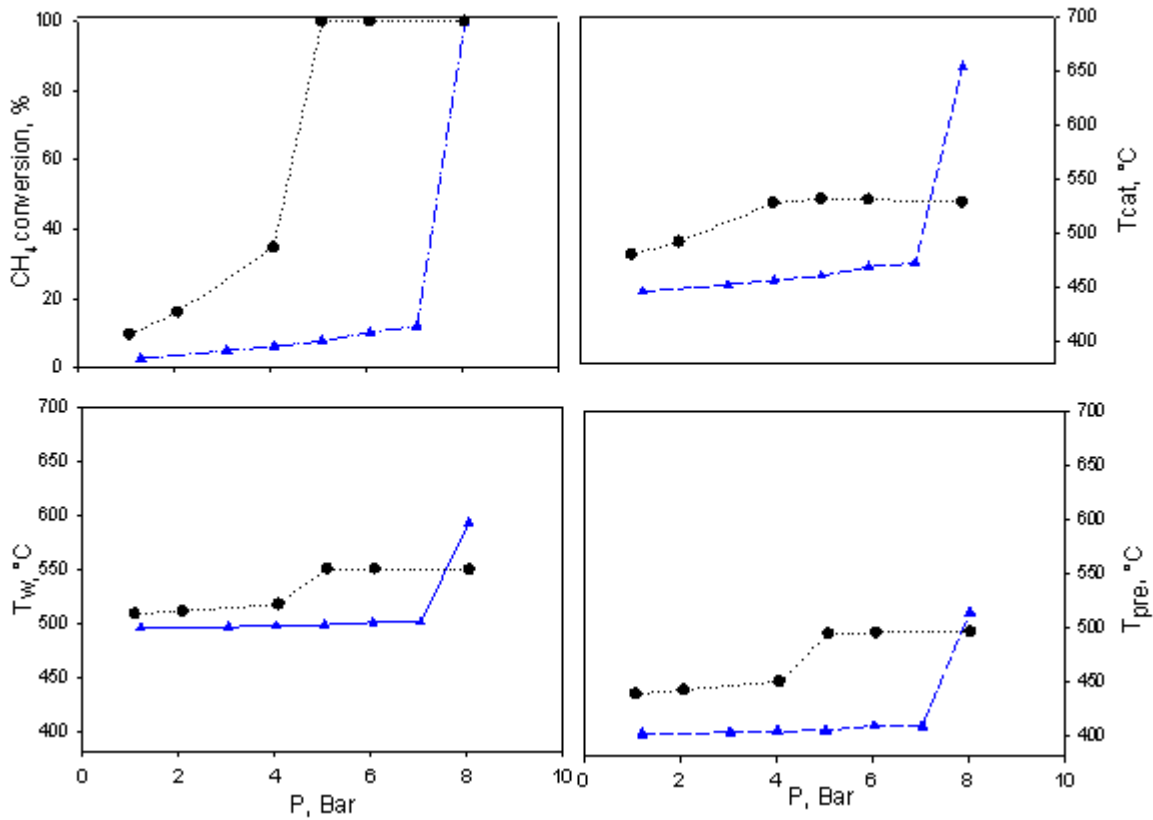


Fig. VI.2.1: conversion and temperatures as a function of the pressure during methane combustion over LM-C900-50 monolith; $\text{O}_2=10\%$; $\text{CH}_4=3,7\%$ $\text{N}_2=\text{balance}$; $T_{\text{jacket}}=600^\circ\text{C}$; (●) $Q_{\text{tot}}=31 \text{ splh}$ (▲) $Q_{\text{tot}}=88 \text{ splh}$.

It clearly appear that the pressure value at which ignition occurs increases from about 5 to 8 bar with the total flow rate.

This effect could be related to the decrease of contact time at the same other reaction conditions. Therefore in order to achieve reaction rates at the end of the catalyst high enough to allow the system ignition, it is necessary to operate at higher pressure in order to improve kinetics at a lower contact time.

Moreover from Fig. VI.2.1 it appears that before the ignition, the measured conversion in the case of the higher flow rate results lower than the analogous at lower flow rate, respectively of 12 and 35%. On the other hand from the analysis of the thermal profiles it appears that also T_{cat} and T_{pre} are lower, the first because of the shift of thermal profile downstream at higher flow rate and the latter caused by the higher thermal power subtracted by the gas flow from the heat shield.

But the temperature of the catalyst end, where ignition occurs, depends on the thermal generated power expressed as follows:

$$P = F_{CH_4} \cdot X \cdot \Delta H_{comb} \quad \text{eq. VI.1}$$

Therefore it could be not excluded that the differences of the temperature measured at the catalyst centre result limited at the end of the catalyst. Nevertheless, the produced thermal power at ignition is lower at the highest flow rate, suggesting a lower exit temperature. As a consequence, the pressure increase, directly acting on the kinetics, could compensate for the temperature decrease.

Fig. VI.2.2 shows the methane conversions and their derivatives at the corresponding ignition pressure for the two flow rates.

At fuel introduction conversions are respectively 25% at 31 slph and 13% at 88 slph, while the time to maximum rate is lower at higher flow rate. Moreover, the ratio between the maximum derivatives, related to the maximum heat production rates obtained at the inflection points of the conversion curves, is about equal to the flow rate ratio. Furthermore, the conversion values showing a derivatives higher than 5% are 55% ($Q = 31$ Slph) and 25% ($Q = 88$ Slph) respectively. All the above phenomena appear to be related to the higher power available at higher flow rate, thus allowing a more rapid run away due to more significant temperature increases.

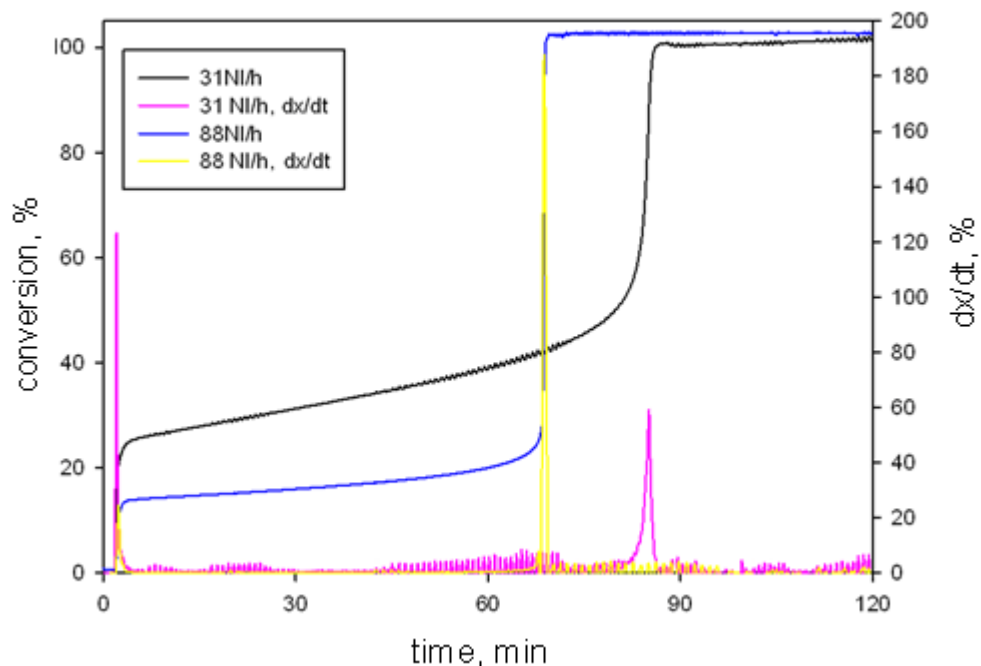


Fig. VI.2.2: CH₄ conversion during ignition over LM-C900-50 monolith at different flow rates. Pressure depends on flow rate: P=5 Bar at Q_{tot}=31 slph; P= 8 Bar at Q_{tot}=88 slph; CH₄ = 3.7%O₂=11%; N₂=balance; T_{jacket}=600°C.

Thermal transients, reported in fig. VI.2.3, confirm the above statements. As a matter of fact, the temperature increase and the reaction front shift are both more rapid by increasing the flow rate; moreover the registered maximum temperature is higher (900°C vs. 650°C). It should be noted that after ignition the catalyst temperature is higher at the highest flow rate, while the opposite is detected under not ignited state. This is due to an higher adiabaticity degree, realizable by increasing the flow rate.

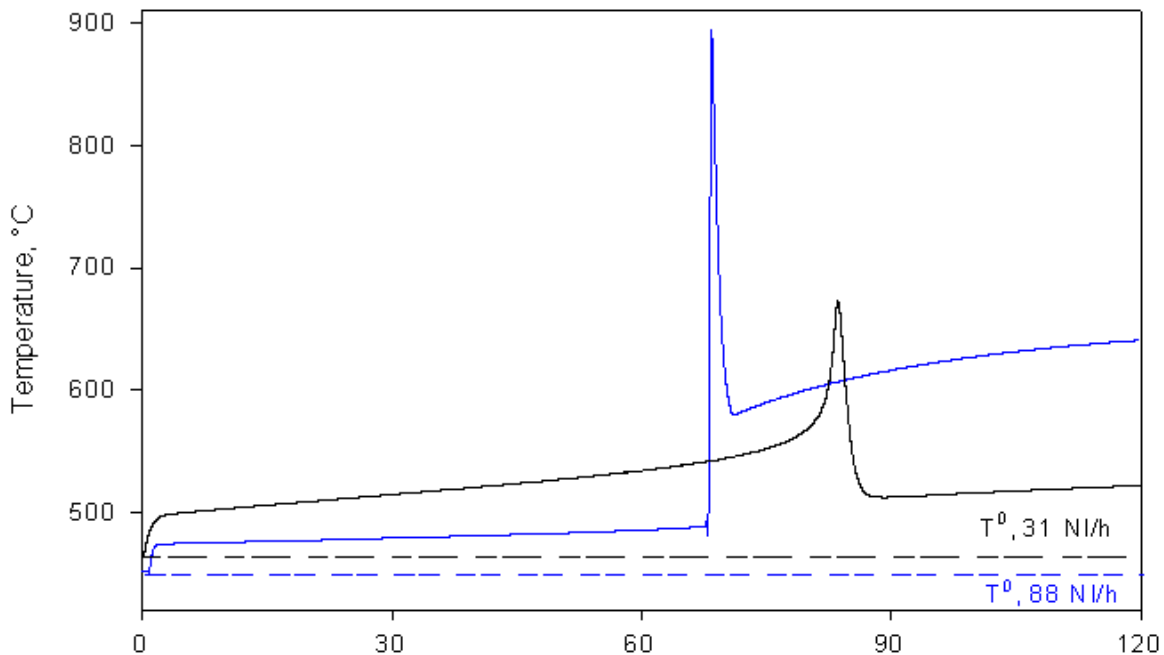


Fig. VI.2.3: Catalyst temperature as a function of the time on stream during ignition over LM-C900-50 monolith at different flow rates. $P=5$ Bar at $Q_{tot}=31$ slph; $P= 8$ Bar at $Q_{tot}=88$ slph; $CH_4 = 3.7\%$; $O_2=11\%$; $N_2=balance$; $T_{jacket}=600^\circ C$.

In order to verify the stability of the ignited state, pressure has been decreased after ignition at 8 bar (flow rate = 88 slph) and results are reported in fig. VI.2.4. It clearly appears that the ignited state is preserved at lower pressures; nevertheless a shift of the reaction front downstream is detected, as pointed out by the increase of the temperature measured in the centre of the catalyst, suggesting that the reaction front is placed in the first part of the reactor. Accordingly a slight decrease of T_{pre} is detected, also due to an higher gas velocity and, consequently, heat exchange. Under the used experimental conditions a quenching has not been detected. Notwithstanding, the above features suggest that at lower pressures quenching could occur through a blowout. The above results also suggest that it is possible to catalytically ignite a mixture by increasing the pressure and then to operate the reactor at lower pressures.

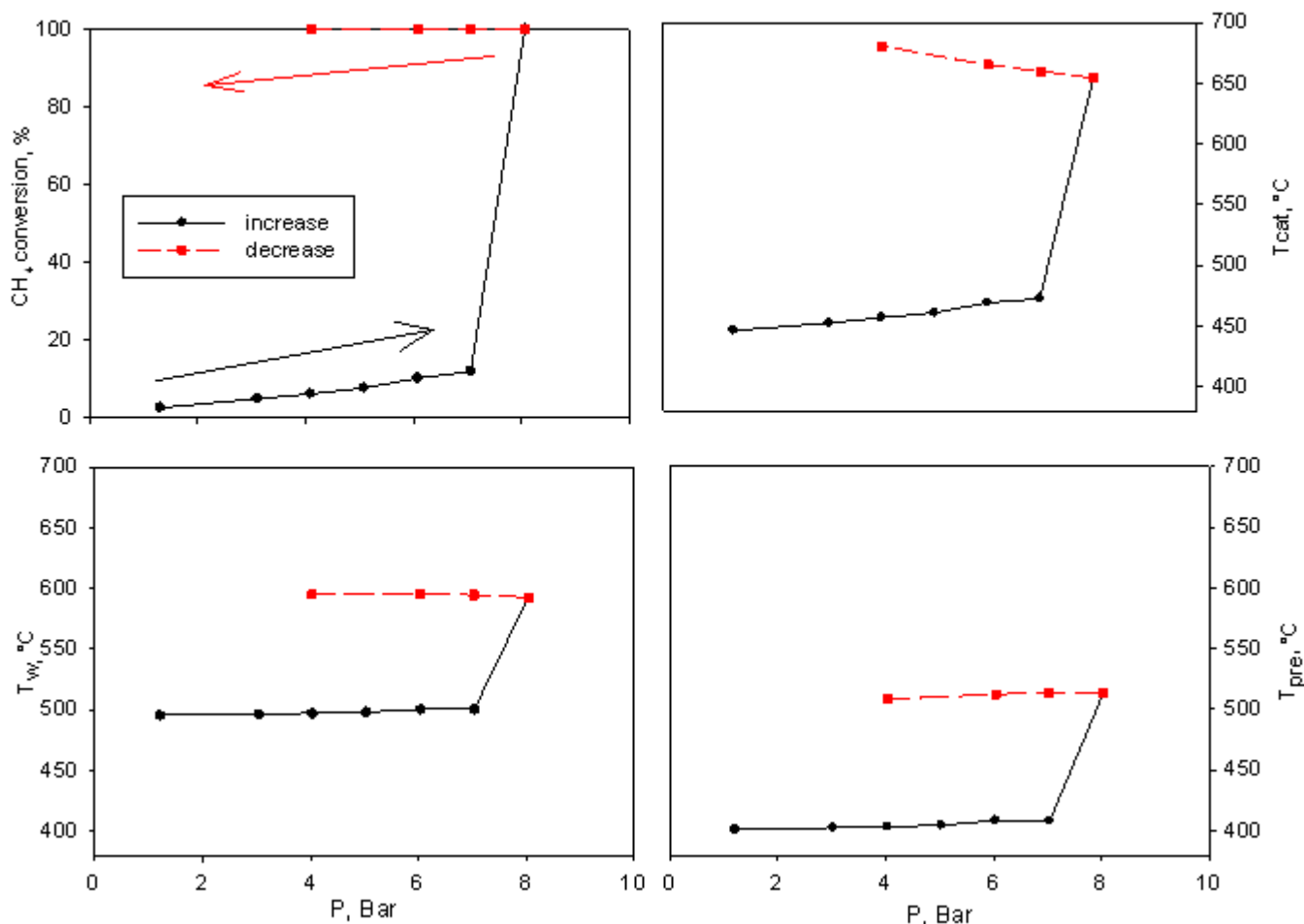


Fig. VI.2.4: CH₄ conversion and temperatures as a function of the pressure during methane combustion over LM-C900-50 monolith. $Q_{\text{tot}}=88$ slph; $O_2=10\%$; $CH_4=3,7\%$ $N_2=\text{balance}$; $T_{\text{jacket}}=600^\circ\text{C}$.

VI.3 Pressure effect on steady state operation

The effect of the pressure on the steady state performance of the perovskite catalyst has been considered too. For the purpose, the heating jacket has been set at 700°C , while the flow rate and oxygen concentration have been kept constant at 40 slph and 105 respectively.

Fig. VI.3.1 shows CH₄ conversion as a function of the pressure for different fuel inlet concentrations. Measured conversions are always over 65% and increase by increasing the fuel concentration. Moreover at fixed composition a beneficial effect of the pressure on the performance is detected.

Obviously, this effect is more pronounced at low pressure or feeding leaner mixtures, due to the lower measured conversions.

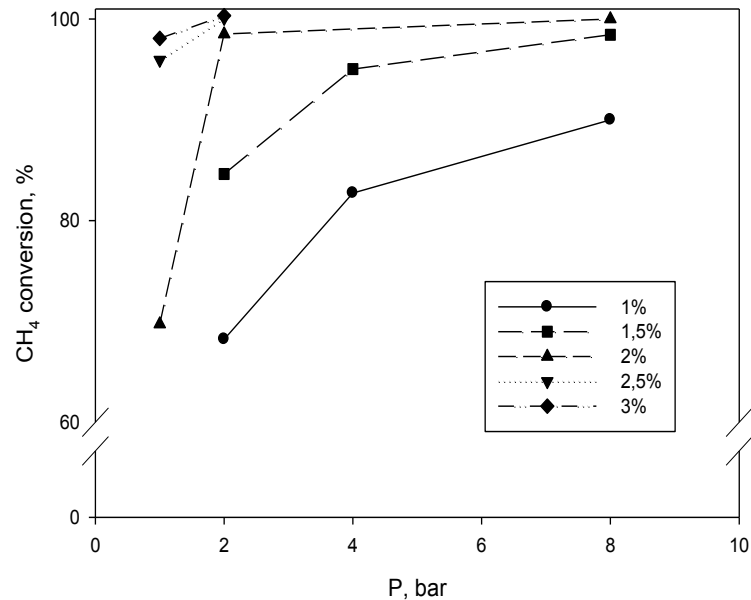


Fig. VI.3.1: CH₄ conversion as a function of the pressure during methane combustion over LM-C900-50 monolith. $Q_{tot}=40$ slph; $O_2=10\%$; $N_2=balance$; $T_{jacket}=700^\circ C$.

Fig. VI.3.2 shows the corresponding temperatures as a function of the pressure (fig. VI.3.2 (a, b, c)) and of the methane inlet concentration (fig. VI.3.2 (d, e, f)). T_w monotonically increases by increasing the fuel concentration as a consequence of the increased developed, and thus exchanged, power also due to improved conversions. The effect of pressure is limited above 4 bar, mainly due to the high conversion level less influenced by changing the pressure. About T_{pre} , a general increase by increasing both pressure and fuel fraction is noted. This is due to two effects: the shift of the reaction front towards the reactor inlet and the increased thermal power developed. Similarly, the behavior of the catalyst temperature is a function of the reaction front position, which by increasing the pressure first approaches, then reaches and finally overcomes the thermocouple shifting from the reactor exit to the inlet. The effect of the fuel concentration can be similarly explained.

VI.4 Pressure effect on ignition of a CH₄/CO/H₂ mixture

The effect of the partial substitution of methane with a H₂/CO mixture on the complete fuel ignition has been studied over the perovskite catalyst. In particular, in order to stress behaviour differences a shorter catalyst (2 cm long) and higher flow rate (100 slph) have been employed. Methane ignition has been conducted by a 2% vol. mixture, while in the CH₄/CO/H₂ mixture the concentrations are respectively 1.5%, 0.6% and 0.9% vol., developing the same thermal power of the CH₄ alone mixture. The concentrations have been chosen in order to obtain a CH₄/(CO+H₂) ratio equal to 1 and a H₂/CO ratio equal to 1.5.

Fig. VI.4.1 shows the results obtained by changing the pressure during the feeding of methane (full symbols) and of the fuels mixture (open symbols). Under these conditions methane ignites at about 8.5 bar; the behaviour has been already described.

The behaviour using mixture appears interesting. As shown in Fig. VI.4.1, CO is mostly converted at atmospheric pressure, while hydrogen conversion appears lower than 50%. This is in agreement with the results previously reported, indicating a higher reactivity of the perovskite towards CO with respect to H₂. But, due to the heat generated by the low BTU fuels combustion, the measured temperature along the overall length of the reactor are higher. Moreover, by increasing pressure CO and mainly H₂ conversions increase allowing a temperature on the surface catalyst high enough to ignite methane at only 4.5 bar. This behaviour resembles to that reported in the chapter IV regarding the CH₄-H₂ mixtures. In this case, CO combustion mainly drives the increase of temperature, responsible for the enhancement of first H₂ and then CH₄ reaction rates up to the ignition of the whole mixture. Looking at the temperature profiles, it is worth noting that after ignition of the multi-fuels mixture a pressure increase shifts the reaction front upstream, as evidenced by the increase of the catalyst temperature and the decrease of the exit temperature.

A direct comparison between the temperature profile after ignition can be performed only at 8.5 bar. It clearly appears that the reaction front of the mixture is upstream with respect to that obtained during the single fuel combustion. This is due to the fast reaction of CO and H₂ in the first part of the reactor, and the consequent more rapid raise of the temperature leading to methane ignition in a previous section of the reactor.

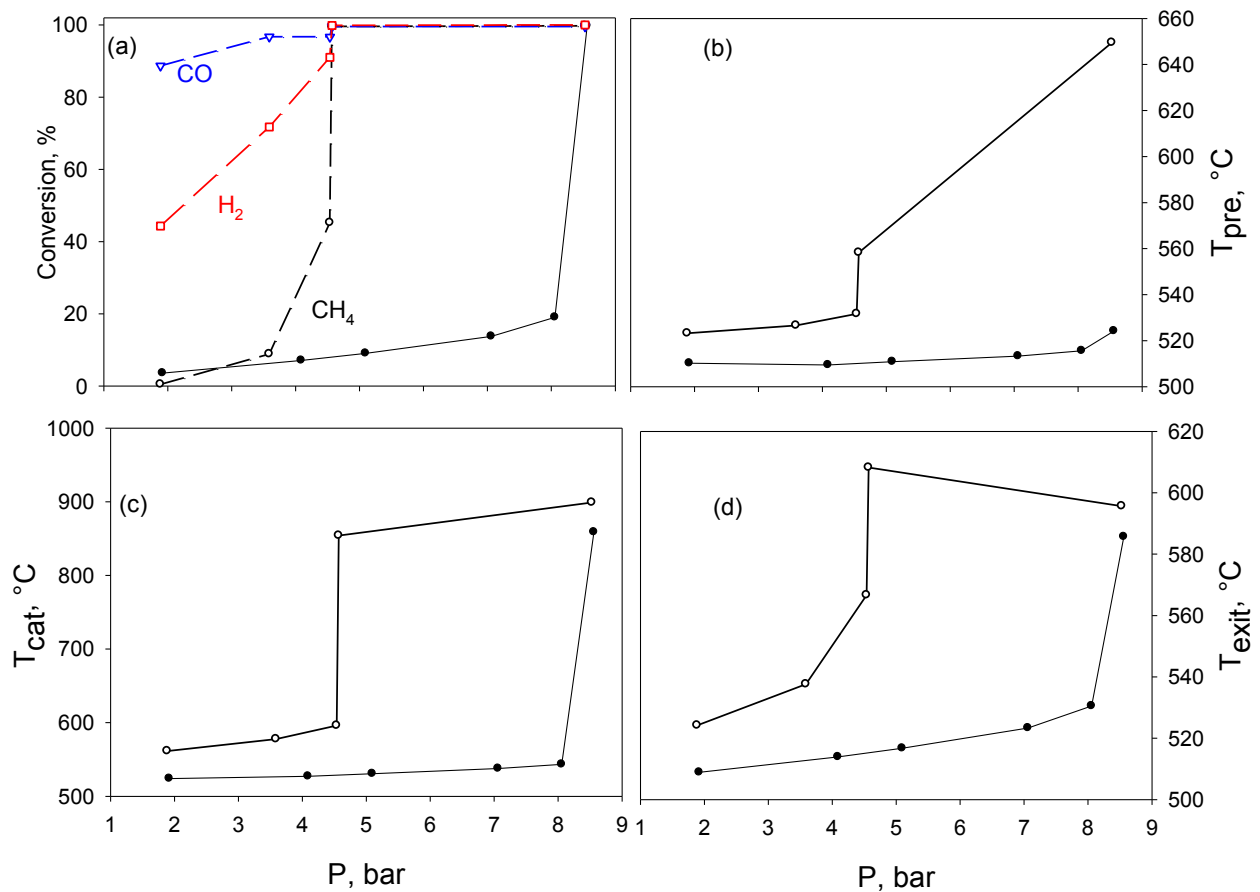


Fig. VI.4.1 Conversions **(a)** and temperatures **(b)**: pre-heating, **(c)**: catalyst, **(d)**: exit as a function of the pressure during ignition test of different fuels: methane (2%vol.; full symbols), CH₄/CO/H₂ (1.5/0.6/0.9% vol.; open symbols) over LM-C600-20 monolith; Q_{tot}=100 slph; O₂=10%; N₂=balance; T_{jacket}=600°C.

The above results show that a synergic effect of low BTU fuels co-feeding on methane ignition is detectable on a perovskite catalyst too. Moreover, even very lean mixture can be ignited at relatively low pressures, i.e. lower than 5 bar, which are of practical interest also for small size gas turbines.

VII CONCLUSIONS AND FUTURE WORK

VII.1 Conclusions

Catalytic combustion of natural gas (NG) has been widely studied as an alternative route to produce electric power with a lower environmental impact, in particular for gas turbine applications. Despite of the potentialities, only few catalytic combustors have been industrially developed, due to the availability of efficient gas turbines producing low pollutants amounts. On the other hand, the development of Integrated Gasification Combined Cycle (IGCC) plants during the last years has shifted the interest from natural gas to syngas combustion in gas turbine cycles with a wide range of output power. But low BTU fuels need less dilution in order to achieve the same power of a NG fuelled gas turbine, thus increasing adiabatic temperature and, as a consequence, nitrogen oxides emissions even for well stated gas turbines. Even if it is generally accepted that the performance of catalysts studied at atmospheric pressure cannot be easily extended to higher pressures, more interesting for gas turbines, the literature availability of high pressure data is very poor and commonly confined to the study of noble metals and methane combustion. As a consequence, the study of catalytic combustion under pressure appears a significant subject, especially if considering not only methane but also hydrogen and carbon monoxide as fuels.

The most part of this study has been conducted onto perovskite-based structured catalyst. From the literature this active phase appears effective and stable at high temperature and cheaper than the more used noble metals. In order to obtain more active catalysts, the perovskite has been doped with small amount of platinum and a Pt-based catalyst has been studied too, as reference in the preliminary atmospheric tests.

Temperature programmed reductions of the different catalysts under H₂ or CO flows revealed that the reducibility of the catalysts, characteristic temperatures and reduction degrees, strongly depends on the reducing agent. In particular, H₂ is the most reducing agent for Pt, while perovskite preferentially interacts with CO. The bi-functional Pt-perovskite catalyst show intermediate properties with respect to the single phases. Due to these intermediate properties, this catalyst has been selected in order to elucidate the behaviour of methane combustion transient phenomena, like

ignition and quenching, and the effect of hydrogen co-feeding. From the results previously reported it clearly appears that methane ignition strongly depends on the local heat balance at the reactor exit and that is a kinetically controlled phenomenon. On the other hand, according to the literature two quenching types have been identified: extinction and blow out. Contrarily to ignition, extinction phenomenon does not appear related to surface kinetics, but to the overall energy balance and in particular to the relative ratio between the heat produced through fuel combustion and the heat losses. As a consequence, an increase of the flow rate, i.e. of the developed power, results in a wider range of operability conditions. This statement is strictly true up to the occurrence of the other quenching mechanism, blow out; in this case, the flow rate is high enough that the reaction front exits the reactor, and, as a consequence, a reduction of the operability range is observed. Because quenching exclusively depends on total flow rate and developable thermal power, methane partial substitution with hydrogen at the same power output does not influence quenching temperatures and the extinction-blow out transition as a function of the flow rate. On the contrary, a positive effect on the ignition temperature has been detected and related to the increase of the catalyst temperature by means of the complete hydrogen conversion on the Pt fraction of the catalyst.

The study of the catalytic combustion of mixtures containing several fuels under pressure needs the preliminary production of kinetic data at above atmospheric pressures, whose availability in the literature is very poor. For this purpose, CH₄, CO and H₂ combustions under isothermal conditions have been separately studied on the perovskite and the noble metal catalyst. H₂ combustion on Pt apart, in all cases it was possible to derive a simple reaction rate well fitting all experimental data. The difficulty encountered with H₂ combustion on Pt seems due to the contemporary occurrence of several steps with different activation energies and, as a consequence, to a different distribution of sites with adsorbed oxygen or hydrogen as a function of the operative conditions (i.e. temperature and reactant partial pressures). On the contrary, for CH₄ and CO combustion a relatively simple reaction rate can represent all experimental data with a good agreement. In these cases the best models have been already reported in the literature and, thus, can be extended at pressures above the atmospheric one.

In the investigated temperature range methane combustion rate can be expressed with a single fractional equation taking into account only methane adsorption. On the other hand, the findings reported in the chapter V underline that methane combustion on perovskite catalyst shows an apparent linear reaction rate only at atmospheric pressure. The extension of such kinetics at higher pressures leads to an overestimation of the reaction rate. The evidence that there is no effect of oxygen (the reaction order with respect to oxygen is zero) suggests that the reaction mainly occurs

with β -oxygen, i.e. with the lattice oxygen. On the contrary, both CO and H₂ combustions on perovskite are influenced by changes of the oxygen partial pressure. In both cases, the best models suggest the reaction of at least a fraction of the fuel with α -oxygen, generally weakly bonded to the catalyst surface. Moreover, according to the strong CO affinity with perovskite as revealed by CO-TPR, the CO combustion rate must take into account the negative effect of CO accumulation on the surface, leading to a less than linear reaction order with respect to the fuel.

As a general conclusion, excluding some conditions of H₂ combustion on Pt, the effect of pressure on the combustion kinetics is positive even if less than linear.

This positive effect has been detected under pseudo auto-thermal conditions too during methane combustion on perovskite. As a matter of fact, methane can be ignited simply by increasing the pressure. As reported above, ignition is a kinetically controlled phenomenon and, thus, the positive effect of the pressure must act on the kinetics. In this case a pressure increase leads to two concomitant effects, both beneficial for the fuel conversion under kinetic control: higher reaction rates, according to the conclusions of the kinetic study, and longer contact times, due to the reduction of the flow velocity. Moreover, once ignited, the pressure can be lowered without the occurrence of quenching phenomena, i.e. keeping stable operation. This effect resembles that of pre-heating temperature, as reported in the chapter IV. Even if no quenching has been detected, the behaviour of the system during pressure decrease suggests that, if any, the quenching should occur more probably by blow out than extinction. This is mainly due to the high pre-heating temperature used in the experiments.

The positive effect of co-feeding on fuel ignition detected at atmospheric pressure has been detected also at higher pressure. In particular the co-feeding of hydrogen and carbon monoxide with methane lowered the pressure leading to methane ignition. Also in this case, the effect is mainly thermal; As a matter of fact, the reported high activity of perovskite towards carbon monoxide combustion allows to convert the most part of CO at atmospheric pressure and the produced heat enhances the catalyst temperature. As a consequence, hydrogen first and following methane can be easily converted due to the highest surface temperatures up to the imbalance between generated and exchanged heat is reached.

VII.2 Future work

Notwithstanding the results reported above, from this study it clearly appears that some issues remain open, thus suggesting future work on this subject. In particular, both kinetic and auto-thermal study can be enlarge according to the following guidelines.

Concerning the kinetics, it appears useful to study under pressure the binary mixtures as H_2/CO , CH_4/H_2 and CO/CH_4 as well as the ternary mixtures $H_2/CO/CH_4$ in order to evaluate the reactants interaction (site competition, synergistic effect, oxygen competition and so on). These studies will be conduct on both Pt and $LaMnO_3$ active phases.

Moreover it seems useful to study the effect of the products (H_2O , CO_2) on kinetics in order to improve the kinetic models reported in this study principally for the prediction of the behavior of the catalyst under less diluted condition (i.e. autothermal condition). Moreover, these compounds can be present in the fuel gas if the syngas is produced by a gasification process.

In the mean while, an effort should be made in order to model the catalytic combustion in the monolithic reactor under pseudo adiabatic condition using the kinetic models proven under pressure. The model will be validated with the aid of the tests conduct in this PhD activity, both at ignition and quenching conditions and at steady state.

In the future, the experimental campaign under pseudo-adiabatic condition should be extended to the study of the addition of H_2 and/or CO to CH_4 combustion, appeared interesting in this thesis, at different pre-heating temperatures, likely lower than that studied at this time, and to different fuel substitution. Moreover, CO_2 and H_2O should be added to the feed in order to better simulate a syngas composition.

Besides, other Pt-based catalysts should be studied under autothermal condition. In particular two concept should be compared: a full bi-functional Pt- $LaMnO_3$ should be compared to a dual stage catalytic concept with Pt based catalyst as first stage followed by a non doped perovskite catalyst.

APPENDIX

This appendix concerns the fluid dynamics description of the reactor developed for the kinetic studies of methane, hydrogen and carbon monoxide combustion on the catalytic platelet as well as the discrimination of the ranges of suitable condition for the study of kinetics mechanism i.e. where interphase and/or intraphase limitations are negligible. At these purposes the fluid dynamics of the reactor is addressed first.

According to the experimental campaign, the following considerations are made for pressure variation at constant of mass flow rate i.e. implying an inverse variation of volumetric flow rate and, as a consequence, of velocity. Moreover, since the mixtures are very diluted, the gas properties (i.e. density viscosity and so on) are those of air.

For the following considerations, the diffusivity evaluation of the different pair of gasses is required. Therefore in table 1, are listed the diffusivities of CH₄, H₂ and CO calculated for 2 different temperatures according to Chapman and Enskog (Eq.1), valid for non polar components, and Brokaw that is valid for polar ones (CO), equations.

$$D_{ab} = \frac{0.001858 \cdot T^{\frac{3}{2}} \cdot \left[\frac{M_a + M_b}{M_a} \cdot M_b \right]^{\frac{1}{2}}}{P \cdot \sigma_{ab}^2 \cdot \Omega_D} \quad \text{eq. 1}$$

Where

- σ_{ab} first Lennard-Jones parameter (i.e. characteristic length) [Å]
- Ω_D adimensional function of temperature and intermolecular potential of the binary gas mixtures gasses.

The Brokaw equation is formally similar to Eq.1 but σ_{ab} and Ω_D are evaluated taking into account the effect of polar interaction.

Tab. 1 – Diffusivities of fuels in air evaluated at P=1 bar and for two temperatures

Diffusivities of fuels in air, m ² /s	400°C	800°C
CH ₄	8,57·10 ⁻⁵	2,01·10 ⁻⁴
H ₂	3,12·10 ⁻⁴	7,13·10 ⁻⁴
CO	6,85·10 ⁻⁵	1,38·10 ⁻⁴

Even if the Chapman-Enskog correlation was derived for low density assumption, it provides good agreement for experimental D_{ab} estimates also up to 70 atm indicating that the $D_{ab}P$ product is constant up to this pressure value. Therefore in the remainder of this consideration it is assumed that the diffusivity is inversely proportional to the pressure.

In table 2, the characteristic dimension of the system (combustion chamber plus platelet) are summarized.

Tab. 2 – Reactor geometrical properties

<i>Platelet</i>	W , width	0.015 m
	L , lenght	0.03 m
	δ_{cat} , catalytic layer thickness	0.000045 m
	S , outer catalytic surface per unit of weight	0,0017 m ² /g
<i>Combustion chamber</i>	δ , channel gap	0.001 m
	$\delta_H = 1 \cdot \frac{W \cdot \delta}{2 \cdot (W + \delta)}$ hydraulic diameter	0.0018 m

1.1 Fluid Dynamic Regime Individuation

Taking into account the value of hydraulic diameter (see Table1) and hypothesizing that total flow rate varies, Q_{tot} , between 40 and 200 splh, the Re number calculated at 4 different temperature are reported in Fig. 1.

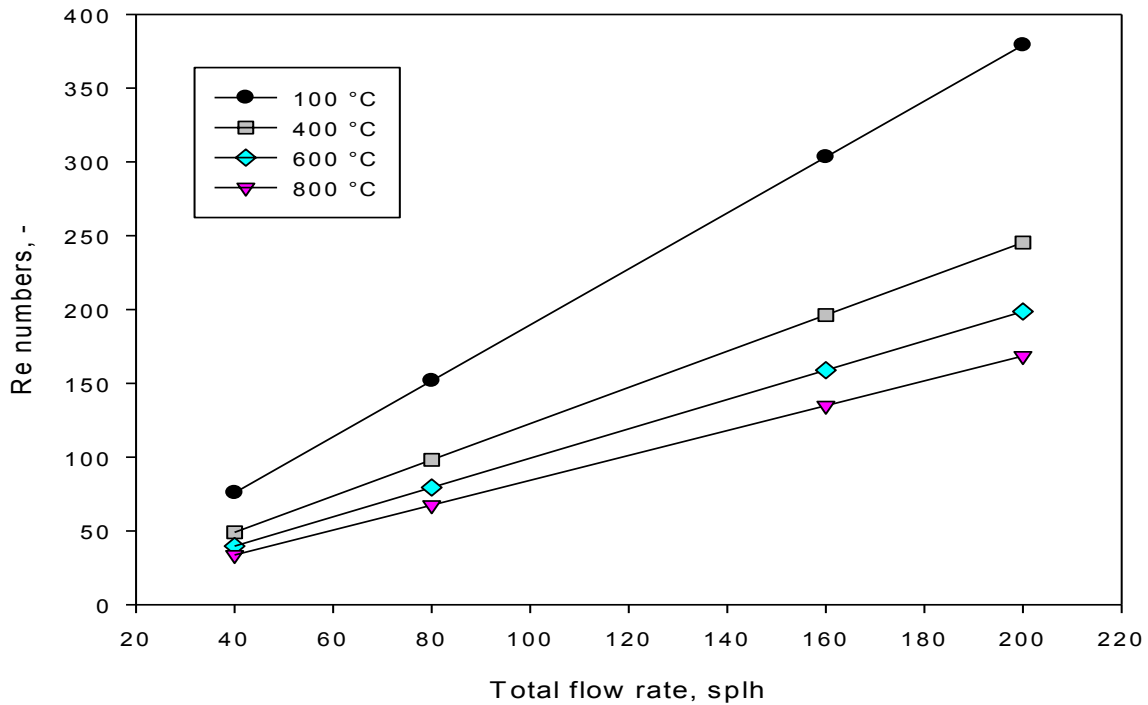


Fig 1-Reynolds number at different temperatures (100:800 °C) as a function of the total flow rate. Gas properties of air @ 1 bar and considered temperatures

It clearly appears that the flow is always laminar, the maximum obtained Re being slightly lower than 400.

The above consideration can be easily extended to pressure above the atmospheric one. As a matter of fact the product $\rho \cdot u$, representing the mass flow rate, is independent on the pressure. Moreover the fluid viscosity dependence on pressure is limited in the range of condition considered, as visible in Fig.2 that reports the dependence of reduced viscosity on reduced pressure and temperature (P_r , T_r). As a matter of fact, changing the pressure from 1 to 12 bar results in a limited variation of the reduced pressure ranging (0,03 to 0,32). In addition, taking into account that the T_r range of variation is 2,8:8,2, it is evident that the curve lies very close to the low pressure limit.

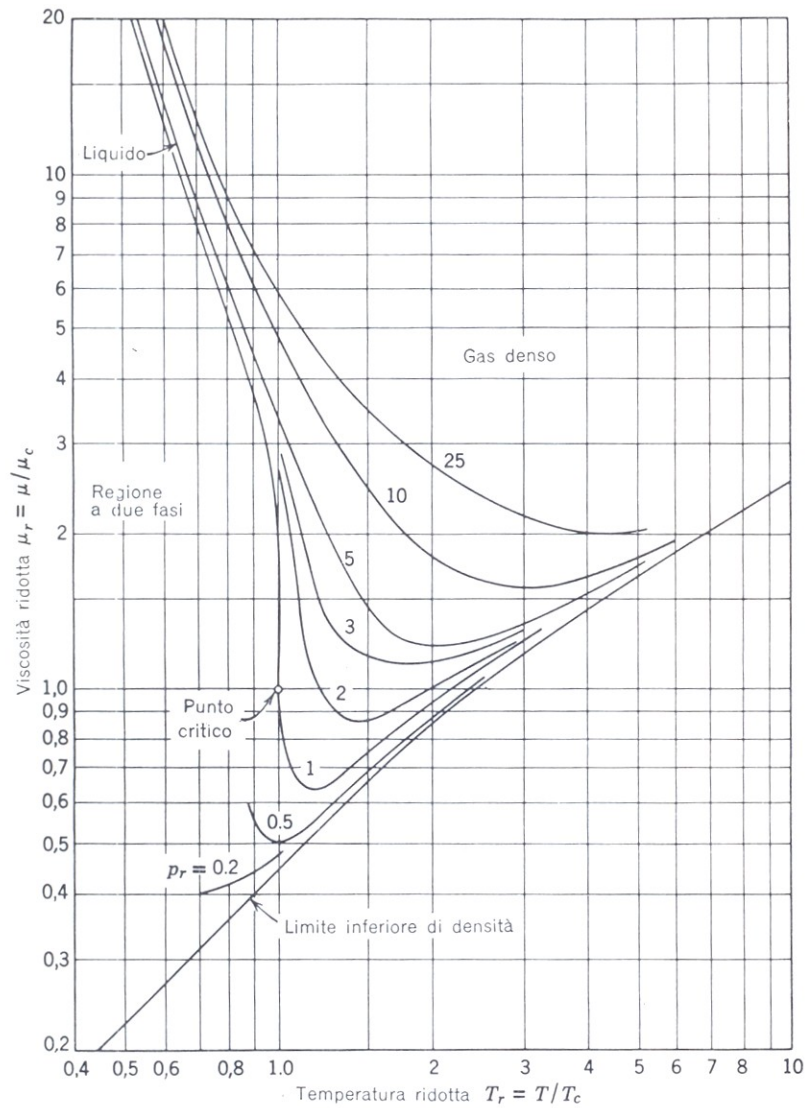


Fig 2-Reynolds number at different temperatures (100:800 °C) varying the total flow rate. Gas properties of air @ 1 bar and temperatures considered

In correspondence of the Re numbers reported in Fig. 1, the hydrodynamic entrance length L_{ent} , was also calculated. This length (see Fig.3), that depends on Re and on the flow condition upstream, corresponds to the length in laminar flow required for the centerline velocity to reach 99 percent of its fully developed value. In the case of uniform velocity profile at the pipe entrance, that is the case under study, a correlation was found by Dombroski et al (1993) (Perry and Green 7th edition):

$$\frac{L_{ent}}{\delta_H} = 0.370 \cdot \exp(-0.148 \cdot Re) + 0.055 \cdot Re + 0.26$$

eq.2.

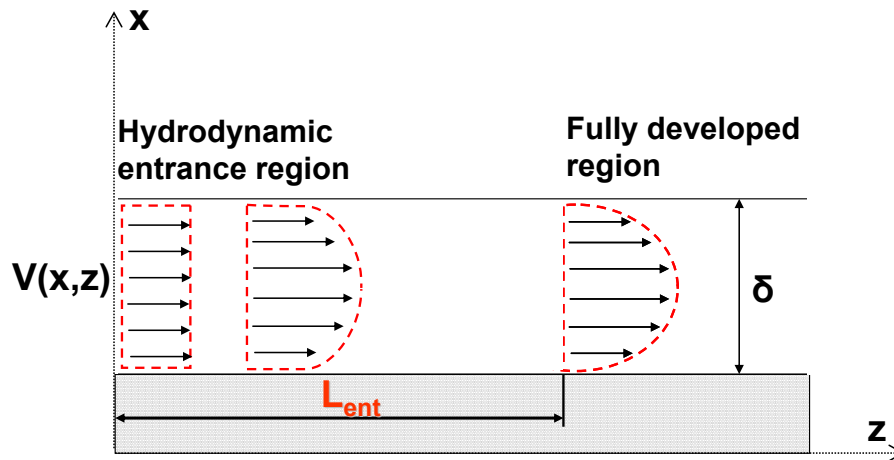


Fig. 3-Velocity profile development in the entrance of the platelet reactor.

The computed L_{ent}/L ratios, according to the correlation of eq.2.,are reported in Fig.4.

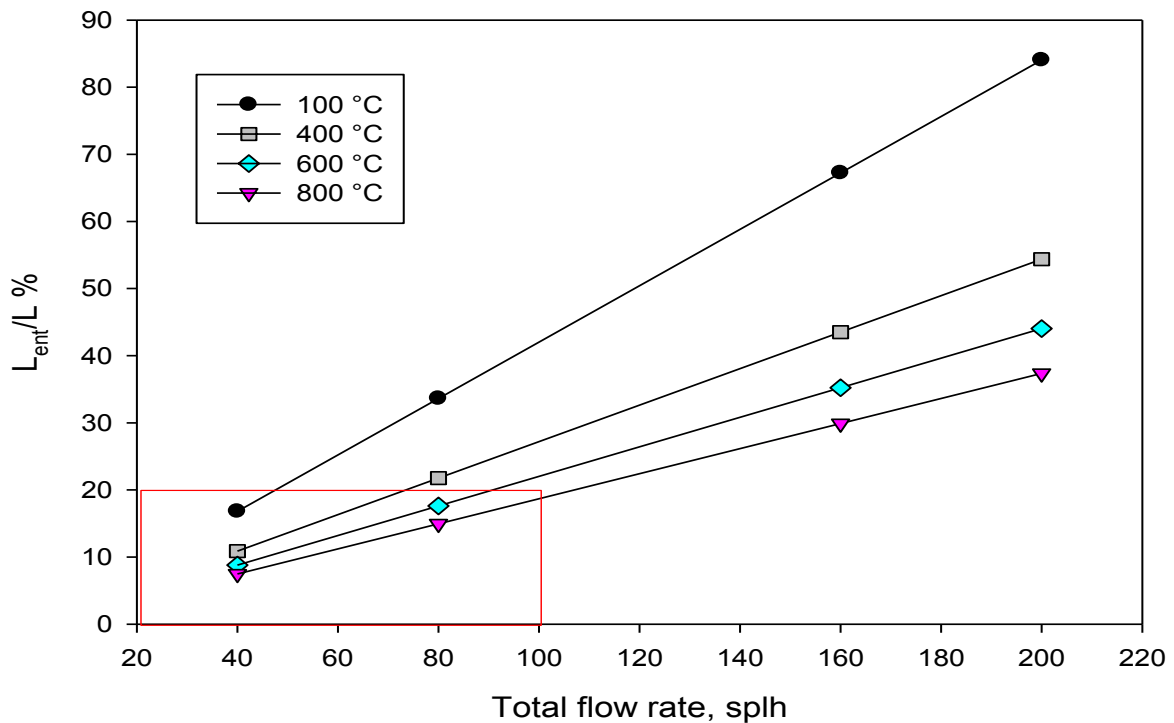


Fig 4- Hydrodynamic entrance length at different temperatures (100±800) varying the total flow rate. Gas properties of air @ 1 bar and temperatures considered

In order to limit the part of the reactor that is devoted to the establishment of laminar profile, it is better to work with relatively low total flow rate and elevated temperature corresponding to Re number below 100.

1.2 Plug flow approximation

The acceptability of the plug flow hypothesis is checked by the evaluation of the axial Peclet (Pe_{ax}) number. According to Levenspiel (1966), for Pe_{ax} values ≈ 30 the flow could be considered plug.

The dispersion coefficient are evaluated from the following empirical correlation (Y. Wen,1982), valid for $1 < Re < 2000$; and $0.2 \leq Sc \leq 1000$:

$$\frac{D_e}{u \cdot \delta_H} = \frac{1}{Re \cdot Sc} + \frac{Re \cdot Sc}{192} \quad \text{eq.4}$$

where the non dimensional group $Re \cdot Sc$, also known as Bodenstein number $Bo = \frac{u \cdot \delta_H}{\mathcal{D}}$ (see Table 3), is pressure independent.

Table 3-Bodeinstein numbers calculated at 800°C for CH₄, H₂ and CO

Total flow rate, splh	CH ₄	H ₂	CO
40	24,9	6,8	36,2
200	124,6	34,2	181,1

This correlation confirms the theoretical one obtained by Taylor and Aris for laminar flow in pipes (1956).

$$D_e = \mathcal{D} + \frac{\delta_H^2 \cdot u^2}{192 \cdot \mathcal{D}} \quad \text{eq.5}$$

From this correlation, it is evident that D_e , the dispersion coefficient, could be of several order of magnitude higher than molecular diffusivity showing its same trend with pressure. Nevertheless the Pe_{ax} results independent on pressure.

In Fig.5 (a,b,c), the different fuels Pe_{ax} , calculated according to Eq.4, are reported as a function of the total flow rate and parametric in the temperature.

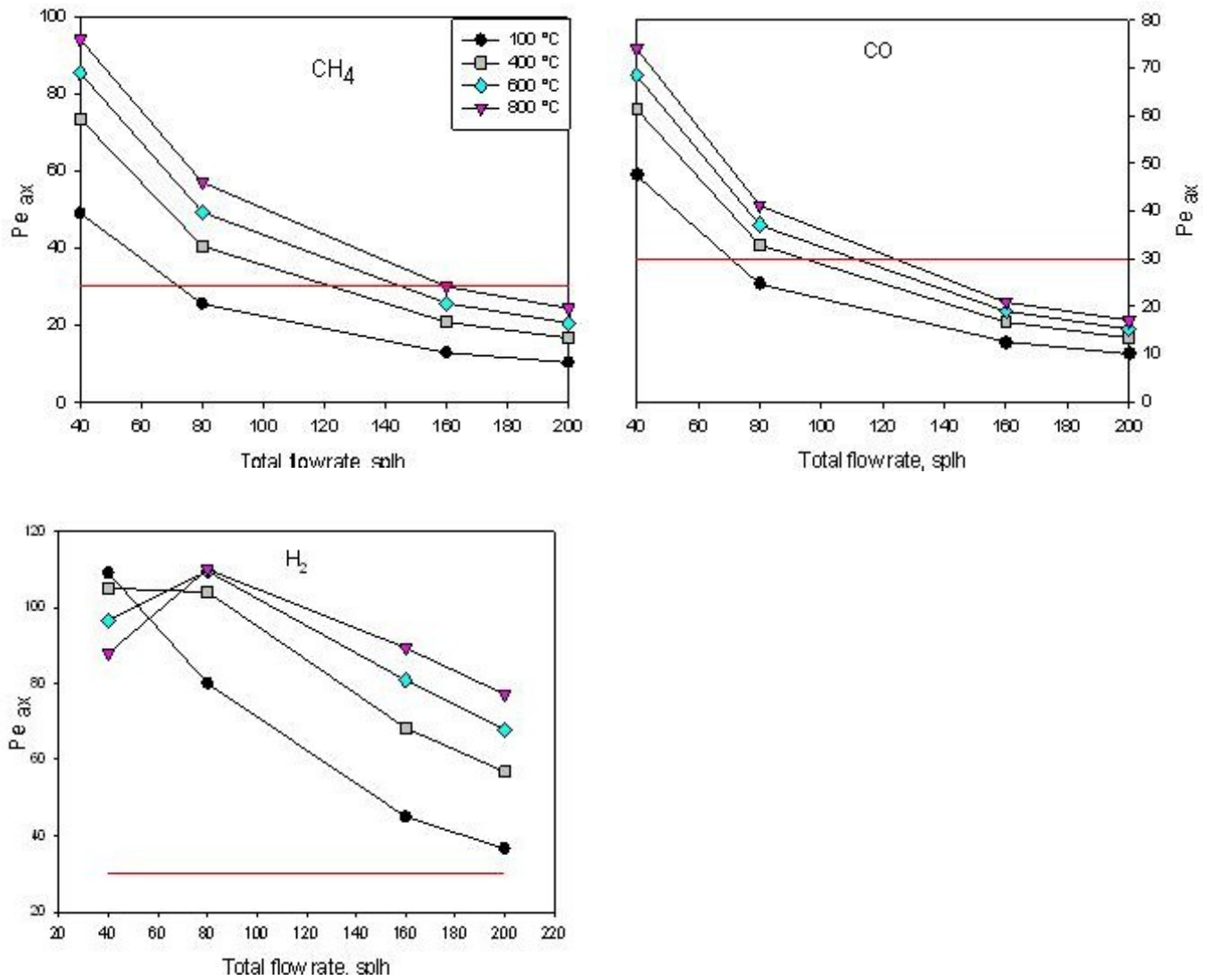


Fig 5-Axial Peclet number at different temperatures (100±800) varying the total flow rate. Gas properties of air @ 1 bar and temperatures considered. Dispersion coefficient calculated according to eq. 5. Diffusivity of CH₄, H₂ and CO calculated by Chapman Enskog and Brokaw (see Table 1).

From Fig.5 it appears that all fuels have axial Peclet decreasing by increasing the flow rate. Methane and carbon monoxide show very similar trends due to the similar value of Bo .

As concerning H_2 , its Pe_{ax} is always higher respect to other fuels even if its molecular diffusivity is higher. This is explained by the lower Bo number with a different relative importance of the terms of eq. 4.

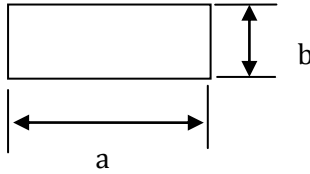
However the Pe_{ax} is always higher than 10, and is possible to achieve values of about 30.

1.3 Heat And Mass Transfer

In fully developed laminar profile (i.e. an entrance region that is less than 10% of the total), it's also possible to estimate a Sh_{∞} number that is independent on velocity and is univocally determined by the geometry and boundary condition as shown in table 4. Actually, the limiting Sh values reported in table 4, are applicable for laminar flow of Graetz numbers are lower than 4.0.

In the case of the reactor used for kinetic test, the aspect ratio is a/b is 15 thus allowing to have a Sh_{∞} higher than 5,60.

Table 4. Limiting Sherwood values for laminar flow and $Gr < 4$ adapted from Bejan, 1998 and Perry and Green 7th edition

	Aspect ratio	Boundary condition
	a/b	Constant Concentration
	1	2.98
	2	3.39
	3	3.96
	4	4.44
	6	5.14
	8	5.60
	∞	7.54

Otherwise, the dependence of Sh number accounting for the entrance effect is taken in account considering the following expression (Beretta et al, 2009):

$$Sh_{loc} = Sh_{\infty} + 8.827 * (1000z / (\delta h Re Sc))^{-0.545} \exp(-48.2z / \delta h Re Sc) \quad \text{eq. 6}$$

As concern the effect of the pressure, once again the product $\delta_h \cdot Re \cdot Sc$ (i.e. $\delta_h^2 \cdot u / \mathcal{D}$) is pressure independent because either u and \mathcal{D} are inversely proportional to the pressure.

In Fig.6, the computed local Sh numbers are reported for the different fuels for total flow rate of 200 splh at 400°C considering Sh_{∞} equal to 5,60.

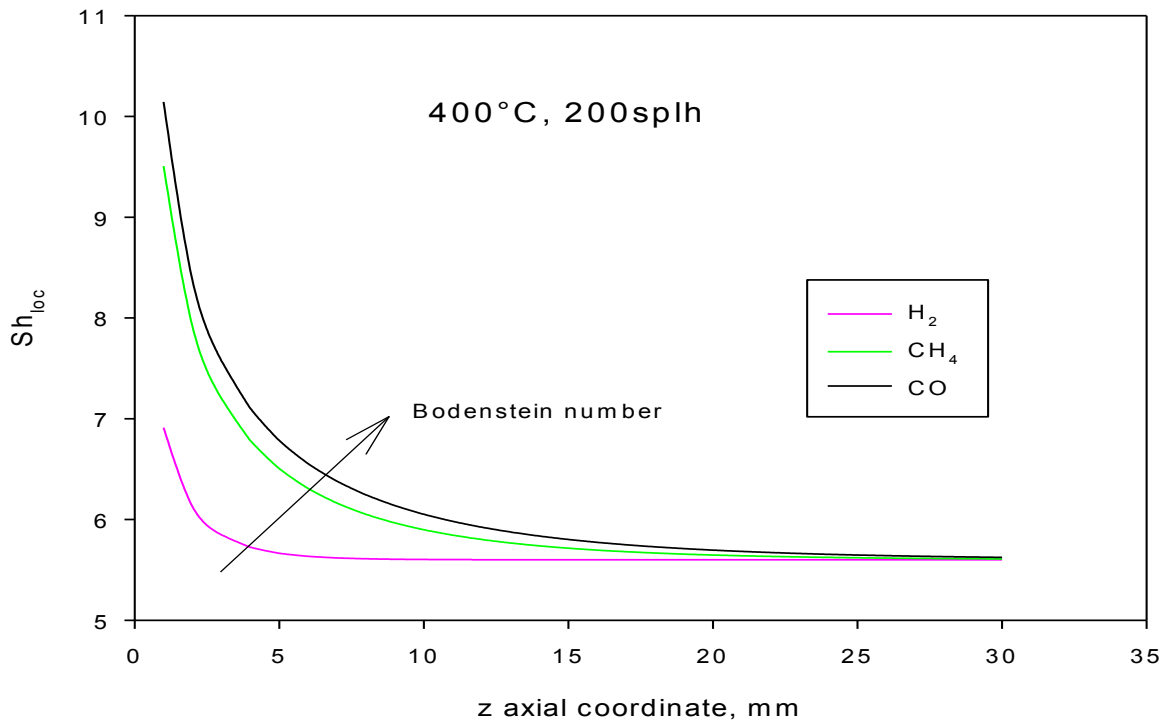


Fig 6-Local Sherwood number along the axial direction for the different fuel at 200 splh and 400°C . Gas properties of air @ 1 bar and temperatures considered. Sh_{loc} calculated according to eq. 6 with Sh_{∞} of 5,60 . Diffusivity of CH_4 , H_2 and CO calculated by Chapman Enskog and Brokaw (see Table 1).

It appears that the local Sh numbers are higher than the limiting value. Moreover, in the first part of the reactor, for low Bo numbers, as in the case of H₂, the limiting value is achieved before; while in the case of CH₄ and CO, the entrance effect is more pronounced.

1.4 Interphase limitation to mass transfer

This paragraph deals with the estimation of the operative condition allowing to neglect the effect of interphase mass transfer of reactants from bulk gas to catalytic surface.

At this purpose, it is useful to write the mass balance at the gas-solid interface as follows:

$$K_m \cdot (P_b - P_s) \cdot a = k \cdot P_s \quad \text{eq.7}$$

where P_b and P_s are the partial pressures of fuel respectively in the bulk gas phase and at the catalyst surface, a is the gas-solid interfacial area per mass of catalyst (m²/g), K_m is the mass transfer coefficient (Kmol/(m²·s·bar)), k is pseudo-first order kinetic constant (Kmol/(g·s·bar)).

Rearranging equation 7 for P_s gives:

$$P_s = \frac{P_b}{1 + \frac{k}{K_m \cdot a}} \quad \text{eq.8}$$

The negligible mass transfer limitation condition implies that the P_s ≈ P_b, or equivalently that the ratio $\frac{k}{K_m \cdot a}$ is much smaller than 1.

At this purpose mass transfer coefficient, K_m is evaluated from Sh according to the eq.9.

$$Sh = \frac{\hat{k}_g \cdot RT \cdot \delta}{D_M \cdot P} = \frac{K_m \cdot RT \cdot \delta}{D_M} \quad \text{eq.9}$$

A Sh value of 5.6 is considered in order to make a conservative valuation (see paragraph 1.3). Concerning kinetic constants, on dependence of active phases and fuels, their values are estimated

at different temperatures considering first order reaction respect to the fuel from literature data, reported in table 5.

Table 5-Literature kinetic parameters used for computing the P_s/P_b ratio

Active phase	CH ₄		H ₂		CO	
	Ea, Kcal·mol ⁻¹	k ⁰ , NI·(g·s) ⁻¹	Ea, Kcal·mol ⁻¹	k ⁰ , NI·(g·s) ⁻¹	Ea, Kcal·mol ⁻¹	k ⁰ , NI·(g·s) ⁻¹
LM20-A	26,2 ^a	3,6·10 ⁵ ^a	14,6 ^b	2.68·10 ³ ^b	13.0 ^b	3.53·10 ³ ^b
1Pt-A	27,7 ^a	3,3·10 ⁵ ^a	9,1 ^a	6,6·10 ⁴ ^a	-	-

a from Scarpa et al, (2009) **b** from Cimino et al (2003);

From the values reported in table 5, it is possible to calculate the iso-conversion curves in the T versus total flow rate plane (Fig.7) calculated for an active phase loading of 26 mg according to a first order reaction, except for CO combustion on 1Pt-A; As a matter of fact a pseudo-first order approximation is not reported in literature.

The computed $\frac{k}{K_m \cdot a}$ and P_s/P_b ratios were calculated and reported in fig. 8 for the different fuel/catalyst systems in their temperature range of interest.

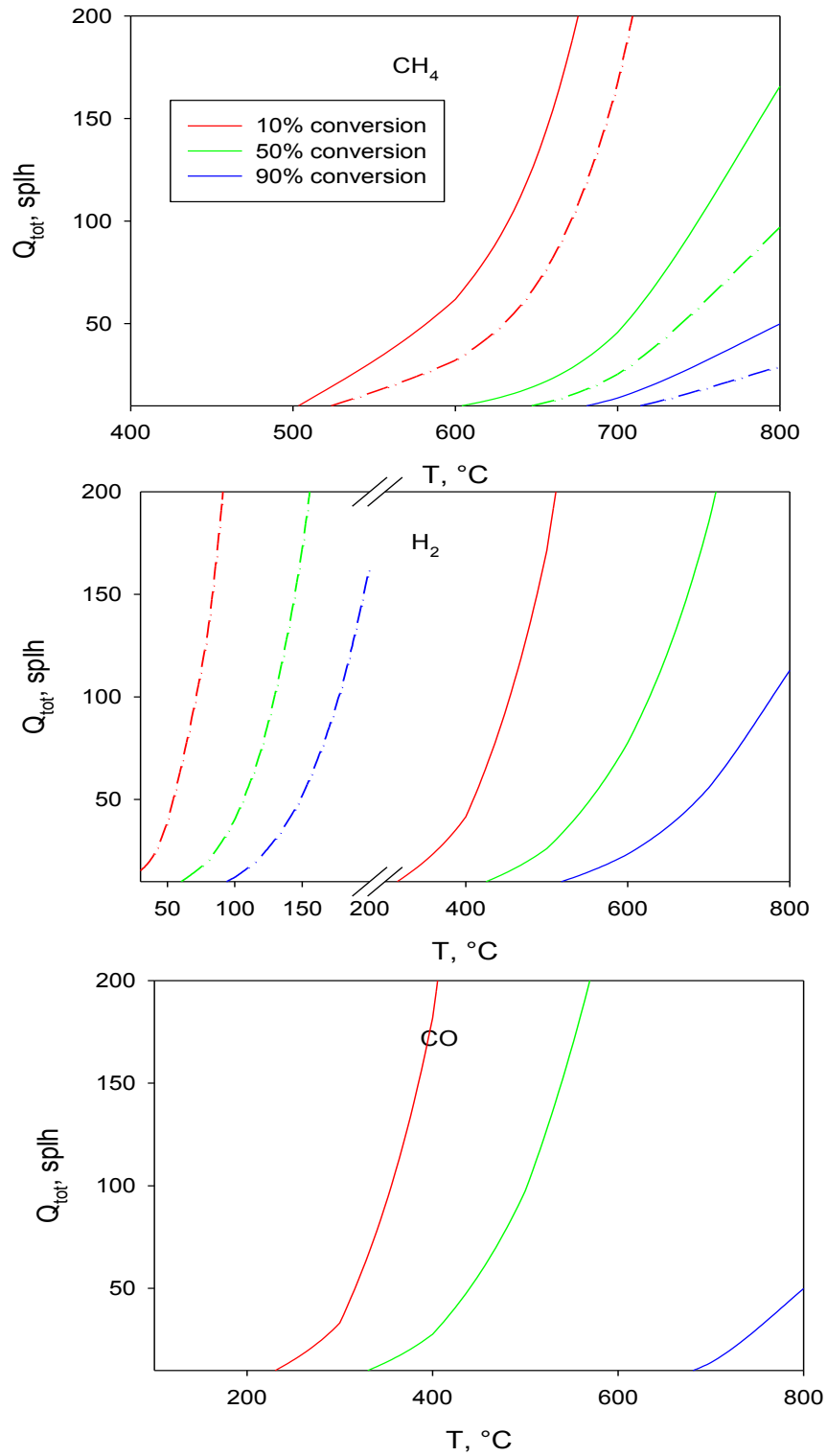


Fig 7- Isoconversion curves in the Q_{tot} vs T plane for CH₄, H₂ and CO combustion. Solid lines: Perovskite catalyst; Dash-dot lines: Pt catalyst.

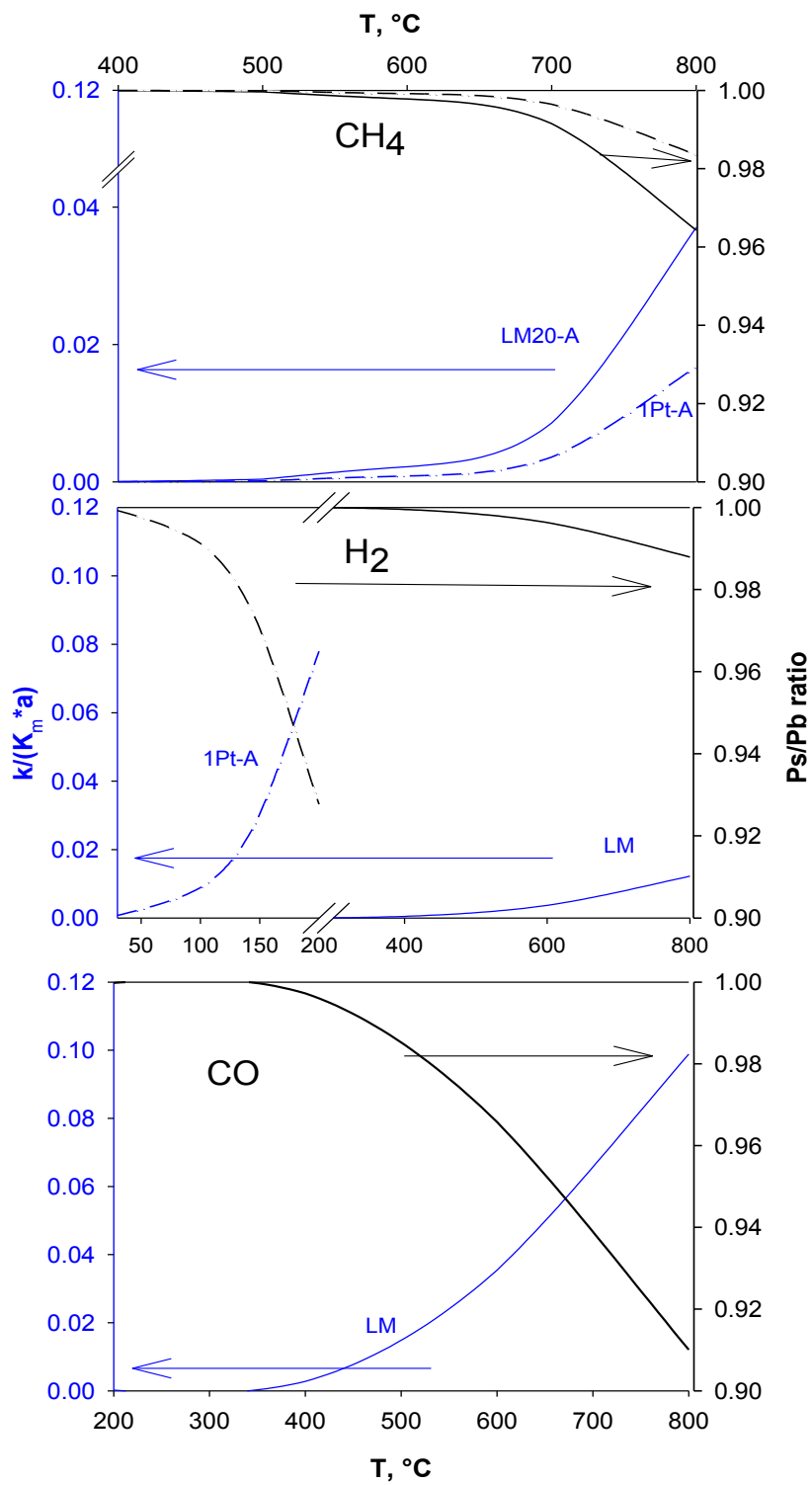


Fig 8- $k/(K_m \cdot S)$ and P_s/P_b ratio varying the temperatures for CH₄, H₂ and CO calculated by kinetic parameters of table 5. Solid lines: Perovskite formulation; dash- dot lines Pt formulation.

1.4 Intraphase limitation to mass transfer

The impact of intraphase transport limitation is considered according to the Weisz-Prater criterion (eq. 11) :

$$\Phi = \phi_I^2 \cdot \eta = \frac{\delta_{cat}^2 \cdot r_v}{C_s \cdot D_{eff}} < 0.3 \quad \text{eq.11}$$

Where

Φ is the Weisz modulus

ϕ_I is the Thiele modulus,

η the efficiency factor

δ_{cat} is the catalytic layer thickness (m)

r_v , volumetric reaction rate, (moli/l/s)

D_{eff} effective diffusion in pores (m²/s)

C_s external surface concentration of reactant (mol/l) (i.e. bulk concentration C_b in the case of negligible resistance to external mass transfer)

This criterion allows to determine the importance of internal diffusion using all observable variables. Properly in the case of integral reactor the C_s or C_b have to be replaced by the proper average of the varying concentrations. For example in the case of first order reaction a logarithmic mean of the concentration inlet and outlet concentration could be used. However in the case of this preliminary study it is enough to estimate the Weisz modulus for the initial concentration.

Concerning the impact of pressure, it is required to study the different mechanism of diffusion into the pores. According to Satterfield and Sherwood (1963), it is known that pore diffusion may occur by one or more of three mechanisms:

- Ordinary diffusion
- Knudsen diffusion
- Surface diffusion.

Concerning the ordinary diffusion, the effective diffusion is estimated by the following equation (eq.12):

$$\mathcal{D}_{M\,eff} = \mathcal{D} \cdot \frac{\theta}{\tau} \quad \text{eq.12}$$

In which are present the void fraction and the τ factor that takes into account for both tortuosity and pore cross section variation.

From eq.12 it appears that the \mathcal{D}_{eff} has the same trend of the molecular diffusivity as a function of pressure (i.e. constant flux with pressure) and is independent on pore size; while Knudsen diffusivity (eq.13) is independent on pressure and dependent on pore size.

$$\mathcal{D}_{K,\,eff} = 9700 \cdot \frac{2\varepsilon}{SSA \cdot \rho_b} \cdot \sqrt{\frac{T}{M}} \frac{\theta}{\tau}; \quad \text{eq.13}$$

were T absolute temperature, SSA the total specific surface area ($1.4 \cdot 10^6 \text{ cm}^2/\text{s}$), ρ_b catalyst density (1.3 g/cm^3).

As a consequence the predominance of Knudsen or ordinary diffusion depends not only on pore size but also on the $\mathcal{D}/\mathcal{D}_K$ ratio. At the same pore size, if $\mathcal{D}/\mathcal{D}_K$ is large, the Knudsen diffusion predominates, on the other hand, for small $\mathcal{D}/\mathcal{D}_K$ ratio the molecular diffusion prevails. It is also evident that pressure can change the relative importance of the two diffusion mechanisms.

As a matter of facts as reported in Satterfield and Sherwood (1963), the diffusion flux for the Knudsen mechanism increases by increasing the pressure and then becomes constant when ordinary diffusivity becomes the predominant mechanism.

This implies that in the case of small pore size, for which is expected that Knudsen diffusion predominates, the increase of pressure cause an increase of diffusion flux allowing to limit the extent of internal mass transfer limit.

Accordingly the Weisz -Prater criterion will be applied for the minimum pressure (i.e. atmospheric one) and higher temperatures for the different fuel/catalyst couples i.e. condition at which the impact of internal mass limitation is expect to be higher. Table 7 summarized the value of both Knudsen and ordinary \mathcal{D}_{eff} and Φ values.

Table 7- Weisz Modulus computed for the different Fuel/catalyst couples at P=1 atm.

Active phase	CH ₄			H ₂			CO		
	$\tilde{\mathcal{D}}_{\text{keff}},$ x10 ⁷ m ² /s	$\tilde{\mathcal{D}}_{\text{M,eff}}$ x10 ⁵ m ² /s	Φ	$\tilde{\mathcal{D}}_{\text{keff}}$ x10 ⁷ m ² /s	$\tilde{\mathcal{D}}_{\text{M,eff}},$ x10 ⁵ m ² /s	Φ	$\tilde{\mathcal{D}}_{\text{keff}}$ x10 ⁷ m ² /s	$\tilde{\mathcal{D}}_{\text{M,eff}}$ x10 ⁵ m ² /s	Φ
LM20-A	1,46	1,51	8·10 ⁻²	1,46	5,48	1.3·10 ⁻¹	1,46	1,04	3.6·10 ⁻¹
1Pt-A	1,46	1,51	3,4·10 ⁻²	0,97 ^b	1,23	6.6·10 ⁻¹	1,1 ^c	0,43	

P=1atm; τ and θ respectively of 4 and 0.3. $S_g=1,4 \cdot 10^6$ cm²/s, $\rho_b=1.3$ g/cm³, Diffusivities are expressed in m²/s, r_v (mol/s/l) calculated from kinetic data of table 5 at the temperature: a) T=800°C; b) T=200°C ; c) 300°C

In every case the Knudsen diffusivity results lower compared to the ordinary one of more than one order of magnitude. The $\tilde{\mathcal{D}}_{\text{eff}}$ evaluated according to the follow expression:

$$\frac{1}{\tilde{\mathcal{D}}_{\text{eff}}} = \frac{1}{\tilde{\mathcal{D}}_{k,\text{eff}}} + \frac{1}{\tilde{\mathcal{D}}_{M,\text{eff}}} \quad \text{eq.14}$$

is with good approximation equal to the effective Knudsen diffusivity. The estimated Φ values for methane combustion on both platelet are always less than 0.3 even at 800°C. In the case of H₂ combustion on perovskite catalyst the Φ values is less than 0.3; while for Pt catalyst this value is about 0.7 at 200°C suggesting that for Pt formulation the maximum temperature adopted for the test must be lower. It is estimated that a 0.3 value of the Weisz-Prater modulus for the H₂-Pt system is obtained for a temperature of about 165°C. As regards CO combustion on perovskite catalyst, the Φ value calculated at 800°C is slightly higher than 0.3 suggesting that the combustion test could be carried out up to 800°C.

NOTATION

Symbols

a	gas-solid interfacial area per mass of catalyst in equation 7 and 8.
ΔH_{comb}	Heat of combustion, kJ/mol
C, C°	molar concentration, initial fuel molar concentration mol·l ⁻¹
$C _z, C _{z+dz}$	Fuel concentration evaluated at z and $z+dz$ axial position, mol·l ⁻¹
C_s, C_b	external surface concentration of reactant, bulk reactant concentration, mol·l ⁻¹
D_e	dispersion coefficient
$\mathcal{D}, \mathcal{D}_{M,\text{eff}}$	Molecular or ordinary diffusivity, ordinary effective diffusion, m ² /s
$\mathcal{D}_{a,b}$	Molecular diffusivity for the binary mixture a,b
$\mathcal{D}_k, \mathcal{D}_{k,\text{eff}}$	Knudsen diffusion, effective diffusivity (m ² /s)
\mathcal{D}_{eff}	effective diffusion in pores (m ² /s)
dW	infinitesimal element of catalyst weight, g
F	ratio of the Model Mean Square to the Error Mean Square
F°	fuel molar flowrate, mol·s ⁻¹
M	Molecular weight, g·mol ⁻¹
MIT, QT	Minum Ignition Temperature, Quenching Temperature, °C in Chapter IV
$MRSS$	Mean Residual Sum of Squares
$N_{\text{obs}}, N_{\text{par}}$	Number of experimental observation, Number of model parameter in eq. II.4.1
$X_{p,n}, X_n$	predicted and experimental final conversion for the nth experiment in eq. II.4.1

k, k', k''	Kinetic constants
K, K_i	Adsorption constants, bar^{-1}
\hat{k}_g	Mass transfer coefficient $\text{kmol}\cdot(\text{m}^2\cdot\text{s})^{-1}$
K_M	Mass transfer coefficient $\text{kmol}\cdot(\text{m}^2\cdot\text{s}\cdot\text{bar})^{-1}$
L	Length, m
L_{ent}	hydrodynamic entrance length, m
m, n, p	apparent reaction order with respect to total pressure, fuel and oxygen
P, P_i	total pressure, partial pressure of the i specie
P_s, P_b	Fuel partial pressure on the surface, in the gas bulk in Appendix
Q_{TOT}	Total volumetric flowrate, splh
r	rate of fuel consumption, $\text{mol}\cdot(\text{g}\cdot\text{s})^{-1}$
r_v	volumetric reaction rate, $\text{mol}\cdot(\text{l}\cdot\text{s})^{-1}$
R	Ideal Gas Constant, $\text{l}\cdot\text{atm}\cdot\text{K}^{-1}\cdot\text{mol}^{-1}$
S	trasversal section of catalyst layer, dm^2 in eq.II.4.3
SSA	Specific Surface Area in Chapter III m^2/g
T_{ad}	Adiabatic Temperature, $^{\circ}\text{C}$
T_{IT}	Turbine Inlet Temperature, $^{\circ}\text{C}$
u	gas velocity, m/s
W	Width, m
w_{cat}	catalyst weight, g
y_i, y_i°	molar fraction of i specie, initial molar fraction of i specie
z	reactor axial coordinate

Greek symbols

β	compressor ratio in Fig.I.5.1
δ	height of the combustion chamber, m
δ_H	hydraulic diameter of the reactor, m
δ_{cat}	thickness of catalytic layer, m
η	efficiency factor
θ	vector of model parameters
θ, τ	void fraction and tortuosity factor in eq.n 12 and 13
θ	surface coverage
μ	gas viscosity
ρ	gas density
ρ_{cat}	apparent density of catalyst layer in eq.II.4.3
ρ_b	catalyst density in eq.13
σ_{LJ}	first Lennard-Jones parameter, Å
τ	contact time, g·s·l ⁻¹
ϕ_l	Thiele modulus,
Φ	Weisz modulus
Ω_{-}	adimensional function of temperature and intermolecular potential of the binary mixture

Subscripts

ad adiabatic

ads	adsorbed
b	bulk
cat	catalyst
eff	effective
lat	lattice
pre	pre-heating
s	surface
w	wall

Non dimensional groups

Re	(Reynolds number)	$\rho \cdot u \cdot \delta H / \mu$
Sc	(Schmidt number)	$\mu / (\rho \cdot D)$
Sh	(Sherwood)	$(K_G \cdot RT \cdot \delta_H / \mathcal{D} \cdot P)$ or $(KD \cdot \delta H / \mathcal{D} \cdot P)$
Gr	(Graetz number)	$Re \cdot Sc \cdot \delta_H / L$
Pe _{axi}	(axial Peclet)	$u \cdot L / De$
Bo	(Bodenstein number)	$Re \cdot Sc$ or $u \cdot \delta_H / \mathcal{D}$

REFERENCES

Alifanti, M.; Blangenois, N.; Florea, M.; Delmon, B.: "Supported Co-based perovskites as catalysts for total oxidation of methane"; *Applied Catalysis, A: General* vol. 280(2) (2005): pp. 255-265.

Appel C., Mantzaras J., Schaeren R., Bombach R., Inauen A., Kaeppli B., Hemmerling B., Stampanoni A.: "An Experimental and Numerical Homogeneous Ignition in Catalytically Stabilized Combustion of Hydrogen/Air Mixtures Over Platinum" *Combustion and Flame* (2002) Vol.128 pp.340-368.

J. C. G. Andrae, D. Johansson, M. Bursell, R. Fakrai, J. Jayasuriya, A. Manrique Carrera ; "High-pressure catalytic combustion of gasified biomass in a Hybrid combustor combustion"; *Applied Catalysis A: General* 293 (2005): pp. 129-136.

Andreini A. and Facchini B. "Gas Turbines Design and Off-Design Performance Analysis With Emissions Evaluation" *ASME Conference Proceedings* (2002) Vol. 4.

H. Arai, T. Yamada, K. Eguchi, T. Seiyama; "Catalytic combustion of methane over various perovskite-type oxides"; *Applied Catalysis*, vol. 26 (1986): pp. 265-276.

Arai, H.; Machida, M. "Thermal Stabilisation of Catalyst Supports and their application to high-temperature catalytic combustion *Applied Catalysis A* (1996), Vol.138, pp 161-176.

M. Balat: "Potential importance of hydrogen as a future solution to environmental and transportation problems" *International Journal of Hydrogen Energy* (2008) Vol.33 pp.4013-4029.

Barbaro P. and Bianchini C "Catalysis for Sustainable Energy production" (2009).

Barbato, P. S.; Landi, G.; Pirone, R.; Russo, G.; Scarpa, A. Auto-thermal combustion of CH₄ and CH₄-H₂ mixtures over bi-functional Pt-LaMnO₃ catalytic honeycomb. *Catalysis Today* (2009), 147(Suppl.),

A. Beretta, G. Groppi, M. Lualdi, I. Tavazzi, and P. Forzatti "Experimental and Modeling Analysis of Methane Partial Oxidation: Transient and Steady-State Behavior of Rh-Coated Honeycomb Monoliths" *Industrial & Engineering Chemical Research* (2009) Vol 48, pp.3825-3836.

R. Carroni, T. Griffin, J. Mantzaras, M. Reinke, "High-pressure experiments and modeling of methane/air catalytic combustion for power-generation applications" *Catalysis Today*, 83 (2003) pp.157-170.

T. V. Choudhary, S. Banerjee, V. R. Choudhary; "Catalysts for combustion of methane and lower alkanes"; *Applied Catalysis A: General*, vol. 234 (2002): pp. 1-23.

Ciambelli, P.; Cimino, S.; De Rossi, S.; Faticanti, M.; Lisi, L.; Minelli, G.; Pettiti, I.; Porta, P.; Russo, G.; Turco, M. "AMnO₃ (A=La, Nd, Sm) and Sm_{1-x}Sr_xMnO₃ perovskites as combustion catalysts: structural, redox and catalytic properties." *Applied Catalysis, B: Environmental* (2000), 24(3,4), 243-253.

F. Cifà, P. Dinka, P. Viparelli, S. Lancione, G. Benedetti, P. L. Villa, M. Viviani, P. Nanni; "Catalysts based on BaZrO₃ with different elements incorporated in the structure I: BaZr_(1-x)Pd_xO₃ systems for total oxidation"; *Applied Catalysis B: Environmental*, vol. 46 (2003): pp. 463-471.

S. Cimino, L. Lisi, R. Pirone, G. Russo, M. Turco; "Methane combustion on perovskite-based structured catalysts"; *Catalysis Today*, vol. 59 (2000): pp. 19-31.

S. Cimino, A. Di Benedetto, R. Pirone, G. Russo; "Transient behaviour of perovskite-based monolithic reactors in the catalytic combustion of methane"; *Catalysis Today*, vol. 69 (2001): pp. 95-103.

Cimino, S.; Di Benedetto, A.; Pirone, R.; Russo, G. "CO, H₂ or C₃H₈ assisted catalytic combustion of methane over supported LaMnO₃ monoliths". *Catalysis Today* (2003), 83(1-4), pp. 33-43.

Cimino S., Lisi L., Pirone R., Russo G., "Dual-Site Pd/Perovskite Monolithic Catalysts for Methane Catalytic Combustion" *Industrial & Engineering Chemistry Research* (2004) Vol.43 (21), pp 6670-6679.

S. Cimino, M.P. Casaletto, L. Lisi and G. Russo "Pd-LaMnO₃ as dual site catalysts for methane combustion" *Applied Catalysis A: General* Vol. 327, Issue 2, (2007), pp. 238-246.

Civera, G. Negro, S. Specchia, G. Saracco, V. Specchia; "Optimal compositional and structural design of a LaMnO₃/ZrO₂/Pd-based catalyst for methane combustion"; *Catalysis Today*, vol. 100 (2005): pp. 275-281.

S. Cocchi, G. Nutini, M. J. Spencer, S. G. Nickolas; "Catalytic combustion system for a 10 MW class power generation gas turbine"; *Catalysis Today*, vol.117 (2006) pp.419- 426.

Cominos, V.; Hessel, V.; Hofmann, C.; Kolb, G.; Zapf, R.; Ziogas, A.; Delsman, E. R.; Schouten, J. C. "Selective oxidation of carbon monoxide in a hydrogen-rich fuel cell feed using a catalyst coated microstructured reactor". *Catalysis Today* (2005), 110(1-2), 140-153.

M.B. Cutrone, K. W. Beebe, R.A. Dalla Betta, J. C. Schlatter, S. G. Nickolas, T. Tsuchiya: "Development of a catalytic Combustor for a heavy-duty utility gas turbine" *Catalysis Today* (1999) Vol 47 pp 391-398.

P. Dagaut, A. Nicolle; "Experimental and detailed kinetic modelling study of hydrogen-enriched natural gas blend oxidation over extended temperature and equivalence ratio ranges"; *Proceedings of the Combustion Institute* 30 (2005): pp. 2631-2638.

R.A Dalla Betta R.A. et al, 1993 U.S. Patent No. 5,248,25.

R.A. Dalla Betta, J.C. Schlatter, D.K. Yee, D.G. Loffler, T. Shoji: "Catalytic combustion technology to achieve ultra low NO_x emissions: Catalyst design and performance characteristic" *Catalysis Today* (1995) Vol.26 pp.329-335.

R. A. Dalla Betta; "Catalytic combustion gas turbine systems: the preferred technology for low emissions electric power production and co-generation"; *Catalysis Today*, Vol. 35(1997): pp. 129-135.

R. A. Dalla Betta, T. Rostrup-Nielsen; "Application of catalytic combustion to a 1.5 MW industrial gas turbine"; *Catalysis Today*, Vol. 47 (1999): pp. 369-375.

B. De Collongue; E. Garbowski; M. Primet; "Catalytic combustion of methane over bulk and supported lanthanum chromium oxide (LaCrO₃) perovskites". *Journal of the Chemical Society, Faraday Transactions* (1991), 87(15): pp. 2493-9.

Davis, S. G.; Joshi, A.V.; Wang, Hai; Egolfopoulos, F.: "An optimized kinetic model of H₂/CO combustion". *Proceedings of the Combustion Institute* (2005), Volume Date 2004, 30(Pt. 1), 1283-1292

Demoulin, O; Seunier, I.; Navez, M; Poleunis, C; Bertrand, P.; Ruiz, P.. "Investigation of the physico-chemical implications of the hydrogen presence during H₂-assisted catalytic combustion of methane using Pd(10 wt.%)/ γ -Al₂O₃ catalyst". *Applied Catalysis, A: General* (2006), 310 40-47

O. Deutschmann, L. I. Maier, U. Riedel, A. H. Stroemman, R. W. Dibble; "Hydrogen assisted catalytic combustion of methane on platinum"; *Catalysis Today*, Vol. 59 (2000): pp. 141-150.

Dubien, C.; Schweich, D.; Mabilon, G.; Martin, B.; Prigent, M.: "Three-way catalytic converter modeling: fast- and slow-oxidizing hydrocarbons, inhibiting species, and steam-reforming reaction" *Chemical Engineering Science* (1997), Volume Date 1998, 53(3), 471-481

Dutta, P., Cowell, L.H., Yee, D.K., Dalla Betta, R.A.: "Design and evaluation of a single-can full scale catalytic combustion system for ultra-low emissions industrial gas turbines" *ASME paper 97-GT-292*.

Ersson, H. Kusar, R. Carroni, T. Griffin, S. Jaras; "Catalytic combustion of methane over bimetallic catalysts a comparison between a novel annular reactor and high-pressure reactor"; *Catalysis Today*, 83 (2003): pp. 265-277.

D. B. Fant, G. S. Jackson, H. Karim, D. M. Newburry, P. Dutta, K. O. Smith, R. W. Dibble; "Status of Catalytic Combustion R&D for the Department of Energy Advanced Turbine Systems Program", *Journal of Engineering for Gas Turbine and Power*, Vol. 124 (2002): pp. 235-238.

R.J. Farrauto, T. Kennelly and E.M. Waterman, US Patent 4 893 465 (1990).

R.J. Farrauto, M.C. Hobson, T. Kennelly, E.M. Waterman; "Catalytic chemistry of supported palladium for combustion of methane"; *Applied Catalysis A: General*, vol. 81 (1992): pp. 227-237.

- Fino, D.;** Russo, N.; Cauda, E.; Saracco, G.; Specchia, V. "La-Li-Cr perovskite catalysts for diesel particulate combustion". *Catalysis Today* (2006), 114(1), 31-39.
- Fino, D.;** Russo, N.; Saracco, G.; Specchia, V. "The role of suprafacial oxygen in some perovskites for the catalytic combustion of soot". *Journal of Catalysis* (2003), 217(2), 367-375.
- L. Forni, I. Rosetti;** "Catalytic combustion of hydrocarbons over perovskites"; *Applied Catalysis B: Environmental*, vol. 38 (2002): pp. 29-37.
- P. Forzatti,** "Status and perspectives of catalytic combustion for gas turbines", *Catalysis Today*, vol 83 (2003): pp.3-18.
- T. Furuya, K. Sasaki, Y. Hanakata, T. Ohhashi, M. Yamada, T. Tsuchiya, Y. Furuse;** "Development of a hybrid catalytic combustor for a 1300°C class gas turbine" *Catalysis today* (1995) Vol.36(3-4) pp.345-350.
- L. Giebler, D. Kiebling, G. Wendt;** "LaMnO₃ perovskite supported noble metal. Catalysts for the total oxidation of methane"; *Chem. Eng. Technol.*, vol. 30 (7) (2007): pp. 889-894.
- Gland, J. L.; Fisher, G. B.** "The hydrogen-oxygen reaction on the platinum(111) surface: temperature programmed reaction of coadsorbed atomic oxygen and atomic hydrogen" .Preprints - American Chemical Society, Division of Petroleum Chemistry (1982)
- G. Groppi, A. Belloli, E. Tronconi and P. Forzatti** "Catalytic combustion of CO---H₂ on Manganese-substituted hexaaluminates" *Catalysis Today* (1996), Vol. 29, (1-4), Pages 403-407.
- Groppi G., Artioli G., Cristiani C., Lietti L., Forzatti P.,** "Decomposition/reformation processes and CH₄ combustion activity of PdO over Al₂O₃ supported catalysts for gas turbine applications" *Studies in Surface Science and Catalysis* Vol. 136, pp.345 (2001)
- Groppi, G.; Ibashi, W.; Tronconi, E.; Forzatti, P.** "Structured reactors for kinetic measurements under severe conditions in catalytic combustion over palladium supported systems". *Catalysis Today* (2001), 69(1-4), 399-408
- Hellsing, B.; Kasemo, B.; Zhdanov, V. P.** "Kinetics of the hydrogen-oxygen reaction on platinum". *Journal of Catalysis* (1991), 132(1), 210-28.
- C.H. Hwang, C.E. Lee, K.O. Lee;** "Numerical investigation on combustion characteristic of methane in a hybrid catalytic combustor"; *Fuel* 83 (2004); pp. 987-996.
- E. M. Johansson, K. M. J. Danielsson, A. G. Ersson, S. G. Jaras;** " Development of Hexaaluminate Catalysts for Combustion of Gasified Biomass in Gas Turbines"; *Journal of Engineering for Gas Turbine and Power*, Vol. 124 (2002): pp. 235-238.
- N. S. Kaisare, S. R. Deshmukh, D. G. Vlachos,** "Stability and performance of catalytic microreactors: simulations of propane catalytic combustion on Pt". *Chemical Engineering Science* 63 (2008) 1098-1116

H. Karim, K. Lyle, S. Etemad, L.L. Smith, W.C. Pfefferle, P. Dutta, K. Smith, "Advanced Catalytic for Low NO_x Industrial Gas Turbines"; Journal of engineering for Gas Turbines and Power (2003), Vol. 125; pp 879-884.

S.T. Kolaczkowski and S. Serbetcioglu : "Development of combustion catalysts for monolith reactors: a consideration of transport limitation" Applied Catalysis A (1996) Vol. 138 pp. 199-214.

B. Kucharczyk, W. Tylus; "Effect of Pd or Ag additive on the activity and stability of monolithic LaCoO₃ perovskites for catalytic combustion of methane"; Catalysis Today, vol. 90 (2004): pp. 121-126.

W.J. Kuper., M. Blaauw, F. van der Berg, G.H. Graaf: "Catalytic combustion concept for gas turbines" Catalysis Today (1999) Vol47 pp.377-389.

A.H. Lefebvre; "Gas Turbine Combustion", Taylor and Francis, 1999.

Li, Juan; Zhao, Zhenwei; Kazakov, Andrei; Chaos, Marcos; Dryer, Frederick L.; Scire, James J., Jr. "A comprehensive kinetic mechanism for CO, CH₂O, and CH₃OH combustion." International Journal of Chemical Kinetics (2007), 39(3), 109-136

Lisi, L.; Bagnasco, G.; Ciambelli, P.; De Rossi, S.; Porta, P.; Russo, G.; Turco, M.. "Perovskite-type oxide II. Redox properties of LaMn_{1-x}Cu_xO₃ and LaCo_{1-x}Cu_xO₃ and methane catalytic combustion" Journal of Solid State Chemistry (1999), 146(1), 176-183

J.Mantzaras.; "Catalytic Combustion of Syngas"; Combustion Science and Technology (2008), vol.180: pp.1137-1168.

Mantzaras, J; Bombach, R; Schaeren, R. "Hetero-/homogeneous combustion of hydrogen/air mixtures over platinum at pressures up to 10 bar." Proceedings of the Combustion Institute (2009), 32(Pt. 2), 1937-1945

L. Marchetti, L. Forni; "Catalytic combustion of methane over perovskites"; Applied Catalysis B: Environmental, vol. 15 (1998): pp. 179-187.

P.E. Marti, M. Maciejewski and A. Baiker: "Methane combustion over La_{0.8}Sr_{0.2}MnO_{3+x} supported on MA₂O₄ (M = Mg, Ni and Co) spinels" Applied catalysis B (1994) Vol.4 pp.225-235.

G.J.Micklrow, S. Roychoudhury, H. Nguyen, M.C Cline; "Emission Reduction by Varing Swirler Airflow Split in Advanced Gas Turbine Combustors"; Journal of Engineering for Gas turbine and Power Vol 115 (1993): pp. 563-569.

J. G. McCarty; "Kinetics of PdO combustion catalysis": Catalysis Today, (1995)Vol. 26(3-4) pp. 283-293.

J. G. McCarty, M. Gusman, D. M. Lowe, D. L. Hildenbrand, K. N. Lau; "Stability of supported metal and supported metal oxide combustion catalysts"; Catalysis Today, Vol. 47 (1999): pp. 5-17.

Natarajan, J.; Kochar, Y.; Lieuwen, T.; Seitzman, J. "Pressure and preheat dependence of laminar flame speeds of H₂/CO/CO₂/O₂/He mixtures". Proceedings of the Combustion Institute (2009), 32(Pt. 1), 1261-1268

J. Neathery, D. Gray, D. Challman, F. Derbyshire; "The pioneer plant concept: co-production of electricity and added-value products from coal"; Fuel, 78 (1999) 815

Ol'khovskii G.G. "Status and Prospects of Heat-Power Engineering" Power Technology and Engineering (2005) Vol. 39 (2) pp. 104-113.

Ozawa, Y.; Tochiyama, Y.; Mori, N.; Yuri, I.; Sato, J.; Kagawa, K.. "Test results of a catalytically assisted combustor for a gas turbine." Catalysis Today (2003), Vol.83(1-4), 247-255.

J. Park, D. G. Hwang, J. S. Park, J. S. Kim, S. I. Keel, H. C. Cho, D. S. Noh, T. K. Kim: "Hydrogen utilization as a fuel: Hydrogen-blending effects in flame structure and NO emission behavior of CH₄-Air flame" International Journal of Energy Research (2007) Vol.31 pp. 472-485.

P.A. Pilavachi, "Power generation with gas turbine systems and combined heat and power", Applied Thermal Engineering . (2000) Vol.20 pp.1421-1429

Pilavachi, P. A.; Chatzipanagi, A. I.; Spyropoulou, A. I. Evaluation of hydrogen production methods using the Analytic Hierarchy Process. International Journal of Hydrogen Energy (2009), 34(13), 5294-5303

K. Persson, A. Ersson, A. Manrique Carrera, J. Jayasuriya, R. Fakrai, T. Fransson, S. Jaras; "Supported palladium-platinum catalyst for methane combustion at high pressure"; Catalysis Today Vol. 100 (2005); pp. 479-483.

S. Petrović, L. Karanović, P. K. Stefanov, M. Zdujić, A. Terlecki-Baričević "Catalytic combustion of methane over Pd containing perovskite type oxides" Applied Catalysis B: Environmental (2005) Vol. 58 (1-2), pp. 133-141.

R.Prasad, L.A. Kennedy, and E. Ruckenstein, "Catalytic combustion" Catalysis. Reviews. Science and Engineering, 26(1) (1984) pp 1-58

Quick L.M. and Kamitomi S. Catalytic combustion reactor design and test results Catalysis. Today (1995), 26(3-4), pp 303-308.

Reinke, M; Mantzaras, J; Schaeren, R; Bombach, R.; Inauen, A.; Schenker, S. Kreutner, W.: Homogeneous ignition in high-pressure combustion of methane/air over platinum: comparison of measurements and detailed numerical predictions. Proceedings of the Combustion Institute (2002)

Reinke, M; Mantzaras, J; Schaeren, R; Bombach, R.; Inauen, A.; Schenker, S. "Homogeneous ignition of CH₄/air and H₂O and CO₂-diluted CH₄/O₂ mixtures over Pt; an experimental and numerical investigation at pressures up to 16 bar." Proceedings of the Combustion Institute (2005), Volume Date 2004, 30(Pt. 2), 2519-2527

Reinke, M; Mantzaras, R; Bombach, R.; Inauen, A.; Schenker, S, Andreas. Gas phase chemistry in catalytic combustion of methane/air mixtures over platinum at pressures of 1 to 16 bar. *Combustion and Flame* (2005), 141(4),448-468

Rentz,; S. Nunge,; M Laforsch, and T., H. (1999); "Technical background document for the actualisation and assessment of UN/ECE protocols related to the abatement of the transboundary transport of nitrogen oxides from stationary sources"

J. Requies, M.C. Alvarez-Galvan, V.L. Barrio, P.L. Arias, J.F. Cambra, M.B. Guemez, A. Manrique Carrera, V.A. de La Peña O'Shea, J.L.G. Fierro; "Palladium-manganese catalysts supported on monolith systems for methane combustion"; *Applied Catalysis B: Environmental* Vol.79 (2008); pp. 122-131.

Russo, N; Fino, D.; Saracco, G.; Specchia, V.. . Studies on the redox properties of chromite perovskite catalysts for soot combustion. *Journal of Catalysis* (2005), 229(2), 459-469

Russo, N; Furfori, S.; Fino, D.; Saracco, G.; Specchia, V.. Lanthanum cobaltite catalysts for diesel soot combustion. *Applied Catalysis, B: Environmental* (2008), 83(1-2), 85-95.

H. Sadamori, T. Tanioka, T. Matsuhisa; "Development of a high-temperature combustion catalyst system and prototype catalytic combustor turbine test results"; *Catalysis Today*, vol. 26 (1995); pp. 337-344.

H. Sadamori; "Application concepts and evaluation of small-scale catalytic combustors for natural gas"; *Catalysis Today*, vol.47 (1999); pp. 325-338.

G. Saracco, F. Geobaldo, G. Baldi; "Methane combustion on Mg-doped LaCrO_3 perovskite catalysts"; *Applied Catalysis B: Environmental*, vol. 20 (1999); pp. 277-288.

C.N. Satterfield and T.K. Sherwood: "the role of diffusion in catalysis"; Addison-Wesley Pub. Co., 1963.

T. Seiyama; "Total oxidation of hydrocarbons on perovskite oxides"; *Catalysis Reviews*, vol. 34 (1992): pp. 281-300.

L.L. Smith, H. Karim, M. J. Castaldi, S. Etemad, W. C. Pfefferle; "Rich-Catalytic Lean-Burn Combustion for Low-Single-Digi NO_x Gas Turbines", *Journal of engineering for Gas Turbines and Power*, (2005) Vol. 127; pp 27-35.

Scarpa, A.; Barbato, P.S.; Landi, G.; Pirone, R.; Russo, G.. "Combustion of methane-hydrogen mixtures on catalytic tablets" *Chemical Engineering Journal* (Amsterdam, Netherlands) (2009), 154(1-3), 315-324

Specchia S.; Finocchio E; Busca G; Palmisano P; Specchia V "Surface chemistry and reactivity of ceria-zirconia-supported palladium oxide catalysts for natural gas combustion" *Journal of Catalysis* (2009) Vol.263 pp.134-145.

Specchia, S; Conti, F; Specchia, V.: "Kinetic studies on Pd/CexZr1-xO2 catalyst for methane combustion" *Industrial & Engineering Chemistry Research* Vol.49 is. 21 pp.11101-11111 (2010).

Tejuca, L.G.; Bell, A.T; Fierro L.G. Tascon M.D.: "Structure and Reactivity of Perovskite-Type Oxides" *Advances in Catalysis* (1989) volume 36

Tejuca, L.G.; Bell, A.T; Fierro L.G. Tascon M.D. : "Temperature programmed desorption study of the interaction of CO and CO, with LaMnO₃," *Chem. SOC., Faraday Trans. I*, 1987, 83 (10), 3149-3159.

Towns B., Skolnik E.G., Miller J., Schefer R.W., Keller J.O.: "Analysis of benefits of carbon credits to hydrogen addition to midsize gas turbine feedstocks" *International Journal of Hydrogen Energy* (2007) Vol. 32 pp.3093-3099.

Verheij, L. K. : "Kinetic modeling of the hydrogen-oxygen reaction on Pt(111) at low temperature (<170K)" *Surface Science* (1997), 371(1), 100-110.

Verheij, L. K.; Huggenschmidt, M. B.: "On the mechanism of the hydrogen-oxygen reaction on Pt(111)" *Surface Science* (1998), 416(1/2), 37-58

Voltz, S.E.; Morgan, Charles R.; Liederman, D.; Jacob, S. M.: "Kinetic study of carbon monoxide and propylene oxidation on platinum catalysis." *Industrial & Engineering Chemistry Product Research and Development* (1973), 12(4), 294-301.

M. Uenishi, M. Tanigushi, H. Tanaka, M. Rimura, Y. Nishihata, J. Mizuki, T. Kobayashi; "Redox behaviour of palladium at start-up in the Perovskite-type LaFePdO_x automotive catalysts showing a self-regenerative function"; *Applied Catalysis B: Environmental*, vol. 57 (2005): pp. 267-273.

Wright I. G. Gibbons T.B.: "Recent developments in gas turbine materials and technology and their implications for syngas firing"; *International Journal of Hydrogen Energy* (2007) Vol. 32 pp. 3610-3621.

Ylmaz, M. Ilbas: "an experimental study on hydrogen-methane mixture fuels" *International Communications in Heat and Mass Transfer* (2008) Vol.35 pp. 178-187.

M. Zwinkels, S. Jaras, P.G. Menon, T. Griffin; "Catalytic materials for high temperature combustion, *Catalysis Reviews: Science and Engineering*, vol.35 (1993) p 319.